In vivo assessment of pathology in Parkinson's disease with Positron Emission Tomography

Benjamin S. Simpson

Thesis submitted in fulfilment of the requirements for the degree of

Doctor in Philosophy

Centre for Neuroinflammation and Neurodegeneration

Division of Brain Sciences

Faculty of Medicine

Imperial College London

Supervisor: Professor David J. Brooks

TABLE OF CONTENTS

Index of tables 9

Index of figures 12

Declaration of originality and acknowledgements 24

Abstract 25

Chapter 1: Introduction 26

1.1 Historical background 26

1.2 Epidemiology 26

1.2.1 Incidence, prevalence and economic burden 26

1.2.2 Gender 27

1.2.3 Racial variation 27

1.3 Aetiology 27

1.3.1 Genetics 27

1.3.2 Toxins 29

1.3.3 Tobacco, caffeine and alcohol 31

1.3.4 Non-steroidal anti-inflammatory drugs 31

1.4 Clinical manifestations of Parkinson's disease 31

1.4.1 Motor phenotype 31

1.4.2 Non-motor symptoms and "pre-motor" Parkinson's disease 32

1.4.3 Olfaction 32

1.4.4 Autonomic dysfunction 33

1.4.5 Depression and anxiety 34

1.4.6 REM sleep behaviour disorder 34

1.4.7 Excessive daytime sleepiness 35

1.4.8 Fatigue 36

1.4.9 Cognition & Dementia 36

1.5 Pathology 39

1.5.1 Dopamine 39

1.5.2 Acetylcholine 41

1.5.3 Serotonin 41

1.5.4 Noradrenaline 42

1.5.5 Lewy Bodies 42

1.5.6 Alpha synuclein 43
1.5.7 Glia 44
1.5.8 Neuroinflammation and microglia 44
1.5.9 Amyloid 44
1.5.10 Synergism between alpha synuclein, amyloid and tau 45
1.5.11 Progression of pathology in PD 46
1.5.12 Infection hypothesis 46
1.5.13 Prion hypothesis 47
Chapter 2: Methodology 49
2.1 Positron Emission Tomography 49
2.2 PET scanners 52
2.3 Kinetic analysis 52
2.4 Simplified Reference Tissue Model 54
2.5 Region of interest analysis 57
2.6 Voxel-based analysis: statistical parametric mapping 57
2.7 Imaging activated microglia with [^{11}C]-PK11195 PET 58
2.7.1 Radiopharmaceutical preparation 60
2.7.2 Scanning protocol 60
2.7.3 Image processing 60
2.7.4 Supervised clustering algorithm 61
2.7.5 Generation of parametric images 61
2.7.6 Spatial normalisation 61
2.7.7 Region of interest approach 61
2.7.8 Statistical parametric mapping 62
2.8 Imaging amyloid with [^{11}C]-PIB PET 62
2.8.1 Radiopharmaceutical preparation 63
2.8.2 Scanning protocol 63
2.8.3 Image processing 63
2.8.4 Spatial normalisation 63
2.8.5 Cerebellar ratio method 64
2.8.6 Region of interest approach 64
2.8.7 Statistical parametric mapping 64
2.9 Imaging cerebral glucose metabolism with [^{18}F]-FDG PET 64
2.9.1 Spectral analysis 66

2.9.2 Scanning protocol 66
2.9.3 Image processing 66
2.9.4 Spatial normalisation 67
2.9.5 Region of interest approach 67
Chapter 3: Activated microglia in Parkinson's disease 68
3.1 Objectives 68
3.2 Summary 68
3.3 Introduction 68
3.3.1 Neuroinflammation and microglia 68
3.3.2 Imaging activated microglia using [^{11}C]-(R)-PK11195 PET 72
3.3.3 [^{11}C]-(R)-PK11195 PET studies in Parkinson's disease 72
3.3.4 Novel TSPO radiotracers 73
3.4 Subjects and methods 74
3.4.1 Ethics and safety 74
3.4.2 Funding 74
3.4.3 Source of subjects 74
3.4.4 Inclusion criteria 74
3.4.5 Exclusion criteria 75
3.4.6 Sub-groups 75
3.4.7 Subgroup inclusion criteria 75
3.4.8 Determination of motor phenotype 76
3.4.9 Subjects 77
3.4.10 Clinical assessment 77
3.4.11 Scans 78
3.4.12 Image analysis 79
3.4.13 Region of interest data extraction 79
3.4.14 Voxel-based analysis: statistical parametric mapping (SPM) 79
3.4.15 Statistical analysis 79
3.5 Results 80
3.5.1 Baseline ROI analysis: controls v PD subjects 82
3.5.2 Baseline ROI analysis: disease duration 83
3.5.3 Baseline ROI analysis: age 84
3.5.4 Baseline ROI analysis: subject-rated motor disability (UPDRS 2) 84
3.5.5 Baseline ROI analysis: clinician-rated motor disability (UPDRS 3) 85

3.5.6 Baseline ROI analysis: depression 88
3.5.7 Baseline ROI analysis: quality of life (PDQ-39) 89
3.5.8 Baseline SPM analysis: healthy control versus PD subjects 89
3.5.9 Baseline SPM analysis: PD subjects at lower v higher dementia risk 91
3.5.10 Baseline SPM analysis: age 93
3.5.11 Baseline SPM analysis: disease duration 94
3.5.12 Baseline SPM analysis: visuospatial cognition 96
3.5.13 Baseline SPM analysis: phonemic fluency 97
3.5.14 Baseline SPM analysis: semantic fluency 99
3.5.15 Baseline SPM analysis: quality of life (PDQ-39) 100
3.5.16 Baseline SPM analysis: PDQ-39 mobility domain 101
3.5.17 Baseline SPM analysis: PDQ-39 cognition domain 102
3.5.18 Baseline SPM analysis: PDQ-39 communication domain 103
3.5.19 Baseline SPM analysis: PDQ-39 social impairment 104
3.5.20 Baseline SPM analysis: PDQ-39 bodily discomfort domain 106
3.5.21 Baseline SPM analysis: depression (GDS-15) 107
3.5.22 Baseline SPM analysis: subject-rated motor disability (UPDRS 2) 109
3.5.23 Baseline SPM analysis: clinician-rated motor disability (UPDRS 3) 110
3.5.24 Follow up ROI analysis: controls v PD subjects 111
3.5.25 Follow up ROI analysis: disease duration 112
3.5.26 Follow up ROI analysis: MoCA 113
3.5.27 Follow up ROI analysis: ACE 114
3.5.28 Follow up ROI analysis: depression (GDS-15) 116
3.5.29 Follow up ROI analysis: semantic fluency 117
3.5.30 Follow up ROI analysis: quality of life (PDQ-39) 117
3.5.31 Follow up ROI analysis: non-motor symptom scale (NMSS) 119
3.5.32 Follow up SPM analysis: disease duration 119
3.5.33 Follow up SPM analysis: MMSE 120
3.5.34 Follow up SPM analysis: UPDRS part 2 122
3.5.35 Follow up SPM analysis: UPDRS part 3) 123
3.5.36 Follow up SPM analysis: somnolence 124
3.5.37 Follow up SPM analysis: non-motor symptom scale (NMSS) 125
3.5.38 Follow up SPM analysis: quality of life (PDQ-39) 127
3.5.39 Follow up SPM analysis: PDQ-39 ADL domain 128

3.5.40 Follow up SPM analysis: PDQ-39 Mobility domain 130
3.5.41 Follow up SPM analysis: PDQ-39 emotion domain 131
3.5.42 Follow up SPM analysis: PDQ-39 bodily discomfort domain 132
3.5.43 Follow up SPM analysis: depression (GDS-15) 134
3.5.44 [^{11}C]-(R)-PK11195 BPND v [^{18}F]-FDG at baseline 135
3.5.45 [^{11}C]-(R)-PK11195 BPND v [^{18}F]-FDG at follow up 135
3.6 Discussion 136
Chapter 4: Amyloid deposition in Parkinson's disease 143
4.1 Objectives 143
4.2 Summary 143
4.3 Introduction 144
4.3.1 Neuropathology 144
4.3.2 Molecular pathology 146
4.3.3 Genetics 147
4.3.4 Cerebrospinal fluid 147
4.3.5 Imaging amyloid in Parkinson's disease using [11C]-PIB PET 148
4.4 Subjects and methods 150
4.4.1 Ethics and safety 150
4.4.2 Funding 150
4.4.3 Source of subjects 151
4.4.4 Inclusion criteria 151
4.4.5 Exclusion criteria 151
4.4.6 Sub-groups 151
4.4.7 Subjects 152
4.4.8 Clinical assessments 152
4.4.9 Scans 152
4.4.10 Image analysis 153
4.4.11 Region of interest data sampling 153
4.4.12 Voxel-based analysis: statistical parametric mapping (SPM) 153
4.4.13 Statistical analysis 153
4.5 Results 154
4.5.1 ROI analysis: controls v PD subjects at baseline 155
4.5.2 ROI analysis: PD subjects at baseline v follow up 156
4.5.4 ROI analysis: baseline PDND v PDD 156

4.5.5 Baseline ROI analysis: UPDRS part 2 157
4.5.6 Baseline ROI analysis: Montréal Cognitive Assessment (MoCA) 157
4.5.7 Baseline ROI analysis: phonemic fluency 158
4.5.8 Baseline SPM analysis: controls v non-demented PD 159
4.5.9 Baseline SPM analysis: non-demented v PD dementia 160
4.5.10 Follow up ROI analysis: verbal fluency 161
4.5.11 Follow up ROI analysis: depression 162
4.5.12 Follow up SPM analysis: verbal fluency 163
4.5.13 Follow up SPM analysis: depression 165
4.5.14 Follow up SPM analysis: PDQ-39 communication domain 166
4.5.15 Follow up SPM analysis: PDQ-39 mobility domain 167
4.5.16 Baseline [11C]-PIB v [18F]-FDG 169
4.5.17 Follow up [11C]-PIB v [18F]-FDG 170
4.6 Discussion 171
Chapter 5: Brain glucose metabolism and gait dysfunction in Parkinson's disease 176
5.1 Objectives 176
5.2 Summary 176
5.3 Introduction 176
5.3.1 Neural basis of normal gait function 176
5.3.2 Cognition and gait dysfunction in normal elderly subjects 177
5.3.3 Cognition and gait dysfunction in the presence of brain pathology 178
5.3.4 Cognition and gait dysfunction in Parkinson's disease 178
5.3.5 Functional imaging studies of gait dysfunction in PD 179
5.4 Subjects and methods 181
5.4.1 Source of subjects & ethics 181
5.4.2 Subjects 181
5.4.3 Gait assessment 181
5.4.4 Equipment 183
5.4.5 Gait characteristics 183
5.4.6 Scans 183
5.4.7 Image analysis 184
5.4.8 Region of interest data sampling 185
5.4.9 Voxel-based analysis: statistical parametric mapping (SPM) 185
5.4.10 Statistical analysis 185

5.5 Results 185
5.5.1 ROI analysis: step velocity 185
5.5.2 ROI analysis: step velocity variability 186
5.5.3 ROI analysis: step time 187
5.5.4 ROI analysis: step time variability 188
5.5.5 ROI analysis: stance time 188
5.5.6 ROI analysis: stance time variability 189
5.5.7 ROI analysis: step length asymmetry 190
5.5.8 ROI analysis: step length variability 190
5.5.9 ROI analysis: step width variability 190
5.5.10 ROI analysis: swing time 190
5.5.11 ROI analysis: swing time variability 191
5.5.12 SPM analysis: step time variability 192
5.5.13 SPM analysis: stance time 193
5.5.14 SPM analysis: stance time variability 194
5.5.15 SPM analysis: step length asymmetry 195
5.5.16 SPM analysis: step length variability 197
5.5.17 SPM analysis: swing time variability 198
5.6 Discussion 199
Chapter 6: Summary of findings and conclusions 204
6.1 Activated microglia in Parkinson's disease 204
6.2 Amyloid deposition in Parkinson's disease 206
6.3 Brain glucose metabolism & gait dysfunction in Parkinson's disease 207
Chapter 7: Appendix 209
Chapter 8: References 295

INDEX OF TABLES

3.1. Regions of interest

3.2. Subject demographics and clinical data

3.3. Regional [^{11}C]-(R)-PK11195 Binding Potentials (mean BP_{ND} ± standard deviation) in healthy controls and Parkinson's disease subjects

3.4. Correlation between regional mean [^{11}C]-(R)-PK11195 Binding Potentials (BP_{ND}) and self-rated depression scores (GDS-15) in PD subjects

3.5. Correlation between baseline regional [^{11}C]-(R)-PK11195 BP_{ND} and PDQ-39 total and sub-domain scores. Data are Spearman rank correlation coefficients (ρ)

3.6. Areas of raised [^{11}C]-(R)-PK11195 BP_{ND} in PD subjects compared to controls

3.7. Areas of greater [^{11}C]-(R)-PK11195 binding in PD subjects at higher risk of dementia compared to lower risk subjects

3.8. Areas of [^{11}C]-(R)-PK11195 binding in PD subjects correlating inversely with disease duration

3.9. Areas of inverse correlation between [^{11}C]-(R)-PK11195 BP_{ND} and the ACE visuospatial sub-score

3.10. Areas of inverse correlation between phonemic fluency (FAS letter task) and [^{11}C]-(R)-PK11195 BP_{ND}

3.11. Areas of inverse correlation between [^{11}C]-(R)-PK11195 BP_{ND} and semantic fluency scores

3.12. Areas of positive correlation between PDQ-39 scores and [^{11}C]-(R)-PK11195 BP_{ND}

3.13. Areas of positive correlation between PDQ-39 mobility scores and [^{11}C]-(R)-PK11195 BP_{ND}

3.14. Areas of positive correlation between baseline PDQ-39 cognition scores and [^{11}C]-(R)-PK11195 BP_{ND}

3.15. Areas of positive correlation between PDQ-39 communication scores and [^{11}C]-(R)-PK11195 BP_{ND}

3.16. Areas of positive correlation between PDQ-39 social impairment scores and [^{11}C]-(R)-PK11195 BP_{ND}

3.17. Areas of positive correlation between PDQ-39 and bodily discomfort scores and [^{11}C]-(R)-PK11195 BP_{ND}

3.18. Areas of positive correlation between GDS-15 depression scores and [^{11}C]-(R)-PK11195 BP_{ND}

3.19. Areas of positive correlation between UPDRS part 2 scores and [^{11}C]-(R)-PK11195 BP_{ND}

3.20 Areas of positive correlation between UPDRS part 3 scores and [^{11}C]-(R)-PK11195 BP_{ND}

3.21. Regional [^{11}C]-(R)-PK11195 Binding Potentials (mean ± standard deviation) in healthy controls and Parkinson's disease subjects

3.22. Correlation between regional [^{11}C]-PK11195 BP_{ND} and PDQ-39 total and sub-domain scores (Spearman rank coefficients) at follow up

3.23. Areas of inverse correlation between [^{11}C]-(R)-PK11195 BP_{ND} and disease duration

3.24. Areas of inverse correlation between [^{11}C]-(R)-PK11195 BP_{ND} and MMSE

3.25. Areas of positive correlation between [^{11}C]-(R)-PK11195 BP_{ND} and UPDRS part 2 scores

3.26. Areas of positive correlation between [^{11}C]-(R)-PK11195 BP_{ND} and UPDRS part 3 scores

3.27. Areas of positive correlation between [^{11}C]-(R)-PK11195 BP_{ND} and somnolence (ESS) scores

3.28. Areas of positive correlation between [^{11}C]-(R)-PK11195 BP_{ND} and non-motor symptom scale (NMSS) scores

3.29. Areas of positive correlation between [^{11}C]-(R)-PK11195 BP_{ND} and PDQ-39

3.30. Areas of positive correlation between [^{11}C]-(R)-PK11195 BP_{ND} and PDQ-39 ADL scores

3.31. Areas of positive correlation between [^{11}C]-(R)-PK11195 BP_{ND} and PDQ-39 mobility scores

3.32. Areas of positive correlation between [^{11}C]-(R)-PK11195 BP_{ND} and PDQ-39 emotional wellbeing scores

3.33. Areas of positive correlation between [^{11}C]-(R)-PK11195 BP_{ND} and PDQ-39 bodily discomfort scores

3.34. Areas of positive correlation between [^{11}C]-(R)-PK11195 BP_{ND} and GDS-15 scores

4.1. Demographic and clinical data for the non-demented (PDND) and PD dementia (PDD) subjects

4.2. Mean regional [^{11}C]-PIB RATIOs (± standard deviation) in healthy controls, non-demented PD subjects (PDND) at baseline and follow up, and subjects with Parkinson's disease dementia (PDD)

4.3. Areas of elevated [^{11}C]-PIB uptake in non-demented PD subjects compared to controls

4.4. Areas of elevated [^{11}C]-PIB uptake in PD subjects with dementia compared to non-demented PD subjects

4.5. Areas of inverse correlation between [^{11}C]-PIB and the ACE verbal fluency

4.6. Areas of inverse correlation between [^{11}C]-PIB uptake and phonemic fluency

4.7. Areas of positive correlation between [^{11}C]-PIB and depression (GDS-15) scores

4.8. Areas of positive correlation between [^{11}C]-PIB and the communication impairment domain of the PDQ-39

4.9. Areas of positive correlation between [^{11}C]-PIB and the PDQ-39 mobility impairment scores

4.10. Correlation between striatal [^{11}C]-PIB RATIO and regional CMRGlu

5.1. Gait characteristics

5.2. Correlation between mean regional [^{18}F]-FDG uptake and step time

5.3. Correlation between mean regional [^{18}F]-FDG uptake and step time variability

5.4. Correlation between mean regional [^{18}F]-FDG uptake and stance time

5.5. Correlation between mean regional [^{18}F]-FDG uptake and stance time variability

5.6. Correlation between mean regional [^{18}F]-FDG uptake and step length variability

5.7. Correlation between mean regional [^{18}F]-FDG uptake and swing time

5.8. Correlation between mean regional [^{18}F]-FDG uptake and swing time variability

5.9. Areas of inverse correlation between [^{18}F]-FDG uptake and step time variability

5.10. Areas of inverse correlation between [^{18}F]-FDG uptake and stance time

5.11. Areas of inverse correlation between [^{18}F]-FDG uptake and stance time variability

5.12. Areas of inverse correlation between [^{18}F]-FDG uptake and step length asymmetry

5.13. Areas of inverse correlation between [^{18}F]-FDG uptake and step length variability

5.14. Areas of inverse correlation between [^{18}F]-FDG uptake and swing time variability

INDEX OF FIGURES

2.1. Schema of annihilation event, coincidence detection and data processing
2.2. The compartment model
2.3. Reference tissue compartmental models
2.4. Compartment model for reference region based kinetic analyses
2.5. [^{18}F]-FDG is derived from D-Glucose by substitution of ^{18}F for the carbon-2 OH group
2.6. Hexokinase
3.1. Correlation between brainstem [^{11}C]-(R)-PK11195 BP_{ND} and disease duration
3.2. Correlation between posterior cingulate [^{11}C]-(R)-PK11195 BP_{ND} and disease duration
3.3. Correlation between putamenal [^{11}C]-(R)-PK11195 BP_{ND} and UPDRS part 2
3.4. Correlation between insula [^{11}C]-(R)-PK11195 BP_{ND} and UPDRS part 2
3.5. Correlation between whole brain [^{11}C]-(R)-PK11195 BP_{ND} and UPDRS part 2
3.6. Correlation between putamenal [^{11}C]-(R)-PK11195 BP_{ND} and UPDRS part 3
3.7. Correlation between frontal lobe [^{11}C]-(R)-PK11195 BP_{ND} and UPDRS part 3
3.8. Correlation between temporal lobe [^{11}C]-(R)-PK11195 BP_{ND} and UPDRS part 3
3.9. Correlation between insula [^{11}C]-(R)-PK11195 BP_{ND} and UPDRS part 3
3.10. Correlation between whole brain [^{11}C]-(R)-PK11195 BP_{ND} and UPDRS part 3
3.11. Regions of elevated baseline [^{11}C]-(R)-PK11195 BP_{ND} in non-demented PD subjects compared to healthy controls
3.12. Regions of elevated baseline [^{11}C]-(R)-PK11195 BP_{ND} in PD subjects at higher risk of dementia compared to those at lower risk
3.13. Inverse correlation between baseline [^{11}C]-(R)-PK11195 BP_{ND} and disease duration
3.14. Inverse correlation between [^{11}C]-(R)-PK11195 BP_{ND} and the visuospatial sub-score of the Addenbrooke's Cognitive Examination (ACE
3.15. Inverse correlation between [^{11}C]-(R)-PK11195 BP_{ND} and phonemic fluency (FAS letter task)
3.16. Inverse correlation between [^{11}C]-(R)-PK11195 BP_{ND} and semantic fluency
3.17. Positive correlation between [^{11}C]-(R)-PK11195 BP_{ND} and PDQ-39
3.18. Positive correlation between [^{11}C]-(R)-PK11195 BP_{ND} and PDQ-39 mobility domain

3.19 Positive correlation between baseline [^{11}C]-(R)-PK11195 BP_{ND} and PDQ-39 cognition domain

3.20. Positive correlation between [^{11}C]-(R)-PK11195 BP_{ND} and PDQ-39 communication domain

3.21. Positive correlation between [^{11}C]-(R)-PK11195 BP_{ND} and PDQ-39 social dimension

3.22. Positive correlation between [^{11}C]-(R)-PK11195 BP_{ND} and PDQ-39 bodily discomfort

3.23. Positive correlation between [^{11}C]-(R)-PK11195 BP_{ND} and GDS-15

3.24. Positive correlation between [^{11}C]-(R)-PK11195 BP_{ND} and UPDRS part 2

3.25. Positive correlation between baseline [^{11}C]-(R)-PK11195 BP_{ND} and UPDRS part 3

3.26. Correlation between follow up striatal [^{11}C]-(R)-PK11195 BP_{ND} and disease duration

3.27. Correlation between striatal [^{11}C]-(R)-PK11195 BP_{ND} and MoCA

3.28. Correlation between globus pallidus [^{11}C]-(R)-PK11195 BP_{ND} and MoCA

3.29. Correlation between globus pallidus [^{11}C]-(R)-PK11195 BP_{ND} and ACE

3.30. Correlation between globus pallidus [^{11}C]-(R)-PK11195 BP_{ND} and ACE verbal fluency

3.31. Correlation between globus pallidus [^{11}C]-(R)-PK11195 BP_{ND} and ACE language

3.32. Correlation between globus pallidus [^{11}C]-(R)-PK11195 BP_{ND} and ACE memory

3.33. Correlation between brainstem [^{11}C]-(R)-PK11195 BP_{ND} and GDS-15

3.34. Correlation between globus pallidus [^{11}C]-(R)-PK11195 BP_{ND} and semantic fluency

3.35. Inverse correlation between follow up [^{11}C]-(R)-PK11195 BP_{ND} and disease duration

3.36. Inverse correlation between follow up [^{11}C]-(R)-PK11195 BP_{ND} and MMSE

3.37. Positive correlation between follow up [^{11}C]-(R)-PK11195 BP_{ND} and UPDRS part 2

3.38. Positive correlation between follow up [^{11}C]-(R)-PK11195 BP_{ND} and UPDRS part 3 3.39. Positive correlation between follow up [^{11}C]-(R)-PK11195 BP_{ND} and ESS

3.40. Positive correlation between follow up [^{11}C]-(R)-PK11195 BP_{ND} and NMSS

3.41. Positive correlation between follow up [^{11}C]-(R)-PK11195 BP_{ND} and PDQ-39
3.42. Positive correlation between follow up [^{11}C]-(R)-PK11195 BP_{ND} and PDQ-39 ADL
3.43. Positive correlation between follow up [^{11}C]-(R)-PK11195 BP_{ND} and PDQ-39 mobility
3.44. Positive correlation between follow up [^{11}C]-(R)-PK11195 BP_{ND} and PDQ-39 emotional
3.45. Positive correlation between follow up [^{11}C]-(R)-PK11195 BP_{ND} and PDQ-39 bodily discomfort
3.46. Positive correlation between follow up [^{11}C]-(R)-PK11195 BP_{ND} and GDS-15
4.1. Example [^{11}C]-PIB RATIO images for control (A), non-demented PD (B), and PD dementia (C) subjects
4.2. [^{11}C]-PIB RATIO images at baseline (A) and at 24 months (B) in a subject developing PDD during this interval
4.3. Correlation between insula [^{11}C]-PIB RATIO and UPDRS part 2
4.4. Correlation between thalamic [^{11}C]-PIB RATIO and MoCA
4.5. Correlation between insula [^{11}C]-PIB RATIO and FAS phonemic fluency
4.6. Regions of elevated baseline [^{11}C]-PIB uptake in non-demented PD compared to controls
4.7. Regions of elevated baseline [^{11}C]-PIB uptake in PDD compared to non-demented PD
4.8. Correlation between striatal [^{11}C]-PIB RATIO and semantic fluency scores
4.9. Correlation between striatal [^{11}C]-PIB RATIO and ACE verbal fluency scores
4.10. Correlation between temporal lobe [^{11}C]-PIB RATIO and GDS-15
4.11. Inverse correlation between [^{11}C]-PIB uptake and ACE verbal fluency
4.12. Inverse correlation between [^{11}C]-PIB uptake and phonemic fluency (FAS letter task)
4.13. Positive correlation between [^{11}C]-PIB uptake and subject-rated depression (GDS-15)
4.14. Positive correlation between [^{11}C]-PIB uptake and PDQ-39 communication
4.15. Positive correlation between [^{11}C]-PIB uptake and PDQ-39 mobility
4.16. Correlation between striatal [^{11}C]-PIB RATIO and occipital lobe CMRGlu
4.17. Correlation between [^{11}C]-PIB RATIO and CMRGlu in anterior cingulate
4.18. Correlation between [^{11}C]-PIB RATIO and CMRGlu in frontal cortex

5.1. Laboratory arrangement for gait analysis
5.2. Illustration of gait parameters assessed: (i) length, (ii) width and (iii) timing
5.3. Correlation between putamenal [^{18}F]-FDG uptake and step velocity
5.4. Correlation between anterior cingulate [^{18}F]-FDG uptake and step velocity variability
5.5. Correlation between posterior cingulate [^{18}F]-FDG uptake and step velocity variability
5.6. Negative correlation between [^{18}F]-FDG uptake and step time variability
5.7. Negative correlation between [^{18}F]-FDG uptake and stance time
5.8. Negative correlation between [^{18}F]-FDG uptake and stance time variability
5.9. Negative correlation between [^{18}F]-FDG uptake and step length asymmetry
5.10. Negative correlation between [^{18}F]-FDG uptake and step length variability
5.11. Negative correlation between [^{18}F]-FDG uptake and swing time variability
A1. Correlation between whole brain [^{11}C]-(R)-PK11195 BP_{ND} and GDS-15
A2. Correlation between brainstem [^{11}C]-(R)-PK11195 BP_{ND} and GDS-15
A3. Correlation between putamenal [^{11}C]-(R)-PK11195 BP_{ND} and GDS-15
A4. Correlation between thalamic [^{11}C]-(R)-PK11195 BP_{ND} and GDS-15
A5 Correlation between frontal lobe [^{11}C]-(R)-PK11195 BP_{ND} and GDS-15
A6. Correlation between insula [^{11}C]-(R)-PK11195 BP_{ND} and GDS-15
A7. Correlation between temporal lobe [^{11}C]-(R)-PK11195 BP_{ND} and GDS-15
A8. Correlation between parietal lobe [^{11}C]-(R)-PK11195 BP_{ND} and GDS-15
A9. Correlation between occipital lobe [^{11}C]-(R)-PK11195 BP_{ND} and GDS-15
A10. Correlation between whole brain [^{11}C]-(R)-PK11195 BP_{ND} and PDQ 39 at baseline
A11. Correlation between brainstem [^{11}C]-(R)-PK11195 BP_{ND} and PDQ 39 at baseline
A12. Correlation between putamenal [^{11}C]-(R)-PK11195 BP_{ND} and PDQ 39 at baseline
A13. Correlation between globus pallidus [^{11}C]-(R)-PK11195 BP_{ND} and PDQ 39 at baseline
A14. Correlation between insula [^{11}C]-(R)-PK11195 BP_{ND} and PDQ 39 at baseline
A15. Correlation between frontal lobe [^{11}C]-(R)-PK11195 BP_{ND} and PDQ 39 at baseline
A16. Correlation between temporal lobe [^{11}C]-(R)-PK11195 BP_{ND} and PDQ 39 at

baseline

A17. Correlation between parietal lobe [^{11}C]-(R)-PK11195 BP_{ND} and PDQ 39 at baseline

A18. Correlation between occipital lobe [^{11}C]-(R)-PK11195 BP_{ND} and PDQ 39 at baseline

A19. Correlation between whole brain [^{11}C]-(R)-PK11195 BP_{ND} and PDQ 39 ADL domain at baseline

A20. Correlation between brainstem [^{11}C]-(R)-PK11195 BP_{ND} and PDQ 39 ADL domain at baseline

A21. Correlation between striatal [^{11}C]-(R)-PK11195 BP_{ND} and PDQ 39 ADL domain at baseline

A22. Correlation between insula [^{11}C]-(R)-PK11195 BP_{ND} and PDQ 39 ADL domain at baseline

A23. Correlation between temporal lobe [^{11}C]-(R)-PK11195 BP_{ND} and PDQ 39 ADL domain at baseline

A24. Correlation between whole brain [^{11}C]-(R)-PK11195 BP_{ND} and PDQ 39 Mobility domain at baseline

A25. Correlation between putamenal [^{11}C]-(R)-PK11195 BP_{ND} and PDQ 39 Mobility domain at baseline

A26. Correlation between insula [^{11}C]-(R)-PK11195 BP_{ND} and PDQ 39 Mobility domain at baseline

A27. Correlation between frontal lobe [^{11}C]-(R)-PK11195 BP_{ND} and PDQ 39 Mobility domain at baseline

A28. Correlation between temporal lobe [^{11}C]-(R)-PK11195 BP_{ND} and PDQ 39 Mobility domain at baseline

A29. Correlation between occipital lobe [^{11}C]-(R)-PK11195 BP_{ND} and PDQ 39 Mobility domain at baseline

A30. Correlation between frontal lobe [^{11}C]-(R)-PK11195 BP_{ND} and PDQ 39 Cognition domain at baseline

A31. Correlation between posterior cingulate [^{11}C]-(R)-PK11195 BP_{ND} and PDQ 39 Communication domain at baseline

A32. Correlation between whole [^{11}C]-(R)-PK11195 BP_{ND} and PDQ 39 Emotional Wellbeing domain at baseline

A33. Correlation between brainstem [^{11}C]-(R)-PK11195 BP_{ND} and PDQ 39 Emotional

Wellbeing domain at baseline

A34. Correlation between putamenal [^{11}C]-(R)-PK11195 BP_{ND} and PDQ 39 Emotional Wellbeing domain at baseline

A35. Correlation between thalamic [^{11}C]-(R)-PK11195 BP_{ND} and PDQ 39 Emotional Wellbeing domain at baseline

A36. Correlation between insula [^{11}C]-(R)-PK11195 BP_{ND} and PDQ 39 Emotional Wellbeing domain at baseline

A37. Correlation between temporal lobe [^{11}C]-(R)-PK11195 BP_{ND} and PDQ 39 Emotional Wellbeing domain at baseline

A38. Correlation between whole brain [^{11}C]-(R)-PK11195 BP_{ND} and PDQ 39 Social domain at baseline

A39. Correlation between anterior cingulate [^{11}C]-(R)-PK11195 BP_{ND} and PDQ 39 Social domain at baseline

A40. Correlation between frontal lobe [^{11}C]-(R)-PK11195 BP_{ND} and PDQ 39 Social domain at baseline

A41. Correlation between temporal lobe [^{11}C]-(R)-PK11195 BP_{ND} and PDQ 39 Social domain at baseline

A42. Correlation between occipital lobe [^{11}C]-(R)-PK11195 BP_{ND} and PDQ 39 Social domain at baseline

A43. Correlation between whole brain [^{11}C]-(R)-PK11195 BP_{ND} and PDQ 39 Stigmatisation domain at baseline

A44. Correlation between anterior cingulate [^{11}C]-(R)-PK11195 BP_{ND} and PDQ 39 Stigmatisation domain at baseline

A45. Correlation between frontal lobe [^{11}C]-(R)-PK11195 BP_{ND} and PDQ 39 Stigmatisation domain at baseline

A46. Correlation between globus pallidus [^{11}C]-(R)-PK11195 BP_{ND} and PDQ 39 bodily discomfort domain at baseline

A47. Correlation between frontal lobe [^{11}C]-(R)-PK11195 BP_{ND} and PDQ 39 Bodily Discomfort domain at baseline

A48. Correlation between whole brain [^{11}C]-(R)-PK11195 BP_{ND} and PDQ 39 at follow up

A49. Correlation between brainstem [^{11}C]-(R)-PK11195 BP_{ND} and PDQ 39 at follow up

A50. Correlation between thalamic [^{11}C]-(R)-PK11195 BP_{ND} and PDQ 39 at follow

up
A51. Correlation between striatal [^{11}C]-(R)-PK11195 BP_{ND} and PDQ 39 at follow up
A52. Correlation between globus pallidus [^{11}C]-(R)-PK11195 BP_{ND} and PDQ 39 at follow up
A53. Correlation between frontal lobe [^{11}C]-(R)-PK11195 BP_{ND} and PDQ 39 at follow up
A54. Correlation between insula [^{11}C]-(R)-PK11195 BP_{ND} and PDQ 39 at follow up
A55. Correlation between temporal lobe [^{11}C]-(R)-PK11195 BP_{ND} and PDQ 39 at follow up
A56. Correlation between parietal lobe [^{11}C]-(R)-PK11195 BP_{ND} and PDQ 39 at follow up
A57. Correlation between occipital lobe [^{11}C]-(R)-PK11195 BP_{ND} and PDQ 39 at follow up
A58. Correlation between whole brain [^{11}C]-(R)-PK11195 BP_{ND} and PDQ 39 ADL domain at follow up
A59. Correlation between brainstem [^{11}C]-(R)-PK11195 BP_{ND} and PDQ 39 ADL domain at follow up
A60. Correlation between caudate [^{11}C]-(R)-PK11195 BP_{ND} and PDQ 39 ADL domain at follow up
A61. Correlation between putamenal [^{11}C]-(R)-PK11195 BP_{ND} and PDQ 39 ADL domain at follow up
A62. Correlation between thalamic [^{11}C]-(R)-PK11195 BP_{ND} and PDQ 39 ADL domain at follow up
A63. Correlation between globus pallidus [^{11}C]-(R)-PK11195 BP_{ND} and PDQ 39 ADL domain at follow up
A64. Correlation between insula [^{11}C]-(R)-PK11195 BP_{ND} and PDQ 39 ADL domain at follow up
A65. Correlation between frontal lobe [^{11}C]-(R)-PK11195 BP_{ND} and PDQ 39 ADL domain at follow up
A66. Correlation between temporal lobe [^{11}C]-(R)-PK11195 BP_{ND} and PDQ 39 ADL domain at follow up
A67. Correlation between parietal lobe [^{11}C]-(R)-PK11195 BP_{ND} and PDQ 39 ADL domain at follow up

A68. Correlation between occipital lobe [^{11}C]-(R)-PK11195 BP_{ND} and PDQ 39 ADL domain at follow up

A69. Correlation between whole brain [^{11}C]-(R)-PK11195 BP_{ND} and PDQ 39 Mobility domain at follow up

A70. Correlation between brainstem [^{11}C]-(R)-PK11195 BP_{ND} and PDQ 39 Mobility domain at follow up

A71. Correlation between striatal [^{11}C]-(R)-PK11195 BP_{ND} and PDQ 39 Mobility domain at follow up

A72. Correlation between frontal lobe [^{11}C]-(R)-PK11195 BP_{ND} and PDQ 39 Mobility domain at follow up

A73. Correlation between insula [^{11}C]-(R)-PK11195 BP_{ND} and PDQ 39 Mobility domain at follow up

A74. Correlation between temporal lobe [^{11}C]-(R)-PK11195 BP_{ND} and PDQ 39 Mobility domain at follow up

A75. Correlation between parietal lobe [^{11}C]-(R)-PK11195 BP_{ND} and PDQ 39 Mobility domain at follow up

A76. Correlation between whole brain [^{11}C]-(R)-PK11195 BP_{ND} and PDQ 39 Cognition domain at follow up

A77. Correlation between brainstem [^{11}C]-(R)-PK11195 BP_{ND} and PDQ 39 Cognition domain at follow up

A78. Correlation between globus pallidus [^{11}C]-(R)-PK11195 BP_{ND} and PDQ 39 Cognition domain at follow up

A79. Correlation between insula [^{11}C]-(R)-PK11195 BP_{ND} and PDQ 39 Cognition domain at follow up

A80. Correlation between frontal lobe [^{11}C]-(R)-PK11195 BP_{ND} and PDQ 39 Cognition domain at follow up

A81. Correlation between whole brain [^{11}C]-(R)-PK11195 BP_{ND} and PDQ 39 Emotional Wellbeing domain at follow up

A82. Correlation between brainstem [^{11}C]-(R)-PK11195 BP_{ND} and PDQ 39 Emotional Wellbeing domain at follow up

A83. Correlation between striatal [^{11}C]-(R)-PK11195 BP_{ND} and PDQ 39 Emotional Wellbeing domain at follow up

A84. Correlation between thalamic [^{11}C]-(R)-PK11195 BP_{ND} and PDQ 39 Emotional Wellbeing domain at follow up

A85. Correlation between insula [^{11}C]-(R)-PK11195 BP_{ND} and PDQ 39 Emotional Wellbeing domain at follow up

A86. Correlation between temporal lobe [^{11}C]-(R)-PK11195 BP_{ND} and PDQ 39 Emotional Wellbeing domain at follow up

A87. Correlation between brainstem [^{11}C]-(R)-PK11195 BP_{ND} and PDQ 39 Bodily Discomfort domain at follow up

A88. Correlation between putamenal [^{11}C]-(R)-PK11195 BP_{ND} and PDQ 39 Bodily Discomfort domain at follow up

A89. Correlation between thalamic [^{11}C]-(R)-PK11195 BP_{ND} and PDQ 39 Bodily Discomfort domain at follow up

A90. Correlation between globus pallidus [^{11}C]-(R)-PK11195 BP_{ND} and PDQ 39 Bodily Discomfort domain at follow up

A91. Correlation between insula [^{11}C]-(R)-PK11195 BP_{ND} and PDQ 39 Bodily Discomfort domain at follow up

A92 Correlation between frontal lobe [^{11}C]-(R)-PK11195 BP_{ND} and PDQ 39 Bodily Discomfort domain at follow up

A93. Correlation between temporal lobe [^{11}C]-(R)-PK11195 BP_{ND} and PDQ 39 Bodily Discomfort domain at follow up

A94. Correlation between parietal lobe [^{11}C]-(R)-PK11195 BP_{ND} and PDQ 39 Bodily Discomfort domain at follow up

A95. Correlation between occipital [^{11}C]-(R)-PK11195 BP_{ND} and PDQ 39 Bodily Discomfort domain at follow up

A96. Correlation between caudate [^{11}C]-(R)-PK11195 BP_{ND} and brainstem CMRGlu at baseline

A97. Correlation between caudate [^{11}C]-(R)-PK11195 BP_{ND} and thalamic CMRGlu at baseline

A98. Correlation between posterior cingulate [^{11}C]-(R)-PK11195 BP_{ND} and occipital lobe CMRGlu at baseline

A99. Correlation between putamenal [^{11}C]-(R)-PK11195 BP_{ND} and putamenal CMRGlu at follow up

A100. Correlation between putamenal [^{11}C]-(R)-PK11195 BP_{ND} and thalamic CMRGlu at follow up

A101. Correlation between putamenal [^{11}C]-(R)-PK11195 BP_{ND} and frontal lobe CMRGlu at follow up

A102. Correlation between putamenal [^{11}C]-(R)-PK11195 BP_{ND} and parietal lobe CMRGlu at follow up

B1. Correlation between striatal [^{11}C]-PIB RATIO and whole brain CMRGlu

B2. Correlation between striatal [^{11}C]-PIB RATIO and striatal CMRGlu

B3. Correlation between striatal [^{11}C]-PIB RATIO and thalamic CMRGlu

B4. Correlation between striatal [^{11}C]-PIB RATIO and anterior cingulate CMRGlu

B5. Correlation between striatal [^{11}C]-PIB RATIO and posterior cingulate CMRGlu

B6. Correlation between striatal [^{11}C]-PIB RATIO and insula CMRGlu

B7. Correlation between striatal [^{11}C]-PIB RATIO and frontal lobe CMRGlu

B8. Correlation between striatal [^{11}C]-PIB RATIO and temporal lobe CMRGlu

B9. Correlation between striatal [^{11}C]-PIB RATIO and parietal lobe CMRGlu

C1. Correlation between whole brain [^{18}F]-FDG uptake and step time

C2. Correlation between brainstem [^{18}F]-FDG uptake and step time

C3. Correlation between putamenal [^{18}F]-FDG uptake and step time

C4. Correlation between globus pallidus [^{18}F]-FDG uptake and step time

C5. Correlation between anterior cingulate [^{18}F]-FDG uptake and step time

C6. Correlation between posterior cingulate [^{18}F]-FDG uptake and step time

C7. Correlation between insula [^{18}F]-FDG uptake and step time

C8. Correlation between frontal lobe [^{18}F]-FDG uptake and step time

C9. Correlation between temporal lobe [^{18}F]-FDG uptake and step time

C10. Correlation between whole brain [^{18}F]-FDG uptake and step time variability

C11. Correlation between putamenal [^{18}F]-FDG uptake and step time variability

C12. Correlation between globus pallidus [^{18}F]-FDG uptake and step time variability

C13. Correlation between anterior cingulate [^{18}F]-FDG uptake and step time variability

C14. Correlation between posterior cingulate [^{18}F]-FDG uptake and step time variability

C15. Correlation between insula [^{18}F]-FDG uptake and step time variability

C16. Correlation between frontal lobe [^{18}F]-FDG uptake and step time variability

C17. Correlation between temporal lobe [^{18}F]-FDG uptake and step time variability

C18. Correlation between brainstem [^{18}F]-FDG uptake and stance time

C19. Correlation between putamneal [^{18}F]-FDG uptake and stance time

C20. Correlation between globus pallidus [^{18}F]-FDG uptake and stance time

C21. Correlation between posterior cingulate [^{18}F]-FDG uptake and stance time

C22. Correlation between insula [^{18}F]-FDG uptake and stance time

C23. Correlation between frontal lobe [^{18}F]-FDG uptake and stance time

C24. Correlation between temporal lobe [^{18}F]-FDG uptake and stance time

C25. Correlation between whole brain [^{18}F]-FDG uptake and stance time variability

C26. Correlation between putamenal [^{18}F]-FDG uptake and stance time variability

C27. Correlation between globus pallidus [^{18}F]-FDG uptake and stance time variability

C28. Correlation between anterior cingulate [^{18}F]-FDG uptake and stance time variability

C29. Correlation between anterior cingulate [^{18}F]-FDG uptake and stance time variability

C30. Correlation between insula [^{18}F]-FDG uptake and stance time variability

C31. Correlation between frontal lobe [^{18}F]-FDG uptake and stance time variability

C32. Correlation between temporal lobe [^{18}F]-FDG uptake and stance time variability

C33. Correlation between caudate [^{18}F]-FDG uptake and step length asymmetry

C34. Correlation between putamenal [^{18}F]-FDG uptake and step length asymmetry

C35. Correlation between caudate [^{18}F]-FDG uptake and step length variability

C36. Correlation between putamenal [^{18}F]-FDG uptake and step length variability

C37. Correlation between globus pallidus [^{18}F]-FDG uptake and step length variability

C38. Correlation between anterior cingulate [^{18}F]-FDG uptake and step length variability

C39. Correlation between posterior cingulate [^{18}F]-FDG uptake and step length variability

C40. Correlation between insula [^{18}F]-FDG uptake and step length variability

C41. Correlation between frontal lobe [^{18}F]-FDG uptake and step length variability

C42. Correlation between temporal lobe [^{18}F]-FDG uptake and step length variability

C43. Correlation between striatal [^{18}F]-FDG uptake and step width variability

C44. Correlation between whole brain [^{18}F]-FDG uptake and swing time

C45. Correlation between brainstem [^{18}F]-FDG uptake and swing time

C46. Correlation between putamenal [^{18}F]-FDG uptake and swing time

C47. Correlation between globus pallidus [^{18}F]-FDG uptake and swing time

C48. Correlation between posterior cingulate [^{18}F]-FDG uptake and swing time

C49. Correlation between frontal lobe [^{18}F]-FDG uptake and swing time

C50. Correlation between temporal lobe [^{18}F]-FDG uptake and swing time

C51. Correlation between parietal lobe [^{18}F]-FDG uptake and swing time

C52. Correlation between occipital lobe [^{18}F]-FDG uptake and swing time

C53. Correlation between putamenal [^{18}F]-FDG uptake and swing time variability

C54. Correlation between globus pallidus [^{18}F]-FDG uptake and swing time variability

C55. Correlation between globus pallidus [^{18}F]-FDG uptake and swing time variability

C56. Correlation between posterior cingulate [^{18}F]-FDG uptake and swing time variability

C57. Correlation between frontal lobe [^{18}F]-FDG uptake and swing time variability

C58. Correlation between temporal lobe [^{18}F]-FDG uptake and swing time variability

DECLARATION OF ORGINALITY, ACKOWLEDGEMENTS, AND COPYRIGHT DECLARATION

I declare that the work contained in this thesis is my own.

My gratitude goes to my supervisor Professor Brooks for setting direction and providing support and wise council. I would also like to thank my mentor, Dr Nicola Pavese, for his support and advice; Professor Barker, of University of Cambridge for supplying some of the patients for the main study; and to Professors Rochester and Burn of the Institute of Neuroscience, Newcastle, for providing the scans and clinical data for analysis in Chapter 5. Most importantly, I am grateful to the patients with Parkinson's disease who participated in this research.

The copyright of this thesis rests with the author and is made available under a Creative Commons Attribution Non-Commercial No Derivatives licence. Researchers are free to copy, distribute or transmit the thesis on the condition that they attribute it, that they do not use it for commercial purposes and that they do not alter, transform or build upon it. For any reuse or redistribution, researchers must make clear to others the licence terms of this work.

Abstract

Twenty-one non-demented Parkinson's disease (PD) subjects had [^{11}C]-(R)-PK11195, [^{11}C]-PIB and [^{18}F]-FDG PET scans to evaluate activated microglia, amyloid and cerebral metabolism, respectively; of these, 19 underwent repeat scanning at an interval of 2 years. Motor, cognitive and non-motor clinical assessments were conducted. 7 subjects with PD dementia had [^{11}C]-PIB and [^{18}F]-FDG scans. 8 [^{11}C]-(R)-PK11195, 9 [^{11}C]-PIB, and 8 [^{18}F]-FDG control scans were obtained. [^{11}C]-(R)-PK11195 uptake correlated with multiple motor and cognitive deficits and other non-motor clinical symptoms, suggesting that neuroinflammation associated with microglial activation is relevant to the clinical phenotypic expression from early disease onwards. [^{11}C]-PIB uptake was elevated throughout the neocortex and in the striatum in the non-demented PD group compared to controls, with a predilection for posterior cortical structures. [^{11}C]-PIB uptake had increased in the non-demented PD group at interval scanning. [^{11}C]-PIB retention in the PD dementia group was higher than in the non-demented PD group, with a relative excess of anterior cortical [^{11}C]-PIB binding. Striatal [^{11}C]-PIB retention correlated inversely with verbal fluency. Subjective motor disability, impaired verbal fluency, and communication difficulties were associated with frontal lobe [^{11}C]-PIB uptake in the non-demented PD group, suggesting that amyloid may contribute to frontal lobe dysfunction in PD before the onset of dementia.

In a separate study, 47 [^{18}F]-FDG PET scans with comprehensive gait analysis data were acquired. Brain metabolic deficits, detected with [^{18}F]-FDG PET, were associated with abnormalities in gait pace and variability. Reduced gait velocity correlated with hypometabolism in the brainstem, putamen, globus pallidus, cingulate and anterior neocortex. The same pattern of metabolic derangement was related to increased gait variability, but spared the brainstem. It is conceived that brainstem locomotor structure contribute to pace, a more rudimentary component of gait function, whilst excess variability is a consequence of impaired supratentorial control of brainstem locomotion structures. Excess gait variability in PD may represent failure of compensatory mechanisms localising to the basal ganglia and anterior neocortex, due to progressive intrinsic PD pathology in these structures.

Chapter 1

Introduction

1.1 Historical background

Parkinson's disease (PD) is a progressive incurable akinetic rigid and tremulous movement disorder usually presenting in later adulthood, although the phenotype is now known to be much broader. The condition is named after the English apothecary and surgeon James Parkinson, who published the first clinical description in his monograph "The Shaking Palsy" based on observations of six subjects in Shoreditch, London (Parkinson, 1817). No convincing description of a condition resembling PD exists in pre-modern history, despite its distinctive phenotype (Stern, 1989). This observation, combined with evidence for putative environmental neurotoxins in the aetiology and pathogenesis of the condition considered below, has led to the suggestion that PD is a disease of the Industrial Age.

1.2 Epidemiology

1.2.1 Incidence, prevalence and economic burden

PD affects 1 million people in North America (Lang and Lozano, 1998) and 1.2 million in Europe (Andlin-Sobocki et al., 2005). Under reporting, especially in lower income and ethnic minority groups, means the real prevalence is likely to be higher. In developing countries where statistics are available, the proportion of undetected cases is probably greater still, while no data exists for other nations, meaning that there is no reliable figure for global prevalence. The incidence and prevalence of PD rises with the age of the population. It is uncommon in those under 50 years, increasing with age thereafter. In the population over 65 years the overall prevalence is of the order 1-1.8% (de Rijk et al., 2000; Driver et al., 2009), rising to 2.6% among persons aged 85-89 years (de Rijk et al., 2000). The overall prevalence of PD in the 10 most populous nations worldwide was projected to increase from 4.1 million in 2005, to 8.67 million in 2030 (Dorsey et al., 2007. The annual economic cost of PD is

estimated to be $23 billion in the US (Huse et al., 2005), and €13.9 billion in Europe (Gustavsson et al., 2011).

1.2.2 Gender

PD is overrepresented in males. In a meta-analysis of 7 epidemiological studies, the risk of PD was 1.5 times greater in men than woman (Wooten et al., 2004). The reasons for this are unknown. There may be an intrinsic biological mechanism, such as excess mitochondrial toxicity in men, or a protective effect of oestrogens in women (Inestrosa et al., 1998). Alternatively, male behavioural patterns may lead to greater exposure to environmental risk factors (Wooten et al., 2004).

1.2.3 Racial variation

In a large epidemiological study of an ethnically heterogeneous North American population, the incidence of PD was highest among Hispanics, with progressively lower rates reported for non-Hispanic Whites, Asians and Blacks (Van Den Eeden et al., 2003). Increased prevalence of established PD susceptibility alleles in well-characterised ethnic groups, such as pathogenic LRRK2 and GBA mutations in Ashkenazi Jews (Liu et al., 2011), explains only a small proportion of the apparent racial variation reported in epidemiological studies. These differences may instead be due to unknown genetic factors, inter-racial variation in environmental risk factor exposure, or ascertainment bias.

1.3 Aetiology

1.3.1 Genetics

In a recent meta-analysis of 26 epidemiological studies, the odds ratio of developing PD in the presence of a first degree relative with the disease was 3.23 (Noyce et al., 2012). Whilst some of this excess risk may be due to shared environment, the genetic contribution to apparently sporadic IPD likely consists of unidentified monogenetic and polygenetic factors. At the time of writing, seven genes are known to cause a

phenotype resembling sporadic PD, with a Mendelian pattern of inheritance; overall these account for 5% of cases of PD (Lesage and Brice, 2009). In genome wide association studies, the most consistently identified PD risk alleles are SCNA (encoding alpha synuclein), MAPT (microtubule associated protein tau) and LRRK2 (Simon-Sanchez et al., 2009; Satake et al., 2009; Sharma et al., 2012).

Four genes (SNCA, LRRK2, EIF4G1 and VPS35) are associated with autosomal dominant inheritance; three (parkin, PINK1, DJ1) are recessive. A point mutation (A53T) in the SNCA (PARK1/4) gene was described in 1996 in the large North American Contursi kindred (Golbe et al., 1996). Two further pathogenic point mutations in SCNA have been identified (Kruger et al., 1998; Zarranz et al., 2004). Duplication of the SCNA gene was shown to cause disease phenotypically indistinguishable from sporadic idiopathic PD (Chartier-Harlin et al., 2004), whilst triplication results in a fulminant PD dementia with median age at onset 20 years earlier (Singleton et al., 2003), suggesting a toxic gene dosage effect.

In 2004, two groups independently reported dominantly inherited PD due to mutations in the LRRK2 (PARK8) gene (Paisan-Ruiz et al., 2004; Zimprich et al., 2004). The common G2019S mutation is the cause of 1-2% of apparently sporadic PD in Europe (Farrer et al., 2005; Gilks et al., 2005), rising to 18.3% in Ashkenashi Jews (Ozelius et al., 2006), and 41% in North African Arabs (Lesage et al., 2006). In 2011, two further autosomal dominant PD genes were identified, EIF4G1 (Chartier-Harlin et al., 2011) and VPS35 (Vilarino-Guell et al., 2011). The pathogenicity of these mutations has been confirmed after their independent identification in separate PD kindreds (Lesage et al, 2012; Schulte et al., 2012).

Mutations in the parkin (PARK2) gene cause autosomal recessive PD (Kitada et al., 1998). The frequency of parkin mutations in PD is inversely related to age at onset, being common in cases presenting before 20 years of age, and exceedingly rare with onset over the age of 45 years (Lucking et al., 2000). The clinical phenotype further differs from sporadic PD with the presence of marked diurnal variation in motor symptoms associated with sleep benefit, as well as early foot dystonia and hyperreflexia, and by the relatively low incidence of cognitive impairment, dysautonomia and other non-motor symptoms (Ahlskog et al., 2009). Moreover, pathology appears to be restricted to the brainstem, and Lewy bodies - the histological

hallmark of sporadic PD - are typically absent (Mori et al., 1998; van de Warrenburg et al., 2001). Mutations in PINK1 (PARK 6; Valente et al, 2004) and DJ-1 (PARK 7; Bonifati et al., 2003) are less common causes of recessive PD: the phenotype is similar to that due to parkin mutations. In a recent meta-analysis of early-onset PD (defined as age at onset under 45 years), the frequency of parkin, PINK1, and DJ-1 mutations was 8.6%, 3.7%, and 0.4% respectively (Kilarski et al., 2012).

Homozygous or compound heterozygous mutations in the glucocerebrosidase (GBA1) gene cause the autosomal recessive lysosomal storage disorder, Gaucher's disease (GD), particularly prevalent among Ashkenazi Jews. The glucocerebrosidase enzyme is a lysosomal hydrolase; deficiency causes lysosomal accumulation of glycolipids. In 2004, Aharon-Peretz et al. reported a high prevalence (31%) of heterozygous GBA1 mutations in Ashkenazi Jewish IPD patients. Several studies have reported an age of onset in GBA1 associated PD cases 5-10 years earlier than in sporadic IPD (Aharon-Peretz et al., 2004; Alcalay et al., 2014), although others report no difference (Aharon-Peretz et al., 2005). Data from cellular models suggest several mechanisms by which GBA1 mutations may precipitate cellular aggregation of α-synuclein, including lysosome, endoplasmic reticulum and mitochondrial dysfunction (Yang et al., 2013). Alpha-synuclein binds specifically with glucocerebrosidase *in vitro* in solution replicating lysosomal physiological conditions (Yap et al., 2011). Glucocerebrosidase was detected in 75% of Lewy bodies examined from the brains of three GD cases and four GBA1 heterozygotes (Goker-Alpan et al., 2010). In brain autopsy samples from subjects with sporadic PD, cellular accumulation of α-synuclein was associated with impaired lysosomal function and loss of lysosomal glucocerebrosidase (Murphy et al., 2014).

1.3.2 Toxins

A history of occupational exposure to herbicides or pesticides is more common in subjects who later develop PD (Liou et al, 1997; Gorell et al, 1998; Noyce et al. 2012). Given their widespread use in agriculture, exposure to such chemicals may be practically unavoidable even in the general population. Nigrostriatal dopaminergic neurons are especially sensitive to oxidative damage, and a range of pesticides,

including paraquat, maneb and rotenone, has been shown to be neurotoxic to cell cultures under experimental conditions (Moretto and Colosio, 2011).

In 1979, a single case report appeared of chronic parkinsonism in a substance abuser who had synthesised and injected an illicit pethidine derivative, 4-propyloxy-4-phenyl-N-methylpiperidine. The parkinsonism was confirmed at autopsy to be due to nigral neurotoxicity of the chemical (Davis et al. 1979). Other such cases were reported in the early 1980s, leading to the identification of the relevant neurotoxin - a by-product of the meperidine synthesis - N-methyl-4-phenyl-1,2,3,6-tetrahydropyridine (MPTP; Langston et al., 1983). This led to the development of the primate MPTP model of PD (Burns et al., 1983). Heavy metal deposition may also cause basal ganglia toxicity. Excess brain copper accumulation is a cause of parkinsonism, typically starting in adolescence, in the recessive genetic disorder, Wilson's disease. Manganese may be deposited in the basal ganglia of patients with cirrhosis, where it is the cause of acquired (non-Wilsonian) hepato-cerebral degeneration (Ferrara and Jankovic, 2009) and in a recently identified genetic disorder due to SLC30A10 mutations, encoding a manganese transporter (Tuschl et al., 2012). In the last five years, numerous cases of parkinsonism in methcathinone/ ephedrone drug users (particularly from eastern Europe) have been attributed to manganese toxicity due to the use of potassium permanganate in its manufacture from ephedrine (Stepens et al., 2008). Occupational manganese exposure ("Manganism") is also a recognised cause of parkinsonism (Calne et al., 1994), affecting miners and steelworkers among others, particularly in previous generations (Couper, 1837; Rodier, 1955; Cook et al., 1974), when occupational exposure to manganese in developed countries was an order of magnitude higher than in the present day (Racette, 2013). There is a controversial recent literature suggesting a raised risk of PD with contemporary lower Mn exposure occupations. While some studies reported an elevated PD risk in welders (Racette et al., 2012), a recent meta-analysis found no association (Mortimer et al., 2012).

Lytico-Bodig disease is a progressive neurological disorder occurring in the Chamorro island population of Guam (Hirano et al., 1961), presenting with a variable phenotype termed amyotrophic lateral sclerosis/parkinsonism/dementia complex. It is caused by the cyanobacterial neurotoxin β-methylamino-L-alanine (BMAA), which accumulates in the seeds of the cycad tree, *Cycas micronesica* (Spencer et al., 1987),

from which the Chamorro derive flour used for tortillas, although a much higher concentration of the toxin is found in fruit bats which also feed on the seeds, and which the Chamorro consume as a delicacy (Cox et al., 2003). Cycad-fed rats develop a parkinsonian disorder with pathological features of PD (α-synuclein containing inclusions in degenerating dopaminergic neurons; Shen et al., 2010).

1.3.3 Tobacco, caffeine and alcohol

Subjects who smoke tobacco have a 25-50% lower relative risk of developing PD compared to those who have never smoked (Allam et al., 2003; Noyce et al. 2012). Coffee drinkers also have a reduced risk (Hernan et al., 2002), and moderate alcohol consumption may be protective (Ragonese et al., 2003), but not tea (Noyce et al. 2012). These phenomena are difficult to explain biologically, and it is unclear whether they represent a genuine neuroprotective effect, or are due to unidentified confounding factors.

1.3.4 Non-steroidal anti-inflammatory drugs

In the last decade, reports emerged of a protective effect of prior non-steroidal anti-inflammatory drug (NSAID) use on the risk of developing PD (Chen et al., 2003; 2005), although others found no association (Hernan et al., 2006; Ton et al., 2006). A subsequent meta-analysis of 7 studies reported a 15% reduction in the risk of PD in non-aspirin NSAID users, and furthermore the effect magnitude was proportional to duration of exposure and cumulative dose (Gagne and Power, 2010).

1.4 Clinical manifestations of Parkinson's disease

1.4.1 Motor phenotype

Parkinson's disease is clinically characterised by the classical motor triad of tremor, limb rigidity and bradykinesia. Asymmetric onset, gait abnormalities including flexed posture, loss of postural reflexes, and freezing, are other key motor features (Tolosa et al., 2006). Bradykinesia - slowness of movement initiation and execution - is the

cardinal clinical sign in PD, being that most closely related to nigral dopaminergic cell loss. Limb tremor has a typical frequency of 3-7 Hz, and is present predominantly at rest, lessening or abating with movement. Tremor may affect other body parts, such as lip or jaw. The lateral asymmetry of limb symptoms at disease onset is preserved throughout the disease (Uitti et al., 2005). Bulbar function may be affected later, leading to hypophonia, dysarthria and dysphagia. Gait is affected by a number of akinetic phenomena: gait ignition failure (difficulty starting to walk), reduced stride length, problematic turning, freezing of gait, and an inability to lift the foot from the floor producing "shuffling". The centre of gravity is held forward, which in association with rapid steps of markedly reduced stride length results in festination. Gait disorder and postural instability are usually refractory to dopaminergic medication (suggesting that they have a non-dopaminergic basis), and, particularly if present early in the course of the disease, are risk factors for later dementia (see paragraph 1.4.9).

Clinico-pathological series indicate that the accuracy of a clinical diagnosis of Parkinson's disease with nigral Lewy body disease as the standard of truth may at best be 90%, even in the hands of experienced movement disorder neurologists, with or without the use of research diagnostic criteria (Hughes et al. 1992; 2001). Thus, PD populations studied in clinical trials are likely to be contaminated by at least 10% of cases with an alternate pathology (most frequently progressive supranuclear palsy if established cases; Williams et al., 2005).

1.4.2 Non-motor symptoms and "pre-motor" Parkinson's disease

It is now recognised that patients with PD may develop non-motor symptoms before the onset of the motor phenotype; these increase in frequency and severity in advanced PD where they become a major source of morbidity, often refractory to treatment.

1.4.3 Olfaction

In the Honolulu-Asia Aging Study, 2267 men aged 71-95 years without clinical (motor) PD underwent olfactory testing, and were followed for 8 years thereafter: the presence of idiopathic hyposmia was associated with an odds ratio of 5.2 for the subsequent development of PD, compared to those with intact baseline olfaction (Ross et al., 2008). In a two year longitudinal study of 361 first degree relatives of PD subjects asymptomatic at enrolment, 40 were hyposmic and seven of these had evidence of nigro-striatal dopamine deficiency on DAT (dopamine transporter) SPECT imaging - four subsequently converted to clinical PD over a two year follow up period. Of those subjects with abnormal baseline DAT scans who did not develop clinical PD, the rate of progression of dopaminergic deficiency was greater in hyposmic cases (Ponsen et al., 2004). The presence of Lewy body pathology in the olfactory bulb has long been recognised (Daniel and Hawkes, 1992), and the Braak model predicts pre-motor hyposmia at the earliest pathological stage (Braak et al., 2003, see). Hyposmia is also the most common detectable non-motor symptom once motor symptoms of PD develop, occurring in 70-100% if sought using objective olfactory testing (Katzenschlager and Lees, 2004).

1.4.4 Autonomic dysfunction

A wide range of autonomic symptoms may occur in PD, involving gastrointestinal, urinary, cardiovascular and sexual dysfunction. This is consistent with the identification of α-synuclein pathology throughout the autonomic nervous system, including medulla, thoracic spinal cord, sympathetic ganglia, vagal and sacral parasympathetic nerves, and gut submucosal plexus. Although early autonomic disturbance, particularly if severe, should prompt consideration of a diagnosis of MSA, autonomic involvement can occur early in the course of PD (Awerbuch and Sandyk, 1994; Verbaan et al., 2007). In a series of 98 autopsy specimens with no motor symptoms of PD in life, 17% had spinal and peripheral Lewy pathology (Bloch et al., 2006). If the pathological origin of PD is indeed in the periphery, some of these ILBD cases may represent “pre-motor” disease.

Constipation predating motor symptoms is frequently reported by PD subjects, yet retrospective studies may be affected by recall bias. In a large prospective cohort of 6790 respondents aged 51-75 (the Honolulu Heart Program) followed for 24 years,

the relative risk of developing PD in those with less the one bowel motion per day was 4.1, compared to those with two or more motions per day (Abbott et al., 2001), suggesting that constipation is a risk marker for PD. In a cross-sectional study of symptomatic PD, 40% of subjects with early (Hohn and Yahr stage 1/2) disease had dysphagia, early abdominal fullness or constipation, suggesting the presence of pharyngeal/ oesophageal dysmotility, gastroparesis or slow colonic transit; whilst the prevalence of symptoms of postural hypotension, urinary dysfunction and erectile dysfunction in males was greater than 50% for each domain (Verbaan et al., 2007).

^{123}I-meta-iodobenzylguanidine (^{123}I-MIBG), an analogue of noradrenaline, is taken up by post-ganglionic sympathetic nerve terminals, and can be used as a marker to assess the functional integrity of a target region's sympathetic innervation. ^{123}I-MIBG scintigraphy has been used to demonstrate cardiac sympathetic denervation in PD (Oka et al., 2007), and can discriminate between PD and MSA with around 80% accuracy since autonomic neuropathy in MSA affects first, not second order sympathetic nerves, resulting in normal ^{123}I-MIBG uptake (Umemura et al., 2013).

1.4.5 Depression and anxiety

In a meta-analysis of 36 studies, the prevalence of major depression in PD was 17%, and that of minor depression 22% (Reijnders et al., 2008). The prevalence of anxiety in PD appears comparable to that of depression, being reported in the range 20-33% (Aarsland et al., 1999; Shulman et al., 2001). Depression and anxiety can also precede motor PD by 3-6 years (Shiba et al., 2000; Leentjens et al., 2003) and this may in part be due to the loss of noradrenergic and/or serotonergic neurons in the pons (see paragraphs 1.5.3 and 1.5.4).

1.4.6 REM sleep behaviour disorder

Rapid Eye Movement (REM) sleep behaviour disorder (RBD) is a parasomnia characterised by the enactment of often vivid and threatening dreams due to the loss of physiological limb atonia during REM sleep. RBD may be a "pre-motor" symptom in PD. In a study of 44 subjects with isolated RBD, 20 developed clinical features of a

synucleinopathy (PD, DLB or MSA) within 11.5 years, 50% being PD (Iranzo et al., 2006). A later study reported isolated RBD present 15-50 years before the clinical diagnosis of a synucleinopathy (Claassen et al., 2010). Further, subjects with idiopathic RBD have reduced striatal dopamine transporter binding intermediate between controls and symptomatic PD when assessed with [^{123}I]-IPT SPECT (Eisensehr et al., 2000), consistent with idiopathic RBD being insipient Lewy body disease in at least some cases.

The pontine coeruleus/subcoeruleus complex is thought to drive atonia in REM sleep. Using MRI to study its integrity by exploiting the paramagnetic properties of neuromelanin-bound iron, it has been shown there is reduced coeruleus/subcoeruleus neuromelanin content in PD which is more pronounced when RBD is also present and correlates with the fractional loss of atonia at polysomnography (García-Lorenzo et al., 2013). In subjects with RBD, comorbid hyposmia increases the risk of developing PD (Postuma et al., 2011).

1.4.7 Excessive daytime sleepiness

Some studies report excessive daytime sleepiness (EDS) in medicated but not treatment naïve PD, leading to the suggestion that EDS is a pharmacological phenomenon (Fabbrini et al., 2002). Whilst it is well recognized that drugs, particularly dopamine agonists, may cause or exacerbate sleepiness in PD, attributing excess somnolence exclusively to medication may be confounded by the effect of underlying disease severity, since pathological progression is broadly associated with increasing medication burden. Of 3078 men aged 71-93 in the Honolulu Aging Study, however, the presence of EDS was associated with an odds ratio of 3.3 for developing PD within the next 3 years compared to those without EDS (Abbott et al., 2005), suggesting that excessive somnolence may be a risk factor for, and a pre-motor symptom of, PD. The definition of excessive sleepiness in this study was self-reported "sleepiness for most of the day", and did not involve objective assessment (such as with the Epworth Sleepiness Scale). EDS is also a risk factor for cognitive impairment and dementia.

1.4.8 Fatigue

Mental and physical fatigue is more common in PD than controls (van Hilten et al., 1993). This finding was confirmed in the ELLDOPA study, in which 37% of 361 subjects were classified as fatigued at baseline (Schifitto et al., 2008). Drawing firm conclusions on role of dopamine in fatigue from the ELLDOPA study is difficult, since, whilst the symptom responded to dopaminergic medication, there was no difference in striatal dopamine transporter binding assessed with [^{123}I]-beta-CIT between the fatigued and non-fatigued groups at baseline. Pavese et al. (2010) also found no difference in striatal dopaminergic function (assessed with ^{18}F-dopa PET) between fatigued and non-fatigued PD cases, but striatal and thalamic serotonin transporter binding, imaged with ^{11}C-DASB PET, was significantly reduced in the fatigued subjects. This finding suggests that serotonin rather than dopamine deficiency may be more relevant to PD fatigue (see paragraph 1.5.3).

1.4.9 Cognition & dementia

In his 1817 essay, Parkinson accurately documented the bradykinesia and tremor of the disorder, but asserted that cognitive impairment was absent ("*the higher senses being unaffected*"). We now know this to be incorrect: the prevalence of dementia after 20 years of symptomatic disease is 80% (Hely et al., 2008). If dementia occurs more than one year after parkinsonism then the condition is known as PD dementia (PDD); if dementia precedes or develops within a year of parkinsonism, a diagnosis of Dementia with Lewy bodies (DLB) is made (McKeith et al., 2005). The development of dementia in PD creates a substantial healthcare and social burden and, in common with other degenerative dementing illnesses, its incidence is likely to increase through the remainder of the 21st century as populations in many countries age. Further, the supervention of dementia in PD often stymies attempts to manage the motor aspects of the condition pharmacologically: most PD drugs tend, to some degree, to exacerbate cognitive symptoms associated with PDD. No proven intervention exists that might prevent or delay the onset of PDD.

Several risk factors have been identified for the development of dementia in PD. Age and more severe motor disability are robustly associated with PDD (Marder, 2010). In

a dichotomised bivariate analysis, Levy et al. (2002) found age >72 years and motor disability greater than a score of 24 in the Unified Parkinson's Disease Rating Scale (part 3) were together associated with a 10 fold elevated risk of PDD. Tremor predominant cases without postural instability are associated with a favourable prognosis in terms of both the rate of accumulation of motor disability and conversion to PDD; conversely, the postural instability gait disorder (PIGD) phenotype, semantic dysfluency, constructional apraxia, and the presence of visual hallucinations, are all risk factors for PDD (Jankovic et al., 1990; Levy et al., 2000; Fenlon et al., 2000; 2006; Williams-Gray et al*.,* 2007; 2013).

Cognitive impairment is frequently present in early motor PD, and may even occur in the premotor phases of the disease (Goldman et al., 2014). It usually consists of a fronto-striatal dysexecutive syndrome, manifesting as impaired working memory, planning and attentional control; slowing of mental processes (bradyphrenia); and cognitive inflexibility (Kehagia al., 2010). Cognitive impairment at this stage appears to be a consequence of dysfunction of nigro-striatal and nigro-frontal dopaminergic neurotransmission. Selective frontal lobe dopamine depletion (using 6-OHDA) in monkeys causes increased distractibility and impaired attentional set-shifting, whilst dopamine depletion of the striatum causes reduced distractibility (Crofts et al. 2001), the adverse clinical consequence of which may be cognitive rigidity (Cools et al., 2010). In animal studies, both pharmacological blockade and overstimulation of frontal lobe D1 receptors caused impairment on working memory tasks (Sawaguchi and Goldman-Rakic 1991; Zahrt et al., 1997), leading to the hypothesis that there is a physiological window for optimal modulation of frontal lobe function by dopamine, alternatively described as an inverted "U"-shaped curve (Williams and Castner, 2006; Mizoguchi et al., 2009).

The synaptic concentration of dopamine in the frontal cortex is dependent on the activity of catechol-O-methyl transferase (COMT), which metabolises dopamine in the synaptic cleft. The substitution of for methionine for valine at codon 158 in the COMT gene, a common polymorphism affecting 50% of European populations (Palmatier et al., 1999), results in significantly lower enzymatic activity (Chen et al., 2004), and is therefore predicted to cause higher frontal lobe dopamine levels. In healthy volunteers, Met/Met homozygotes performed better on a frontal executive set-shifting task (the Wisconsin Card Sorting Test) than those with one or more Val

alleles, suggesting the latter have suboptimal frontal lobe dopamine levels (Malhotra et al. 2002). The opposite effect is observed for early PD patients, however: Met/Met genotype subjects performed less well compared to Val/Val cases on the Tower of London (ToL) task, a test of planning (Foltynie et al., 2004), and had defective attentional control (William-Gray et al., 2008), leading to the hypothesis that a hyperdopaminergic state, arising as a compensatory response to nigrostriatal dopamine depletion, is deleterious to cognitive function in early PD (Williams-Gray et al, 2007; 2008; Cools et al., 2010). Dopaminergic drugs may exacerbate this effect, since medicated recent-onset PD subjects have greater impairment in ToL and spatial working memory tasks than non-medicated otherwise matched PD cases (Owen et al., 1992). Met/Met PD subjects also showed reduced activation of fronto-parietal cortex, assessed using fMRI, which correlated with poorer cognitive performance (Williams-Gray et al. 2007; 2008). Subsequently, Wu et al. (2012) confirmed the presence of higher frontal lobe dopamine in PD subjects with the Met/Met genotype compared to Val/Val, using [^{18}F]-DOPA PET.

It is intuitive that a patient with a progressive neurodegenerative disease ultimately causing dementia should transition through an intermediate clinical phase. This concept, termed mild cognitive impairment (MCI), was initially developed in the Alzheimer's disease literature (Petersen et al., 2001; Albert et al., 2011), but has since been introduced for PD (Litvan et al., 2012). The reported prevalence of MCI in recent-onset PD is 20-35%, rising to over 50% at 5 years (Aarsland et al., 2009; 2010; Broeders et al., 2013). In contrast to MCI in AD, which is dominated by amnesia (Ferman et al., 2013), MCI in PD is characterised by a range of cognitive deficits, most often affecting executive, memory, verbal fluency or visuospatial function, alone or in combination (Mahieux et al. 1998; Levy et al., 2002; Williams-Gray et al., 2007). The most common presentation is with a unimodal non-amnestic disorder (Litvan et al., 2011).

Degeneration of cholinergic neurons in the basal forebrain nucleus of Meynert in PD has long been recognised (Rogers et al., 1985). PET studies using N-[^{11}C]-methyl-4-piperidyl acetate, a marker of acetylcholinesterase (AChE) activity, show that progressive loss of cholinergic terminals is detectable from an early stage, being most severe in PDD (Shimada et al., 2009; Gilman et al., 2010). Cholinergic dysfunction may contribute to cognitive impairment in PD (Kehagia al., 2010); treatment of PDD

subjects with cholinesterase inhibitors improves cognitive performance and subjective disability (Rolinski et al., 2012).

In addition to dysfunction in dopaminergic and cholinergic systems, intrinsic cortical pathology also contributes to cognitive impairment in PD (Jellinger, 2012). Neural glucose uptake is a function of metabolic demand, principally determined by synaptic activity. Intrinsic cortical pathology is associated with hypometabolism due to progressive dysfunction and dying back of neurons. The glucose analogue [^{18}F]-FDG is a PET marker of hexokinase activity that allows the effect of local pathology on regional brain glucose utilisation to be studied. The pattern of cortical hypometabolism seen with [^{18}F]-FDG PET in non-demented PD is similar to AD, involving temporal and dorsal parietal lobes, precuneus and posterior cingulate (Peppard et al., 1992; Hu et al., 2000), but in addition targets occipital cortex (Lyoo et al. 2010; Bohnen et al., 2011). There is also a relative increase in metabolism in the putamen, globus pallidus, and thalamus, which may be a compensatory mechanism (Eidelberg et al., 1994; Antonini et al., 1997). Progression of disease culminating in PDD is characterized by progressive cortical and subcortical hypometabolism, with frontal lobe involvement (Peppard et al., 1992; Bohnen et al., 2011).

1.5 Pathology

1.5.1 Dopamine

A century after Parkinson's clinical observations, Konstantin Tretiakoff reported loss of pigmented neurons in the midbrain substantia nigra pars compacta (SNc) in necropsy specimens from PD cases (Tretiakoff, 1919). In 1960, Ehringer and Hornykiewicz demonstrated profound dopamine depletion in the striatum (comprising the caudate and putamen), due to loss of dopaminergic neurons in the SNc, which project to the striatum (Ehringer and Hornykiewicz 1960; Hirsch et al., 1988). Subsequently, Birkmayer and Hornykiewicz (1961) demonstrated improvement of bradykinesia in PD patients after injection with the dopamine precursor levodopa (L-dopa), confirming the dopaminergic deficit as the principal cause of the motor features of the disease, and resulting in the widespread deployment of the drug to treat the disorder (Cotzias et al., 1967).

Neurodegeneration in the SNc begins in the ventrolateral tier, which projects to the dorsolateral putamen (Kish et al., 1988); thereafter degeneration of the ventral SNc continues with extension into the dorsal SNc, leading ultimately to denervation of the rostral putamen, head of caudate and globus pallidus (Kish et al., 1988; Damier et al., 1999). Normal control subjects exhibit 10-fold slower nigral cell attrition, with the opposite anatomical pattern (Fearnley and Lees, 1991). By extrapolating these data from control and PD subjects, the threshold loss of nigral cells required to cause motor symptoms has been estimated to be 50% (Fearnley and Lees, 1991).

Evidence from [^{18}F]-DOPA PET in living PD subjects confirmed that dopamine depletion targets the posterior putamen compared to the ventral striatum (Brooks et al., 1990). In drug naïve early PD, the putamen contralateral to the more affected limb has lower [^{18}F]-DOPA uptake, but greater D2 dopamine receptor availability (assessed with [^{11}C]-raclopride), which may represent compensatory receptor upregulation and/or the presence of reduced striatal dopamine (Brooks et al., 1992; Sawle et al., 1993). In advanced PD treated with L-Dopa, D2 receptor availability is normalised or reduced (Brooks et al. 1992, Turjanski et al. 1997), which may be a consequence of chronic non-physiological dopamine stimulation leading to downregulation of D2 receptors. Neuropathology from patients in whom [^{18}F]-DOPA PET had ben performed in late life show a good correlation between nigral dopaminergic cell counts and striatal [^{18}F]-DOPA uptake (Snow et al., 1993).

Whilst neuropathology series are by nature cross-sectional, longitudinal PET and SPECT studies have investigated the progression of loss of dopaminergic function in PD. Using [^{123}I]-β-CIT SPECT, the annual decline in striatal dopamine transporter availability was 11.2% (Marek et al., 2001), whilst a [^{18}F]-DOPA PET study reported an annual loss of dopamine of 8% in the putamen and globus pallidus (Pavese et al., 2011). In a PET study using [^{11}C]-dihydrotetrabenazine (DTBZ, a marker for vesicular monoamine transporter type 2), the rate of decline in VMAT2 binding was the same across all striatal regions (Lee et al., 2004). This finding has since been replicated using three radiotracers that assess dopaminergic function: [^{18}F]-DOPA, [^{11}C]-DTBZ, and [^{11}C]-d-threo-methylphenidate (MP, a dopamine transporter marker); the rate of dopaminergic loss was similar with all the tracers and was uniform across the striatum (Nandhagopal et al., 2009). This suggests that the cause

of the initial rostro-caudal and side-to-side asymmetry in striatal pathology may be independent of the mechanisms that drive subsequent neurodegeneration.

In addition to nigrostriatal degeneration, marked dopamine depletion in the globus pallidus also occurs in PD, and may contribute to basal ganglia dysfunction (Rajput et al., 2008). Using [^{18}F]-DOPA PET, Whone et al. (2003) reported increased [^{18}F]-DOPA uptake in the GPi in early PD that is lost later in the disease, whilst dopamine depletion in the GPe was progressive from onset. This may represent a compensatory response to nigrostriatal dopamine depletion, similar to the nigro-frontal dopaminergic upregulation discussed above.

1.5.2 Acetylcholine

Loss of cholinergic neurons in the basal forebrain nucleus of Meynert in PD is well established from neuropathology series (Candy et al., 1983; Arendt et al., 1983; Nakano and Hirano, 1984). Functional imaging data *in vivo* confirm the pathological findings. In a SPECT study using [^{123}I]-iodobenzovesamicol (IBVM), a marker of the vesicular acetylcholine transporter, non-demented PD subjects had reduced density of cholinergic terminals in parieto-occipital cortex, whilst subjects with PDD had a more extensive cortical cholinergic deficit (Kuhl et al., 1996). Using the PET radiotracer N-[^{11}C]-methyl-4-piperidyl acetate (MP4A), which binds to acetylcholinesterase, Hilker et al. (2005) found a posterior cholinergic deficit in non-demented PD subjects, which was more severe in PDD. A subsequent SPECT study using [^{123}I]-5-iodo-3-[2(S)-2-azetidinylmethoxy]-pyridine, a marker of nicotinic acetylcholine receptors, reported extensive cholinergic deficiency in non-demented early PD, involving cortical and subcortical regions (Fujita et al., 2006). These data provide a biological rationale for the use of acetylcholinestrase inhibitors in PDD, in agreement with trial data demonstrating clinical efficacy (Rolinski et al. 2012).

1.5.3 Serotonin

Brain serotonin (5-hydroxytryptamine; 5-HT) is synthesised by neurons of the pontine raphe nuclei, which project to the frontal cortex and limbic system, where it has

cognitive and affective functions (Albert et al., 2014). In PD, neuropathology data shows reduced serotonin (5-hydroxytryptamine; 5-HT) in caudate, limbic and frontal cortex (Scatton et al., 1983). In support of this, Guttman et al. (2007) reported reduced serotonin transporter (SERT) binding in the midbrain, striatum, and orbitofrontal cortex in PD, assessed using [^{11}C]-3-amino-4-(2-dimethylaminomethyl-phenylsulfanyl)-benzonitrile (DASB) PET.

Because of the role of 5-HT in depression in the general population (Albert et al., 2014), and the widespread use of serotonin-selective reuptake inhibitors (SSRIs) as anti-depressants, several studies have addressed the question of whether depression in PD has a serotonergic aetiology, with conflicting results. In a neuropathology series of 45 PD cases, those with a history of depression had greater neuron loss in the dorsal raphe nuclei (Paulus and Jellinger, 1991). Functional imaging studies, however, have not supported this. No difference between PD subjects with and without depression was found in 5HT1A receptor availability, assessed using [^{11}C]-WAY100635 (Doder et al., 2000), or SERT density, using [^{123}I]-β-CIT SPECT (Kim et al., 2003). 5-HT may instead be involved in fatigue in PD, since non-depressed PD subjects with fatigue had reduced SERT availability compared to non-fatigued cases, using [^{11}C]-DASB PET (Pavese et al., 2010).

1.5.4 Noradrenaline

Loss of noradrenergic neurons in the locus coerulus in PD is well established (Mann, 1983; German et al., 1992). Brainstem Lewy body pathology involves the locus coreulus, as well as the SNc and raphe nuclei (Zarow et al, 2003, Braak et al, 2003). The rate of noradrenergic attrition is comparable to that of dopamine (Pavese et al., 2011). Uptake of [^{11}C]RTI-32, which binds both dopamine and noradrenaline transporters, was lower in depressed than non-depressed PD subjects in the locus coerulus and limbic system (Remy et al., 2005). Since the locus coerulus does not contain dopamine, noradrenaline may contribute to depression in PD.

1.5.5 Lewy Bodies

In 1912, German pathologist Fritz Heinrich Lewy discovered neuronal inclusions in the brains of patients with "paralysis agitans" (Rodrigues e Silva et al., 2010). These became known as Lewy bodies, and are today considered the histological hallmark of the disease, their presence being mandatory for a pathological diagnosis of PD (Hughes et al., 1992). Whilst Lewy bodies are a highly specific pathological marker of PD, they are not the pivotal event in the pathogenesis of the condition, and the focus in recent years has shifted to the principal constituent of Lewy bodies, aggregated alpha synuclein (Ozansoy and Başak, 2013).

1.5.6 Alpha synuclein

In 1997, the molecular composition of Lewy bodies was shown to contain aggregated alpha synuclein (Spillantini et al*.,* 1997). Triplication of the alpha synuclein gene (SCNA) results in early adult onset rapidly progressive PD (Singleton et al., 2003), whilst SCNA duplication results in disease phenotypically indistinguishable from sporadic late adult onset idiopathic PD (Chartier-Harlin et al., 2004). Transgenic mice constitutively expressing human alpha synuclein develop a complex motor disorder associated with the development of neuronal inclusions containing alpha synuclein similar to Lewy bodies (Giasson et al., 2002).

Alpha synuclein pathology in axonal processes ("Lewy neurites") is detectable before the development of Lewy bodies (Braak et al., 1999). Axonal dysfunction and degeneration correlates better with clinical status in PD than Lewy body density (Chen et al., 2010). It was previously thought that alpha synuclein aggregation was the central pathological event in PD (Caughey and Lansbury, 2003). Striatal dopamine transporter density, however, correlates with total SNc alpha-synuclein burden, not Lewy body counts (Kovacs et al., 2008). Abundant recent evidence points to soluble alpha synuclein oligomers as the most toxic species (Danzer et al., 2007; Tsigelny et al., 2008; Winner et al., 2011), and the Lewy body may play a protective role as well as providing a disease biomarker. Alpha synuclein oligomers may have a deleterious effect on several cellular targets, including the synapse, mitochondria, endoplasmic reticulum, and axonal transport (Katsuse et al., 2003; Nakamura et al., 2011; Ferrer et al., 2011).

1.5.7 Glia

Gliosis, which accompanies all neurodegenerative diseases, has been previously regarded as a non-specific response to tissue injury. In recent years, however, a central role for glia as pathologic effectors has been proposed (Halliday and Stevens, 2011), due to a direct toxic effect on adjacent neurons (McGeer and McGeer, 2004). The distribution of alpha synuclein positive astrocytes exceeds that of Lewy body positive neurons, as they are present in the midbrain, where Lewy body containing cell bodies of the SNc reside, and the striatum, to which those neurons project. It has been hypothesised that astrocytes may take up alpha synuclein from adjacent neurites (Braak et al., 2004). Transfer of alpha synuclein from neurons to astrocytes has been demonstrated *in vitro*, and is associated with astrocytic release of inflammatory cytokines that may be directly neurotoxic and/or recruit microglia and hence promote further inflammatory injury (Lee et al., 2010). Glia may be cellular intermediaries, transmitting alpha synuclein pathology to previously healthy neurons, in a manner analogous to prion diseases (Braak et al., 2003, 2004; Halliday and Stevens, 2011).

1.5.8 Neuroinflammation and microglia

Evidence is accumulating for an inflammatory component in a variety of neurodegenerative diseases (McGeer and McGeer, 2004; Mrak and Griffin, 2007), including PD (Phani et al., 2012). The role of microglia is PD is discussed further in Chapter 4.

1.5.9 Amyloid

Some neuropathology studies have reported a correlation between cortical Lewy body density and dementia in PD (Hurtig et al., 2000; Braak et al., 2005; Aarsland et al., 2005); others have found no such association (Colosimo 2003 et al.; Ballard et al*.,* 2006; Lashley et al., 2008; Parkkinen et al., 2005; 2008). Given the likelihood that Lewy bodies are a marker of alpha synucleinopathy and not directly toxic (paragraph 1.5.5), other pathological processes must contribute to cognitive impairment in PD.

Several clinicopathological series report a significant contribution from beta amyloid deposition (Apaydin et al. 2002*;* Jellinger and Attems, 2008; Lashley et al., 2008; Compta et al., 2011). The role of amyloid in PD is discussed further in Chapter 5.

1.5.10 Synergism between alpha synuclein, amyloid and tau

Microtubule-associated protein tau (MAPT; tau protein) stabilises axonal microtubules (Weingarten et al., 1975; Harada et al., 1994). Hyperphosphorylation of tau causes microtubule destabilisation, and is a key pathologic event in AD, progressive supranuclear palsy, and other "tauopathies" (Iqbal et al., 2005). In PD, there is evidence of a synergistic relationship between amyloid, alpha synuclein and tau, whereby each facilitates the aggregation of the other two. In an alpha synuclein/Amyloid Precursor Protein (APP) dual transgenic murine model, greater alpha synuclein accumulation occurred compared to that in the single transgenics, and Aß amyloid peptides were shown to promote alpha synuclein accumulation *in vitro* (Masliah et al., 2001). Alpha synuclein induces the formation of tau fibrils, and tau and alpha synuclein act synergistically in effecting the polymerization of each into fibrillar amyloid aggregates (Giasson et al., 2003). In a transgenic mouse which manifests alpha synuclein, Aß amyloid and tau pathologies, mutual synergism in the accumulation of all three proteins was seen and was associated with phenotypic severity (Clinton et al., 2010*)*. Alpha synuclein promotes tau phosphorylation and aggregation (Qureshi and Paudel, 2011; Waxman and Giasson, 2011), and may thereby disrupt axonal transport, which depends on normal microtubule function.

In genome-wide association studies, polymorphisms in the SNCA gene (encoding alpha synucelin), and the MAPT H1 haplotype (encoding tau) were the most potent genetic contributors to both familial and sporadic PD risk (Goris et al., 2007; Pankratz et al*.,* 2009; Simon-Sanchez et al., 2009; Elbaz et al., 2011). APOE genotype, robustly associated with amyloid deposition in AD, may also contribute to PDD risk (Lashley et al*.,* 2008; Williams-Gray et al*.,* 2009). In a large clinicopathological series, PD dementia was independently associated with alpha synuclein, tau and amyloid loads (Compta et al., 2011).

1.5.11 Progression of pathology in PD

According to Braak staging (Braak et al*.,* 2003; 2005), Lewy body pathology starts in the medullary dorsal motor nucleus of vagus, and/or in the olfactory bulb and anterior olfactory nuclei (stage 1); and progresses rostrally through the neuraxis, affecting the pontine locus coeruleus, gigantocellular reticular nucleus, and raphe nuclei (stage 2); causes the cardinal motor symptoms once pathology affects the midbrain SNc (stage 3); and results in cognitive impairment and ultimately dementia with involvement of limbic (stage 4) and primary and association neocortex (stages 5 and 6). Although the Braak staging has gained broad acceptance, its universality has been contested (Burke et al., 2008; Halliday et al., 2008). If all cases of PD followed the Braak model, lower brainstem Lewy bodies should be detectable in every symptomatic PD subject, and in all cases of incidental Lewy body disease (iLBD). In support of this, lower brainstem Lewy body pathology was found with midbrain Lewy bodies in 71 consecutive cases of autopsy-proven PD (Parkkinen et al., 2008). Eleven cases of iLBD had reduced striatal tyrosine hydroxylase (the enzyme catalysing the rate-limiting in dopamine synthesis), suggesting that iLBD is "pre-symptomatic" PD (Beach et al., 2008; Halliday et al., 2006). Further, striatal and epicardial nerve tyrosine hydoxylase levels in iLBD are intermediate between those of controls and PD subjects (Dickson et al., 2008).

Other studies, however, have reported that a significant minority of cases diverge from the Braak staging model. Of 76 brains with Lewy bodies (a mixture of symptomatic and iLBD cases), cortical pathology in the absence of lower brainstem involvement occurred in 17% (Zaccai et al., 2008). In a series of 226 pure iLBD cases, pontine and medullary Lewy bodies were also absent in 17% (Parkkinen et al., 2008). A modification of the Braak model proposes two routes by which pathology may spread to the neocortex: ascent through the brainstem as originally proposed, or alternatively via the limbic system, bypassing the brainstem (Beach et al., 2009).

1.5.12 Infection hypothesis

Pathology in PD is not confined to the central nervous system. Lewy bodies have been found in the peripheral autonomic and enteric nervous systems (Wakabayashi et al., 1988; 1993); indeed they are nearly universal at autopsy (Beach et al., 2009). An obvious question is the temporal relationship between central and peripheral nervous system involvement in the pathologic evolution of PD. Considering the connection of the olfactory bulb and dorsal vagal nucleus, via the olfactory and vagal nerves, to mucosa interfacing with the external environment, a centripetal model of progression has been proposed in which enteric nervous system pathology occurs early, and seeds the central nervous system via retrograde axonal transport ("the infection hypothesis"; Braak et al., 2003). In support of this, alpha-synuclein has been detected in colonic submucosa in early, untreated PD (median disease duration 1.5 years; Shannon et al., 2012), and even from colonic biopsies taken from "pre-symptomatic" cases, up to 8 years prior to the onset of motor symptoms (Hilton et al., 2014). The existence of two portals of entry to the central nervous system may account for the minority of cases that do not conform to the original Braak model, since pathology spreading through the olfactory tracts to the olfactory cortex in the temporal lobe is consistent with the system proposed by Beach et al. (2009).

1.5.13 Prion hypothesis

Stem cell-based neural replacement therapies have long been a desired therapeutic goal, despite considerable technical and ethical challenges, and generally disappointing clinical results (Linvall, 2013). In 2008, independent groups in the United States and Sweden reported the presence of Lewy pathology in engrafted foetal mesencephalic dopaminergic neurons at autopsy (Kordower et al., 2008; Li et al., 2008), leading the authors to speculate that alpha synuclein was transferred from diseased host to healthy graft neurons via a conformational template mechanism analogous to the propagation of misfolded proteins in prion diseases. Subsequently this theory was propounded for the endogenous spread of pathology in PD and other synucleinopathies (Olanow and Prusiner, 2009; Angot et al., 2010). *In vitro* support for this hypothesis comes from the demonstration that intracellular injection of alpha synuclein fibrils into cultured cells constitutionally overexpressing alpha synuclein "seeds" the recruitment of endogenous soluble alpha synuclein into insoluble

aggregates similar to Lewy bodies (Luk et al., 2009). Injection of recombinant alpha synuclein fibrils into the brain of transgenic mice expressing human alpha synuclein induces a widespread fulminant synucleinopathy (Luk et al., 2012a), and the same authors have shown that a less aggressive synucleinopathy radiating from an intra-striatal site of injection is seen in wild type (non-transgenic) mice, a more physiological condition (Luk et al., 2012b). A Japanese group has since replicated these findings, and also showed that insoluble alpha synuclein isolated from DLB brains induces similar pathology (Masuda-Suzukake et al, 2013).

Several strands of evidence presented above may be unified as follows. No infectious agent has been reliably implicated in the aetiology of PD, and instead a non-infectious environmental toxin or other factor, entering via the nasal and/or gut mucosa, may trigger a prion-like process leading to spread of alpha synuclein pathology in the central nervous system in a manner broadly consistent with the Braak model.

Chapter 2

Methodology

2.1 Positron Emission Tomography

Positron Emission Tomography (PET) is a sensitive imaging technique for the *in vivo* study of a variety of specific biological processes. A radioisotope (usually ^{11}C or ^{18}F) is conjugated to a chemical compound with high specific affinity for a receptor or protein of interest to produce a radiotracer, which is then injected intravenously into the subject. The use of radioisotopes with a relatively short half-life (^{11}C, 20.4 minutes; ^{18}F, 109.8 minutes) allows for the administration of an experimentally adequate quantity of radioactivity, whilst minimising the total radiation exposure to the subject. Depending on the radiotracer's molecular target, PET may be used to quantify cell surface receptor availability, metabolic reactions, or blood flow.

PET radioisotopes are usually synthesised in a particle accelerator known as a cyclotron, in which positively charged subatomic particles such protons, deuterons (consisting of two protons) or helium nuclei (two protons and two neutrons) are accelerated into a high velocity focussed beam by interacting with a rapidly alternating electrical field and a perpendicular stable magnetic field. The beam is then directed at a static target containing a stable isotope in a chemical compound to produce the short-lived positron-emitting radioisotope. An example is proton beam irradiation of stable $^{14}N_2$ gas to produce ^{11}C that is collected as $^{11}CO_2$ and then converted to $^{11}CH_3I$. For short-lived ^{11}C radiotracers, the cyclotron and PET scanner must in practice be on the same site, essentially limiting use to the research setting.

A positron is the anti-matter equivalent of an electron, discharged from the nucleus when a radioisotope decays. Within a short distance (*in vivo*, typically 1-3mm) it collides with an electron. The interaction of a pair of matter/anti-matter particles results in their annihilation, in which the total mass is converted to energy ($e=mc^2$) in the form of two high energy (gamma range) photons travelling in opposite directions. Since the mass in the reaction is constant, the energy yielded is also an invariable 511 keV per photon. These photons are then simultaneously detected at opposing points of

a circumferential ring of detectors containing photoluminescent crystals, from which can be inferred the location of the decay event, being the point on a line drawn between the two detector locations. Since the photons by definition travel at the speed of light, the latency between detection events caused by radioisotope decay within the target is in the range 4-12 nanoseconds. Detection of photon pairs within this interval is therefore considered by the scanner software to be simultaneous. The detection process itself relies on the interaction between the high-energy photons and scintillation crystals in the PET detector ring, which yields low energy photons in the visible spectrum, which are then amplified and converted to an electrical signal by a photomultiplier tube. The data is recorded by the PET computer as a two-dimensional matrix known as a sinogram, consisting of the response count for a given pair of detectors (figure 2.1).

The maximal theoretical image resolution is approximately 1.2x the width of the detection crystals assuming no positron movement. Early PET scanners had a single detector ring and were therefore capable of generating only two-dimensional images. Modern scanners, however, have multiple detector rings in a cylinder arrangement. By registering paired detection events across different rings, a three-dimensional image can be constructed. Sensitivity is also increased, since a greater proportional of annihilation events are detected.

Two types of false positives must be accounted for – random and scatter events. Random events occur when a photon unrelated to annihilation strikes the detector within the “true event” nanosecond timeframe. The random event rate can be estimated in real-time by introducing a delay into one side of the coincidence detection circuit to create a “delayed coincidence channel” (Dyson, 1960). The delay is long enough that none of the paired events in this scenario will be from genuine annihilations. Scatter events occur when a photon travelling through soft tissue strikes an orbital electron and is deflected from its original course with an accompanying loss of energy (Compton Effect). The near-simultaneous detection of a pair of photons, in which one (or both) has been deflected by Compton scattering would lead to an erroneously inferred annihilation location. These “scatter events” can be identified as photons below a certain energy threshold (eg 380 keV) and excluded from the analysis (Grootoonk et al., 1996).

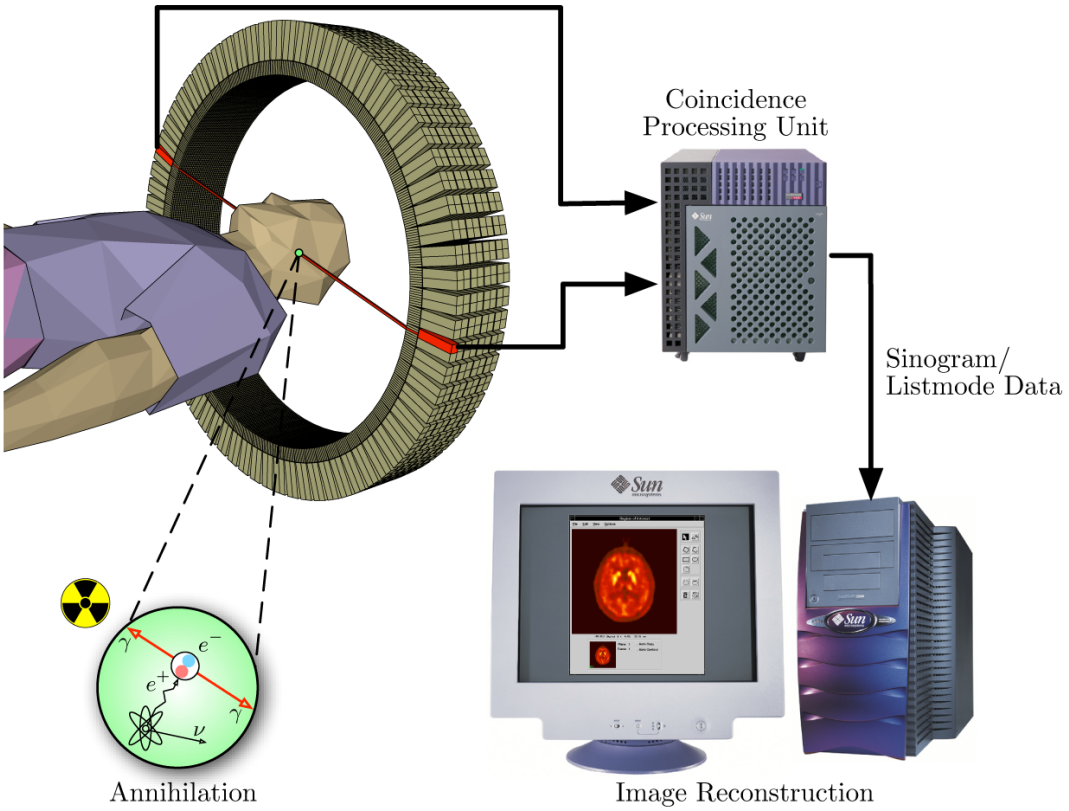


Figure 2.1. Schema of annihilation event, coincidence detection and data processing

In addition to scatter events, photons may be absorbed by soft tissue and thus fail to reach the detector. This tissue attenuation is in the range 50-95%. It can be estimated from two control scans - blank emission and transmission - typically performed before radiotracer injection. The blank emission scan is a measure of background radiation and is performed with no subject in the scanner. In the transmission scan, the subject is exposed to a rotating external positron source (^{68}Ga), which emits 511 keV photons. The tissue attenuation along all coincidence lines is derived from the ratio of blank emission and transmission data. Attenuation correction is then applied to the data, which serves to increase the signal to noise ratio and is necessary for accurate quantitative analysis.

The three-dimensional PET image is reconstructed by applying a filtered back-projection algorithm to sinograms from all lines of coincidence. Data is typically acquired either continuously (list mode) or as a series of dynamic time frames. The

first frames are short (60-90 seconds) and represent the period delivery of the radiotracer in the bloodstream from the site of intravenous injection to the target tissue. The duration of subsequent time frames progressively increases to maintain signal to noise ratio despite the inevitable reduction in radioactivity due to tracer decay. The exact time frame profile varies with the ligand employed and the requirements of the kinetic model used in subsequent analysis.

2.2 PET scanners

Two PET scanners were used in this study. Baseline scans were acquired using a Siemens ECAT EXACT HR+ (CTI/Siemens 962) scanner at IMANET, Cyclotron Building, Hammersmith Hospital, London. Follow up imaging was performed using a GE Advance scanner at the Wolfson Brain Imaging Centre (WBIC), Addenbrooke's Hospital, Cambridge. Head position was checked using a short (2 min) transmission scan, with stability of head position monitored during the scan by video observation. A longer (10 min) transmission scan was used for attenuation correction. The radiotracer was delivered by injection over 30 seconds into an intravenous cannula previously sited in the subject's forearm

2.3 Kinetic analysis

Several categories of methodology have been devised for the kinetic analysis of PET brain uptake time activity curves (TACs) that include spectral, compartmental, graphical and equilibrium models (Slifstein and Laruelle, 2001). Reference region methods to define levels of non-specific uptake can avoid the need for a measured arterial input function, but their accuracy rests on the validity of the assumptions used in the model.

Compartmental modeling predefines multiple plasma and brain compartments (figure 2.2). The radiotracer enters the venous compartment (C_V) and then the arterial plasma compartment (C_A) following intravenous injection. It then enters a free brain tissue compartment (C_F). It may then bind non-specifically to a variety of sites within the tissue compartment (collectively termed C_{NS}) or specifically with the receptor or

protein of interest, represented by C_B. The kinetics of transfer of the ligand between the compartments is defined by rate constants $k_{1\text{-}6}$. If equilibrium between free and non-specific brain compartments is rapid these can be treated as a single compartment.

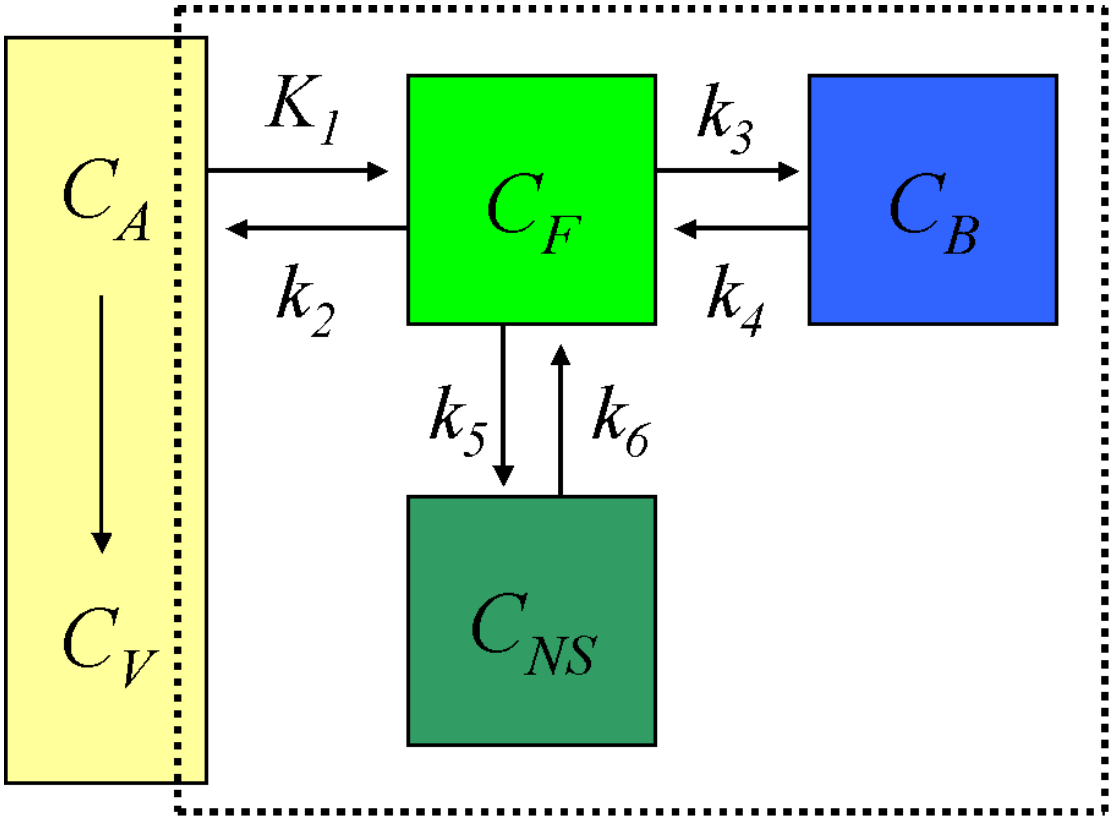


Figure 2.2. C_A and C_V are the arterial and venous vascular compartments, respectively. The tissue compartment is represented by the hatched rectangle. C_F, C_{NS} and C_B are the free ligand, non-specifically bound and specifically bound tissue compartments, respectively. $K_{1\text{-}6}$ are the rate constants for ligand transfer between the various compartments. The binding potential (BP_{ND}) is defined as k_3/k_4 in true equilibrium.

The binding potential (BP_{ND}) is given by the equation:

$BP_{ND} = k_3/k_4$

BP_{ND} is also known as the "specific to nonspecific equilibrium partition coefficient" (Innis et al., 1997). In a state of true equilibrium, C_F plus C_{NS} is defined as the non-displaceable (ND) fraction, and BP_{ND} is then the ratio of specifically bound to non-displaceable tracer in tissue at equilibrium.

2.4 Simplified Reference Tissue Model

The ideal reference region contains no specific binding sites. In the reference tissue model (RTM) as originally developed, the free, non-specifically bound, and specifically bound fractions of the target tissue, and the free and non-specifically bound fractions in the reference tissue were considered as separate compartments (Lammertsma et al., 1996).

The simplified reference tissue model (SRTM) makes two further assumptions (Lammertsma and Hume, 1996; Turkheimer et al., 2007; figures 2.3 and 2.4):

1. The volume of distribution of the non-specifically bound tracer in target and reference tissue is the same.

2. The free and non-specifically bound fractions equilibrate rapidly in both target and reference regions, allowing C_F and C_{NS} to be considered as a single compartment in both regions.

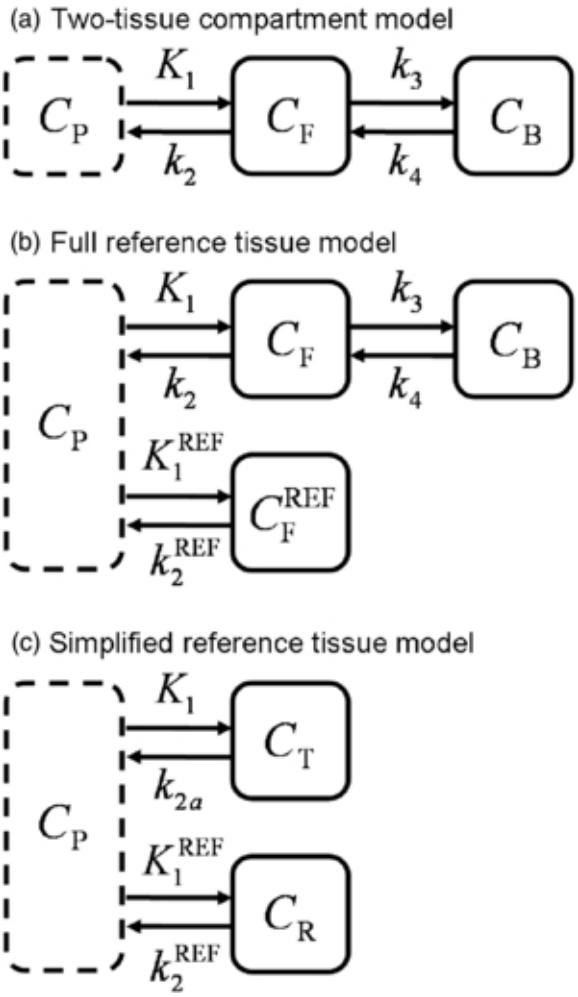


Figure 2.3. Reference tissue compartmental models

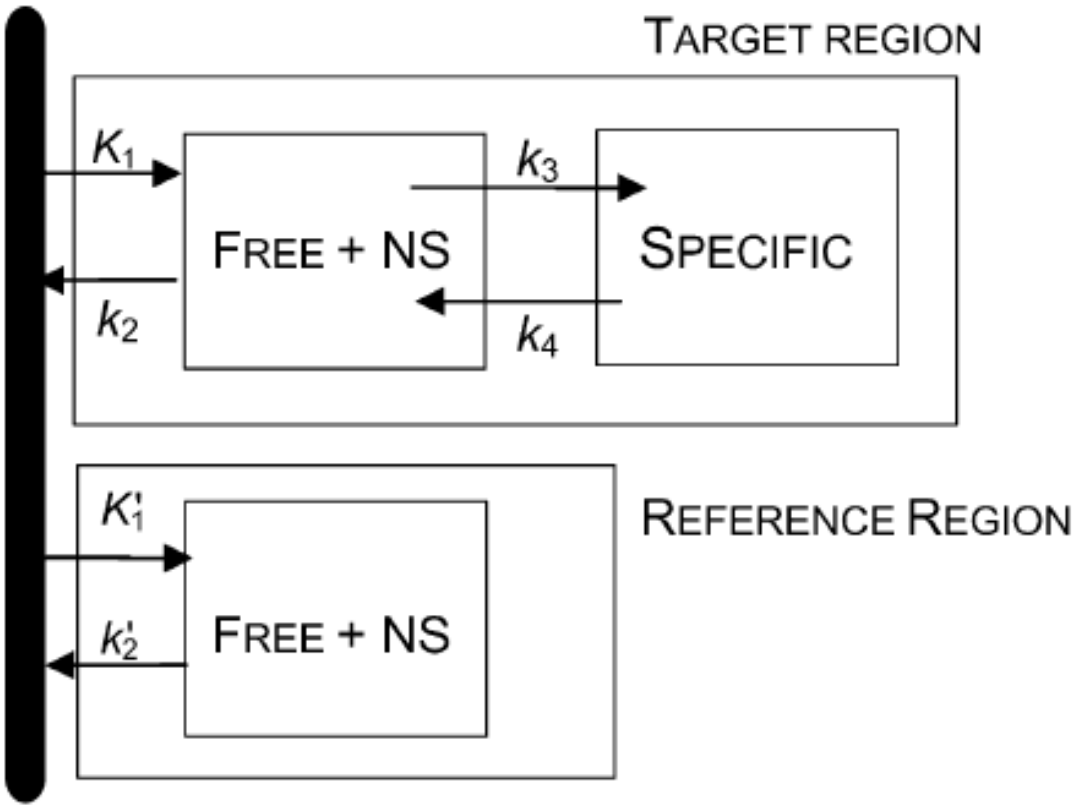


Figure 2.4. Compartment model for reference region based kinetic analyses. The ideal reference region tissue should be devoid of specific binding. The model assumes free ligand rapidly equilibrates with any non-specific (NS) binding sites, thereby allowing the free and non-specific fractions to be considered as a single compartment, which is then in equilibrium with the plasma compartment as described by rate constants k'_1 and k'_2 (Turkheimer et al., 2007). The Binding Potential (BP_{ND}) is given by k_3/k_4.

In practice only the total concentration C_T (C_F+ C_B) can be measured. In this case, the rate of change of total binding (C_T) within the target tissue is given by:

$$dC_T(t)/dt = k_1C_P(t) - k_{2a}C_T(t)$$

k_{2a} is the apparent (overall) rate constant for transfer from specific compartment (C_T) to plasma (C_P) and k_1 is the rate constant for the opposite direction.

The rate of change of total binding (C_R) within the reference tissue is then given by:

$$dC_R(t)/dt = k_1^{REF}C_P(t) - k_2^{REF}C_R(t)$$

where k_1^{REF} is the rate constant for transfer from the plasma compartment (C_P) to the reference tissue compartment (C_R), and k_2^{REF} is the rate constant for the opposite direction.

Also:

$C_T(t) = R_1C_R(t) + \{k_2 - R_1k_2/(1 + BP)\}C_R(t) * \exp\{-k_2t/(1 + BP)\}$

$R_1 = k_1/k_1^{REF}$ which accounts for any difference in the delivery of ligand to target and reference tissues.

By measuring C_T and C_R, the other three parameters, R_1, k_2 and BP can be estimated using regression analysis.

2.5 Region of interest analysis

The region of interest (ROI) approach quantitates radiotracer uptake in a priori investigator-determined defined anatomical regions. This may involve the application of a generic brain atlas, consisting of a set of anatomical regions defined in standard stereotaxic space, or the investigator may manually select an *ad hoc* region for study.

2.6 Voxel-based analysis: statistical parametric mapping

An exploratory voxel-by-voxel whole brain analysis does not rest on an *a priori* anatomical hypothesis, in contrast to the ROI approach above. The most common method employs Statistical Parametric Mapping (SPM) software (Wellcome).

SPM is based on the general linear model (GLM, Friston et al., 1995), which can be expressed as:

$Y = X\beta + \epsilon$

In this instance, Y is the observed (measured) response variable, X is a design matrix consisting of a set of explanatory variables; β is a matrix representing the response coefficients for each of the explanatory variables; and ϵ represents the error or "noise". An important assumption is that the error field behaves as random field with

a multivariate Gaussian (normal) distribution, ie "noise". All statistical tests performed in SPM, whether t-tests, simple regression (correlation) or multiple regression can be described by the GLM.

For example, consider multiple linear regression with two known explanatory variables, x and y:

$$Y = \beta_0 + \beta_1 x + \beta_2 y + \epsilon$$

Here, β_0 is the y-intercept, and β_1 and β_2 are the response coefficients of the known variables, x and y, respectively.

The chosen statistical test is applied to all voxels, the result of which can be expressed as an image, known as a statistical parametric map (SPM). The values for each voxel in an SPM express the extent to which that voxel deviates from a known probability function if the null hypothesis is true, usually the Student's t-distribution, expressed as a t-statistic for each voxel, SPM(t), with the overall SPM then known as a T-map. Since the t-statistic is dependent on the degrees of freedom, direct comparison of T-maps would not be valid if there was a disparity in the degrees of freedom (e.g. different sample sizes). For this reason, SPM(t) is transformed to a Z score, SPM(Z), which follows a Gaussian distribution and is not affected by degrees of freedom.

A further issue relates to the statistical problem of multiple comparisons. If an analysis of all voxels in an image is performed, and each voxel is considered a discrete statistical test, the most conservative correction for multiple comparisons would be the Bonferroni method. Each voxel is not fully discrete, however, being spatially and functionally related to its neighbours. A less severe (and therefore more sensitive) method for correcting for multiple comparisons in SPM employs random field theory (RFT). Here correction for statistical significance is applied at the level of voxel clusters, which are the phenomena of physiological interest, rather than at the level of individual voxels.

2.7 Imaging activated microglia with [^{11}C]-PK11195 PET

When activated, microglia express translocator protein (TSPO), previously known as the peripheral benzodiazepine receptor, on the outer surface of their mitochondria.

TSPO can be detected *in vivo* using [^{11}C]-PK11195, an isoquinoline that binds to this protein (Banati et al., 1997). PK thereby allows the detection and quantification of the earliest cellular component of neuroinflammation. Ouchi et al. (2005) studied 10 early onset drug naïve PD subjects and 10 age matched controls with [^{11}C]-PK11195 PET and the dopamine transporter marker [^{11}C]-CFT PET, a measure of dopamine transporter (DAT) availability. They reported elevated PK in the midbrain contralateral to the symptomatic side, which correlated with clinical disability and inversely with putamen DAT binding. Gerhard et al. (2006) studied 18 PD subjects with [^{11}C]-PK11195 and [^{18}F]-DOPA PET (another measure of dopamine terminal function) compared to 11 controls. PD subjects had increased [^{11}C]-PK11195 binding in the fronto-temporal cortices, pons and striatum, but not consistently in the midbrain. Nigral PK binding in their study did not correlate with either clinical severity or levels of striatal [^{18}F]-dopa uptake.

Selection of a reference tissue region for [^{11}C]-PK11195 that is devoid of specific binding is problematic, since TSPO is expressed on a number of cell types in addition to activated microglia, including perivascular macrophages, neutrophils and lymphocytes, as well as myocytes of leptomeningeal and parenchymal arteries, meninges, and ependyma (Banati, 2002). To address this, Turkheimer et al. (2007) developed a supervised clustering algorithm using six pre-defined kinetic classes: specific pathological (microglial) TSPO binding, nonspecific grey matter, nonspecific white matter, blood pool, skull, and muscle (referred to here as SVCA6). The kinetics of specific pathological TSPO binding were derived empirically from [^{11}C]-PK11195 PET scans of 3 symptomatic, genetically-confirmed Huntington's disease subjects, with striatum and globus pallidus as regions of interest (ROI), sites known to be associated with intense microglial activation in this disease (Sapp et al., 2001). The other kinetic classes were derived from ROIs drawn over grey matter, white matter, venous sinus, sternocleidomastoid muscle and skull, respectively, in 12 control subjects. The supervised clustering algorithm uses a regression operation to derive the relative contribution to a voxel from each kinetic class. By applying the time activity curve (TAC) therein derived for specific pathological TSPO binding to a subject's dynamic PET image, a parametric BP_{ND} image may be produced. The method has been validated against the "gold standard" plasma input function derived BP_{ND} model (Turkheimer et al., 2007).

In collaboration with Boellaard‘s group in Amsterdam, Turkheimer further rationalised the supervised clustering algorithm by applying an inclusive whole brain mask to the analysis, allowing the bone and muscle clusters to be discarded, thus deriving a four-cluster method (SVCA4). This was superior in discriminating Alzheimer’s subjects from controls compared to SVCA6 (Yaqub et al., 2012).

2.7.1 Radiopharmaceutical preparation

[^{11}C]-PK11195 PET was synthesised on-site by Hammersmith IMANET for baseline scans, and by the Wolfson Brain Imaging Centre, Cambridge for follow up imaging.

2.7.2 Scanning protocol

A short (2 minute) transmission scan was performed to check head position, and a longer (10 minute) transmission scan for attenuation correction. After bolus injection of 370 MBq of [^{11}C]-(R)-PK11195, a 3D dynamic emission scan was acquired over 18 frames (30s background frame, 1x 15s; 1x 5s; 1x 10s; 1x 30s; 4x 60s; 7x 300s; 2x 600s). Frame reconstruction and correction for scatter, randoms and attenuation were performed using proprietary software supplied with the camera.

2.7.3 Image processing

The subject’s volumetric T1 weighted MRI image was segmented into grey matter, white matter, and CSF compartments using the probabilistic function native to the SPM software. A binary grey matter image was also derived using a 50% probabilistic threshold. All frames (1-18) of the dynamic PET image were summed using in-house software to produce an “ADD image”, which has higher spatial resolution than the dynamic image. This was then used as an anatomical template for the co-registration and subsequent three-dimensional transformation (“re-slicing”) of the whole MRI, grey matter, and white matter images into PET space, performed in SPM8.

2.7.4 Supervised clustering algorithm

The SVCA4 algorithm first normalises the dynamic PET image by subtracting from each frame its mean and dividing it by the standard deviation. The algorithm then models the kinetic of each voxel of the normalised dynamic image, using a regression procedure to derive the scaling coefficient of each of the 4 pre-specified kinetic classes, which are then recorded in coefficient maps displaying their spatial distribution. The reference tissue time activity curve (TAC) is then extracted by applying the coefficient map from the normal grey matter kinetic class to the (non-normalised) dynamic image (Turkheimer et al., 2007; Yaqub et al., 2012).

2.7.5 Generation of parametric images

The extracted reference TAC is then applied to the dynamic image using the basis function approach of SRTM (Gunn et al., 1997), a function supplied with the SVCA4 software, to produce the BP_{ND} image.

2.7.6 Spatial normalisation

A three-dimensional transformation of the BP_{ND} image is then performed in SPM8, using a standard T1 template to bring the PET image into Montreal Neurological Institute (MNI) space. A standard atlas (derived in MNI space) can then be applied to the normalised BP_{ND} image for ROI analysis, and within-group and between-group phenomena can be investigated with voxel-based SPM.

2.7.7 Region of interest approach

A standard probabilistic object map in MNI space was convolved with the subject's binary grey matter image in Analyze 11.0 (Mayo clinic) to derive an ROI atlas for that subject (Hammers et al., 2003). The atlas was then overlaid on the BP_{ND} image and mean BP_{ND} values for each region of the atlas were systemically sampled in Analyze.

2.7.8 Statistical parametric mapping

Spatially normalised images were smoothed with a 6mm FHWM kernel in SPM8. Smoothing reduces the effect of structural variation between subjects, and increases the signal-to-noise ratio, at the expense of some loss of spatial resolution, an effect that increases with the width of the smoothing kernel. The use of coarser smoothing (8mm FHWM or higher) is often used in PET SPM, but was avoided in this study to retain anatomical detail. Smoothed normalised images are then entered into the SPM design matrix allowing between-group or within-group phenomena to be examined at the voxel level.

2.8 Imaging amyloid with [^{11}C]-PIB PET

The PET radiotracer [^{11}C]-PIB (N-methyl-$^{11}C_2$-(40-methylaminophenyl)-6-hydroxybenzothiazole) binds with nanomolar affinity to fibrillar beta amyloid and has been used extensively in the study of Alzheimer's disease (Klunk et al., 2004). Recently, several groups have used PIB to examine amyloid deposition *in vivo* in dementia with Lewy bodies (DLB), PD with dementia (PDD), and PD without dementia (Brooks, 2009). Edison et al. (2008) reported levels of PIB uptake in the AD range in the majority of cases (10/12) of dementia with Lewy bodies (DLB). Only 2/12 PDD subjects, however, were reported to have elevated PIB to the same degree. Similarly, Maetzler et al. (2008) reported PIB retention in the AD range in a minority of PDD cases (2/10). Gomperts et al. (2008) found AD range PIB levels in 7/8 DLB, 2/7 PDD, but also in 2/11 non-demented PD and 10/37 controls. Their analysis used a Logan graphical approach, however, rather than the standard cerebellar ratio method used in the other studies. Burack et al., (2010) examined autopsy data from 3 PDD subjects in whom PIB imaging had been undertaken within 15 months of death. 2/3 had elevated PIB binding, which was explained pathologically by diffuse, rather than the neuritic, plaques of amyloid characteristic of Alzheimer's disease.

The selection of a non-specific reference region for [^{11}C]-PIB PET is more straightforward than for [^{11}C]-PK11195. The cerebellum is devoid of fibrillar amyloid in control and AD subjects, and has consequently become the standard reference

tissue region in [^{11}C]-PIB studies (Price et al., 2005; Lopresti et al., 2005). A standardised index of [^{11}C]-PIB uptake is obtained by dividing voxel uptake throughout the PET image by the mean cerebellar [^{11}C]-PIB uptake value. This is ratio uptake image is usually generated using 40-60 min or 60-90 min time frames, where [^{11}C]-PIB signal is highest.

2.8.1 Radiopharmaceutical preparation

[^{11}C]-PIB was synthesised on-site by Hammersmith Imanet, GE Healthcare, at the Cyclotron Building, Hammersmith Hospital for baseline scans, and by the Wolfson Brain Imaging Centre, Cambridge for follow up imaging.

2.8.2 Scanning protocol

Head position was confirmed with a short (2 minute) transmission scan, with a longer (10 minute) transmission scan performed for attenuation correction. After bolus injection of 370 MBq of [^{11}C]-PIB, a three dimensional dynamic emission scan was acquired as 32 frames over 90 minutes according to a predetermined protocol (1x 15s, 1x 5s, 1x 10s, 2x 30s, 9x 60s, 3x 180s, 14x 300s). Frame reconstruction and correction for scatter, randoms and attenuation were performed using proprietary software.

2.8.3 Image processing

SPM8 was used to segment the volumetric T1 weighted MRI into grey matter, white matter, and CSF compartments, and to create a binary grey matter image with a 50% probability threshold. A “late ADD image”, representing the last 30 minutes of the dynamic emission scan (frames 27-32) was derived using in-house software.

2.8.4 Spatial normalisation

The T1 whole MRI, binary grey matter and late ADD images were normalised into Montréal Neurological Institute (MNI) space in SPM8 using a standard T1 template. A standard object map was convolved with the binary grey matter image in Analyze 11.0 (Mayo clinic) to define and sample ROIs.

2.8.5 Cerebellar ratio method

The normalised late ADD image was then divided by the sampled mean uptake value for the cerebellum using Analyze 11.0, to produce a target region to cerebellar ratio (RATIO) image.

2.8.6 Region of interest approach

A standard object map was convolved with the normalised binary grey matter image in Analyze 11.0 to define ROIs which were then used to sample activity in the normalised RATIO image to generate mean relative uptake values for each region were systemically sampled.

2.8.7 Statistical parametric mapping

Spatially normalised RATIO images were smoothed with a 6mm FHWM kernel in SPM8. These images are then entered into the SPM design matrix, allowing voxel-by-voxel analysis of between-group or within-group effects.

2.9 Imaging cerebral glucose metabolism with [^{18}F]-FDG PET

[^{18}F]-FDG is synthesised from the D-isomer of glucose by substitution of a radioactive Flourine-18 atom for the hydroxyl group at the 2nd carbon position (figure 2.5). The brain derives most of its metabolic energy from glucose, which is taken up directly into neurons from the extracellular fluid. The glucose rate of uptake is proportional to metabolic activity, which is in turn a proxy for electrical activity.

Once inside the neuron, glucose is converted to glucose-6-phosphate by hexokinase, the first step in glycolysis (figure 2.6).



Figure 2.5. [^{18}F]-FDG is derived from D-Glucose by substitution of ^{18}F for the carbon-2 hydroxyl (OH) group.

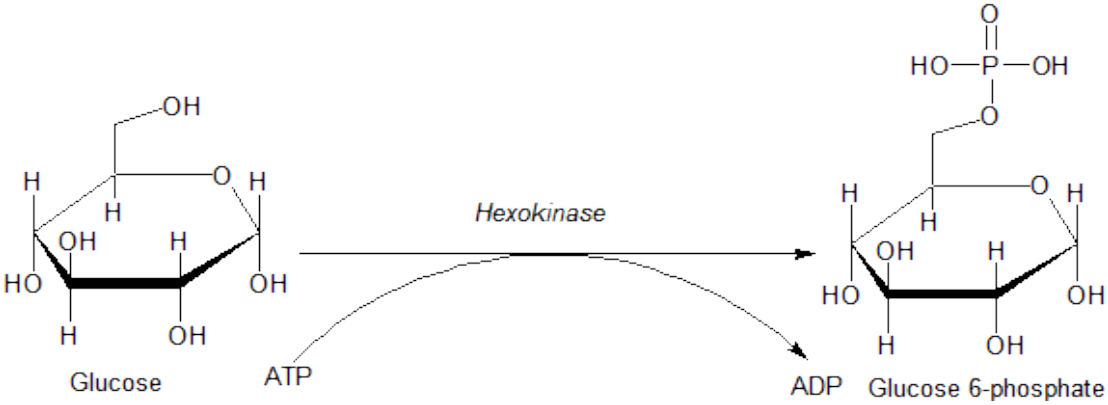


Figure 2.6. In the first step of glycolysis, hexokinase coverts glucose to glucose-6-phosphate

Hexokinase also performs the same reaction on [^{18}F]-FDG to produce [^{18}F]-FDG-6-phosphate, but the next enzyme in the glycolytic pathway, glucose-6-phosphate isomerase, is unable to open the glucose ring in [^{18}F]-FDG-6-phosphate due to the loss of the carbon-2 hydroxyl group. The phosphorylated molecule is only slowly dephosphorylated and so is effectively trapped while the ^{18}F atom decays (half-life 110 minutes) with the emission of a positron, accompanied by the conversion of a nuclear proton to a neutron, to produce $^{18}O^{-}$. The latter rapidly binds covalently with a free proton produce a hydroxyl group, to form glucose-6-phosphate, which is then metabolised normally by glucose-6-phosphate isomerase. FDG PET, therefore, is a marker of hexokinase activity that in turn reflects glycolytic activity in the brain.

2.9.1 Spectral analysis

Spectral analysis models the relationship between the target tissue time-activity function and the plasma input time-activity function by resolving the kinetics governing this relationship into a spectrum of kinetic components which best fit the observed data (Cunningham and Jones, 1993). The target tissue's unit impulse response function can then be derived form the sum of the kinetic components and, when integrated, it provides a volume of distribution. Unlike the SRTM, the technique does not make any *a priori* assumptions about the number of compartments in the kinetic model. The use of a plasma input function allows the absolute quantification of the rate of regional [^{18}F]-FDG uptake, which in turn can provide a measure of rCMRGlu (regional cerebral metabolic rate of glucose) if its uptake is corrected for differences in brain transport and phosphorylation rates between glucose and FDG by multiplying the influx constant by a lump constant. This modelling approach contrasts to the methods described previously for [^{11}C]-PK11195 and [^{11}C]-PIB, which express target tissue binding relative to a specified reference region.

2.9.2 Scanning protocol

Subjects fasted for at least 4 hours prior to scanning. 185 MBq [^{18}F]-FDG was administered by bolus injection over 30 seconds. A dynamic emission scan was acquired as 28 time frames over 60 minutes according to a predefined protocol (1x 30s background frame, 1x 15s, 1x 5s, 4x 10s, 4x 30s, 4x 60s, 4x 120s, 9x 300s). Intra-arterial blood sampling via a radial artery cannula was performed at baseline, 5, 10, 15, 20, 30, 40, 50, and 60 minutes). Image reconstruction and correction were performed using Siemens software.

2.9.3 Image processing

A late ADD image representing frames 24-28 was created for use as a template in subsequent co-registration using in-house software. Parametric images were generated using spectral analysis in RPM (Gunn et al., 1997). The volumetric T1 MRI was

segmented into grey matter, white matter, and CSF compartments, and a binary grey matter image with a 50% probability threshold was created in SPM8.

2.9.4 Spatial normalisation

The T1 whole MRI, binary grey matter, CMRGlu parametric and ADD images were co-registered and normalised into Montreal Neurological Institute (MNI) space in SPM8 using a standard T1 template. A standard object map was convolved with the binary grey matter image in Analyze 11.0 (Mayo clinic) to define ROIs.

2.9.5 Region of interest approach

A standard object map was convolved with the normalised binary grey matter image in Analyze 11.0 to define ROIs which then used to sample activity in the normalised CMRGlu image as described above (paragraph 2.7.7).

Chapter 3

Activated microglia in Parkinson's disease

3.1 Objectives

1. To image in vivo activated microglia in the brains of subjects with Parkinson's disease using [^{11}C]-(R)-PK11195 PET.
2. To correlate levels of local microglial activation with objective measures of clinical status in motor, cognitive and other non-motor domains, using region of interest and voxel-based analyses.
3. To correlate levels of regional microglial activation and tissue metabolism, assessed with [^{11}C]-(R)-PK11195 and [^{18}F]-FDG respectively.

3.2 Summary

Local levels of microglial activation, imaged using [^{11}C]-(R)-PK11195 PET, correlate with multiple motor and cognitive deficits and other non-motor clinical symptoms in a group of non-demented PD subjects with a broad range of disease duration, suggesting that neuroinflammation is relevant to the clinical phenotypic expression, from early disease onwards. Subjects with a greater burden of microglial associated cortical inflammation may be at higher risk of PD dementia. These data from living PD subjects suggest that most early clinical cases are advanced on the Braak model for pathologic staging based on post mortem data. The presence of activated microglia on PET imaging appears to be a valid biomarker of disease activity.

3.3 Introduction

3.3.1 Neuroinflammation and microglia

Evidence is accumulating for an inflammatory component manifesting as microglial activation to a variety of neurodegenerative diseases including PD, dementia with Lewy bodies (DLB), Alzheimer's disease (AD), amyotrophic lateral sclerosis, progressive supranuclear palsy (PSP) and other tauopathies (McGeer and McGeer, 2004; Mrak and Griffin, 2007). Epidemiological data provides support for an inflammatory contribution to the aetiology and pathogenesis of PD. In a genome-wide association study, late onset sporadic PD was associated with a polymorphism in a non-coding region of the Human Leukocyte Antigen (HLA) locus involved in the regulation of HLA-DR expression, a surface antigen expressed by microglia (Hamza et al., 2010). Raised plasma IL-6, a component of the systemic inflammatory response, was reported to be associated with elevated risk of PD (Chen et al., 2008). Subjects receiving certain non-steroid anti-inflammatory drugs (NSAIDs) appear to have a lower risk of developing PD (see paragraph x.x). Cyclo-oxygenase (COX), the enzymatic target of NSAIDs, is upregulated in dopaminergic neurons of post mortem PD subjects and in animals previously exposed to the nigral toxin MPTP. In the latter pharmacological inhibition of COX is neuroprotective (Knott et al., 2000; Teismann et al., 2003). These observations have led to the proposal that neuroinflammation could be a therapeutic target in PD (Qian et al., 2010).

Microglia are of monocyte lineage and are the intrinsic macrophages of the central nervous system. They are widely distributed throughout the brain, normally existing in a quiescent state with neither secretory activity nor cell-cell contact. Their spidery processes probably act to monitor the local brain milieu. They become activated, however, by any change injurious to the brain and represent the earliest stages of the neuroinflammatory response (Kreutzberg, 1996). Microglia exhibit polarized activation states: a "classical" proinflammatory phenotype (M1) involved in the response to pathogens; and an "alternative" anti-inflammatory phenotype (M2) concerned with adaptation to inflammation and repair, although interconversion between these extreme phenotypes and mixed states are now thought to occur (Shechter and Schwartz, 2013). From 1996 to 2013, the annual number of scientific papers on the subject of microglia and Parkinson's disease increased progressively from 10 to 131. Whilst most experimental data support a deleterious role for microglia in PD, a neuroprotective effect has also been demonstrated under certain experimental conditions and it has been suggested that the balance of these opposing

actions is critical *in vivo*, perhaps varying with disease stage (Li et al., 2007; Sanchez-Guajardo et al., 2010).

Monkeys and humans exposed acutely to the toxin MPTP exposure may show activated microglia in their substantia nigra many years later (Langston et al., 1999; McGreer et al., 2003; Barcia et al., 2013). In PD patients at post-mortem activated microglia are found in the substantia nigra and striatum (McGeer et al., 1988) and throughout limbic and cortical association areas where they maintain a cytokine secreting pro-inflammatory phenotype into end-stage disease (Imamura et al., 2003). Persistently activated microglia could potentially drive neurodegeneration in animal models and human PD through a variety of effector mechanisms, including cytokine production (Imamura et al., 2003; Theodore et al., 2008), phagocytosis (Kohutnicka et al., 1998; Barcia et al., 2013), and release of nitric oxide (Knott et al., 2000; Gao et al., 2008) and reactive oxygen species (Liberatore et al., 1999; Block et al., 2007). Alpha synuclein is secreted from rat cortical neurons by exocytosis in both soluble and aggregated forms when these cells have been transfected with human α-syn genes (Lee et al., 2005). Secretion of A53T mutated α-syn by transgenic mouse neurons has been demonstrated, and α-syn can be detected in brain parenchymal interstitial fluid from both transgenic mice and humans at necropsy (Emmanouilidou et al., 2011). Exogenous α-syn, whether in an aggregated or soluble state, is internalized by microglia, which then become activated and secrete pro-inflammatory cytokines associated with subsequent dopaminergic neurodegeneration in co-culture assays (Zhang et al., 2005; Alvarez-Erviti et al., 2011).

Microglial activation precedes neurodegeneration in animal models of PD suggesting that microglia are not merely phagocytic scavengers recruited to clear cellular debris. In rotenone and 6-hydroxydopamine toxin models of PD, activated microglia are detected hours after the initial insult, well before any neural loss (Sherer et al., 2003; Rodriguez-Pallares et al., 2007*)*; in transgenic mice expressing human α-syn, microglial activation also precedes neural death (Su et al*.,* 2009*)*. Activated microglia secrete a range of pro-inflammatory cytokines including tumour necrosis factor alpha (TNFα), interleukin 1-beta (IL-1β), IL-6 and nuclear factor kappa B (Suzumura et al., 1996; Hartlage-Rübsamen et al., 1999). Lipopolysaccaride induced dopamine

degeneration is associated with IL-1β production, and blockade of the cytokine prevented neural death (Arai et al., 2004). Inhibition of TNF-α has reduced dopaminergic neuron loss in multiple rodent and *in vitro* models of PD (McCoy et al., 2006).

Leucine-rich repeat kinase-2 (LRRK2) mutations cause dominantly inherited PD (see Chapter 1, paragraph 1.3.1), and the protein is implicated in the pathogenesis of sporadic PD, although its normal and patholoigcal functions are still unclear. Recently, LRRK2 was implicated in monocyte and macrophage maturation (Thévenet et al., 2011). Marked expression of LRRK2 in microglia was reported in a rodent model of neuroinflammation, whilst inhibition of LRRK2 in cultured microglia blocked TNFα secretion, iNOS induction, and microglial process outgrowth and chemotaxis (Moehle et al., 2012). Murine microglia overexpressing the PD-linked LRRK2 (R1441G) mutation demonstrated greater proinflammatory cytokine secretion compared to wild type microglia, and conditioned medium from the transgenic microglia induced death of cultured neurons (Gillardon et al., 2012). Microglial activation *in vivo* may occur predominantly through Toll-like receptor (TLR) signaling (Lehnardt, 2010). It was recently shown that microglia preconditioned with α-syn exhibit an augmented proinflammatory cytokine response to TLR stimulation (Roodveldt et al., 2013).

Pharmacological blockade of microglial activation protects against neuronal loss in the MPTP rodent model (Wu et al., 2002*).* In mice constitutionally overexpressing human a-syn, microglial inhibition also prolongs neuron survival (Gu et al., 2010). In the rotenone model, dopaminergic neurodegeneration can be prevented by blockade of microglial phagocytosis (Emmrich et al., 2013). The protective effect of the cytokine TGFβ against dopaminergic neural death induced by reactive oxygen species is mediated by microglial inhibition (Qian et al., 2008). Silencing of inducible nitric oxide synthetase (iNOS) expression by RNA interference attenuates neural loss induced by 6-hydroxydopamine (Li et al., 2012). Overall, the evidence supports a model in which microglia become activated after taking up oligomeric α-syn released by neurons, resulting in cytokine release and neural injury.

3.3.2 Imaging activated microglia using [^{11}C]-(R)-PK11195 PET

Activated microglia express translocator protein (TSPO) in their outer mitochondrial membranes (Banati, 2002). TSPO was formerly called the peripheral benzodiazepine receptor, although it has no classical receptor properties;. it is a steroid and anion transporter and regulates membrane potential but may also be involved in controlling cytokine production (Choi et al., 2002). PK11195 has been shown in animal models to bind selectively to an isoquinoline site on TSPO (Banati et al., 1997). Radiolabelled [^{11}C]-(R)-PK11195 PET can, therefore, be used to visualize activated microglia via their TSPO expression in living human subjects (Pike et al., 1993; Banati et al., 1999; 2000).

3.3.3 *[^{11}C]-(R)-PK11195 PET studies in Parkinson's disease*

There have been five [^{11}C]-(R)-PK11195 PET studies on PD subjects published to date: Ouchi et al. (2005) scanned 10 subjects with early drug naïve PD with [^{11}C]-PK11195 and [^{11}C]-CFT (a dopamine transporter marker) PET and compared findings with those for 10 healthy controls. Using a region of interest approach, they found significantly elevated [^{11}C]-(R)-PK11195 in the midbrain contralateral to the more clinically affected side in PD subjects compared to controls. Within the PD group, they reported a positive correlation between midbrain [^{11}C]-(R)-PK11195 BP_{ND} and clinical motor severity (assessed using the Unified Parkinson's disease rating scale, UPDRS) and an inverse relationship between midbrain PK and putamen [^{11}C]-CFT binding. To date, this is the only PET study in PD to report such an association between levels of midbrain microglial activation and clinical phenotype.

Our group reported elevated [^{11}C]-(R)-PK11195 BP_{ND} in the pons, basal ganglia, frontal and temporal cortices in 18 non-demented PD subjects compared to 11 controls (Gerhard et al., 2006a). No correlation was found between [^{11}C]-(R)-PK11195 BP_{ND} in any region of interest and clinical disability (assessed using the UPDRS, Mini Mental State Examination, and the Frontal Assessment Battery). There was no significant change in [^{11}C]-(R)-PK11195 BP_{ND} in the 8 subjects where repeat

scanning was performed a mean interval of 22.9 months later. More recently, our unit reported elevated [^{11}C]-(R)-PK11195 binding in the temporal and occipital cortex of non-demented PD and more extensive cortical microglial activation in subjects with PD dementia (Edison et al., 2013). An inverse correlation between cortical [^{11}C]-(R)-PK11195 binding and MMSE scores was detected using voxel-wise statistical parametric mapping.

In a study of 14 PD subjects and 8 controls, Bartels et al. (2010) reported a non-significant trend towards elevated PK in PD putamen and substantia nigra. [^{11}C]-(R)-PK11195 BP_{ND} did not change significantly after a relatively brief (one month) course of the COX2 inhibitor, celecoxib. In contrast, Iannaccone et al. (2013) found significantly elevated [^{11}C]-PK11195 in the substantia nigra and putamen in PD and DLB subjects compared to controls and the DLB subjects also had raised neocortical [^{11}C]-(R)-PK11195 uptake.

3.3.4 Novel TSPO radiotracers

[^{11}C]-PK11195 has several limitations: in addition to the selection of a suitable reference region (see Chapter 2, paragraph 2.7), the tracer has high non-specific binding and a low signal to noise ratio (Chauveau et al., 2008). This has led to the development of "second generation" TSPO ligands, including [^{11}C]-PBR28 (Fujita et al., 2008); [^{11}C]-DAA1106 (Ikoma et al., 2007); [^{11}C]-PBR111 (Fookes et al., 2008); and [^{18}F]-FEPPA (Wilson et al., 2008). Of these, increased microglial infiltration in AD has been demonstrated using [^{11}C]-DAA1106 (Yasuno et al., 2008) and [^{11}C]-PBR28 (Kreisi et al., 2013), but there are no published studies in PD. In addition, there are pharmacokinetic issues affecting novel TSPO ligands. 14-23% of healthy control subjects exhibit no detectable TSPO binding in either brain or periphery using [^{11}C]-PRB28 PET (Fujita et al., 2008; Owen et al., 2010). This has been attributed to the existence of a very low TSPO binding affinity for PBR28 in these cases. Moreover, of those with detectable [^{11}C]-PRB28 binding, intermediate and high binding affinity states were resolved, further complicating kinetic analysis (Owen et al., 2010). Subsequently, all novel TSPO ligands have been shown to bind to three affinity states *in vitro* (Owen et al., 2011). By contrast, PK11195 binds TSPO in all

subjects with a single binding affinity (Doble et al., 1987; Rao and Butterworth, 1998; Owen et al., 2011).

3.4 Subjects and methods

3.4.1 Ethics and safety

Ethical approval for this study was obtained from Hammersmith Hospitals Trust Ethics Committee (REC 08/H07711/135). The radiation exposure was justified by Professor Myers of Imperial College London, and by the Ethics committee. Permission to use the relevant radiotracers in human subjects was obtained from the Administration of Radioactive Substances Advisory Committee (ARSAC), as required by law. The candidate obtained the necessary IRMER radiation protection training and certification from Imperial College London, also a legal requirement.

3.4.2 Funding

This project was financed by grants from Parkinson's UK and the Medical Research Council.

3.4.3 Source of subjects

Subjects were recruited from two sources:

1. General neurology/movement disorder clinics at Imperial College London NHS Trust (Prof D. Brooks, Dr P. Bain, Dr S. Molloy).
2. The Cambridge Centre for Brain Repair, where a countywide study of incident PD (CamPaIGN) began in 2004.

3.4.4 Inclusion criteria

1. Age 35-79 years at enrolment
2. Clinical diagnosis of PD by Queen Square Brain Bank Criteria (Hughes et al., 1992)
3. Capacity to give informed consent
4. Able to complete neuropsychological assessment

3.4.5 Exclusion criteria

1. Extensive microvascular disease on MRI disproportionate for age
2. Pregnant or breast feeding
3. Current or recent (within 5 years) alcohol or drug dependency
4. Other illness causing inability to undergo neuropsychological testing or scanning

3.4.6 Sub-groups

PD subjects were classified into two groups by clinical criteria:

Low Risk (PDND-Lo)

High Risk (PDND-Hi)

3.4.7 Subgroup inclusion criteria

Subjects were classified at higher risk of developing PD dementia (PDND-Hi) in the presence of two or more of the following:

1. Age ≥ 70 years
2. Postural Instability Gait Disorder (PIGD) phenotype (see below)
3. Unified Parkinson's Disease Rating Scale (UPDRS) part 3 score ≥33 (revised MDS-UPDRS 2008 version)
4. Semantic fluency deficiency (<20 animals spontaneously named in 90s)
5. Constructional apraxia (inability to copy intersecting pentagons figure)
6. History of visual hallucinations

3.4.8 Determination of motor phenotype

The original literature method (Jankovic *et al*., 1990) derived a Tremor Score (TS) from the sum of the scores for the tremor specific questions from the 1987 version of the Unified Parkinson's Disease Rating Scale (UPDRS), divided by the number of such questions (nine). The Postural Instability Gait Disorder (PIGD) score was similarly obtained from the sum of the UPDRS questions pertinent to that domain divided by the number of those questions (five). The TS/PIGD index was then calculated by dividing the TS by the PIGD score. Motor phenotype was then assigned according to:

Tremor Dominant (TD) phenotype: TS/PIGD ≥ 1.5
PIGD phenotype: TS/PIGD ≤ 1.0
Intermediate phenotype: 1.0 < TS/PIGD < 1.5

In the present study, a modified TS/PIGD method was derived using sections from the updated and expanded 2008 MDS-UPDRS, but which preserves the original arithmetic weighting:

Tremor Score (9 domains):

Tremor history (2 - left & right)
Postural/kinetic tremor of hands (2)
Rest tremor amplitude (5 domains – head, all four limbs)
TS = total / 9

PIGD Score (5 domains):

Walking & balance (history)
Freezing (history)
Gait (examination)
Freezing (examination)
Postural instability (examination)
PIGD Score = Total / 5

TS/PIGD Index = TS / PIGD score

3.4.9 Subjects

21 PD subjects fulfilling a diagnosis of PD using Queen Square Brain Bank criteria (Hughes et al., 1992) were recruited. None had PD dementia according to consensus criteria (Emre et al., 2007). The spouses of 8 of the PD subjects were recruited as healthy controls. 2 PD subjects withdrew from the study after baseline scanning and clinical assessment; 19 completed follow up imaging and clinical testing. Due to the potential for systematic bias as a result of differences between the PET scanners at Hammersmith and Cambridge, 6 control [^{11}C]-PK11195 scans with paired MRI were obtained from the local WBIC archive for analysis with the follow up PD dataset.

3.4.10 Clinical assessment

A full clinical history and examination were obtained for each subject. Additionally, the formal assessment tools below were utilised:

Unified Parkinson's Disease Rating Scale (UPDRS) Parts 2 and 3. Part 2 assesses activities of daily living in 13 domains with severity scores 0-4 for each. Part 3 documents the physical examination of the motor system in 18 sections, each with severity scores 0-4.

Montréal Cognitive Assessment (MoCA). A global cognitive screening tool with greater sensitivity to cognitive change in early PD than the MMSE, in part due to its assessment of frontal executive function.

Addenbrooke's Cognitive Examination-Revised. The ACE-R incorporates and expands upon the MMSE. In addition to the total score for global cognition, a sub-score for 5 cognitive domains may be derived, for orientation, memory, fluency, language, and visuospatial function.

Letter & semantic fluency from the Frontal Assessment Battery. Fluency is particularly disturbed in frontal and temporal lobe disease.

Epworth Sleepiness Scale. The ESS is a self reported assessment of daytime somnolence.

Geriatric Depression Scale. The GDS-15 is a self-reported assessment of depressive symptoms.

PDQ-39. The 39 item Parkinson's disease quality of life questionnaire allows the derivation of sub-scores for impairment in activities of daily living, mobility, cognition, communication, social functioning, stigmatisation, emotional wellbeing and bodily discomfort, in addition to a total score for overall impaired quality of life.

Non-motor symptom score. The NMSS is self-reported assessment of overall non-motor symptom burden.

3.4.11 Scans

Baseline PET scanning was performed at the Cyclotron Building, Hammersmith Hospital, Hammersmith Imanet, GE Healthcare, London, UK, using an ECAT EXACT HR+ (CTI/Siemens 962) camera. Follow up scanning occurred at the Wolfson Brain Imaging Centre, Cambridge, UK using a GE Advance scanner (General Electric Medical Systems). The scanning protocol for baseline and follow up scans was identical, and involved 3D acquisition over 60 minutes following a bolus injection of 370 MBq of [^{11}C]-(R)-PK11195.

3.4.12 Image analysis

Parametric binding potential (BP_{ND}) images were created as described in Chapter 2. Spatial normalisation of BP_{ND} and MR images into standard MNI stereotaxic space was performed using SPM8 implemented in Matlab 7. Subject-specific object maps

for region of interest analysis were generated in ANALYZE (see Chapter 2, paragraph 2.7.7).

3.4.13 Region of interest data extraction

The subject-specific object map was laid over the spatially normalized BP_{ND} image in ANALYZE (Mayo Clinic, Rochester, MN), followed by systematic sampling of the regions of interest shown in table 3.1.

Table 3.1. Regions of interest
Anterior and posterior cingulate
Thalamus
Striatum, head of caudate, and putamen
Globus pallidus
Frontal lobe
Insula
Temporal lobe
Parietal lobe
Occipital lobe
Brainstem
Whole brain (excluding CSF spaces)

3.4.14 Voxel-based analysis: statistical parametric mapping (SPM)

Significant differences in mean [^{11}C]-(R)-PK11195 BP_{ND} between control and non-demented PD groups at the voxel level were localised using SPM8 software (Wellcome Trust Centre for Neuroimaging, UCL, London) as described in Chapter 2. Within the PDND group, significant voxel level correlation between [^{11}C]-(R)-PK11195 BP_{ND} and clinical parameters were interrogated with SPM8.

3.4.15 Statistical analysis

Statistical analysis of ROI and clinical data was performed in SSPS 21.0 (IBM, New York). Normality of data distributions was checked with the Kolmogorov-Smirnov test. Correlations between variables were interrogated with Spearman rank statistics.

3.5 Results

Table 3.2 shows the demographics and clinical data for the PD group at baseline and follow up.

Several ROI datasets and distributions of clinical variables failed the Kolmogorov-Smirnov test of normality at baseline and follow up, confirming the appropriateness of non-parametric statistical tests, which were therefore used throughout.

Table 3.2. Subject demographics and clinical data

	Baseline	**Follow up**
Number	21 (13 male)	19 (12 male)
Age, years	66.7 (6.4)	69.4 (6.6)
Onset age, years	61.7 (7.4)	62.7 (6.8)
Duration, months	60.8 (56.3)	78.2 (51.9)
MMSE	29.1 (1.3)	28.4 (2.3)
MoCA	25.3 (2.7)	22.7 (4.9)
ACE	88.1 (9.1)	84.2 (13.4)
ACE Memory	20.4 (4.4)	21.0 (4.7)
ACE Fluency	10.2 (2.8)	8.9 (3.4)
ACE Language	24.7 (2.4)	23.6 (3.3)
ACE Visuospatial	14.7 (1.6)	13.6 (3.8)
Phonemic fluency	11.6 (4.8)	11.5 (5.0)
Semantic fluency	15.2 (5.0)	13.0 (7.3)
UPDRS part 2	9.9 (5.0)	15.7 (8.7)
UPDRS part 3	27.8 (6.9)	34.5 (12.0)
ESS	7.4 (5.6)	7.7 (5.6)
GDS-15	4.4 (3.4)	3.9 (3.7)
PDQ-39	99.3 (66.2)	110.9 (72.7)
PDQ-39 ADL	14.8 (29.2)	22.7 (15.6)
PDQ-39 Mobility	34.7 (29.2)	34.7 (32.6)
PDQ-39 Cognition	7.7 (6.7)	7.7 (5.8)
PDQ-39	7.3 (7.9)	7.2 (7.4)
PDQ-39 Emotion	13.9 (13.2)	14.7 (16.0)
PDQ-39 Social	4.4 (5.9)	4.7 (6.6)
PDQ-39 Stigma	7.5 (9.6)	6.4 (9.9)
PDQ-39 Bodily	11.6 (6.9)	12.2 (8.4)

Data are mean with standard deviation in parentheses. MMSE (Mini Mental State Examination); MoCA (Montréal Cognitive Assessment); ACE (Addenbrooke's Cognitive Examination); UPDRS (Unified Parkinson's Disease Rating Scale); ESS (Epworth Sleepiness Scale); GDS-15 (Geriatric Depression Scale); PDQ-39 (Parkinson's disease quality of life 39 item questionnaire).

Baseline [^{11}C]-(R)-PK11195 imaging

Region of interest analysis

3.5.1 Baseline ROI analysis: controls v PD subjects

PD subjects had elevated [^{11}C]-(R)-PK11195 binding compared to controls in the brainstem, posterior cingulate, thalamus, putamen, insula, and in temporal and occipital cortex, and a trend towards higher [^{11}C]-(R)-PK11195 uptake at whole brain level (table 3.3).

Table 3.3. Regional [^{11}C]-(R)-PK11195 Binding Potentials (mean BP_{ND} ± standard deviation) in healthy controls and Parkinson's disease subjects

	Controls (n=7)	PD (n=21)
Anterior cingulate	0.1940 ± 0.0349	0.1976 ± 0.0636
Posterior cingulate	0.1763 ± 0.0215	0.2154 0.0601*
Thalamus	0.3240 ± 0.0476	0.3818 ± 0.0574*
Caudate	0.1270 ± 0.0291	0.1548 ± 0.0543
Putamen	0.2354 ± 0.0288	0.2932 ± 0.0720*
Globus pallidus	0.2369 ± 0.0539	0.3213 ± 0.0947*
Frontal lobe	0.17443 ± 0.0277	0.1969 ± 0.0600
Insula	0.1901 ± 0.0272	0.2251 ± 0.0476*
Temporal lobe	0.1796 ± 0.0196	0.2237 ± 0.0482**
Parietal lobe	0.1584 ± 0.0183	0.1832 ± 0.0504
Occipital lobe	0.1946 ± 0.0286	0.2290 ± 0.0474*
Brainstem	0.2877 ± 0.0282	0.3353 ± 0.0584*
Whole brain	0.1810 ± 0.0205	0.2127 ± 0.0501†

Mann-Whitney U test, ** $p<0.01$; * $p<0.01$; † $p=0.071$

Clinical correlations

3.5.2 Baseline ROI analysis: disease duration

Positive correlations were found between disease duration and [^{11}]-(R)-PK11195 BP_{ND} in the brainstem (ρ=0.564, p=0.008, figure 3.1) and posterior cingulate (ρ=0.456, p=0.038, figure 3.2).

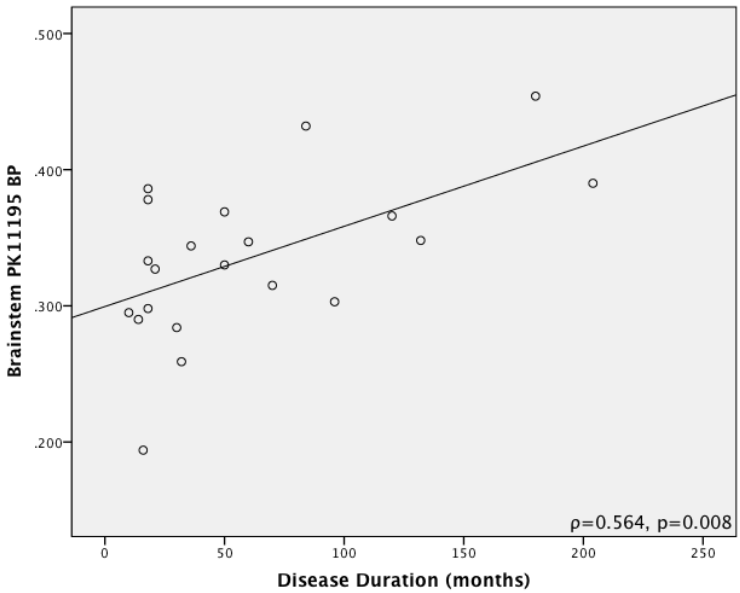


Figure 3.1. Correlation between brainstem [^{11}C]-(R)-PK11195 BP_{ND} and disease duration

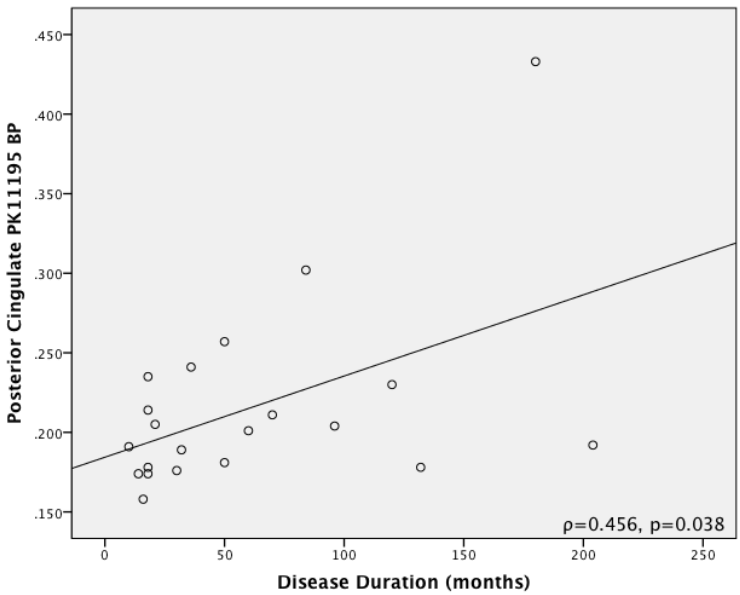


Figure 3.2. Correlation between posterior cingulate [^{11}C]-(R)-PK11195 BP_{ND} and disease duration

3.5.3 Baseline ROI analysis: age

There was no significant correlation between regional [^{11}C]-(R)-PK11195 uptake and age.

3.5.4 Baseline ROI analysis: subject-rated motor disability (UPDRS part 2)

Self-reported impairment of motor activities of daily living, rated with part 2 of the UPDRS, correlated positively with [^{11}C]-(R)-PK11195 BP_{ND} in the putamen (ρ=0.549, p=0.014), insula (ρ=0.604, p=0.007), and whole brain (ρ=0.427, p=0.0497), shown in figures 3.3-3.5.

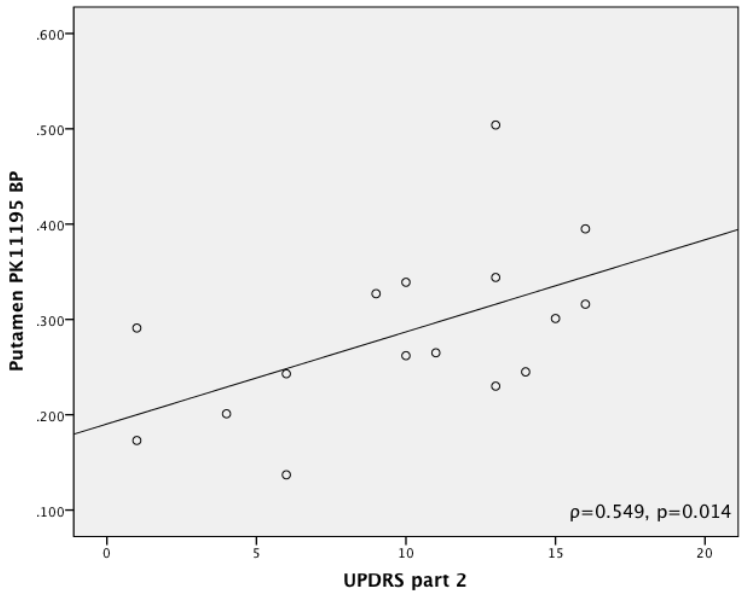


Figure 3.3. Correlation between putamenal [^{11}C]-(R)-PK11195 BP_{ND} and UPDRS part 2

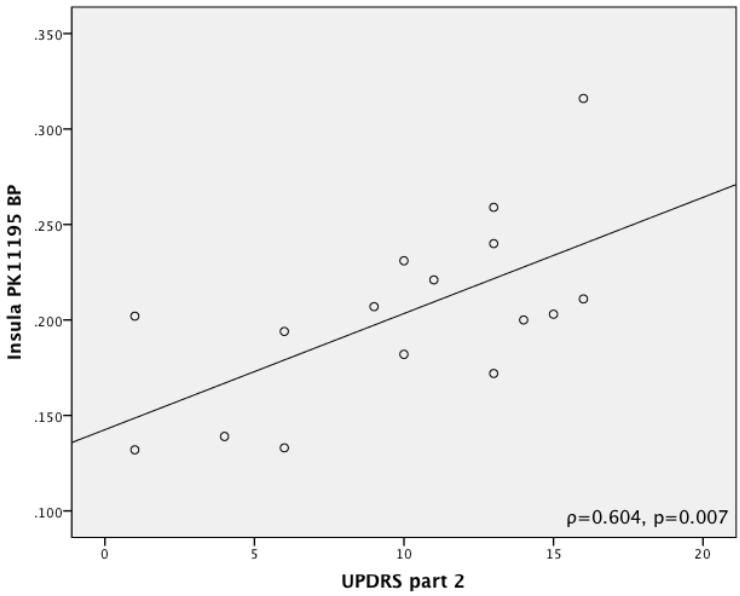


Figure 3.4. Correlation between insula [^{11}C]-(R)-PK11195 BP_{ND} and UPDRS part 2

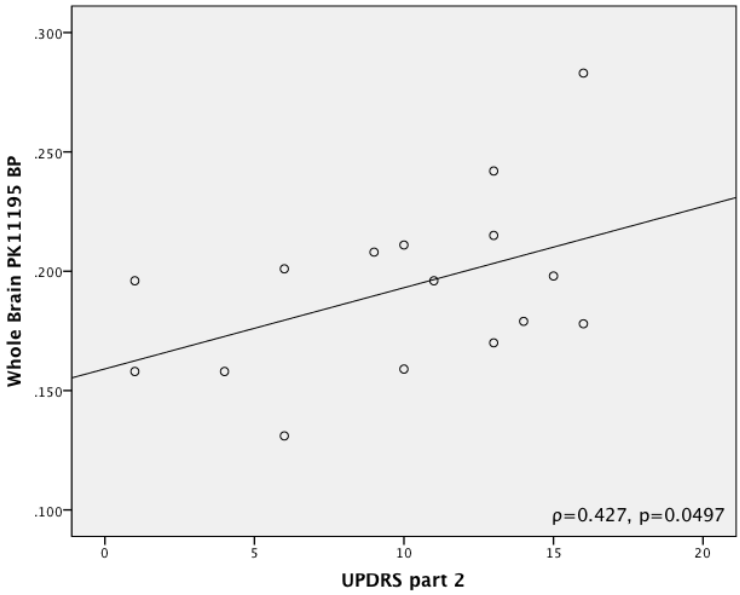


Figure 3.5. Correlation between whole brain [^{11}C]-(R)-PK11195 BP_{ND} and UPDRS part 2

3.5.5 Baseline ROI analysis: clinician-rated motor disability (UPDRS part 3)

Clinician-rated motor disability (rated with the UPDRS part 3) correlated positively with [^{11}C]-(R)-PK11195 BP_{ND} in putamen (ρ=0.444, p=0.043), frontal lobe (ρ=0.432, p=0.047), insula (ρ=0.488, p=0.028), temporal lobe (ρ=0.500, p=0.024) and whole brain (ρ=0.461, p=0.036), as shown in figures 3.6-3.10.

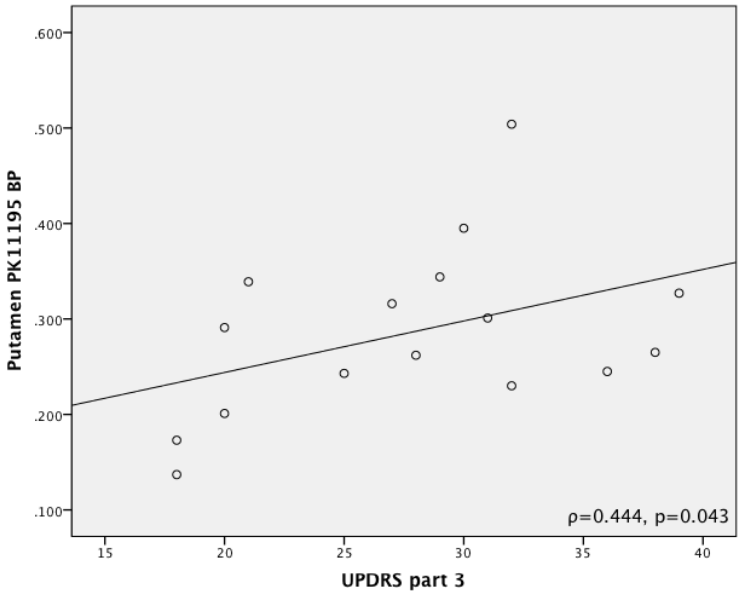


Figure 3.6. Correlation between putamenal [^{11}C]-(R)-PK11195 BP_{ND} and UPDRS part 3

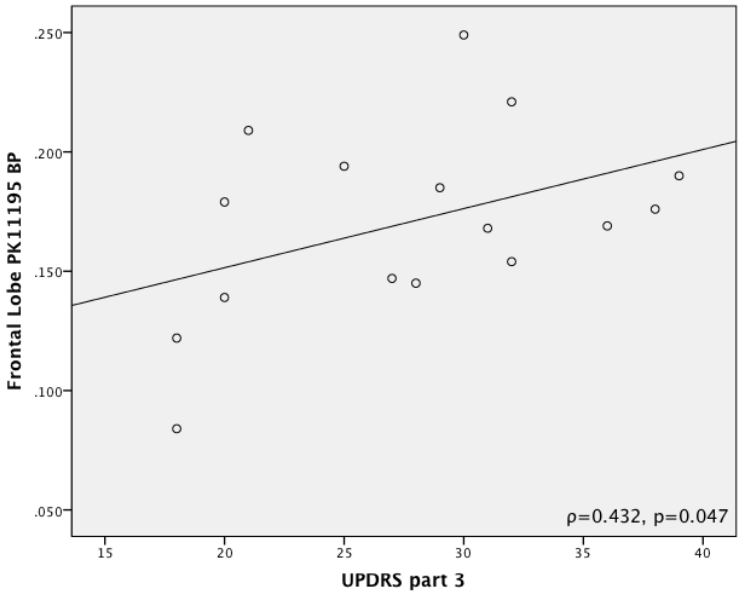


Figure 3.7. Correlation between frontal lobe [^{11}C]-(R)-PK11195 BP_{ND} and UPDRS part 3

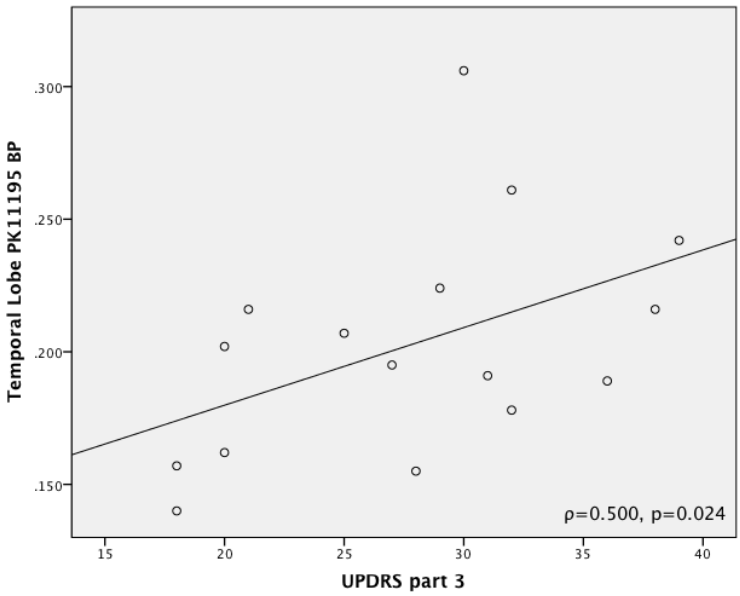


Figure 3.8. Correlation between temporal lobe [^{11}C]-(R)-PK11195 BP_{ND} and UPDRS part 3

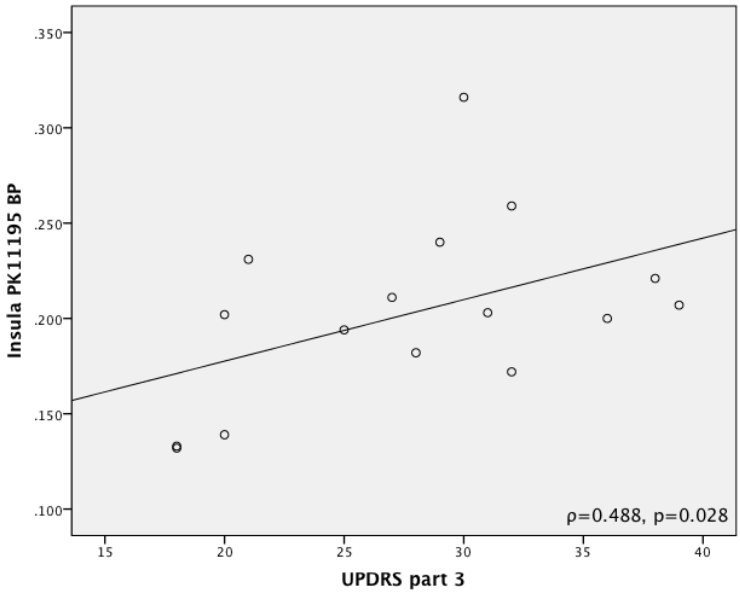


Figure 3.9. Correlation between insula [^{11}C]-(R)-PK11195 BP_{ND} and UPDRS part 3

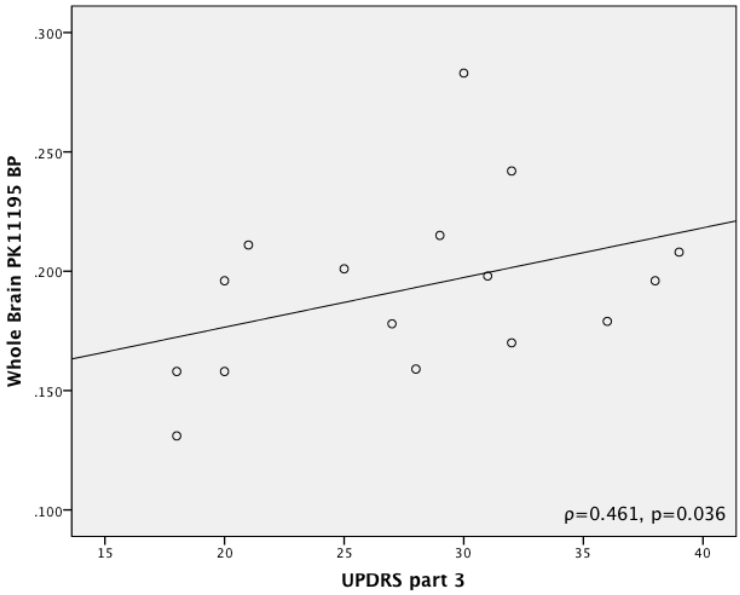


Figure 3.10. Correlation between whole brain [^{11}C]-(R)-PK11195 BP_{ND} and UPDRS part 3

3.5.6 Baseline ROI analysis: depression

Self reported GDS-15 depression scores correlated positively with [^{11}C]-(R)-PK11195 BP_{ND} at whole brain level and in brainstem, putamen, thalamus, insula, and in frontal, temporal, parietal and occipital cortices (table 3.4; Appendix, figures A1-9).

Table 3.4. Correlation between regional mean [^{11}C]-(R)-PK11195 Binding Potentials (BP_{ND}) and self-rated depression scores (GDS-15) in PD subjects

	Correlation coefficient (Spearman Rho)	**p value**
Anterior cingulate	0.411	0.050
Posterior cingulate	0.392	0.060
Caudate	0.307	0.115
Putamen	0.615	0.007**
Thalamus	0.417	0.048*
Globus pallidus	0.259	0.158
Frontal lobe	0.680	0.0013**
Insula	0.709	0.0007***
Temporal lobe	0.687	0.0012**

Parietal lobe	0.642	0.003**
Occipital lobe	0.594	0.006**
Brainstem	0.732	0.0004***
Whole brain	0.657	0.002**

Spearman rank correlation coefficient, *** p<0.001; ** p<0.01; * p<0.05

3.5.7 Baseline ROI analysis: quality of life (PDQ-39)

Significant positive correlations were found between subject-rated impairment in quality of life (rated with the PDQ-39), and mean whole brain [^{11}C]-(R)-PK11195 BP_{ND}, and with regional [^{11}C]-(R)-PK11195 BP_{ND} in the brainstem, putamen, globus pallidus, insula, and in frontal, temporal, parietal and occipital cortex (Table 3.5; Appendix, figures A10-18). Impaired activities of daily living (ADL), assessed with the PDQ-39 ADL sub-score, correlated positively with [^{11}C]-(R)-PK11195 BP_{ND} at whole brain level, and in brainstem, striatum, insula and temporal lobes (table 3.5; Appendix, figures A19-23). Self-reported mobility problems, assessed with the PDQ-39 mobility score, correlated with whole brain, putamenal, insular and frontal, temporal and occipital lobe [^{11}C]-(R)-PK11195 BP_{ND} (table 3.5, Appendix, figures A24-29). Subjective cognitive impairment correlated with frontal lobe [^{11}C]-(R)-PK11195 BP_{ND}, whilst problematic communication correlated with posterior cingulate [^{11}C]-(R)-PK11195 uptake (table 3.5; Appendix, figures A30 and A31). Impairment in emotional wellbeing correlated with mean whole brain [^{11}C]-(R)-PK11195 BP_{ND}, and with regional [^{11}C]-(R)-PK11195 BP_{ND} in brainstem, putamen, thalamus, globus pallidus, anterior cingulate, insula, and in frontal and temporal cortex (table 3.5; Appendix, figures A32-37). Greater perceived social problems correlated positively with whole brain, anterior cingulate, and with frontal, temporal and occipital lobe [^{11}C]-(R)-PK11195 BP_{ND} (table 3.5; Appendix, figures A38-42). Subjective PDQ-39 stigmatisation scores correlated with whole brain, anterior cingulate and frontal lobe [^{11}C]-(R)-PK11195 BP_{ND} (table 3.5; Appendix, figures A43-45). Bodily discomfort correlated with globus pallidus and frontal lobe [^{11}C]-(R)-PK11195 BP_{ND} (table 3.5; Appendix, figures A46 and A47).

Table 3.5. Correlation between baseline regional [^{11}C]-(R)-PK11195 BP_{ND} and PDQ-39 total and sub-domain scores. Data are Spearman rank correlation coefficients (ρ).

	PDQ-39	ADL	Mobility	Cognition	Communication	Emotion	Social	Stigma	Bodily discomfort
Anterior	0.449	0.201	0.409	0.276	0.271	0.566*	0.694***	0.475*	0.398
Posterior	0.189	0.188	0.129	0.276	0.463*	0.321	0.387	0.072	0.111
Thalamus	0.385	0.354	0.157	0.393	0.415	0.536*	0.203	0.305	0.431
Caudate	-0.002	-0.010	-0.026	0.186	0.332	0.135	0.197	0.103	0.060
Putamen	0.532*	0.351	0.428*	0.260	0.246	0.444*	0.293	0.199	0.398
Globus	0.525	0.308	0.322	-0.040	0.041	0.426*	0.271	0.268	0.463*
Frontal lobe	0.727**	0.373	0.600**	0.536*	0.354	0.463*	0.527*	0.509*	0.503*
Insula	0.605*	0.498*	0.443*	0.379	0.289	0.507*	0.232	0.182	0.415
Temporal lobe	0.726**	0.557*	0.598**	0.273	0.314	0.704***	0.551*	0.403	0.242
Parietal lobe	0.530*	0.194	0.343	0.323	0.131	0.305	0.425	0.3121	0.381
Occipital lobe	0.546*	0.248	0.441*	0.062	0.056	0.265	0.496*	0.253	0.264
Brainstem	0.464*	0.512*	0.244	0.182	0.116	0.723***	0.266	0.269	-0.009
Whole brain	0.796***	0.468*	0.589*	0.320	0.226	0.570*	0.500*	0.428*	0.455

Spearman rank correlation coefficient: *** p<0.001; ** p <0.01; *p<0.05

Voxel-based analysis: statistical parametric mapping (SPM)

3.5.8 Baseline SPM analysis: healthy control versus Parkinson's disease subjects

SPM localised relatively greater [^{11}C]-(R)-PK11195 binding in PD subjects compared to controls in frontal lobes, putamena, midbrain and pons (figure 3.11; table 3.6).

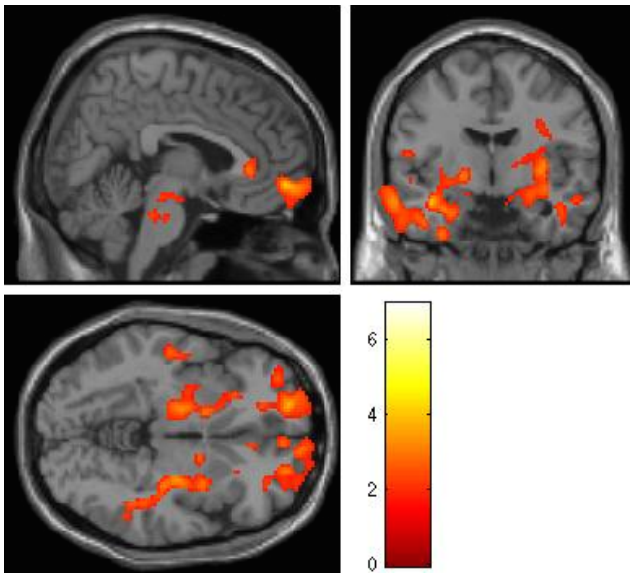


Figure 3.11. Regions of elevated baseline [^{11}C]-(R)-PK11195 BP_{ND} in non-demented PD subjects compared to healthy controls. Statistical parametric map (SPM) showing relative excess of [^{11}C]-(R)-PK11195 uptake in the basal ganglia, frontal and temporal lobes, midbrain and pons. (voxel threshold p=0.05; cluster significance p<0.001, corrected). The colour stripe indicates Z score.

Table 3.6. Areas of raised [^{11}C]-(R)-PK11195 BP_{ND} in PD subjects compared to controls

Z score	MNI coordinates			Area
	x	*y*	*z*	
5.18	28	0	-16	Right parahippocampal gyrus
4.15	24	8	-40	Right temporal pole
3.84	-18	58	-6	Left superior frontal gyrus
4.06	-42	12	10	Left precentral gyrus
3.99	-64	-10	-16	Left middle temporal gyrus
3.67	6	-23	-17	Brainstem

3.5.9 Baseline SPM analysis: PD subjects at lower v higher risk of dementia

SPM localised relatively greater [^{11}C]-(R)-PK11195 BP_{ND} in the dorsal parietal lobes (including precuneus), occipital and frontal lobes in subjects classified as being at higher risk of PD dementia compared to lower risk subjects (figure 3.12; table 3.7).

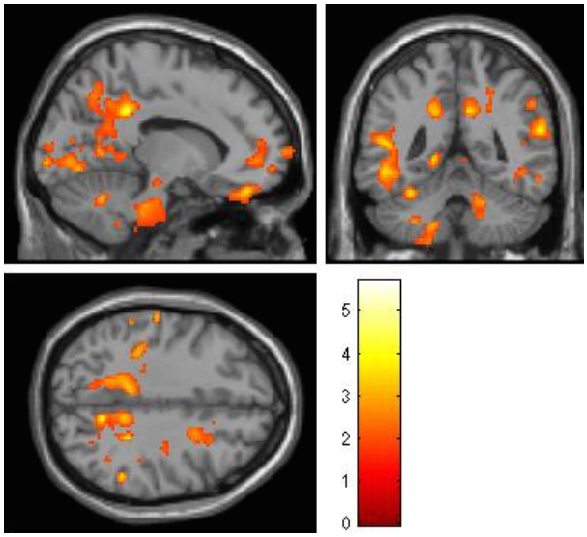


Figure 3.12. Regions of elevated baseline [^{11}C]-(R)-PK11195 BP_{ND} in PD subjects at higher risk of dementia compared to those at lower risk. Statistical parametric map (SPM) showing relative excess of [^{11}C]-(R)-PK11195 uptake in the dorsal parietal lobes, precuneus (arrows), occipital and frontal lobes in higher risk subjects (voxel threshold p=0.05; cluster significance p<0.001, corrected). The colour stripe indicates *Z* score.

Table 3.7. Areas of greater [^{11}C]-(R)-PK11195 binding in PD subjects at higher risk of dementia compared to lower risk subjects

Z score	MNI coordinates			Area
	x	*y*	*z*	
4.15	12	-58	6	Posterior cingulate
3.83	20	-80	0	Right lingual gyrus
3.80	20	-34	-16	Right culmen
3.79	22	-80	-46	Inferior semi-lunar lobule
3.77	10	-58	42	Right precuneus
3.68	12	-56	34	Right precuneus
3.36	34	-10	14	Right insula
3.34	50	-54	16	Right superior temporal gyrus
3.34	44	-70	2	Right fusiform gyrus
4.02	-32	-40	56	Left precentral gyrus
3.65	-54	-54	22	Left supramarginal gyrus
3.50	-14	-42	34	Left dorsal posterior cingulate

3.26	-42	-42	6	Left superior temporal gyrus
3.23	-44	-62	10	Left middle temporal gyrus
3.02	-58	-20	36	Left superior temporal gyrus
2.99	-16	-44	0	Left parahippocampal gyrus
3.94	24	54	-14	Right superior frontal gyrus
3.55	-24	56	12	Left middle frontal gyrus
3.15	-18	64	4	Left superior Frontal gyrus
3.14	10	52	10	Right medial Frontal gyrus
3.13	26	52	4	Right anterior prefrontal
3.08	-20	-68	-10	Left lingual gyrus
3.04	-32	-84	2	Left middle occipital gyrus
2.99	-16	-44	0	Left parahippocampal gyrus
3.94	24	54	-14	Right superior frontal gyrus
3.55	-24	56	12	Left middle frontal gyrus
3.15	-18	64	4	Left superior frontal gyrus
3.14	10	52	10	Right medial frontal gyrus
3.13	26	52	4	Right anterior prefrontal
2.93	24	60	-4	Right superior frontal gyrus
2.91	0	60	-8	Left medial orbitofrontal
2.56	8	66	-20	Right superior orbitofrontal
3.75	32	2	-18	Right parahippocampal gyrus
3.18	-26	-40	-26	Left culmen
3.17	16	-16	-18	Midbrain
3.03	-32	-14	-6	Left putamen
3.03	-32	-46	-24	Left culmen
2.93	-34	-10	-8	Left claustrum
2.91	-18	-34	-34	Pons

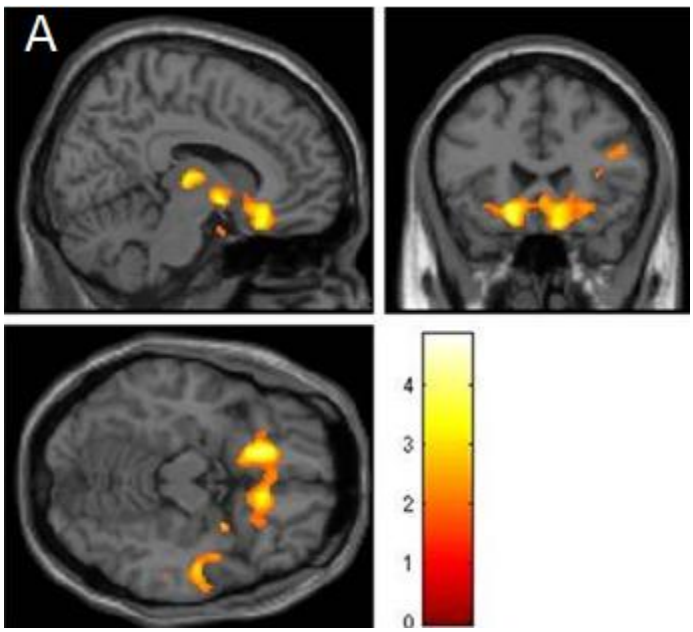
Baseline SPM analysis: clinical correlation

3.5.10 Baseline SPM analysis: age

There was no significant correlation between [^{11}C]-(R)-PK11195 binding and age.

3.5.11 Baseline SPM analysis: disease duration

An inverse correlation was found between disease duration and [^{11}C]-(R)-PK11195 BP_{ND} in the basal ganglia and basal forebrain, the latter location containing the anterior olfactory nuclei (figure 3.13; table 3.8).



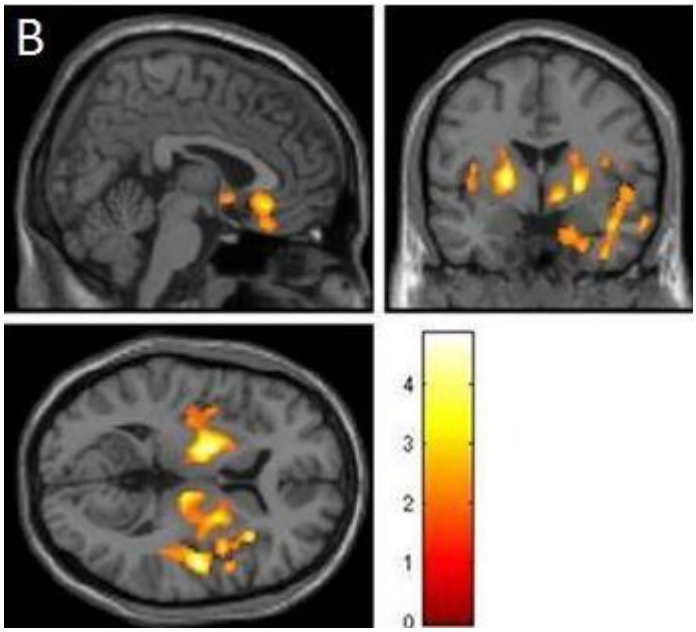


Figure 3.13. Inverse correlation between baseline [^{11}C]-(R)-PK11195 BP_{ND} and disease duration. Statistical parametric map (SPM) showing shorter disease duration correlates with [^{11}C]-(R)-PK11195 uptake in the basal forebrain (A), a region containing the anterior olfactory nuclei, and in the basal ganglia (B). Voxel threshold p=0.05; cluster significance p<0.01, corrected. The colour stripe indicates Z score.

Table 3.8. Areas of [^{11}C]-(R)-PK11195 binding in PD subjects correlating inversely with disease duration

	MNI coordinates			Area
Z score	*x*	*y*	*z*	
3.84	-19	-5	12	Left putamen
3.74	-18	-4	6	Left external globus pallidus
3.41	-16	-30	-16	Left inferior frontal gyrus pars
3.37	24	-2	2	Right putamen
3.35	2	32	-10	Anterior cingulate
3.11	-18	14	-2	Left putamen
3.08	10	26	-20	Right medial frontal gyrus
2.98	12	-18	6	Right thalamus
2.93	10	28	-14	Right medial frontal gyrus
2.91	26	-10	12	Right putamen
2.81	-40	0	12	Left insula
3.82	50	-10	6	Right premotor

3.62	56	-32	-22	Right inferior temporal gyrus
3.60	34	18	4	Right insula
3.43	28	4	-18	Right entorhinal
3.34	62	-42	20	Right superior temporal gyrus
3.26	30	6	-22	Right entorhinal
3.11	40	2	16	Right insula
3.05	50	-10	-8	Right superior temporal gyrus
3.04	28	14	-34	Right superior temporal gyrus
3.04	26	-4	-34	Right uncus
2.97	42	-32	12	Right auditory cortex
2.95	40	4	8	Right insula
2.95	38	40	24	Right anterior prefrontal lobe

3.5.12 Baseline SPM analysis: visuospatial cognition

SPM revealed an inverse correlation between visuospatial cognitive function (assessed with the visuospatial ACE sub-score) and [^{11}C]-(R)-PK11195 BP_{ND} in the dorsal parietal lobes (figure 3.14; table 3.9).

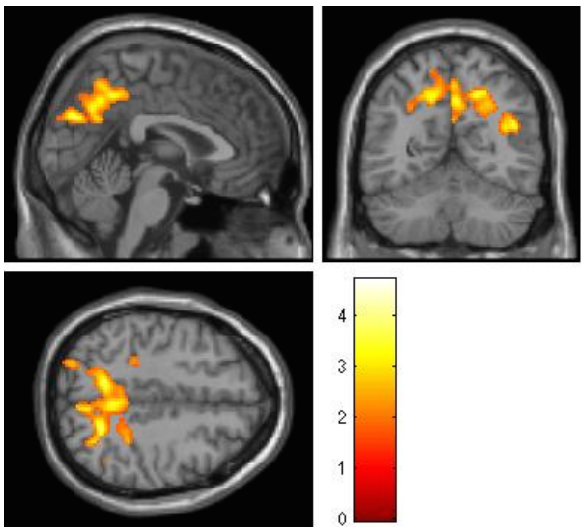


Figure 3.14. Inverse correlation between [^{11}C]-(R)-PK11195 BP_{ND} and the visuospatial sub-score of the Addenbrooke's Cognitive Examination (ACE). Statistical parametric map (SPM) showing bilateral dorsal parietal lobe [^{11}C]-(R)-PK11195 signal correlates with greater impairment in visuospatial cognitive function

(voxel threshold p=0.05; cluster significance p<0.001, corrected). The colour stripe indicates Z score.

Table 3.9. Areas of inverse correlation between [^{11}C]-(R)-PK11195 BP_{ND} and the ACE visuospatial sub-score

Z score	MNI coordinates			Area
	x	*y*	*z*	
3.76	-16	-38	70	Left postcentral gyrus
3.23	4	-60	40	Left somatosensory association
3.22	20	-58	46	Right precuneus
3.18	-12	-56	46	Left precuneus
3.14	-20	-46	62	Left somatosensory association
3.13	-14	-50	70	Left postcentral gyrus
3.12	46	-60	24	Right angular gyrus
3.12	2	-78	30	Left cuneus
3.10	40	-54	22	Right superior temporal gyrus
3.01	-30	-32	58	Left primary motor cortex
3.00	4	-50	46	Right somatosensory association
2.93	-20	-30	60	Right postcentral gyrus
2.91	-20	-32	64	Left primary somatosensory
2.88	-30	-48	64	Left postcentral gyrus
2.83	6	-70	48	Right precuneus

3.5.13 Baseline SPM analysis: phonemic fluency

SPM revealed an inverse relationship between phonemic fluency (FAS letter task) scores and [^{11}C]-(R)-PK11195 BP_{ND} in the frontal lobes (figure 3.15; table 3.10).

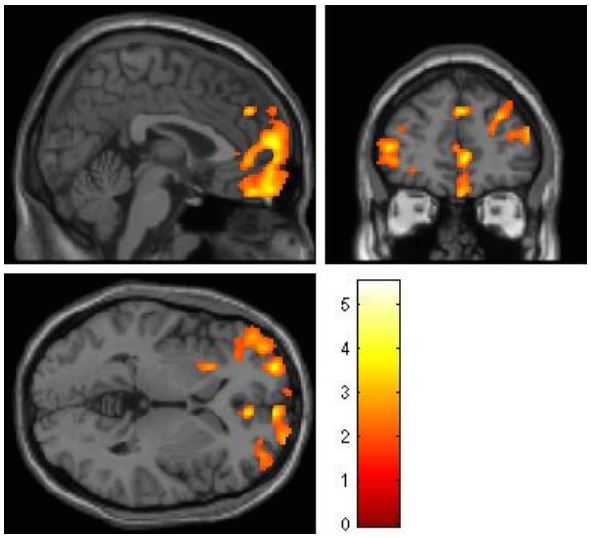


Figure 3.15. Inverse correlation between [^{11}C]-(R)-PK11195 BP_{ND} and phonemic fluency (FAS letter task). Statistical parametric map (SPM) showing [^{11}C]-(R)-PK11195 uptake in the frontal lobes correlates with greater impairment in phonemic fluency (voxel threshold p=0.05; cluster significance p<0.001, corrected). The colour stripe indicates Z score.

Table 3.10. Areas of inverse correlation between phonemic fluency (FAS letter task) and [^{11}C]-(R)-PK11195 BP_{ND}

	MNI coordinates			
Z score	*x*	*y*	*z*	Area
4.02	8	58	-18	Right medial frontal gyrus
3.49	2	64	10	Right superior medial frontal
3.47	6	58	12	Right medial frontal gyrus
3.43	-38	16	32	Left middle frontal gyrus
3.34	-46	44	8	Left inferior frontal gyrus
3.32	-32	32	42	Left middle frontal gyrus
3.29	32	56	-6	Right anterior prefrontal
3.09	44	54	20	Right anterior prefrontal
3.09	6	64	0	Right medial frontal gyrus
3.08	8	46	2	Anterior cingulate
3.07	4	46	34	Right dorsolateral prefrontal
3.06	-26	64	0	Left anterior prefrontal
3.01	4	48	-22	Right orbitofrontal
3.01	10	60	28	Right superior frontal gyrus

2.95	34	56	34	Right anterior prefrontal
2.88	22	72	10	Right dorsolateral prefrontal

3.5.14 Baseline SPM analysis: semantic fluency

A negative correlation between semantic fluency scores and [^{11}C]-(R)-PK11195 BP_{ND} in the frontal lobes and left insula was found (figure 3.16; table 3.11).

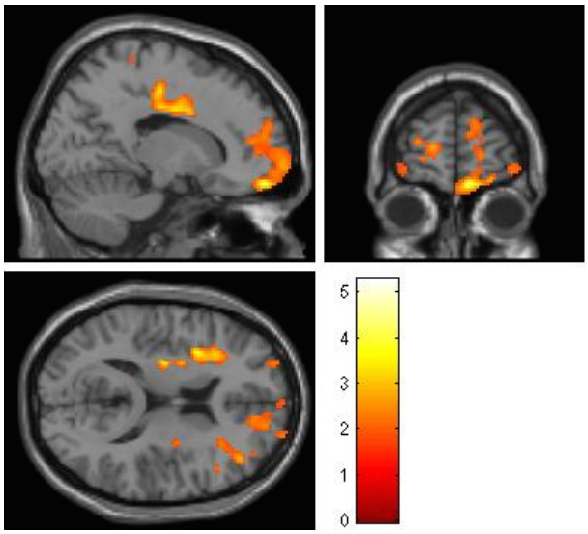


Figure 3.16. Inverse correlation between [^{11}C]-(R)-PK11195 BP_{ND} and semantic fluency (number of animals named in 1 minute). Statistical parametric map (SPM) showing [^{11}C]-(R)-PK11195 signal in frontal cortex and left insula correlates with greater impairment in semantic fluency (voxel threshold p=0.05; cluster significance p<0.001, corrected). The colour stripe indicates Z score.

Table 3.11. Areas of inverse correlation between [^{11}C]-(R)-PK11195 BP_{ND} and semantic fluency scores

	MNI coordinates			Area
Z score	*x*	*y*	*z*	
3.91	-28	44	-8	Left middle frontal gyrus
3.89	42	26	28	Right middle frontal gyrus
3.58	10	60	-18	Right medial frontal gyrus
3.36	54	-42	38	Right supramarginal gyrus
3.34	30	40	-6	Right middle frontal gyrus

3.30	-34	10	12	Left insula
3.25	16	56	-18	Right orbitofrontal
3.09	24	-30	62	Right postcentral gyrus
2.95	34	52	-4	Right middle frontal gyrus
2.93	18	-6	34	Cingulate
2.91	-30	36	-2	Left middle frontal gyrus
2.89	38	-34	26	Right inferior parietal lobule

3.5.15 Baseline SPM analysis: quality of life (PDQ-39)

SPM analysis revealed a positive correlation between total PDQ-39 scores and neocortical [^{11}C]-(R)-PK11195 uptake, especially in the frontal lobes (figure 3.17; table 3.12).

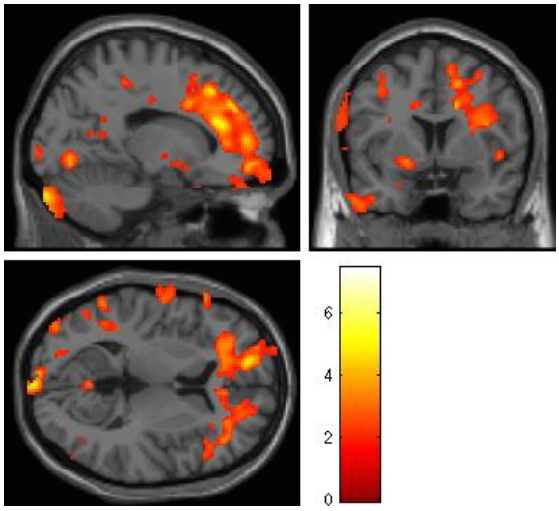


Figure 3.17. Positive correlation between [^{11}C]-(R)-PK11195 BP_{ND} and subject-rated impaired quality of life scores (PDQ-39). Statistical parametric map (SPM) showing cortical [^{11}C]-(R)-PK11195 signal correlates with higher PDQ-39 scores, predominantly in the frontal lobes (voxel threshold p=0.05; cluster significance p<0.001, corrected). The colour stripe indicates Z score.

Table 3.12. Areas of positive correlation between PDQ-39 scores and [^{11}C]-(R)-PK11195 BP_{ND}

MNI coordinates			Area

Z score	*x*	*y*	*z*	
4.21	-42	0	-36	Left middle temporal gyrus
4.07	10	40	36	Right medial frontal gyrus
3.92	-16	42	32	Posterior cingulate
3.87	-12	32	22	Anterior cingulate
3.87	48	-82	-18	Right angular gyrus
3.85	-52	-10	-24	Left inferior temporal gyrus
3.72	14	22	40	Anterior cingulate
3.71	-62	-22	14	Left supramarginal gyrus

3.5.16 Baseline SPM analysis: PDQ-39 mobility domain

Subjective mobility difficulties, rated with the mobility dimension of the PDQ-39, correlated with diffuse neocortical [^{11}C]-(R)-PK11195, particularly the frontal lobes (figure 3.18; table 3.13).

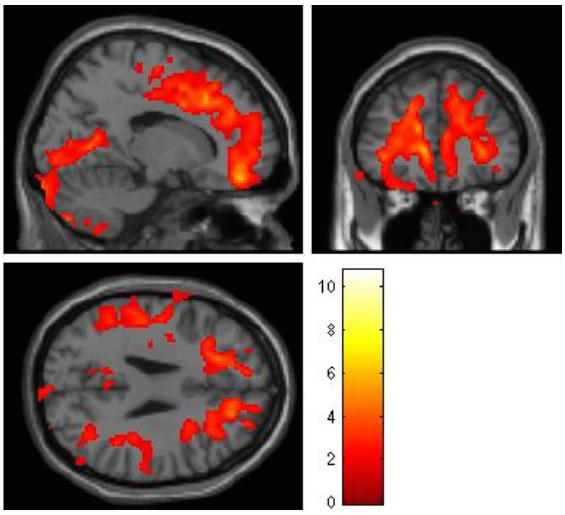


Figure 3.18. Positive correlation between [^{11}C]-(R)-PK11195 BP_{ND} and subject-rated impaired mobility (PDQ-39 mobility domain). Statistical parametric map (SPM) showing cortical [^{11}C]-(R)-PK11195 signal correlates with higher PDQ-39 mobility scores, especially in the frontal lobes (voxel threshold p=0.05; cluster significance p<0.001, corrected). The colour stripe indicates Z score.

Table 3.13. Areas of positive correlation between PDQ-39 mobility scores and [^{11}C]-(R)-PK11195 BP_{ND}

Z score	MNI coordinates			Area
	x	*y*	*z*	
5.29	50	-80	-16	Right middle occipital gyrus
4.80	-10	40	0	Anterior cingulate
4.50	38	-92	-18	Right secondary visual cortex
4.37	14	46	-14	Right inferior frontal gyrus
4.20	14	22	42	Right superior frontal gyrus
4.09	28	-92	-30	Right inferior occipital gyrus
4.01	22	14	-16	Right insula
3.98	-56	-54	0	Left middle temporal gyrus
3.95	-12	36	18	Anterior cingulate
3.88	24	54	-2	Right superior frontal gyrus
3.88	-52	-10	-22	Left middle temporal gyrus

3.5.17 Baseline SPM analysis: PDQ-39 cognition domain

Subject-rated cognitive impairment, assessed using the cognition domain of the PDQ-39, correlated with frontal lobe [^{11}C]-(R)-PK11195 BP_{ND} (figure 3.19; table 3.14).

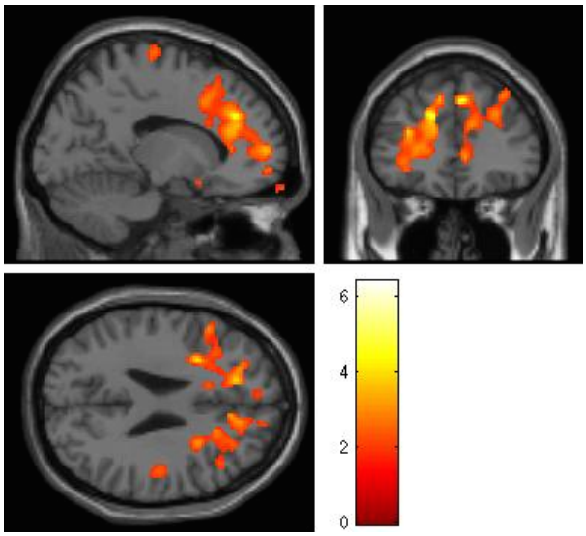


Figure 3.19. Positive correlation between baseline [^{11}C]-(R)-PK11195 BP_{ND} and subject-rated cognitive impairment (PDQ-39 cognition domain). Statistical parametric

map (SPM) showing frontal lobe [^{11}C]-(R)-PK11195 signal correlates with higher cognitive impairment scores (voxel threshold p=0.05; cluster significance p<0.001, corrected). The colour stripe indicates Z score.

Table 3.14. Areas of positive correlation between baseline PDQ-39 cognition scores and [^{11}C]-(R)-PK11195 BP_{ND}

Z score	MNI coordinates			Area
	x	*y*	*z*	
4.28	6	38	42	Right middle frontal gyrus
3.71	6	28	50	Right superior frontal gyrus
3.60	-34	24	12	Left insula
3.26	32	28	42	Right middle frontal gyrus
3.25	-30	12	30	Left middle frontal gyrus
3.22	-16	36	32	Left medial frontal gyrus
3.15	-34	24	30	Left middle frontal gyrus
3.01	-14	38	24	Left dorsolateral prefrontal cortex
2.92	12	50	14	Right medial frontal gyrus

3.5.18 Baseline SPM analysis: PDQ-39 communication domain

Self assessed difficulty with communication, assessed with the communication subscale of the PDQ-39, correlated [^{11}C]-(R)-PK11195 uptake in the frontal lobes (figure 3.20; table 3.15).

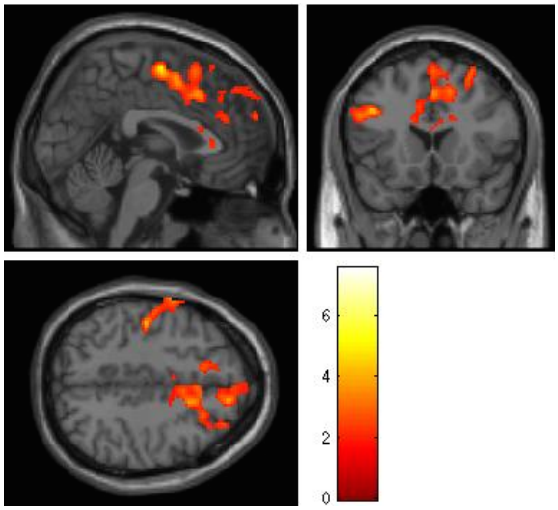


Figure 3.20. Positive correlation between [^{11}C]-(R)-PK11195 BP_{ND} and subject-rated communication impairment (PDQ-39 communication domain). Statistical parametric map (SPM) showing [^{11}C]-(R)-PK11195 uptake in the frontal lobes correlates with greater communication impairment (voxel threshold p=0.05; cluster significance p<0.001, corrected). The colour stripe indicates Z score.

Table 3.15. Areas of positive correlation between PDQ-39 communication scores and [^{11}C]-(R)-PK11195 BP_{ND}

	MNI coordinates			
Z score	*x*	*y*	*z*	Area
4.50	-72	-4	18	Left medial frontal gyrus
4.17	-62	-2	42	Left precentral gyrus
4.06	-72	-14	22	Left precentral gyrus
4.01	-54	-12	50	Left postcentral gyrus
3.57	-42	20	32	Left middle frontal gyrus
3.39	-56	-34	38	Left inferior parietal lobule
3.19	-44	-20	46	Left postcentral gyrus
3.06	-50	20	28	Left inferior frontal gyrus
2.99	-68	-14	36	Left postcentral gyrus
2.96	-52	-6	30	Left precentral gyrus
2.50	-54	4	20	Left inferior frontal gyrus
2.49	-52	14	16	Left insula

3.5.19 Baseline SPM analysis: PDQ-39 social impairment

Subjective social impairment, rated with the social dimension of the PDQ-39, correlated with widespread neocortical signal (figure 3.21; table 3.16).

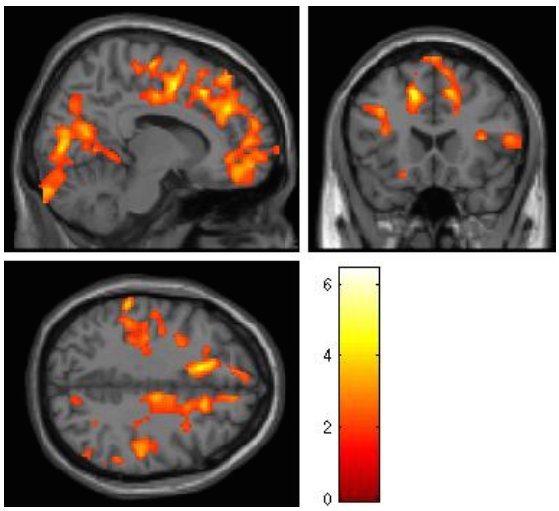


Figure 3.21. Positive correlation between [^{11}C]-(R)-PK11195 BP_{ND} and subject-rated social impairment (PDQ-39 social dimension). Statistical parametric map (SPM) showing widespread cortical [^{11}C]-(R)-PK11195 signal correlates with higher subjective social impairment (voxel threshold $p=0.05$; cluster significance $p<0.001$, corrected). The colour stripe indicates Z score.

Table 3.16. Areas of positive correlation between PDQ-39 social impairment scores and [^{11}C]-(R)-PK11195 BP_{ND}

	MNI coordinates			
Z score	*x*	*y*	*z*	Area
4.32	42	-32	-20	Right fusiform gyrus
3.93	20	-96	0	Right cuneus
3.69	44	-62	-4	Right middle temporal gyrus
3.57	64	-46	12	Right superior temporal gyrus
3.49	52	-72	22	Right middle temporal gyrus
3.49	-6	-82	-12	Left secondary visual cortex
3.45	-24	-94	-36	Left inferior occipital gyrus
3.41	-8	-86	-12	Left lingual gyrus
3.32	4	-68	20	Posterior cingulate
3.31	48	-36	-14	Right middle temporal gyrus
3.29	-32	-94	-34	Left inferior occipital gyrus

4.22	-14	28	44	Left superior frontal gyrus
4.20	14	2	50	Cingulate
4.09	62	-20	20	Right postcentral gyrus
4.06	12	22	44	Anterior cingulate
3.92	50	26	12	Right inferior frontal gyrus
3.83	68	-12	16	Right postcentral gyrus
3.55	10	40	34	Right medial frontal gyrus
3.50	-12	30	54	Left superior frontal gyrus
3.45	8	38	-4	Anterior cingulate
3.41	0	56	-4	Left orbitofrontal cortex
3.36	-48	-6	8	Left precentral gyrus
3.32	-40	-42	12	Left superior temporal gyrus
3.31	-44	-18	50	Left primary motor cortex

3.5.20 Baseline SPM analysis: PDQ-39 bodily discomfort domain

PDQ-39 bodily discomfort scores correlated positively with [^{11}C]-(R)-PK11195 BP_{ND} in the frontal lobes (figure 3.22; table 3.17).

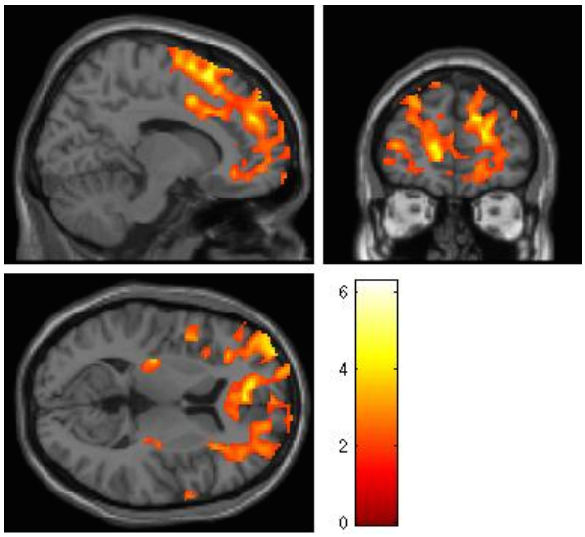


Figure 3.22. Positive correlation between [^{11}C]-(R)-PK11195 BP_{ND} and PDQ-39 bodily discomfort scores. Statistical parametric map (SPM) showing frontal lobe [^{11}C]-(R)-PK11195 uptake correlates with higher bodily discomfort scores (voxel

threshold p=0.05; cluster significance p<0.001, corrected). The colour stripe indicates Z score.

Table 3.17. Areas of positive correlation between PDQ-39 and bodily discomfort scores and [^{11}C]-(R)-PK11195 BP_{ND}

Z score	MNI coordinates			Area
	x	*y*	*z*	
4.09	-6	64	0	Left medial frontal gyrus
3.94	-16	58	20	Left superior frontal gyrus
3.90	-2	64	-10	Left orbitofrontal cortex
3.75	22	48	18	Left superior frontal gyrus
3.74	12	16	36	Anterior cingulate
3.73	-20	-46	78	Left superior parietal lobe
3.69	20	38	42	Right dorsolateral prefrontal cortex
3.65	14	18	60	Right premotor cortex
3.52	-20	38	36	Left dorsolateral prefrontal cortex
3.47	18	20	66	Right premotor cortex
3.41	-46	-12	26	Left postcentral gyrus
3.40	20	44	30	Right superior frontal gyrus
3.40	-42	58	10	Left middle frontal gyrus
3.40	6	34	-4	Anterior cingulate

3.5.21 Baseline SPM analysis: depression (GDS-15)

Subject-rated GDS-15 depression scores correlated positively with diffuse cortical [^{11}C]-(R)-PK11195 uptake (figures 3.23; table 3.18).

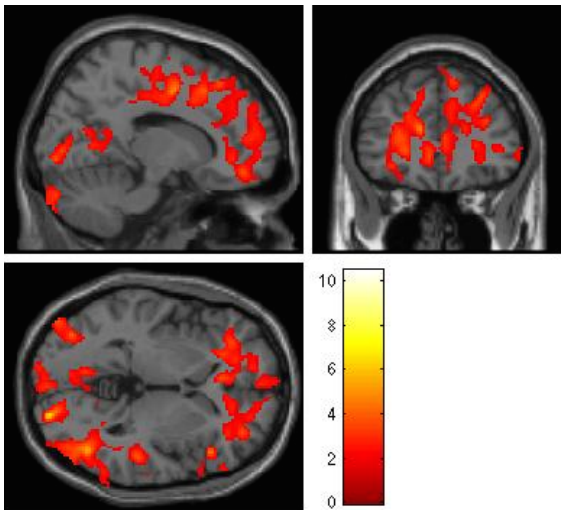


Figure 3.23. Positive correlation between [^{11}C]-(R)-PK11195 BP_{ND} and self-rated depression (GDS-15) scores. Statistical parametric map (SPM) showing widespread cortical [^{11}C]-(R)-PK11195 signal correlates with higher depression scores (voxel threshold p=0.05; cluster significance p<0.001, corrected). The colour stripe indicates *Z* score.

Table 3.18. Areas of positive correlation between GDS-15 depression scores and [^{11}C]-(R)-PK11195 BP_{ND}

Z score	MNI coordinates			Area
	x	*y*	*z*	
5.56	20	-92	-4	Right lingual gyrus
3.98	48	-66	-2	Right fusiform gyrus
3.94	-36	38	-6	Left middle frontal gyrus
3.90	44	-68	-4	Right fusiform gyrus
3.73	-14	-78	-10	Left secondary visual cortex (V2)
3.72	28	-92	14	Right middle occipital gyrus
3.66	62	-24	16	Right supramarginal gyrus
3.64	-12	34	18	Anterior cingulate
3.61	14	-4	46	Cingulate
3.50	66	-38	12	Right superior temporal gyrus
3.48	38	-94	-18	Right association visual cortex
3.47	52	-28	2	Right superior temporal gyrus
3.47	46	-84	-14	Right secondary visual cortex (V2)

3.5.22 Baseline SPM analysis: subject-rated motor disability (UPDRS part 2)

Subject-rated impairment in motor activities of daily living (assessed with part 2 of the UPDRS) correlated positively with [^{11}C]-(R)-PK11195 BP_{ND} in the posterior putamen bilaterally and the frontal lobes (figures 3.24; table 3.19).

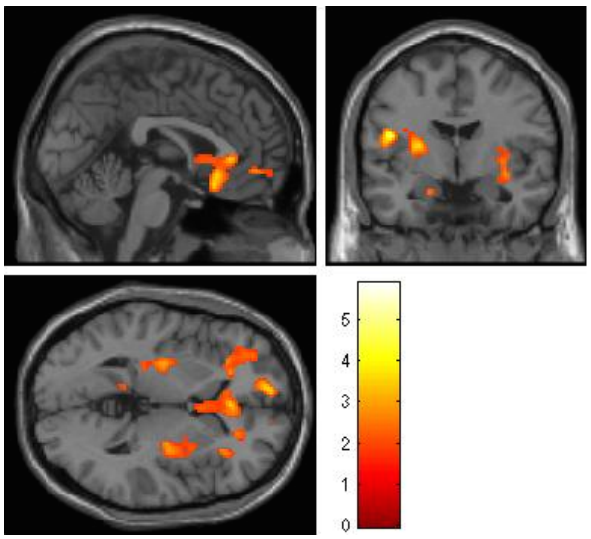


Figure 3.24. Positive correlation between [^{11}C]-(R)-PK11195 BP_{ND} and UPDRS part 2 scores. Statistical parametric map (SPM) showing widespread cortical [^{11}C]-(R)-PK11195 signal in the frontal lobes and posterior putamen bilaterally correlates with greater subject-rated impairment of motor activities of daily living (voxel threshold p=0.05; cluster significance p<0.001, corrected). The colour stripe indicates Z score.

Table 3.19. Areas of positive correlation between UPDRS part 2 scores and [^{11}C]-(R)-PK11195 BP_{ND}

Z score	MNI coordinates			Area
	x	*y*	*z*	
4.10	-24	2	12	Left putamen
3.86	28	38	-10	Right inferior frontal gyrus pars
3.75	36	12	14	Right insula
3.67	20	-18	-20	Right entorhinal cortex
3.64	8	50	20	Right medial frontal gyrus
3.55	-20	-12	-18	Left entorhinal cortex
3.40	-30	18	14	Left insula

3.30	29	-12	4	Right putamen
3.25	-10	42	20	Left medial frontal gyrus
3.23	-28	-16	8	Left insula
3.18	10	58	-6	Right anterior prefrontal
3.12	-14	58	4	Left anterior prefrontal

3.5.23 Baseline SPM analysis: clinician-rated motor disability (UPDRS part 3)

Clinician-assessed motor disability (rated with the UPDRS part 3) correlated positively with PK uptake in the posterior putamen bilaterally, and in the frontal and right temporal lobes (figure 3.25; table 3.20).

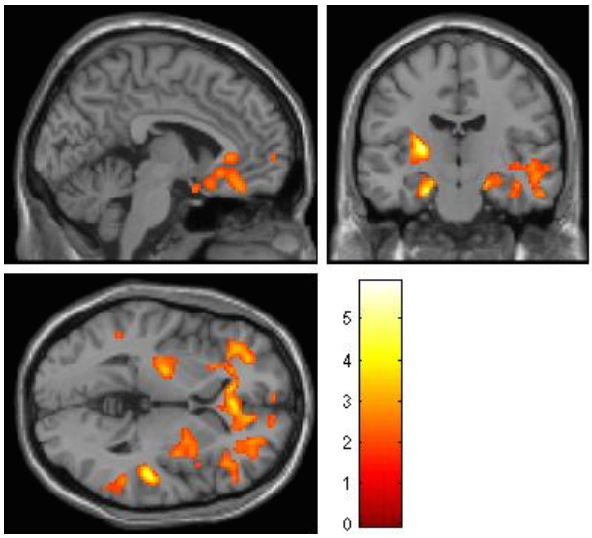


Figure 3.25. Positive correlation between baseline [^{11}C]-(R)-PK11195 BP_{ND} and UPDRS part 3 scores. Statistical parametric map (SPM) showing [^{11}C]-(R)-PK11195 uptake in the frontal lobes, right temporal lobe and posterior putamen bilaterally (arrows) correlates with greater clinician-rated motor disability (voxel threshold p=0.05; cluster significance p<0.001, corrected). The colour stripe indicates Z score

Table 3.20 Areas of positive correlation between UPDRS part 3 scores and [^{11}C]-(R)-PK11195 BP_{ND}

	MNI coordinates			Area
Z score	*x*	*y*	*z*	
4.12	-24	-14	6	Left putamen
3.57	50	-26	2	Right superior temporal gyrus

3.49	-22	-16	-22	Left parahippocampal gyrus
3.49	-12	32	-2	Anterior cingulate
3.39	-22	36	24	Left medial frontal gyrus
3.27	18	32	18	Anterior cingulate
3.26	-11	6	10	Left putamen
3.20	-40	2	34	Left inferior frontal gyrus
3.19	-20	30	24	Anterior cingulate
3.17	-36	40	-4	Left middle frontal gyrus

Follow up [^{11}C]-(R)-PK11195 imaging

Region of interest analysis

3.5.24 Follow up ROI analysis: controls v PD subjects

Two subjects withdrew from the study after baseline scanning and clinical assessment. The remaining 19 subjects underwent follow up [^{11}C]-(R)-PK11195 PET imaging and clinical evaluation at a mean interval of 21.4 months. The follow up [^{11}C]-(R)-PK11195 PD dataset was compared with a set of controls obtained with the same scanner. Significant increases in [^{11}C]-(R)-PK11195 BP_{ND} in PD subjects compared to controls was found in anterior cingulate, posterior cingulate, striatum, putamen, frontal, temporal, parietal and occipital cortex and at whole brain level (table 3.21).

Table 3.21. Regional [^{11}C]-(R)-PK11195 Binding Potentials (mean ± standard deviation) in healthy controls and Parkinson's disease subjects

	Controls (n=6)	**PD (n=19)**
Anterior cingulate	0.1285 ± 0.0134	0.1680 ± 0.0449*
Posterior cingulate	0.1623 ± 0.0179	0.2103 ± 0.0399*
Thalamus	0.3635 ± 0.0433	0.3987 ± 0.0807
Striatum	0.2007 ± 0.0365	0.2572 ± 0.0636*
Caudate	0.1403 ± 0.0435	0.1434 ± 0.0443
Putamen	0.2263 ± 0.0352	0.2901 ± 0.0676*
Globus pallidus	0.2838 ± 0.0366	0.3320 ± 0.0897
Frontal lobe	0.1317 ± 0.0185	0.1992 ± 0.0661**
Insula	0.1740 ± 0.0326	0.2004 ± 0.0512
Temporal lobe	0.1417 ± 0.0225	0.2007 ± 0.0499**
Parietal lobe	0.1233 ± 0.0199	0.1646 ± 0.0367**
Occipital lobe	0.1525 ± 0.0275	0.2063 ± 0.0473**
Brainstem	0.3273 ± 0.0343	0.3088 ± 0.0756
Whole brain	0.1445 ± 0.0199	0.1926 ± 0.0389**

Mann-Whitney U test: ** $p<0.01$; * $p<0.05$.

Clinical correlation

3.5.25 Follow up ROI analysis: disease duration

At follow up imaging, disease duration correlated with [^{11}C]-(R)-PK11195 BP_{ND} in the striatum (**ρ**=0.482, p=0.037; figure 3.26).

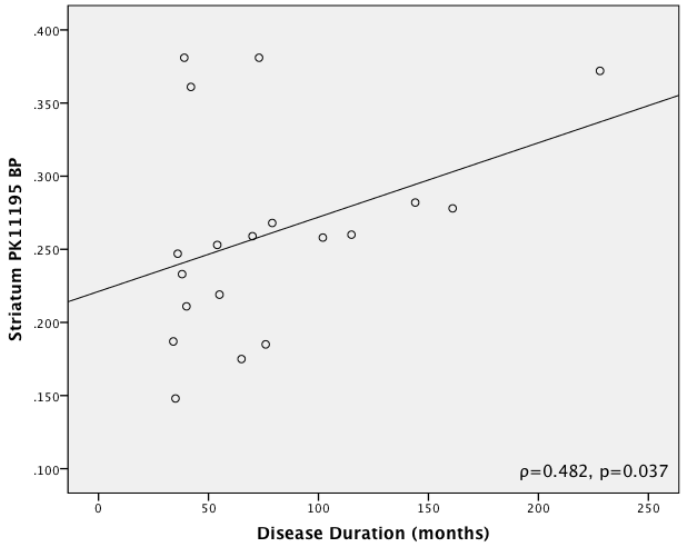


Figure 3.26. Correlation between striatal [^{11}C]-(R)-PK11195 BP_{ND} and disease duration.

3.5.26 Follow up ROI analysis: Montréal Cognitive Assessment (MoCA)

An inverse correlation was found between performance on the Montréal Cognitive Assessment and [^{11}]-(R)-PK11195 BP_{ND} in the globus pallidus (**ρ** = -0.543, p=0.008, figure 3.27) and striatum (**ρ** = -0.426, p=0.035, figure 3.28).

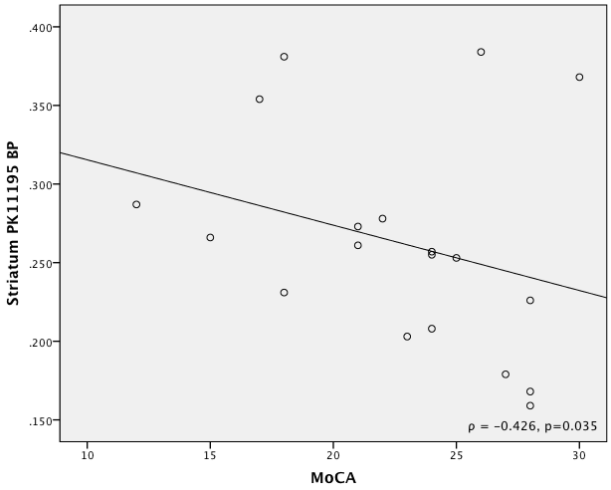


Figure 3.27. Correlation between striatal [^{11}C]-(R)-PK11195 BP_{ND} and Montréal Cognitive Examination (MoCA) scores.

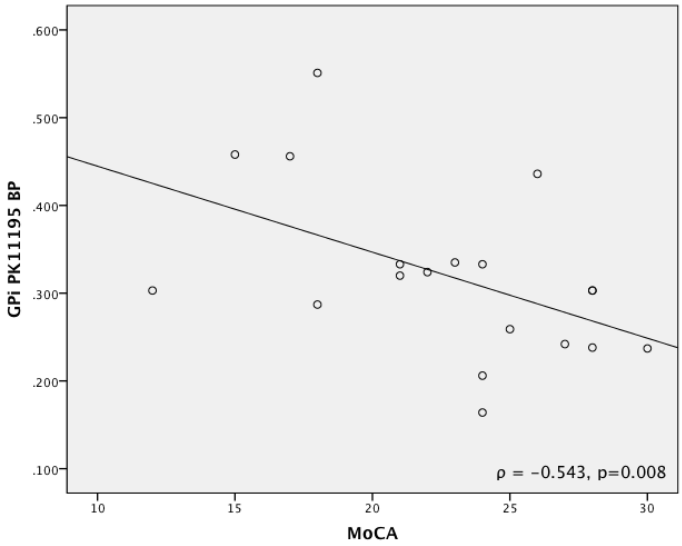


Figure 3.28. Correlation between globus pallidus [^{11}C]-(R)-PK11195 BP_{ND} and Montréal Cognitive Examination (MoCA) scores.

3.5.27 Follow up ROI analysis: Addenbrooke's Cognitive Assessment (ACE)

A negative correlation was seen between [^{11}C]-(R)-PK11195 BP_{ND} in the globus pallidus and performance on the Addenbrooke's cognitive examination (ACE, **ρ** = -0.607, p=0.003, figure 3.29); a negative relationship was also found between globus pallidus PK11195 BP_{ND} and the verbal fluency (**ρ** = -0.423, p=0.036), language (**ρ** = -0.506, p=0.013) and memory (**ρ** = -0.700, p<0.001) subscales of the ACE (figures 3.30-3.32).

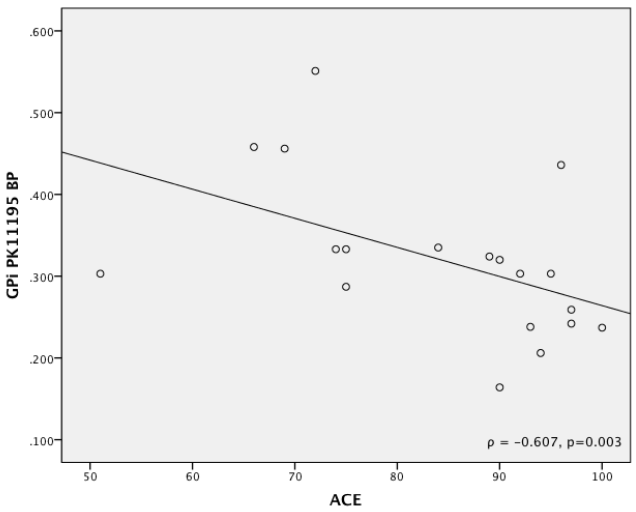


Figure 3.29. Correlation between globus pallidus [^{11}C]-(R)-PK11195 BP_{ND} and

Addenbrooke's Cognitive Examination (ACE) scores.

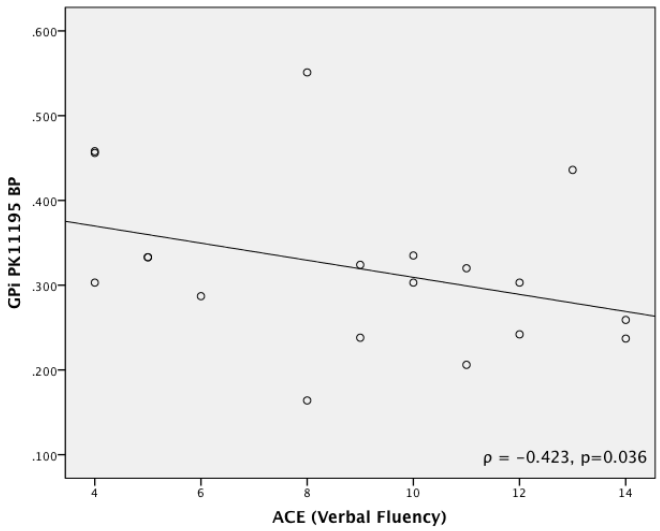


Figure 3.30. Correlation between globus pallidus [^{11}C]-(R)-PK11195 BP_{ND} and Addenbrooke's Cognitive Examination (ACE) verbal fluency sub-scores.

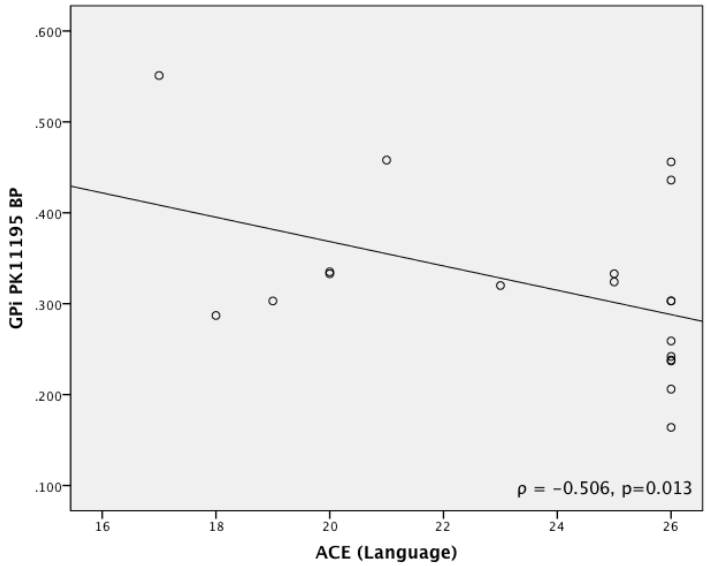


Figure 3.31. Correlation between globus pallidus [^{11}C]-(R)-PK11195 BP_{ND} and Addenbrooke's Cognitive Examination (ACE) language sub-scores.

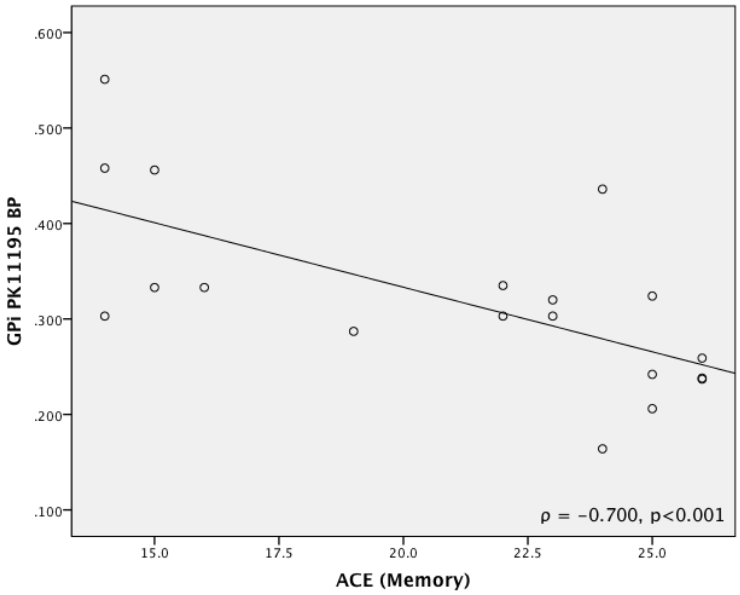


Figure 3.32. Correlation between globus pallidus [^{11}C]-(R)-PK11195 BP_{ND} and Addenbrooke's Cognitive Examination (ACE) memory sub-scores.

3.5.28 Follow up ROI analysis: depression (GDS-15)

A positive correlation was found between self-rated depression (GDS-15) scores and [^{11}C]-(R)-PK11195 BP_{ND} in the brainstem (**ρ**=0.571, p=0.013; figure 3.33) and at the whole brain level (**ρ**=0.410, p=0.045; figure 3.33).

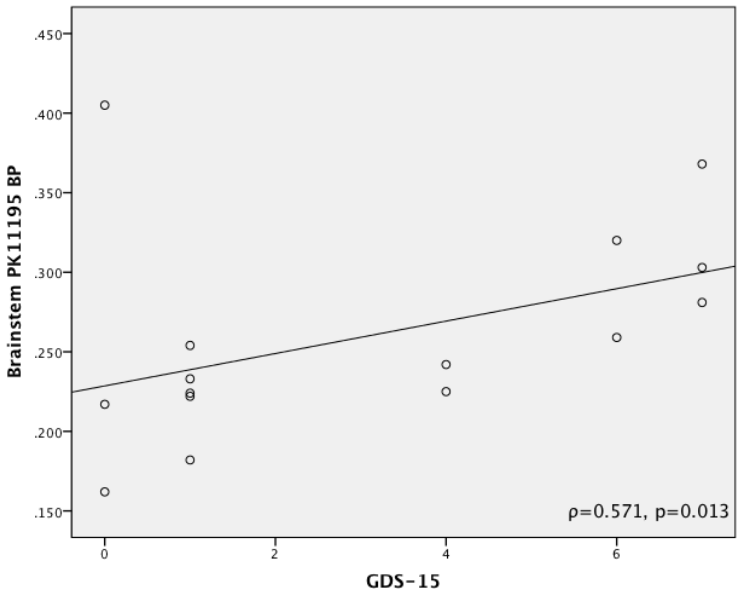


Figure 3.33. Correlation between brainstem [^{11}C]-(R)-PK11195 BP_{ND} and self-rated

depression (GDS-15) scores.

4.5.29 Follow up ROI analysis: semantic fluency

Semantic fluency scores correlated inversely with PK11195 BP_{ND} in the globus pallidus (**ρ**=-0.462 p=0.023, figure 3.34).

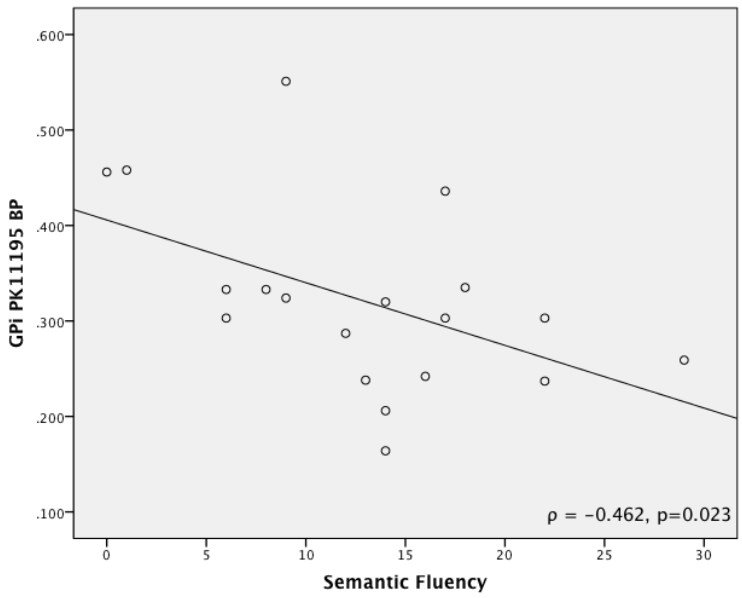


Figure 3.34. Correlation between globus pallidus [^{11}C]-(R)-PK11195 BP_{ND} and semantic fluency.

3.5.30 Follow up ROI analysis: quality of life (PDQ-39)

At follow up assessment, PDQ-39 scores correlated with whole brain [^{11}C]-(R)-PK11195 BP_{ND} and with regional [^{11}C]-(R)-PK11195 uptake in brainstem, striatum, thalamus, globus pallidus, insula, and frontal, temporal, parietal and occipital lobes (table 3.22; Appendix, figures A48-57). Impaired activities of daily living (ADL) correlated with [^{11}C]-(R)-PK11195 BP_{ND} at whole brain level, and in the brainstem, striatum, caudate, putamen, thalamus, globus pallidus, insula, and frontal, temporal, parietal and occipital cortex (table 3.22; Appendix, figures A58-68). Mobility impairment correlated with [^{11}C]-(R)-PK11195 BP_{ND} in whole brain, brainstem, striatum, caudate, thalamus, insula, and frontal, temporal, parietal lobes (table 3.22;

Appendix, figures A69-75). Subjective cognitive difficulties correlated with [^{11}C]-(R)-PK11195 BP_{ND} in whole brain, brainstem, globus pallidus, insula, and frontal cortex (table 3.22; Appendix, figures A76-80). No significant association between regional [^{11}C]-(R)-PK11195 BP_{ND} and subjective communication disorder, social impairment or stigmatisation was found. Greater impairment to emotional wellbeing correlated with [^{11}C]-(R)-PK11195 BP_{ND} at whole brain level, and in the brainstem, striatum, thalamus, insula and temporal lobe (table 3.22; Appendix, figures A81-86). Bodily discomfort scores correlated positively with [^{11}C]-(R)-PK11195 BP_{ND} in brainstem, thalamus, putamen, thalamus, globus pallidus, insula, and frontal, temporal, parietal and occipital cortex (table 3.22; Appendix, figures A87-95).

Table 3.22. Correlation between regional [^{11}C]-PK11195 BP_{ND} and PDQ-39 total and sub-domain scores (Spearman rank coefficients) at follow up

	PDQ-39	ADL	Mobility	Cognition	Communication	Emotion	Social	Stigma	Bodily discomfort
Anterior	0.294	0.305	0.426	0.224	-0.201	0.259	-0.289	0.086	0.214
Posterior	0.271	0.417	0.208	0.222	-0.202	0.283	-0.161	-0.096	0.134
Thalamus	0.732***	0.781***	0.523*	0.502*	0.220	0.751***	-0.035	0.079	0.660**
Striatum	0.699***	0.723***	0.608**	0.372	-0.204	0.619**	-0.140	0.240	0.603**
Caudate	0.452*	0.462*	0.556*	0.100	0.017	0.311	-0.221	-0.077	0.313
Putamen	0.412	0.545*	0.377	0.247	0.017	0.384	-0.157	-0.076	0.462*
Globus	0.600*	0.664**	0.395	0.517*	0.005	0.198	0.090	0.156	0.554*
Frontal lobe	0.614**	0.549*	0.586**	0.427*	-0.032	0.410	-0.004	0.215	0.560*
Insula	0.614**	0.736***	0.492*	0.462*	0.040	0.567*	-0.182	0.033	0.509*
Temporal	0.700***	0.796***	0.550*	0.395	-0.003	0.498*	-0.053	0.197	0.537*
Parietal lobe	0.621**	0.647**	0.594**	0.384	-0.003	0.368	0.066	-0.035	0.678*
Occipital	0.493*	0.604**	0.324	0.224	-0.063	0.268	-0.205	-0.070	0.504*
Brainstem	0.780***	0.841***	0.645**	0.562*	0.016	0.801***	0.113	0.060	0.856***
Whole brain	0.642*	0.703***	0.538*	0.462*	0.159	0.460*	0.070	0.261	0.424

Spearman Rank correlation coefficient: *** p<0.001; ** p <0.01; * p<0.05.

4.5.31 Follow up ROI analysis: non-motor symptom scale (NMSS)

No correlation was found between regional [^{11}C]-(R)-PK11195 BP_{ND} and NMSS scores.

Follow up SPM analysis

3.5.32 Follow up SPM analysis: disease duration

An inverse correlation was found between [^{11}C]-(R)-PK11195 uptake in the putamen and frontal lobes bilaterally and disease duration (figure 3.35, table 3.23).

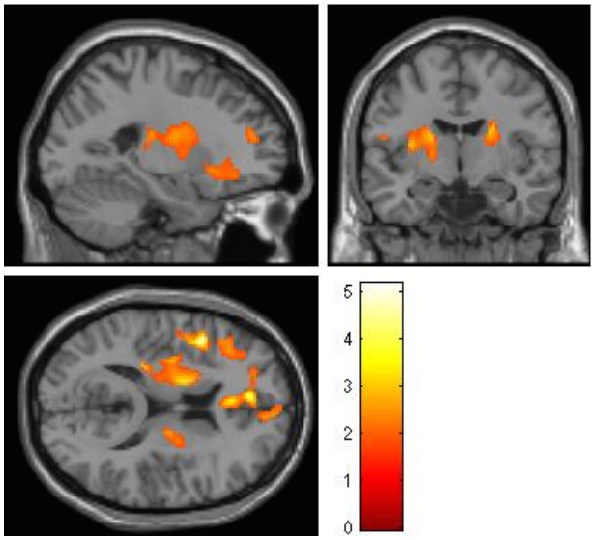


Figure 3.35. Inverse correlation between follow up [^{11}C]-(R)-PK11195 BP_{ND} and disease duration. Statistical parametric map (SPM) showing [^{11}C]-(R)-PK11195 uptake in the putamena and frontal lobes correlates shorter disease duration (voxel threshold p=0.05; cluster significance p<0.001, corrected). The colour stripe indicates *Z* score.

Table 3.23. Areas of inverse correlation between [^{11}C]-(R)-PK11195 BP_{ND} and disease duration

	MNI coordinates			Area
Z score	*x*	*x*	*z*	
3.96	-46	12	14	Left inferior frontal gyrus
3.70	-42	16	34	Left dorsolateral prefrontal cortex
3.48	-6	46	12	Anterior cingulate
3.39	-38	18	30	Left middle frontal gyrus
3.22	-34	42	32	Left middle frontal gyrus
3.09	34	18	30	Right insula
2.95	-34	40	20	Left middle frontal gyrus
2.89	-24	-5	16	Left putamen
2.89	6	46	4	Anterior cingulate
2.83	-16	0	12	Left putamen
2.82	-46	32	10	Left inferior frontal gyrus

3.5.33 Follow up SPM analysis: MMSE

An inverse correlation was found between [^{11}C]-(R)-PK11195 binding in the anterior cingulate and caudate bilaterally and MMSE scores (figure 3.36, table 3.24).

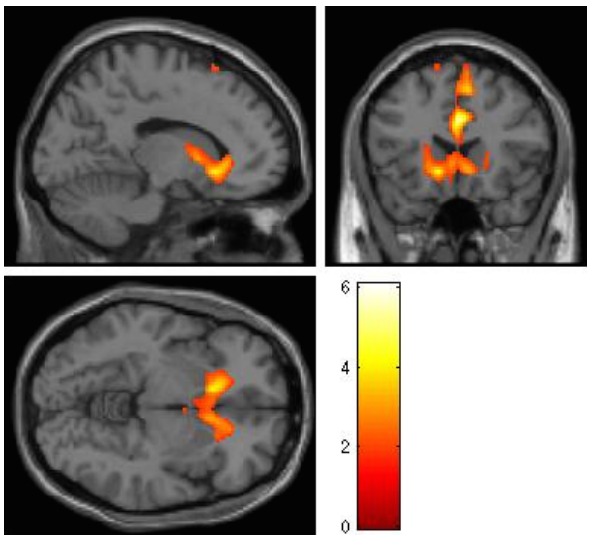


Figure 3.36. Inverse correlation between follow up [^{11}C]-(R)-PK11195 BP_{ND} and MMSE scores. Statistical parametric map (SPM) showing [^{11}C]-(R)-PK11195 uptake in the caudate bilaterally and anterior cingulate correlates with greater global cognitive impairment (voxel threshold p=0.05; cluster significance p<0.01, corrected). The colour stripe indicates Z score.

Table 3.24. Areas of inverse correlation between [^{11}C]-(R)-PK11195 BP_{ND} and MMSE scores

	MNI coordinates			Area
Z score	*x*	*y*	*z*	
4.37	4	24	30	Anterior cingulate
3.84	0	34	10	Anterior cingulate
3.69	0	24	20	Corpus callosum
3.35	-12	20	-6	Left caudate
3.17	4	2	42	Anterior cingulate
3.07	6	2	46	Anterior cingulate
3.04	6	24	56	Right superior frontal gyrus
3.04	12	44	8	Anterior cingulate
3.01	9	22	0	Right caudate
2.97	-4	58	20	Right anterior prefrontal

2.87	0	58	22	Left superior mediofrontal
2.68	6	58	20	Right medial frontal gyrus

3.5.34 Follow up SPM analysis: subject-rated motor disability (UPDRS part 2)

A positive correlation was found between UPDRS part 2 scores and [^{11}C]-(R)-PK11195 in posterior putamen, thalamus and globus pallidus bilaterally (figure 3.37, table 3.25).

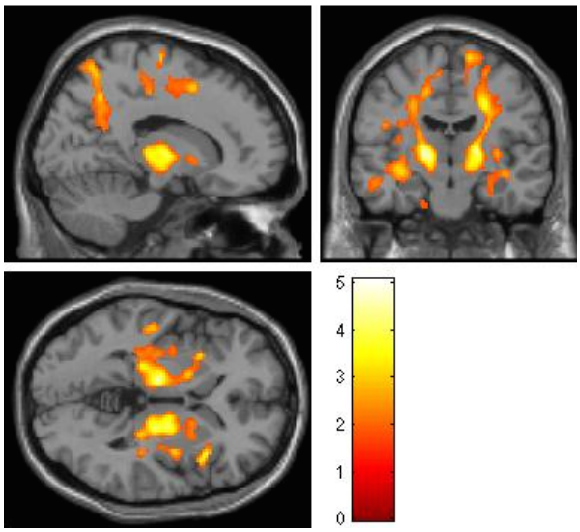


Figure 3.37. Positive correlation between follow up [^{11}C]-(R)-PK11195 BP_{ND} and UPDRS part 2 scores. Statistical parametric map (SPM) showing [^{11}C]-(R)-PK11195 uptake in the left posterior putamen (arrow) correlates with greater subject-rated impairment of motor activities of daily living (voxel threshold p=0.05; cluster significance p<0.001, corrected). The colour stripe indicates Z score.

Table 3.25. Areas of positive correlation between [^{11}C]-(R)-PK11195 BP_{ND} and UPDRS part 2 scores

	MNI coordinates			Area
Z score	*x*	*y*	*z*	
3.86	-16	-16	4	Left thalamus
3.37	-18	6	-6	Left putamen
3.35	-32	14	2	Left insula

3.34	-56	-32	36	Left supramarginal gyrus
3.24	-34	-22	-6	Left insula
3.13	-16	-20	50	Left medial frontal gyrus
3.09	-48	-46	56	Left supramarginal gyrus
3.03	-58	-22	18	Left postcentral gyrus
3.56	20	-16	6	Right thalamus
3.24	22	-26	58	Right primary motor cortex
3.23	14	10	52	Dorsal cingulate
3.17	28	-10	36	Right middle frontal gyrus
3.11	38	18	0	Right insula
2.98	38	-6	10	Right middle temporal gyrus
2.92	36	-26	38	Right postcentral gyrus
2.72	14	-14	72	Right premotor cortex
2.68	38	-4	2	Right insula
2.51	34	-22	46	Right precentral gyrus

3.5.35 Follow up SPM analysis: physician-rated motor disability (UPDRS part 3)

Greater physician-rated motor disability, assessed with the UPDRS part 3, correlated positively with [^{11}C]-(R)-PK11195 binding in the right frontal lobe, insula and posterior putamen (figure 3.38, table 3.26).

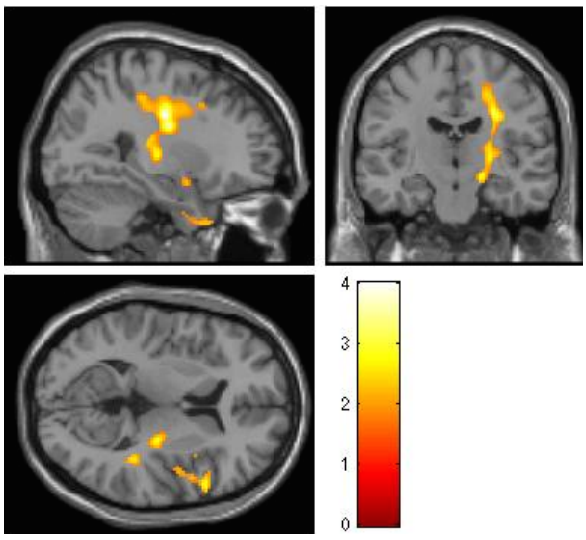


Figure 3.38. Positive correlation between follow up [^{11}C]-(R)-PK11195 BP_{ND} and UPDRS part 3 scores. Statistical parametric map (SPM) showing [^{11}C]-(R)-PK11195 uptake in the right frontal lobe, insula and right posterior putamen (arrow) correlates with greater clinician-rated motor disability (voxel threshold p=0.05; cluster significance p<0.05, corrected). The colour stripe indicates Z score.

Table 3.26. Areas of positive correlation between [^{11}C]-(R)-PK11195 BP_{ND} and UPDRS part 3 scores

Z score	MNI coordinates			Area
	x	*y*	*z*	
3.31	28	-14	34	Right inferior temporal gyrus
3.30	54	10	2	Right insula
3.29	26	-10	26	Right superior frontal gyrus

3.5.36 Follow up SPM analysis: somnolence

Epworth Somnolence Scale (ESS) scores correlated positively with diffuse [^{11}C]-(R)-PK11195 uptake (figure 3.39, table 3.27).

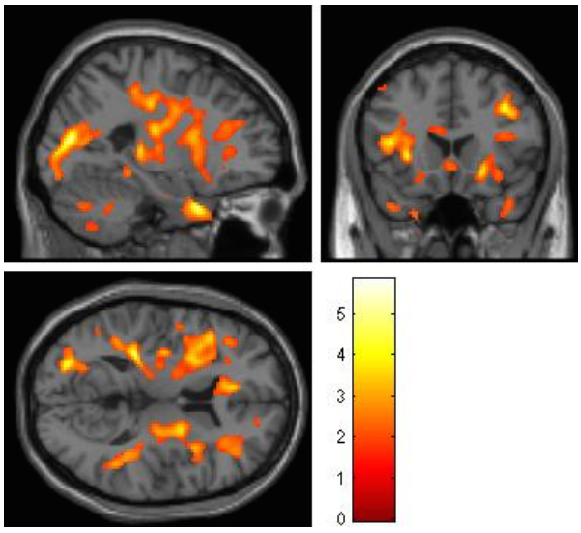


Figure 3.39. Positive correlation between follow up [^{11}C]-(R)-PK11195 BP_{ND} and the daytime somnolence scores (Epworth Sleepiness Scale). Statistical parametric map (SPM) showing diffuse cortical [^{11}C]-(R)-PK11195 uptake correlates with greater self-rated somnolence (voxel threshold p=0.05; cluster significance p<0.001, corrected). The colour stripe indicates Z score.

Table 3.27. Areas of positive correlation between [^{11}C]-(R)-PK11195 BP_{ND} and somnolence (ESS) scores

Z score	MNI coordinates			Area
	x	*y*	*z*	
4.15	10	-44	-40	Pons
3.83	-24	-78	14	Left cuneus
3.75	-24	10	-34	Left temporal pole
3.71	-54	-22	-2	Left superior temporal gyrus
3.57	-52	-2	28	Left precentral gyrus
3.51	0	-34	-36	Pons
3.36	-32	6	-44	Left middle temporal gyrus
4.02	38	18	38	Right middle frontal gyrus
3.57	52	-6	-20	Right middle temporal gyrus
3.44	38	-64	32	Right angular gyrus
3.36	30	-12	-18	Right hippocampus
3.17	38	6	-42	Right middle temporal gyrus
3.00	34	10	12	Right insula
2.98	20	0	10	Right putamen
2.90	30	-20	52	Right precentral gyrus

3.5.37 Follow up SPM analysis: non-motor symptom scale (NMSS)

Greater overall burden of non-motor symptoms, rated with the non-motor symptom scale (NMSS), correlated with cingulate and right hemispheric neocortical and putamenal [^{11}C]-(R)-PK11195 binding (figure 3.40, table 3.28).

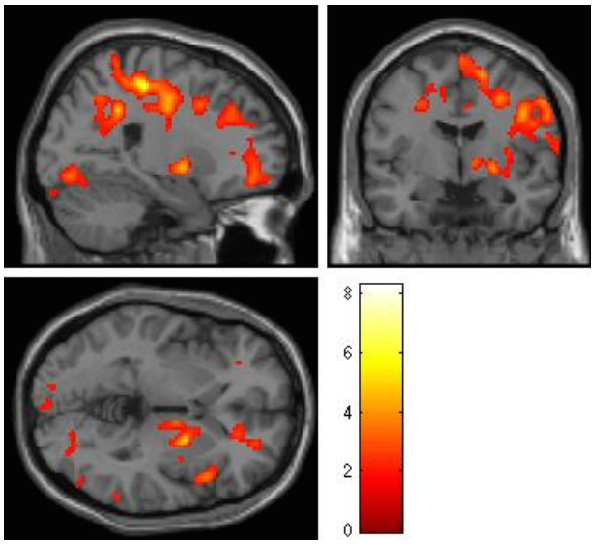


Figure 3.40. Positive correlation between follow up [^{11}C]-(R)-PK11195 BP_{ND} and the non-motor symptom scale (NMSS) scores. Statistical parametric map (SPM) showing [^{11}C]-(R)-PK11195 uptake in the right hemispheric neocortex and putamen correlates with greater NMSS scores (voxel threshold p=0.05; cluster significance p<0.001, corrected). The colour stripe indicates Z score.

Table 3.28. Areas of positive correlation between [^{11}C]-(R)-PK11195 BP_{ND} and non-motor symptom scale (NMSS) scores

Z score	MNI coordinates			Area
	x	*y*	*z*	
4.69	66	-48	24	Right supramarginal gyrus
4.34	26	-28	52	Right primary motor cortex
4.32	34	-24	48	Right postcentral gyrus
4.03	54	-62	28	Right angular gyrus
4.02	52	-58	32	Right supramarginal gyrus
3.94	12	4	62	Right superior frontal gyrus
3.83	50	-74	-16	Right middle occipital gyrus
3.71	42	-8	38	Right premotor cortex
3.69	28	-14	48	Right middle frontal gyrus
3.68	-12	-56	14	Posterior cingulate
3.66	-24	-22	56	Left precentral gyrus
3.61	22	0	-2	Right putamen

3.5.38 Follow up SPM analysis: quality of life (PDQ-39)

At follow up, greater impairment in quality of life, rated with the PDQ-39, correlated with [^{11}C]-(R)-PK11195 uptake, mainly in the fronto-temporal cortex and basal ganglia (figure 3.41, table 3.29).

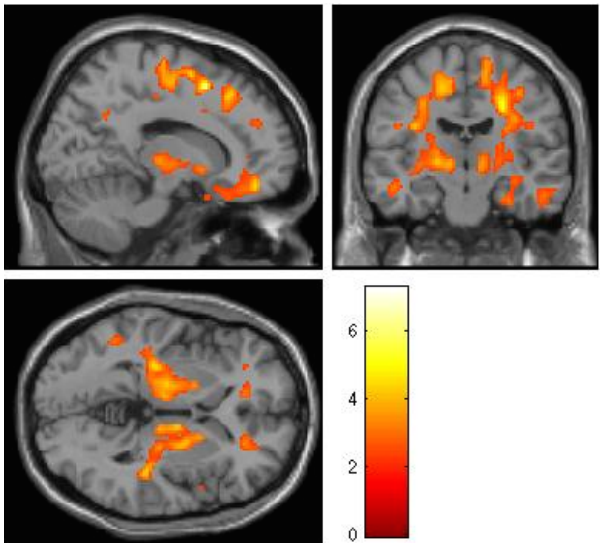


Figure 3.41. Positive correlation between follow up [^{11}C]-(R)-PK11195 BP_{ND} and the PDQ-39 scores. Statistical parametric map (SPM) showing PDQ-39 scores correlated with [^{11}C]-(R)-PK11195 uptake predominantly in fronto-temporal cortex and basal ganglia (voxel threshold p=0.05; cluster significance p<0.001, corrected). The colour stripe indicates Z score.

Table 3.29. Areas of positive correlation between [^{11}C]-(R)-PK11195 BP_{ND} and PDQ-39 scores

	MNI coordinates			
Z score	*x*	*y*	*z*	Area
4.60	-48	-52	-14	Left middle temporal gyrus
4.09	-10	-10	58	Left premotor cortex
3.91	-32	-34	44	Left inferior parietal lobule
3.58	-16	-16	0	Left thalamus
3.57	-30	-20	30	Left postcentral gyrus
3.57	-30	-15	1	Left putamen
3.54	-16	2	56	Left premotor cortex
3.47	-30	-28	32	Left supramarginal gyrus

3.44	-21	-11	-4	Left globus pallidus
3.44	-40	-52	28	Left supramarginal gyrus
3.41	-56	-30	-16	Left middle temporal gyrus
3.38	-34	-18	26	Left supramarginal gyrus
3.37	-42	-66	-12	Left fusiform gyrus
3.32	-22	-22	60	Left precentral gyrus
4.20	14	12	52	Right medial frontal gyrus
4.12	28	-12	34	Right inferior frontal gyrus
4.03	48	4	16	Right insula
3.89	26	-14	42	Right primary motor cortex
3.79	23	-8	-4	Right globus pallidus
3.76	22	-1	-4	Right putamen
3.64	48	-8	20	Right premotor cortex
3.61	18	-56	44	Right precuneus
3.48	16	0	60	Right superior frontal gyrus
3.44	26	8	38	Right dorsolateral prefrontal cortex
3.44	38	-40	28	Right inferior parietal lobule
3.36	14	28	46	Right superior frontal gyrus

3.5.39 Follow up SPM analysis: PDQ-39 ADL domain

Subject-rated impairment in activities of daily living, rated with the ADL sub-score of the PDQ-39, correlated with [^{11}C]-(R)-PK11195 uptake predominantly in fronto-temporal cortex and basal ganglia, but also involving the midbrain and pons (figure 3.42, table 3.30).

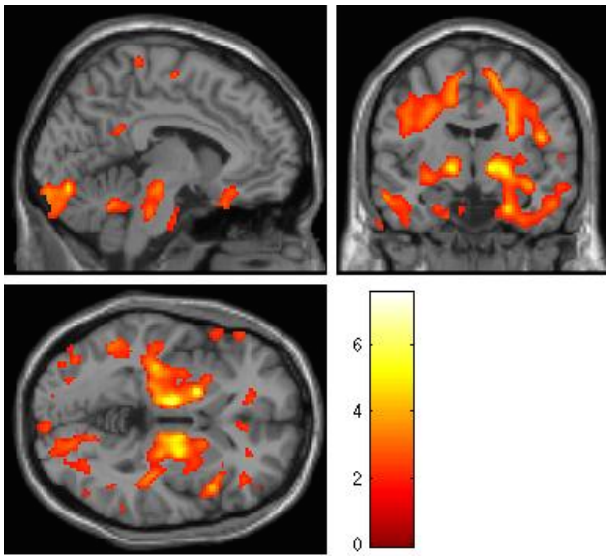


Figure 3.42. Positive correlation between follow up [^{11}C]-(R)-PK11195 BP_{ND} and PDQ-39 impaired activities of daily living (ADL) scores. Statistical parametric map (SPM) showing [^{11}C]-(R)-PK11195 uptake in the fronto-temporal cortex, basal ganglia and brainstem correlates with greater PDQ-39 ADL scores (voxel threshold p=0.05; cluster significance p<0.001, corrected). The colour stripe indicates Z score.

Table 3.30. Areas of positive correlation between [^{11}C]-(R)-PK11195 BP_{ND} and PDQ-39 ADL scores

Z score	MNI coordinates			Area
	x	*y*	*z*	
4.69	-50	-32	-18	Left middle temporal gyrus
4.37	34	-38	-18	Right fusiform gyrus
4.22	-18	6	-4	Left putamen
4.16	-12	-20	50	Left globus pallidus
4.12	-12	-12	-2	Left subthalamic nucleus
4.03	46	16	2	Right inferior gyrus
3.93	14	-8	0	Right globus pallidus
3.69	-36	-44	12	Left superior temporal gyrus
3.67	24	1	0	Right putamen
3.64	-32	-28	30	Left superior parietal lobule
3.64	12	30	46	Right superior frontal gyrus
3.63	2	-24	-24	Midbrain
3.63	20	-92	-20	Right fusiform gyrus

3.5.40 Follow up SPM analysis: PDQ-39 Mobility domain

Subject-rated impaired mobility, rated with the PDQ-39 mobility sub-score, correlated with [^{11}C]-(R)-PK11195 binding in fronto-temporal cortex, basal ganglia, midbrain and pons (figure 3.43, table 3.31).

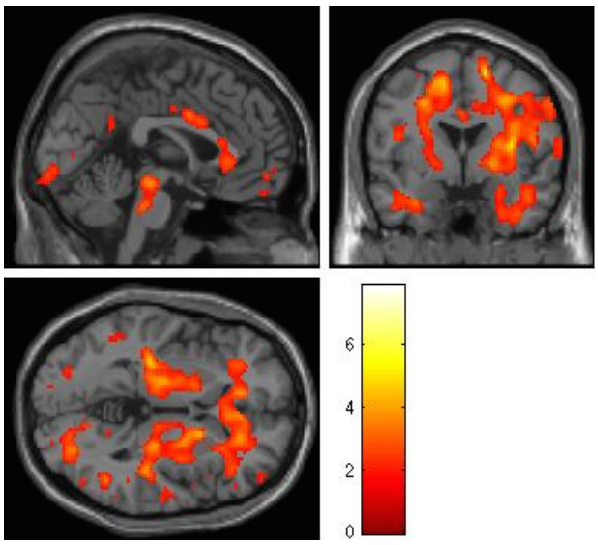


Figure 3.43. Positive correlation between follow up [^{11}C]-(R)-PK11195 BP_{ND} and PDQ-39 impaired mobility scores. Statistical parametric map (SPM) showing [^{11}C]-(R)-PK11195 uptake predominantly in frontal and temporal lobes, basal ganglia and brainstem correlates with greater PDQ-39 mobility scores (voxel threshold p=0.05; cluster significance p<0.001, corrected). The colour stripe indicates Z score.

Table 3.31. Areas of positive correlation between [^{11}C]-(R)-PK11195 BP_{ND} and PDQ-39 mobility scores

	MNI coordinates			
Z score	*X*	*y*	*z*	Area
4.80	34	-24	48	Right postcentral gyrus
4.70	24	-28	52	Right primary motor cortex
4.42	38	-24	42	Right primary somatosensory cortex
4.35	18	-30	58	Right primary motor cortex
4.16	25	-13	1	Right globus pallidus
4.15	66	-50	24	Right supramarginal gyrus
4.14	-17	-11	5	Left thalamus

4.07	23	2	2	Right putamen
4.06	-22	-42	54	Left primary somatosensory cortex
4.06	-28	-46	44	Left inferior parietal lobule
4.03	-12	-60	34	Left precuneus
3.97	20	-44	42	Right precuneus
3.96	2	-26	-21	Midbrain
3.95	-16	-58	46	Left precuenus
3.89	12	4	64	Right premotor cortex

3.5.41 Follow up SPM analysis: PDQ-39 emotion domain

Emotional dysfunction, rated with the relevant PDQ-39 sub-score, correlated with [^{11}C]-(R)-PK11195 uptake in temporo-parietal cortex and the right putamen (figure 3.44, table 3.32).

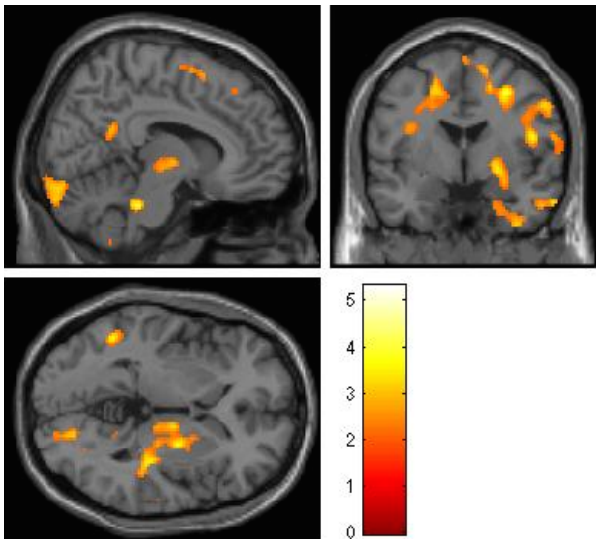


Figure 3.44. Positive correlation between follow up [^{11}C]-(R)-PK11195 BP_{ND} and PDQ-39 impaired emotional wellbeing scores. Statistical parametric map (SPM) showing [^{11}C]-(R)-PK11195 uptake in the correlates with greater subject-rated emotional impairment scores (voxel threshold p=0.05; cluster significance p<0.001, corrected). The colour stripe indicates Z score.

Table 3.32. Areas of positive correlation between [^{11}C]-(R)-PK11195 BP_{ND} and PDQ-39 emotional wellbeing scores

Z score	MNI coordinates			Area
	x	*y*	*z*	
3.87	-44	-54	-14	Left middle temporal gyrus
3.78	44	-48	-20	Right fusiform gyrus
3.74	42	10	-40	Right middle temporal gyrus
3.61	22	-44	38	Right inferior parietal lobule
3.54	12	-34	-30	Pons
3.54	16	-56	32	Right precuneus
3.52	-32	-32	30	Left inferior parietal lobule
3.45	34	-38	-20	Right inferior temporal gyrus
3.45	-40	-54	22	Left superior temporal gyrus
3.41	26	-14	7	Right putamen
3.40	14	-10	54	Right medial frontal gyrus

3.5.42 Follow up SPM analysis: PDQ-39 bodily discomfort domain

Bodily discomfort PDQ-39 scores correlated with widespread neocortical [^{11}C]-(R)-PK11195 binding, especially in the temporal lobes, and also in the basal ganglia and midbrain (figure 3.45, table 3.33).

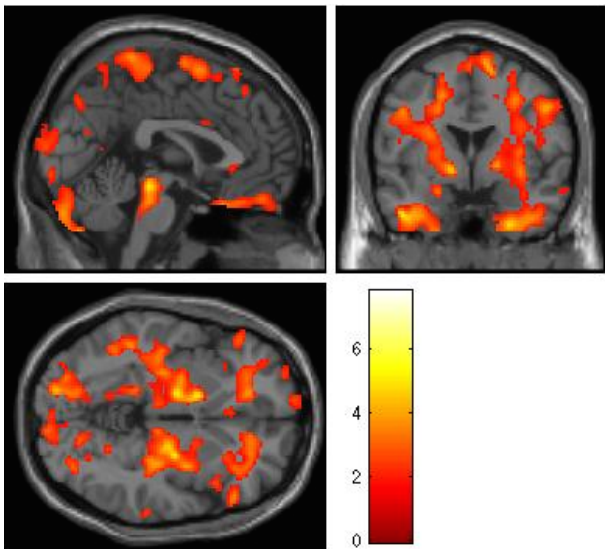


Figure 3.45. Positive correlation between follow up [^{11}C]-(R)-PK11195 BP_{ND} and PDQ-39 bodily discomfort scores. Statistical parametric map (SPM) showing greater subject-rated bodily discomfort scores correlate with [^{11}C]-(R)-PK11195 uptake in the midbrain, basal ganglia and neocortex, especially the temporal lobes (voxel threshold p=0.05; cluster significance p<0.001, corrected). The colour stripe indicates Z score.

Table 3.33. Areas of positive correlation between [^{11}C]-(R)-PK11195 BP_{ND} and PDQ-39 bodily discomfort scores

Z score	MNI coordinates			Area
	x	*y*	*z*	
4.62	32	-30	-14	Right medial temporal lobe
4.19	6	-26	-12	Right middle temporal gyrus
4.18	22	-6	-28	Right perirhinal cortex
4.10	34	-8	4	Right insula
3.92	26	-10	-2	Right globus pallidus
3.81	14	-24	2	Right thalamus
3.80	52	-14	-26	Right inferior temporal gyrus
3.71	-2	-28	-14	Midbrain
3.69	56	-16	-30	Right fusiform gyrus
3.63	32	-16	0	Right putamen
3.55	58	-8	-18	Right middle temporal gyrus
3.47	16	-18	6	Right thalamus
4.57	-8	-82	-14	Left secondary visual cortex
4.42	-14	-86	-14	Left lingual gyrus
4.34	46	-48	-22	Right fusiform gyrus
4.23	12	-92	-12	Right lingual gyrus
4.03	36	-80	-10	Right association visual cortex
4.60	-20	-18	12	Left thalamus
3.96	-14	6	-2	Left globus pallidus
3.91	-22	-8	-28	Left parahippocampal gyrus
3.88	-20	-26	2	Left thalamus
3.73	-46	0	-34	Left middle temporal gyrus
3.73	-18	-10	-2	Left globus pallidus

3.60	-38	-22	-12	Left insula
3.48	-28	-24	-10	Left hippocampus
3.07	-24	-4	-42	Left fusiform gyrus
2.99	-54	-28	-20	Left inferior temporal gyrus

3.5.43 Follow up SPM analysis: depression (GDS-15)

SPM showed a positive correlation between depression scores (GDS-15) and [^{11}C]-(R)-PK11195 in the parietal lobes and right insula (figure 3.46, table 3.34).

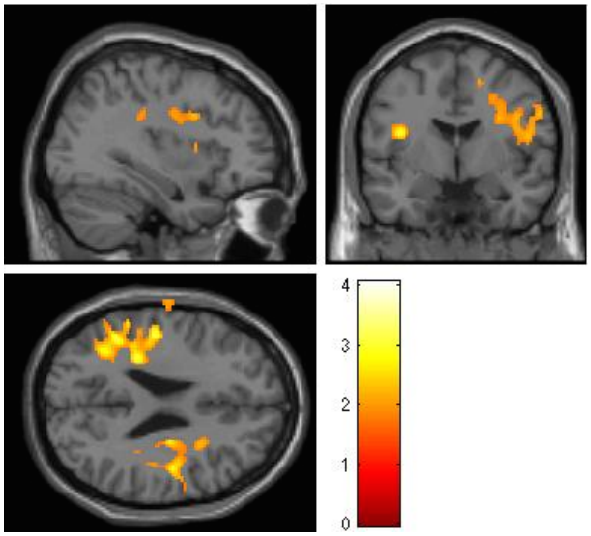


Figure 3.46. Positive correlation between follow up [^{11}C]-(R)-PK11195 BP_{ND} and depression scores (GDS-15). Statistical parametric map (SPM) showing [^{11}C]-(R)-PK11195 uptake in the parietal lobes and right insula correlates with greater subject-rated depression scores (voxel threshold p=0.05; cluster significance p<0.05, corrected). The colour stripe indicates Z score.

Table 3.34. Areas of positive correlation between [^{11}C]-(R)-PK11195 BP_{ND} and GDS-15 scores

Z score	MNI coordinates			Area
	x	*y*	*z*	
3.32	24	-32	36	Cingulate
2.88	14	-56	34	Right precuneus
2.85	28	-10	30	Right precentral gyrus
3.26	-44	-52	12	Left superior temporal gyrus
3.16	-48	-18	24	Left postcentral gyrus
2.89	-44	-46	28	Left inferior parietal lobule

Correlation between [^{11}C]-(R)-PK11195 BP_{ND} and [^{18}F]-FDG

3.5.44 [^{11}C]-(R)-PK11195 BP_{ND} v [^{18}F]-FDG at baseline

A significant negative correlation was found between baseline [^{11}C]-(R)-PK11195 BP_{ND} in the caudate and cerebral metabolic rate of glucose (CMRGlu) in the brainstem (ρ = -0.489, p=0.012; Appendix, figure A96) and thalamus (ρ = -0.472, p=0.015; Appendix, figure A97). An inverse correlation was also observed between [^{11}C]-(R)-PK11195 BP_{ND} in the posterior cingulate and CMRGlu in the occipital lobes (ρ = -0.431, p=0.026; Appendix, figure A98). No correlation was found between [^{11}C]-(R)-PK11195 BP_{ND} and CMRGlu within any given region of interest.

3.5.45 [^{11}C]-(R)-PK11195 BP_{ND} v [^{18}F]-FDG at follow up

At follow up imaging, putamenal [^{11}C]-(R)-PK11195 BP_{ND} correlated inversely with CMRGlu in the putamen (ρ = -0.488, p=0.038; Appendix, figure A99), thalamus (ρ = -0.618, p=0.009; Appendix, figure A100), and in frontal (ρ = -0.481, p=0.041; Appendix, figure A101) and parietal cortex (ρ = -0.473, p=0.044; Appendix, figure A102).

3.6 Discussion

This work confirms the presence of activated microglia in the brainstem, basal ganglia and cortex of non-demented PD subjects, as previously reported by our group and others (Gerhard et al., 2006a). It is, however, the first study to demonstrate in PD that activated microglia correlate with a wide range of motor, cognitive and other non-motor markers of clinical severity.

This study found a correlation between subject and clinician rated motor disability, measured using the UPDRS part 2 and 3 respectively, and [^{11}C]-(R)-PK11195 uptake in cortical and basal ganglia regions involved in the planning and execution of movement. In the ROI analysis, UPDRS part 2 scores, which assess subjective impairment in motor activities of daily living, correlated with baseline [^{11}C]-(R)-PK11195 BP_{ND} in the putamen, insula and at the whole brain level, whilst part 3 of the UPDRS, a measure of clinician-rated motor disability, correlated with [^{11}C]-(R)-PK11195 uptake in the putamen, insula, frontal and temporal lobes, and at whole brain level. Exploratory voxel based analysis using SPM complemented the ROI findings, localising raised frontal lobe and posterior putamen [^{11}C]-(R)-PK11195 signal which correlated with both UPDRS part 2 and 3, and additional temporal lobe signal which correlated with the UPDRS part 3. This is in agreement with pathological (Kish et al., 1988) and functional imaging studies (Brooks et al., 1990; Haapaniemi et al., 2001) demonstrating a relative excess of dorsal putamenal dopaminergic neuron loss in early disease, with preservation of the antero-posterior gradient with progression. Our data demonstrating an association between putamenal [^{11}C]-(R)-PK11195 uptake and UPDRS is in contrast to a Japanese study that reported a correlation between midbrain [^{11}C]-(R)-PK11195 and UPDRS (Ouchi et al., 2005). Recent research, however, indicates that the axon may be a more important target for alpha synuclein pathology in PD (Cheng et al., 2010). Different mechanisms have been demonstrated for somatic apoptosis and Wallerian degeneration in response to local axon injury without neural death (Finn et al., 2000; Raff et al., 2002; Ries et al., 2008). Neuronal loss in the substantia nigra at of PD subjects at autopsy is 60-80 % (Fearnley and Lees, 1991; Pakkenberg et al., 1991), whilst accompanying striatal dopamine depletion is considerably greater at 96-99 % (Kish et al., 1988; Rajput et

al., 2008). Following the discovery of alpha synuclein as the major component of Lewy bodies (Spillantini et al., 1997), and the subsequent exposition of a rostral pathological progression model by Braak et al. in 2003, it is often presumed that somatic aggregation of alpha synuclein leads to centrifugal neurodegeneration. In fact, the Braak group previously reported extensive alpha synuclein pathology in presynaptic "Lewy neurites" (Braak et al., 1999), which has been confirmed by others (Galvin et al., 1999; Duda et al., 2002), and it has since been shown that this presynaptic alpha synuclein pathology, not somatic Lewy bodies, is more closely associated with neurodegeneration (Kramer et al., 2007; Cheng et al., 2010). Further support for the centripetal model comes from studies of cardiac sympathetic denervation in incidental Lewy body disease and PD in which cardiac sympathetic nerve degeneration precedes loss of cell bodies in the paravertebral sympathetic ganglion (Orimo et al., 2005a; Orimo et al., 2008); and from post mortem specimens from subjects at a relatively early stage of clinical disease, where activated microglia are predominantly associated with dopaminergic neurites in the putamen, whilst in those from more advanced cases show a greater association with neurons in the SNc (Sawada et al., 2006).

PET studies of depression in PD have not demonstrated a consistent pattern of neurotransmitter imbalance. Guttman et al. (2007) reported reduced serotonin transporter availability in the midbrain, striatum, and orbitofrontal cortex in PD subjects compared to controls using [^{11}C]-3-amino-4-(2-dimethylaminomethyl-phenylsulfanyl)-benzonitrile ([^{11}C]-DASB). Kim et al. (2003), however, found no difference in serotonin transporter function in Parkinson's disease subjects with or without depression, assessed using [^{123}I]-beta-CIT SPECT, and similarly there was no difference in brainstem serotonin 5HT1A receptor availability between depressed and non-depressed PD patients, measured by [^{11}C]-WAY100635 PET (Doder et al., 2000). More recently, a [^{11}C]-DASB PET study reported relatively raised serotonin transporter concentrations in the raphe nuclei and limbic structures in depressed compared to non-depressed PD subjects, hypothesised to be an inappropriate response to the loss of presynaptic neurons in surviving terminals, which could exacerbate synaptic 5-HT depletion and hence depression (Politis et al., 2010). In the present study, depression severity correlated strongly with baseline [^{11}C]-(R)-PK11195 binding in the brainstem, striatum and throughout the neocortex, and whilst the

relationship was less pronounced at follow up assessment, there was still a significant correlation between depression severity and both brainstem and whole brain [^{11}C]-(R)-PK11195. This suggests that depression is not universally determined by localised neurotransmitter dysfunction, but reflects widespread cortical and subcortical pathology, and this may explain some of the inconsistency in published studies. Since depression can precede the diagnosis of PD, there has been an expectation in the literature that it reflects serotonergic and/or noradrenergic pathology occurring in the pons at Braak stage 2 disease. As the present study demonstrates a correlation between depression and widespread cortical microglial pathology in non-demented PD with both ROI and SPM methods, it seems likely that supratentorial pathology plays a role. In support of this, Kostić et al. (2010) reported greater limbic cortex atrophy in depressed compared to non-depressed PD subjects.

There has also been controversy in the literature as to whether excessive daytime sleepiness (EDS) in PD is driven by underlying pathology, or is a side effect of dopaminergic medication (Gjerstad et al., 2006). Yet since EDS can precede the diagnosis of motor PD (Abbott et al., 2005) and, therefore, exposure to PD drugs, the effect cannot be purely pharmacological. EDS is known to be a risk factor in the development of cognitive decline and dementia (Foley et al., 2001; Merlino et al., 2010; Jaussent et al., 2012). Recently, cortical gray matter atrophy was reported in non-demented PD subjects with high somnolence scores (ESS $\geq$10), but was absent in those with low scores (ESS $\leq$3), suggesting a role for cortical pathology (Kato et al., 2012). In the present study, SPM demonstrated an association between greater daytime somnolence scores and diffuse cortical [^{11}C]-(R)-PK11195 uptake, and this provides further evidence for the role of primary neocortical pathology in EDS in PD before the development of dementia.

Using SPM, impaired visuospatial cognition, demonstrated by poor performance on the visuospatial section of the ACE, correlated with bilateral dorsal parietal lobe [^{11}C]-(R)-PK11195 BP_{ND}. The parietal lobe is critical to visuospatial processing (Marshall and Fink, 2001), and impairment in this domain occurs in PD in the absence of dementia (Uc et al., 2005): the present study suggests that activated microglia associated pathology is relevant to its clinical expression. SPM also localised increased bilateral frontal lobe [^{11}C]-(R)-PK11195 uptake in association

with impairment in both phonemic and semantic fluency, tasks dependent on frontal lobe function. Specific impairment in verbal fluency in the absence of aphasia has been proven to occur in subjects with pure frontal lesions (Chapados and Petrides, 2013).

Baseline region of interest analysis demonstrated a marked correlation between total PDQ-39 quality of life scores and [^{11}C]-(R)-PK11195 uptake at the whole brain level, and with all neocortical and the majority of subcortical regions sampled, including the brainstem and striatum. These findings were confirmed at follow up evaluation. In the SPM analysis, PDQ-39 scores correlated predominantly with frontal and temporal lobe [^{11}C]-(R)-PK11195 BP_{ND} at both baseline and follow up, with additional localisation of thalamic and putamenal signal in the latter. Impaired activities of daily living, assessed with the PDQ-39 ADL domain, correlated with extensive cortical and subcortical [^{11}C]-(R)-PK11195 uptake in the ROI analysis at baseline and follow up, and with diffuse neocortical and especially basal ganglia [^{11}C]-(R)-PK11195 BP_{ND} in the follow up SPM analysis. Baseline PDQ-39 mobility impairment correlated with widespread neocortical and striatal [^{11}C]-(R)-PK11195 uptake in the ROI analysis and with diffuse [^{11}C]-(R)-PK11195 binding in the voxel-wise analysis, whilst at follow up, impaired mobility correlated with widespread neocortical, striatal and ponto-mesencephalic [^{11}C]-(R)-PK11195 BP_{ND}. Whilst these data are broadly in agreement with the UPDRS results discussed above, it is notable that midbrain [^{11}C]-(R)-PK11195 signal correlated with subjective mobility impairment, whilst no correlation was seen between midbrain [^{11}C]-(R)-PK11195 uptake and the UPDRS in the present study. This is in contrast to Ouchi et al. (2005), who reported a correlation between midbrain [^{11}C]-(R)-PK11195 and the UPDRS in early PD. This group used a hypothesis driven region of interest approach, rather than SPM, which does not depend on an *a priori* anatomical hypothesis.

Widespread [^{11}C]-(R)-PK11195 uptake correlated with PDQ-39 impaired emotional wellbeing scores at both baseline and follow up, with the strongest correlation being with the brainstem, a pattern similar to that reported above for subject-reported depression (GDS-15). In this setting, the marked correlation with brainstem [^{11}C]-(R)-PK11195 could be due to disruption of monoaminergic (5-HT and noradenaline) systems, or it may simply reflect worsening of symptoms with disease progression,

since the latter also correlated with brainstem [^{11}C]-(R)-PK11195 BP_{ND}. Whilst it could be argued that the association of GDS-15 depression and PDQ-39 scores with diffuse neocortical [^{11}C]-(R)-PK11195 uptake is also confounded by disease progression, it will be recalled that no correlation between neocortical [^{11}C]-(R)-PK11195 binding and disease duration was found, which argues for a direct role for cortical microglia associated pathology in phenotypic manifestation. Self-reported cognitive impairment correlated with frontal lobe [^{11}C]-(R)-PK11195 uptake at both baseline and interval assessment in the ROI analysis and with frontal lobe [^{11}C]-(R)-PK11195 binding in the baseline SPM analysis, in agreement with the inverse correlation between frontal lobe [^{11}C]-(R)-PK11195 and phonemic fluency. Baseline PDQ-39 communication impairment also correlated with frontal lobe [^{11}C]-(R)-PK11195 in the voxel based analysis. At follow up, correlation with ROI whole brain, brainstem, insula, pallidal and thalamic [^{11}C]-(R)-PK11195 was seen, but not in the SPM analysis, which could be explained if the relevant signal was diffusely distributed. At baseline ROI and SPM analysis, impairment in social function correlated with [^{11}C]-(R)-PK11195 binding in fronto-limbic structures (anterior cingulate, frontal and temporal lobes), regions involved in social cognition (Harmon-Jones and Winkielman, 2007). Furthermore, perceived stigmatisation, which is a form of social cognition, correlated with anterior cingulate, frontal lobe and whole brain [^{11}C]-(R)-PK11195 BP_{ND} at baseline in the voxel-based analysis. Bodily discomfort is a common non-motor symptom in PD, even in the early stages of disease (Duncan et al., 2014). The present study found a correlation between PDQ-39 bodily discomfort scores at baseline and frontal and basal ganglial [^{11}C]-(R)-PK11195 uptake, whilst at follow up there was a strong correlation between diffuse neocortical and subcortical [^{11}C]-(R)-PK11195 signal, including in the brainstem and striatum. This is consistent with the evidence that pain in PD is a consequence of abnormal central “top down” nociceptive input processing (Berardelli et al., 2012; Defazio et al., 2013).

The non-motor symptom scale (NMSS) has been validated in PD and correlates highly with the PDQ-39 (Martinez-Martin et al., 2011). The present study reports a correlation between NMSS scores and [^{11}C]-(R)-PK11195 uptake predominantly in fronto-temporal regions and right putamen in the SPM analysis. This data suggests that the correlation between two clinical instruments for assessing non-motor symptoms is at least partly explained by underlying neuropathology.

It has been known for many years from animal studies that dopamine modulates the function of GABAergic neurons in the globus pallidus (Bergstrom and Walters, 1984; Koshikawa et al., 1990) and dopamine is depleted by 50-80% in the globus pallidus in human PD (Hornykiewicz, 1998; Rajput et al., 2008), potentially affecting the clinical phenotype and response to dopaminergic medication. At follow up imaging, this study reports an inverse correlation between [^{11}C]-(R)-PK11195 uptake in the globus pallidus and cognitive performance using two different instruments (ACE and MoCA), as well as with verbal fluency, memory and language sub-scores of the ACE. There was also a negative correlation between semantic fluency and [^{11}C]-(R)-PK11195 uptake in the globus pallidus and caudate. ROI analysis also revealed an inverse relationship between MoCA scores and [^{11}C]-(R)-PK11195 binding in the caudate. SPM revealed that global cognitive impairment was associated with increased [^{11}C]-(R)-PK11195 binding in the caudate bilaterally and in the anterior cingulate. The existence of a functional topography within the basal ganglia, broadly corresponding to motor, cognitive and affective domains, has been demonstrated in monkeys using invasive tracing methods (Alexander et al., 1990; Hoover and Strick, 1993), and confirmed in human functional imaging studies (Lehéricy et al., 2004; Di Martino et al., 2008): the dorsal putamen is principally concerned with the facilitation of movement; the ventral striatum and head of caudate are more important in motivation and cognition. In PET studies of PD, cognitive dysfunction correlates with dopamine depletion in the caudate (Rinne et al., 2000; Brück et al., 2001; Niethammer et al., 2013).

With SPM analysis, shorter disease duration correlated with [^{11}C]-(R)-PK11195 signal in the putamen and medial basal forebrain, the latter region containing the anterior olfactory nuclei, which is the first cortical structure predicted to be affected by the Braak hypothesis. Region of interest analysis showed a correlation between disease duration and baseline brainstem [^{11}C]-(R)-PK11195 uptake, and at follow-up between disease duration and striatal [^{11}C]-(R)-PK11195. These results can be explained by the early involvement of the nigrostriatal and olfactory systems as predicted by Braak et al., with subsequent progressive accumulation of activated microglia in brainstem and striatum. No statistically significant change in [^{11}C]-(R)-PK11195 uptake was found at follow up assessment, as has been reported by our

group (Gerhard et al., 2006a), although this may be due to a lack of statistical power. Further, the possibility that a difference in sensitivity between the PET cameras used for baseline and follow up imaging may have offset a biological effect cannot be excluded.

Brainstem hypometabolism, assessed with [^{18}F]-FDG, was associated with [^{11}C]-(R)-PK11195 signal in the caudate, which may reflect loss of brainstem cell bodies. At follow-up, putamenal [^{11}C]-(R)-PK11195 uptake correlated with a typical pattern of hypometabolism seen with disease progression, involving the putamen, thalamus and fronto-parietal cortex. PD subjects at higher risk of conversion to dementia based on their phenotype showed raised [^{11}C]-(R)-PK11195 binding predominantly in the dorsal parietal lobes (including the precuneus) and frontal lobes relative to lower risk subjects, which is consistent with published data showing reduced cortical metabolism in the precuneus, occipital and frontal lobes in PD-MCI subjects compared to controls (Pappatà et al., 2011).

In summary, this project has demonstrated for the first time that activated microglial pathology, imaged in non-demented PD subjects *in vivo* using [^{11}C]-(R)-PK11195 PET is widespread and correlates with a broad range of motor, cognitive and other non-motor clinical manifestations. The group of subjects had a wide range of symptomatic duration suggesting that activated microglia are relevant to phenotypic expression throughout the disease. These data from living PD subjects are further consistent with the predications of the Braak hypothesis, which has hitherto rested on extrapolation from necropsy material. Activated microglia imaged using PET therefore appears to be a valid biomarker of the disease. No other putative biomarker identified to date so extensively represents the phenotypic spectrum of the disease.

Chapter 4

Amyloid deposition in Parkinson's disease

4.1 Objectives

1. To image extracellular brain amyloid in Parkinson's disease subjects with and without dementia using [^{11}C]-PIB PET.
2. To measure change in brain amyloid in non-demented Parkinson's disease subjects by interval scanning.
3. To correlate brain amyloid with clinical measurements in motor, cognitive and other non-motor domains, using region of interest and voxel-based analyses.
4. To correlate regional amyloid load and tissue metabolism, assessed with [^{11}C]-PIB and [^{18}F]-FDG respectively.
5. To correlate regional amyloid and activated microglia loads, assessed with [^{11}C]-PIB and [^{11}C]-(R)-PK11195, respectively.

4.2 Summary

[^{11}C]-PIB uptake was elevated throughout the neocortex and in the striatum in the non-demented PD group compared to controls, with a predilection for posterior cortical structures. Interval scanning in the non-demented PD group at two years demonstrated further accumulation of amyloid. [^{11}C]-PIB uptake in the PD dementia group was higher still, with greater involvement of anterior cortical structures. Striatal [^{11}C]-PIB retention was also elevated in the non-demented PD group, and correlated inversely with verbal fluency. Subjective motor disability, impaired verbal fluency, and communication difficulties were associated with frontal lobe [^{11}C]-PIB uptake, suggesting that amyloid may contribute to frontal lobe dysfunction in PD.

4.3 Introduction

4.3.1 Neuropathology

Neurodegenerative diseases, such as Parkinson's disease (PD) and other synucleinopathies, Alzheimer's disease (AD), frontotemporal dementia, Huntington's disease, motor neuron disease and prion disorders, appear to have a common pathologic basis in the form of abnormal protein aggregation. This may take the form of intracellular inclusions such as Lewy Bodies in PD, or extracellular protein aggregates consisting of fibres arranged in a beta-pleated sheet conformation, such as Aβ amyloid (Ross and Poirier, 2004), considered further below.

Aβ amyloid deposition in neurodegenerative disease is traditionally associated with AD, in which it is usually considered the central pathological process ("the amyloid hypothesis"; Hardy and Allsop, 1991). Whilst the histology of "pure" AD, as defined by current consensus criteria, consists of Aβ amyloid plaques and neurofibrillary tangles, the latter containing abnormally phosphorylated tau protein (Hyman et al., 2012), the existence of "mixed" pathology in AD has long been recognised. In 1990, Hansen et al. reported the presence of Lewy body (LB) pathology in 13/33 (36%) of subjects otherwise fulfilling clinical and pathological criteria at the time for AD, designating this the "Lewy Body variant" of AD (LVAD). Clinically this subgroup had a cognitive profile that would today be regarded as typical of dementia with Lewy Bodies (DLB) and PD dementia (PDD), rather than canonical AD, with deficits in attention, fluency, and visuospatial processing, as well as motor features typical of PD, such as facial hypomimia, limb bradykinesia and tremor. Further, there was a similar loss of neurons in the substantia nigra and locus coeruleus to that seen in classical PD. Subsequent larger autopsy series reported an even greater frequency of LB pathology in sporadic AD (43% by Uchikado et al., 2006; 60% by Hamilton, 2000), far in excess of that predicted by chance association, with significant co-localisation of amyloid and LB pathology. Further, cognitive deterioration is faster in cases with dual AD/LB pathology than in "pure" AD (Olichney et al*.,* 1998; Kraybill et al*.,* 2005). The revised consensus criteria for the pathological diagnosis of AD now

acknowledge the frequent co-occurrence and clinical relevance of Lewy body pathology (Hyman et al., 2012; Montine et al., 2012).

As Lewy pathology occurs in and may modulate the phenotype of cases formally classified as AD, evidence also exists for a role for amyloid in canonical Lewy body (LB) disorders. In an autopsy study of 12 PDD subjects, amyloid plaques were highly correlated with Lewy body load (Apaydin et al., 2002). A subsequent series of 21 PDD and DLB cases also reported a correlation between Aβ amyloid and cortical alpha-synuclein load (Pletnikova et al., 2005). In a larger study of 29 DLB and 28 PDD subjects, amyloid load was higher in DLB than PDD subjects, but within the PDD group, amyloid burden correlated inversely with duration of Parkinsonism before dementia, supporting the contention that the operational distinction between DLB and PDD is arbitrary, and cannot be reduced to genuinely discrete pathological entities (Ballard et al., 2006). In a large autopsy series of 56 subjects with non-demented PD, 44 with PDD, and 20 with DLB, cortical amyloid plaque load was lowest in PD without dementia, and highest in DLB (Jellinger and Attems, 2008a). In a clinico-pathological study of 242 non-demented PD subjects, non-tremor dominant phenotype, a known risk factor for PDD, was associated with a higher burden of Lewy body and amyloid pathology and greater cognitive impairment compared to tremor dominant cases (Selikhova et al., 2009). Compta et al. (2011) reported a clinico-pathological series of 27 non-demented PD and 29 PDD cases in which cortical and striatal amyloid, tau, Lewy body and Lewy neurite scores were all significantly greater in the PDD group. Alpha synuclein, tau and amyloid pathologies were all correlated, with a model incorporating all variables being a better predictor of dementia than the severity of any individual pathology; cortical amyloid load exhibited a stronger association with cognitive impairment than tau or synuclein. Furthermore, the presence of amyloid pathology appears to be associated with shorter survival compared to cases with pure synucleinopathy (Kotzbauer et al., 2012). Alpha synuclein and tau co-pathology was detected in olfactory bulb neurons in 38/41 (93 %) of AD subjects with amygdala Lewy bodies subjects, hypothesised to be due to the anatomical connectivity between these regions (Fujishiro et al., 2008). This data is notable in the context of the Braak hypothesis for pathological progression in PD (see Chapter 1, paragraph 1.5.11), in which the olfactory bulb and medullary vagal dorsal motor nucleus are postulated to be the earliest sites for alpha synuclein pathology,

offering two possible routes for pathologic seeding of the cortex: upwards through the brainstem; and via the olfactory pathway into the temporal lobes.

In AD, amyloid classically takes the form of neuritic (senile) plaques, consisting of a central core of Aß amyloid surrounded by dystrophic neural processes and activated microglia. Diffuse amyloid plaques also exist, characterised by a lower density of Aß amyloid and the absence of neurites. Whilst classical AD pathology - neuritic plaques and neurofibrillary tangles – occurs in LVAD, in the primary Lewy body disorders (PD and DLB), diffuse amyloid predominates (Burack et al., 2010). Lashley et al., (2008) demonstrated that diffuse amyloid plaque burden correlated strongly with cortical LB load, with an effect magnitude greatest in those with moderate to high amyloid loads, a subgroup in which APOE4 was also more common. Jellinger and Attems (2008b) reported greater striatal amyloid of the diffuse rather than classical AD senile plaque type in DLB compared to PDD brains. This was in agreement with Halliday et al. (2011), who found striatal amyloid in DLB but not PDD. Kalaitzakis et al. (2011), however, detected amyloid in the striatum of both DLB and PDD brains, but not in PD without dementia, MSA or PSP cases. In an autopsy study of 92 PDD and 48 non-demented PD subjects, the coexistence of AD pathology and the Apolipoprotein E4 (APOE4) genotype were significantly overrepresented in PDD cases, and correlated with Lewy body and Lewy neurite load (Irwin et al., 2012).

Since concomitant amyloid pathology is common in PDD, and is even more prevalent in DLB, it may be that the clinical phenotypes and associated neuropathology that are currently resolved by consensus criteria into discrete nosological entities - PD, PDD, DLB and LVAD – are instead part of a clinical spectrum resulting from a variable interaction between “classical” PD and amyloid pathology.

4.3.2 Molecular pathology

At the molecular level, there is growing evidence for a reciprocally synergistic relationship between Aß amyloid, α-syn and tau. In an α-syn/Amyloid Precursor Protein (APP) dual transgenic murine model, greater α-syn accumulation occurred compared to that in either single transgene mouse, and Aß amyloid peptides were

shown to promote α-syn accumulation *in vitro* (Masliah et al*.,* 2001). Giasson et al. (2003) showed that α-syn induces the formation of tau fibrils and that tau and α-syn act synergistically in effecting the polymerization of each into fibrillar amyloid aggregates. In the first transgenic mouse developed which manifests both LB (α-syn) and AD (Aß and tau) pathologies, mutual synergism in the accumulation of all 3 proteins was seen and was associated with phenotypic severity (Clinton et al., 2010). Synaptic injury induced by the addition of recombinant human alpha-synuclein to cultured neurons is potentiated by co-incubation with amyloid-beta1–42 (Bate et al., 2010). Inhibition of alpha-synuclein aggregation *in vitro* by anti-amyloid agents has been recently demonstrated (Herva et al., 2014).

4.3.3 Genetics

The apolipoprotein E epsilon 4 (APOE4) genotype is robustly associated with the risk of AD (Corder et al., 1993; Farrer et al., 1997), an effect that appears to be driven by an absolute increase in amyloid deposition (Kok et al., 2009; Reiman et al., 2009), potentiated by a clinically deleterious interaction between APOE4 and amyloid itself (Kantarci et al., 2012; Mormino et al., 2014). APOE4 is also overrepresented in LVAD (Galasko et al. 1994; Tsuang et al. 2005) and in PDD and DLB (Williams-Gray et al., 2009b; Tsuang et al., 2013).

4.3.4 Cerebrospinal fluid

Data from examination of cerebrospinal fluid (CSF) broadly support the neuropathologic evidence. CSF Aβ1-42 concentrations are lower in PD than in controls, and are reduced further in PDD (Compta et al. 2009; Montine et al., 2010). In a longitudinal study, lower baseline CSF Aβ1-42 was associated with faster cognitive decline (Siderowf et al., 2010). Recently, Kang et al. (2013) reported an association between lower CSF Aβ1-42 concentrations and the postural instability gait disorder (PIGD) phenotype, itself a risk factor for cognitive decline and dementia in PD (see chapter 1, paragraph 1.4.9). Further, lower CSF Aβ1-42 levels correlated with UPDRS scores at baseline, and were predictive of UPDRS change. In a

prospective study over 5 years of 104 PD subjects, low Aβ42 predicted onset of dementia (Alves et al., 2014).

Whilst it is difficult to draw conclusions about the timing of amyloid deposition from neuropathology data, CSF studies indicate that amyloid deposition begins early in symptomatic disease and may even precede it. In a study of LRRK2 mutation carriers, CSF Aβ1-42 concentrations were reduced in asymptomatic carriers compared to controls, but not to the degree found in symptomatic LRRK2 PD subjects, where levels were comparable with those reported in symptomatic IPD (Aasly et al., 2012). Further, CSF Aβ1-42 concentrations in the LRRK2 group overall correlated with striatal dopaminergic function assessed using three PET radiotracers ([^{18}F]-flourodopa, [^{11}C]-α-dihydrotetrabenazine, and [^{11}C]-d-threo-methylphenidate), suggesting the amyloid deposition may begin in the pre-symptomatic stage.
In idiopathic PD, Bayer et al. (2013) reported an inverse correlation between CSF Aβ38, Aβ40, and Aβ42 and ventricular enlargement in 91 drug naïve early PD cases. Lower CSF Aβ40 and Aβ42 were reported in newly diagnosed incident PD subjects with cognitive impairment compared to those with intact cognition (Yarnall et al., 2014).

4.3.5 Imaging amyloid in Parkinson's disease using [^{11}C]-PIB PET

Researchers at the University of Pittsburgh showed that the neutral thioflavin-T derivative 2-(4'-methylaminophenyl)benzothiazole (or BTA-1) bound to Aβ amyloid fibrils with high (nanomolar) affinity *in vitro*, and that the radiolabeled carbon-11 compound showed good brain penetration and clearance in normal laboratory mice (Klunk et al., 2001). Subsequently this radiotracer was shown to bind to brain amyloid *in vivo* in transgenic mice, demonstrating its potential for use as a PET ligand for imaging amyloid in humans (Mathis et al., 2002). BTA-1 was duly shown to bind to amyloid in brain homogenates from AD subjects (Klunk et al., 2003). On the basis of comparable brain entry and specific Aβ binding affinity, but faster clearance from normal mouse and baboon brains, the 6-hydroxy derivative [N-methyl-(11)C]2-(4'-methylaminophenyl)-6-hydroxybenzothiazole (or [(11)C]6-OH-BTA-1), also known as Pittsburgh Compound B (PIB), was selected for further development (Mathis et al.,

2003). [^{11}C]-PIB was shown to perform favourably in a transgenic mouse model (Bacskai et al., 2003). This led to the first [^{11}C]-PIB clinical study in which 16 AD subjects were shown to have 1.5 to 2 times greater cortical [^{11}C]-PIB uptake than 9 controls (Klunk et al. 2004). This finding was broadly replicated by Edison et al. (2007), who reported 2 times greater association and cingulate cortical [^{11}C]-PIB retention in 19 AD subjects compared to 14 controls. Quantitative pathological assessment of brain amyloid from an AD subject at post-mortem showed good correlation with regional [^{11}C]-PIB uptake at PET scanning performed 3 months before death (Bacskai et al., 2007).

[^{11}C]-PIB PET has since been used to investigate the association of amyloid with Lewy body disorders. Initial studies reported cortical and striatal [^{11}C]-PIB binding elevated to levels approaching those seen in AD (i.e. $\geq$ 1.5 times normal) in DLB, but not in PD or PDD. Edison et al. (2008) found AD range [^{11}C]-PIB uptake in 9/13 DLB but only 2/12 PDD subjects. Maetzler et al. (2008) also reported [^{11}C]-PIB retention elevated to AD levels in 2/10 PDD subjects, whilst in non-demented PD cases raised [^{11}C]-PIB was only detected in the pons and midbrain. Similarly, Gomperts et al. (2008; 2012) reported significantly elevated [^{11}C]-PIB binding only in DLB cases, whilst PDD and non-demented PD subjects could not be differentiated from controls. From these data it was concluded that amyloid was unlikely to play a significant role in driving PD dementia.

Whilst it is accepted that amyloid deposition to the degree typical of AD is rare in PD, other PET data suggest that amyloid is relevant to cognitive impairment in PD. Foster et al. (2010) found no significant difference in [^{11}C]-PIB uptake between PD, PDD and DLB subgroups, but when Lewy disorders were considered as single group, [^{11}C]-PIB uptake correlated inversely with cognitive performance. Petrou et al. (2012) reported a negative relationship between [^{11}C]-PIB retention and global cognitive function in a group of 40 non-demented PD subjects, despite only 6 having AD range [^{11}C]-PIB uptake. Subsequently, Gomperts et al. (2013) showed that a raised baseline [^{11}C]-PIB retention predicted greater cognitive decline in non-demented PD subjects, despite the absence of a significant difference in [^{11}C]-PIB uptake between those with and without mild cognitive impairment (MCI). This is in line with previous work on amnestic MCI, in which subjects with raised [^{11}C]-PIB binding were more likely to

convert to clinical AD (Okello et al., 2009). Furthermore, PD subjects with the postural instability gait disorder (PIGD) phenotype, which is itself a risk factor for PD dementia, had elevated neocortical [^{11}C]-PIB binding compared to tremor dominant cases (Müller et al., 2013).

In addition to the amyloid load issues above, there appear to be differences in the nature and distribution of amyloid deposition between AD and PD. Autopsy data indicate that the predominant form of plaque amyloid in PDD is the diffuse rather than the classical neuritic type typical in AD (Burack et al., 2010). [^{11}C]-PIB is a non-specific marker of Aβ amyloid, being unable to distinguish neuritic from diffuse plaque amyloid or cerebral amyloid angiopathy (Lockhart et al., 2007). The spatial distribution of amyloid deposition also seems to be different in the two conditions: using principal component analysis, Campbell et al. (2013) showed that the PD specific pattern has greater prefrontal and posterior cingulate involvement compared to AD cases.

4.4 Subjects and methods

4.4.1 Ethics and safety

Hammersmith Hospitals Trust Ethics Committee provided ethical approval for the study, including radiation exposure (REC 08/H07711/135). Permission to use the relevant radiotracers was obtained from the Administration of Radioactive Substances Advisory Committee (ARSAC). The candidate obtained the statutory radiation protection certification (IRMER) from Imperial College London.

4.4.2 Funding

The project was financed by grants from Parkinson's UK and the Medical Research Council.

4.4.3 Source of subjects

PD subjects were recruited from two sources:

1. General neurology/movement disorder clinics at Imperial College London NHS Trust (Prof DJ. Brooks, Dr P. Bain, Dr S. Molloy).
2. The Cambridge Centre for Brain Repair.

4.4.4 Inclusion criteria

1. Age 35-79 years at enrolment
2. Clinical diagnosis of PD by QSBB Criteria (Hughes et al., 1992)
3. Capacity to give informed consent
4. Able to complete neuropsychological assessment

4.4.5 Exclusion criteria

1. Extensive microvascular disease on MRI disproportionate for age
2. Major depression (DSM IV criteria)
3. Pregnant or breast-feeding
4. Current or recent (within 5 years) alcohol or drug dependency
5. Other illness causing inability to undergo scanning

4.4.6 Sub-groups

Non-demented PD subjects were classified as having a higher or lower risk of conversion to PD dementia as defined in chapter 3 (paragraphs 3.4.7 and 3.4.8). Subjects were classified as having PD dementia (PDD) according to the Movement Disorders Society Task Force criteria (Dubois et al., 2007):

1. Diagnosis of PD (Queen Square Brain Bank criteria)
2. Diagnosis of PD precedes onset of dementia by at least 1 year
3. Mini Mental State Examination (MMSE) < 26
4. Cognitive deficits in two domains that impact on daily living (Caregiver interview or Pill Questionnaire)
5. Impairment in at least two of the following tests:
    a) Months reversed *or* serial sevens
    b) Lexical fluency *or* clock drawing
    c) Intersecting pentagons
    d) 3-Word recall

4.4.7 Subjects

Nine [^{11}C]-PIB scans performed on healthy volunteers were obtained from our unit's archive (courtesy Dr P. Edison). 21 non-demented subjects meeting the Queen Square Brain Bank criteria for the diagnosis of PD (Hughes et al., 1992) were recruited. 7 subjects fulfilling consensus criteria for the diagnosis of PDD were also recruited (Emre et al., 2007). 2 non-demented PD subjects withdrew from the study after baseline scanning and clinical assessment; 19 completed follow up imaging and clinical testing.

4.4.8 Clinical assessments

Motor, cognitive and other non-motor clinical assessments utilised are detailed in chapter 3 (paragraph 3.4.10).

4.4.9 Scans

Baseline PET scans were acquired with a Siemens ECAT EXACT HR+ (CTI/Siemens 962) camera located at the Cyclotron Building, Hammersmith Hospital, Hammersmith Imanet, GE Healthcare, London, UK. Follow up imaging occurred at

the Wolfson Brain Imaging Centre, Cambridge, UK using a GE Advance scanner (General Electric Medical Systems). The scanning protocol consisted of 3D acquisition over 60 minutes following a bolus injection of 370 MBq of [^{11}C]-PIB.

4.4.10 Image analysis

[^{11}C]-PIB target region to cerebellar ratio (RATIO) images were created as described in Chapter 2 (paragraph 2.8.5). Spatial normalisation of RATIO and MR images into standard MNI stereotaxic space was performed using SPM8 implemented in Matlab 7. Subject-specific object maps for region of interest analysis were generated in ANLAYZE as described in Chapter 2 (paragraph 2.8.6).

4.4.11 Region of interest data sampling

The subject-specific object map was laid over the spatially normalized [^{11}C]-PIB RATIO image in ANALYZE (Mayo Clinic, Rochester, MN), followed by systematic sampling of the regions of interest.

4.4.12 Voxel-based analysis: statistical parametric mapping (SPM)

Voxel level differences in [^{11}C]-PIB RATIO between study groups were identified using SPM8 software (Wellcome Trust Centre for Neuroimaging, UCL, London) as described in Chapter 2 (paragraph 2.8.7). Correlation between RATIO and clinical parameters was similarly assessed in SPM8.

4.4.13 Statistical analysis

Statistical analysis was performed in SPSS 21.0 (IBM, NY). Normality of data distributions was interrogated with the Kolmogorov-Smirnov test. Correlations between variables were analysed with the Spearman Rank correlation test.

4.5 Results

Table 4.1 shows comparative demographic and clinical data for the non-demented and PD dementia groups. Apart from the UPDRS part 3, clinical testing was not possible in 3 of the PDD subjects due to poor attention. Further clinical evaluation in the remainder of the PDD group was not pursued due to lack of numbers to allow meaningful statistical comparisons.

Table 4.1. Demographic and clinical data for the non-demented (PDND) and PD dementia (PDD) subjects

	PDND	**PDD**
Number	21 (13 male)	7 (all male)
Age, years	66.7 (6.4)	70.0 (2.6)
Onset age, years	61.7 (7.4)	58 (4.4)
Duration, months	60.8 (56.3)	142 (46.4)
UPDRS part 3	27.8 (6.9)	51 (8.7)

Data are mean with standard deviation in parentheses

Several ROI and clinical variables in the baseline and follow up datasets failed the Kolmogorov-Smirnov test of normality. Non-parametric statistical tests were therefore appropriate.

Figure 4.1 shows example [^{11}C]-PIB RATIO images for a control, non-demented PD, and PDD subject, illustrating the progressive increase in [^{11}C]-PIB retention with disease progression. Figure 4.2 shows the increase in [^{11}C]-PIB binding from baseline to interval scanning in a subject clinically converting to PD dementia during this period.

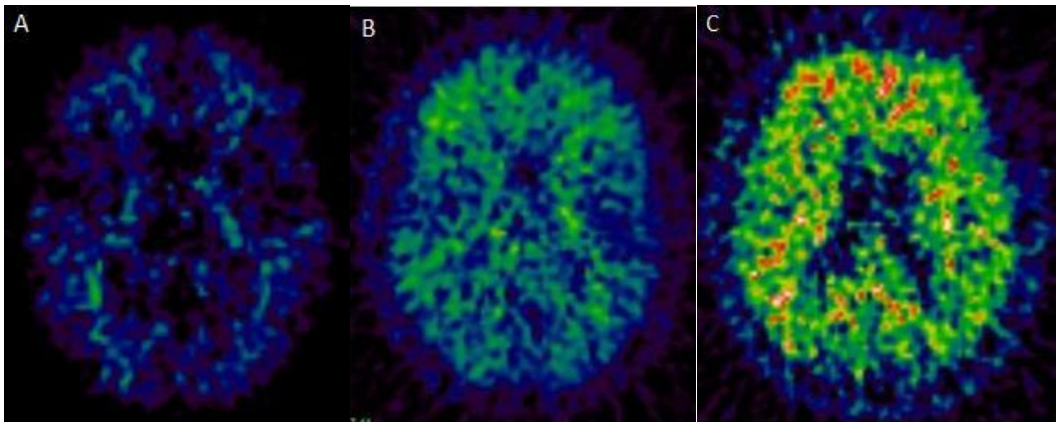


Figure 4.1. Example [^{11}C]-PIB RATIO images for control (A), non-demented PD (B), and PD dementia (C) subjects.

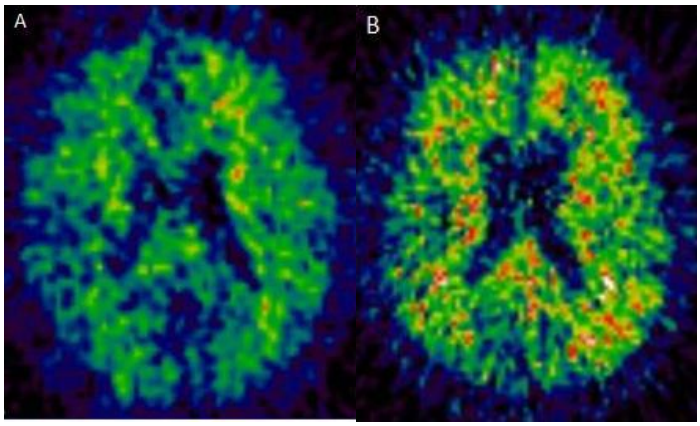


Figure 4.2. [^{11}C]-PIB RATIO images at baseline (A) and at 24 months (B) in a subject developing PDD during this interval.

Baseline [^{11}C]-PIB imaging

Region of interest analysis

4.5.1 ROI analysis: controls v PD subjects at baseline

Non-demented PD subjects (PDND) had significantly greater [^{11}C]-PIB uptake compared to controls at whole brain level, and in the putamen, insula, and frontal, temporal, parietal, occipital lobes (table 4.2).

4.5.2 ROI analysis: PD subjects at baseline v follow up

[^{11}C]-PIB retention was greater in PDND subjects at follow up compared to baseline in anterior and posterior cingulate, caudate, putamen, brainstem, and in frontal and parietal lobes (table 4.2).

4.5.3 ROI analysis: controls v PDD

PDD subjects had significantly greater [^{11}C]-PIB uptake in the posterior cingulate, thalamus, caudate, putamen, insula, and in frontal, temporal, parietal and occipital cortex (table 4.2).

4.5.4 ROI analysis: baseline PDND v PDD

PDD subjects had higher [^{11}C]-PIB signal compared to PDND subjects at baseline in the posterior cingulate, thalamus, putamen and insula (table 4.2).

Table 4.2. Mean regional [^{11}C]-PIB RATIOs (± standard deviation) in healthy controls, non-demented PD subjects (PDND) at baseline and follow up, and subjects with Parkinson's disease dementia (PDD).

	Controls	**PDND baseline**	**PDND follow up**	**PDD**
Anterior cingulate	1.184 ± 0.116	1.240 ± 0.216	1.336 ± 0.330††	1.600 ± 0.518
Posterior cingulate	1.182 ± 0.073	1.275 ± 0.203	1.479 ± 0.352††	1.585 ± 0.471*§
Thalamus	1.105 ± 0.074	1.165 ± 0.093	1.231 ± 0.223	1.270 ± 0.120**§
Caudate	1.073 ± 0.089	1.139 ± 0.178	1.272 ± 0.309†	1.331 ± 0.318**
Putamen	1.194 ± 0.072	1.352 ± 0.159**	1.447 ± 0.258†	1.629 ± 0.259***§§
Frontal lobe	1.110 ± 0.075	1.200 ± 0.158*	1.254 ± 0.212†	1.457 ± 0.401*
Insula	1.162 ± 0.041	1.250 ± 0.144*	1.271 ± 0.213	1.502 ± 0.364***§
Temporal lobe	1.099 ± 0.040	1.185 ± 0.128**	1.226 ± 0.171	1.386 ± 0.329**
Parietal lobe	1.100 ± 0.043	1.211 ± 0.154**	1.289 ± 0.265†	1.410 ± 0.364*
Occipital lobe	1.132 ± 0.055	1.246 ± 0.147**	1.226 ± 0.187	1.311 ± 0.194**

Brainstem	1.461 ± 0.094	1.381 ± 0.116	1.425 ± 0.163†	1.490 ± 0.147
Whole brain	1.115 ± 0.049	1.210 ± 0.142**	1.257 ± 0.198	1.416 ± 0.340*

Mann-Whitney U test: *** p<0.001 compared to controls; ** p<0.01 compared to controls; * p<0.05 compared to controls; §§ p<0.01 compared to baseline PDND; § p<0.05 compared to baseline PDND. Wilcoxon Signed Ranks test: PDND at follow up > baseline †† p<0.01; † p<0.05.

Clinical correlation

4.5.5 Baseline ROI analysis: UPDRS part 2

A positive correlation was found between [^{11}C]-PIB uptake in the insula cortex and UPDRS part 2 scores (ρ=0.526, p=0.018; figure 4.3).

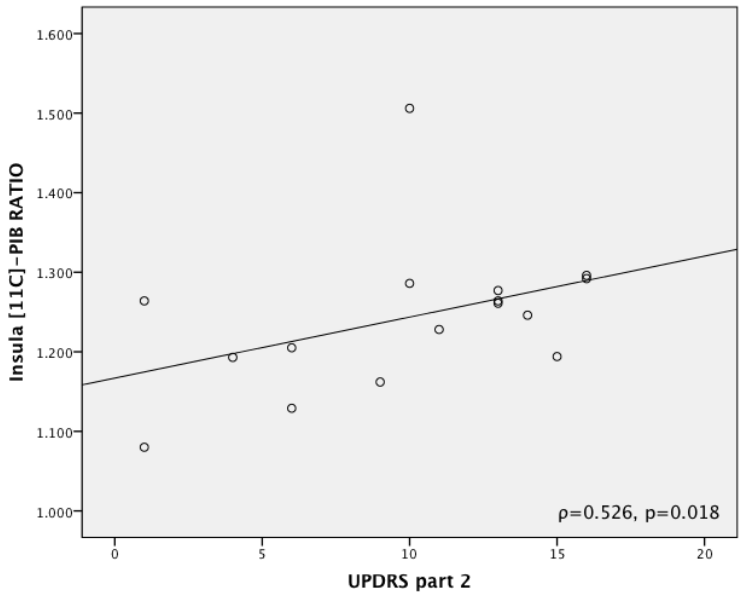


Figure 4.3. Correlation between insula [^{11}C]-PIB RATIO and UPDRS part 2 scores

4.5.6 Baseline ROI analysis: Montréal Cognitive Assessment (MoCA)

MoCA scores correlated inversely with thalamic [^{11}C]-PIB signal (ρ= -0.587, p=0.007; figure 4.4).

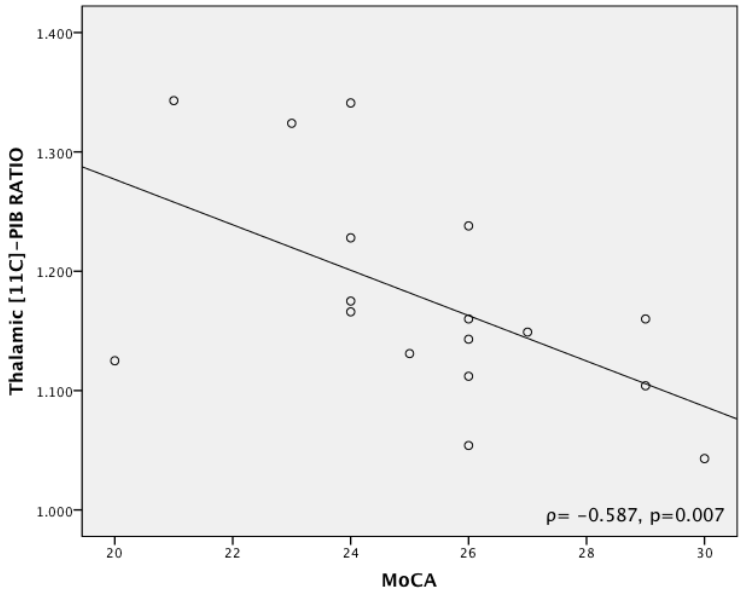


Figure 4.4. Correlation between thalamic [^{11}C]-PIB RATIO and MoCA scores

4.5.7 Baseline ROI analysis: phonemic fluency

Phonemic fluency scores, assessed with the FAS letter task, correlated inversely with [^{11}C]-PIB uptake in the frontal lobes (ρ= -0.455, p=0.033; figure 4.5).

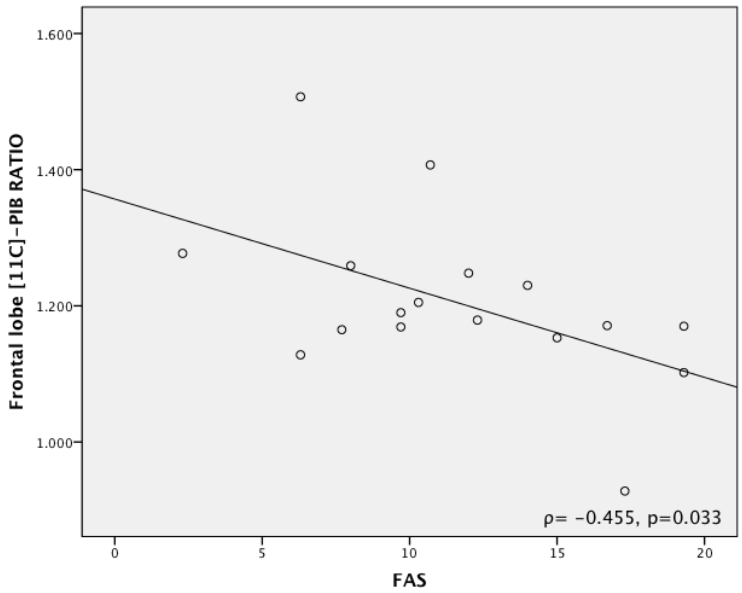


Figure 4.5. Correlation between insula [^{11}C]-PIB RATIO and FAS phonemic fluency scores

Voxel-based analysis: statistical parametric mapping (SPM)

4.5.8 Baseline SPM analysis: controls v non-demented Parkinson's disease

Compared to controls, non-demented PD subjects had greater [^{11}C]-PIB uptake in the occipital and inferior temporal lobes, and especially the posterior cingulate (figure 4.6; table 4.3).

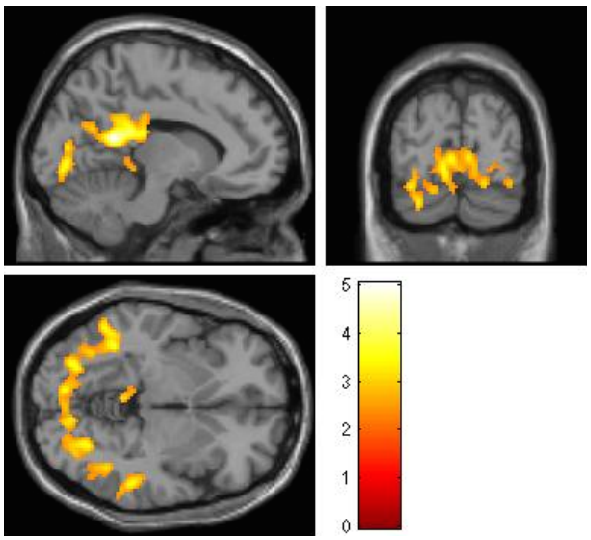


Figure 4.6. Regions of elevated baseline [^{11}C]-PIB uptake in non-demented PD subjects compared to healthy controls. Statistical parametric map (SPM) showing relative excess of [^{11}C]-PIB uptake in the posterior cingulate, occipital and inferior temporal lobes. (voxel threshold p=0.01; cluster significance p<0.001, corrected). The colour scale indicates Z score.

Table 4.3. Areas of elevated [^{11}C]-PIB uptake in non-demented PD subjects compared to controls.

Z score	MNI coordinates			Area
	x	*y*	*z*	
4.21	-10	-50	16	Posterior cingulate
4.07	-36	-68	-14	Left inferior occipital gyrus
4.05	-12	-42	18	Corpus callosum
3.68	-32	-74	-16	Left lingual gyrus
3.65	-32	-80	-16	Left middle occipital gyrus
3.62	26	-74	12	Right cuneus
3.51	-42	-72	-20	Left association visual cortex (V3-5)

3.50	22	-68	2	Right lingual gyrus
3.48	6	-80	4	Left cuneus
3.31	-42	-48	-4	Left middle temporal gyrus
3.16	-4	-84	2	Left primary visual cortex (V1)
3.92	52	-8	-24	Right inferior temporal gyrus
3.82	62	-14	-22	Right middle temporal gyrus
3.34	66	-40	4	Right superior temporal gyrus
2.77	54	-68	-16	Right association visual cortex (V3-
2.77	52	-66	4	Right fusiform gyrus

4.5.9 Baseline SPM analysis: non-demented v demented Parkinson's disease subjects

A relative excess of [^{11}C]-PIB uptake was found in the frontal lobes and posterior cingulate of PD subjects with dementia compared non-demented subjects (figure 4.7, table 4.4).

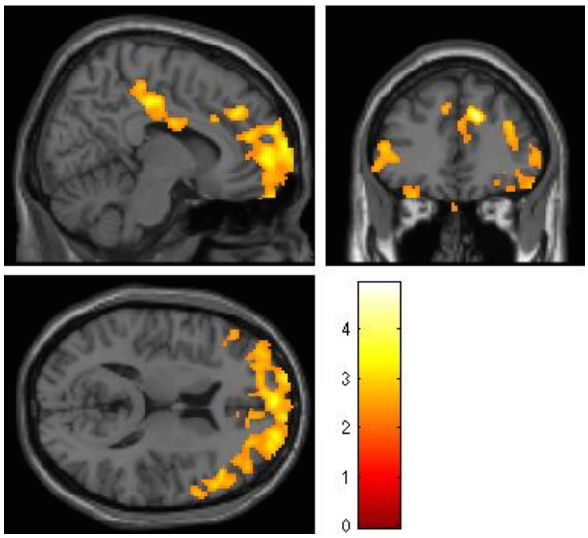


Figure 4.7. Regions of elevated baseline [^{11}C]-PIB uptake in PD subjects with dementia compared to non-demented PD subjects. Statistical parametric map (SPM) showing relative excess of [^{11}C]-PIB binding in the posterior cingulate and frontal lobes. (voxel threshold p=0.01; cluster significance p<0.001, corrected). The colour stripe indicates Z score.

Table 4.4. Areas of elevated [^{11}C]-PIB uptake in PD subjects with dementia compared to non-demented PD subjects.

Z score	MNI coordinates			Area
	x	*y*	*z*	
4.10	24	24	-16	Right inferior frontal gyrus
4.08	16	40	32	Right medial frontal gyrus
3.78	-52	34	8	Left inferior frontal gyrus
3.45	26	48	18	Right superior frontal gyrus
3.40	6	54	-32	Right dorsolateral prefrontal cortex
3.35	0	14	40	Cingulate
3.32	6	58	-26	Right superior frontal gyrus
3.31	60	34	-4	Right orbitofrontal cortex
3.30	-2	-28	50	Posterior cingulate
3.25	48	24	-8	Right inferior gyrus
3.24	12	60	0	Right medial frontal gyrus
3.23	-36	56	4	Right anterior prefrontal cortex

Baseline SPM analysis: clinical correlation

No significant correlation was found between baseline [^{11}C]-PIB uptake and locomotor function.

Follow up [^{11}C]-PIB imaging

ROI analysis: clinical correlation

4.5.10 Follow up ROI analysis: verbal fluency

Semantic fluency scores correlated inversely with [^{11}C]-PIB uptake in the striatum (ρ= -0.424, p=0.035; figure 4.8). The verbal fluency domain of the Addenbrooke's cognitive examination also correlated inversely with striatal [^{11}C]-PIB retention (ρ= -0.406, p=0.042; figure 4.9).

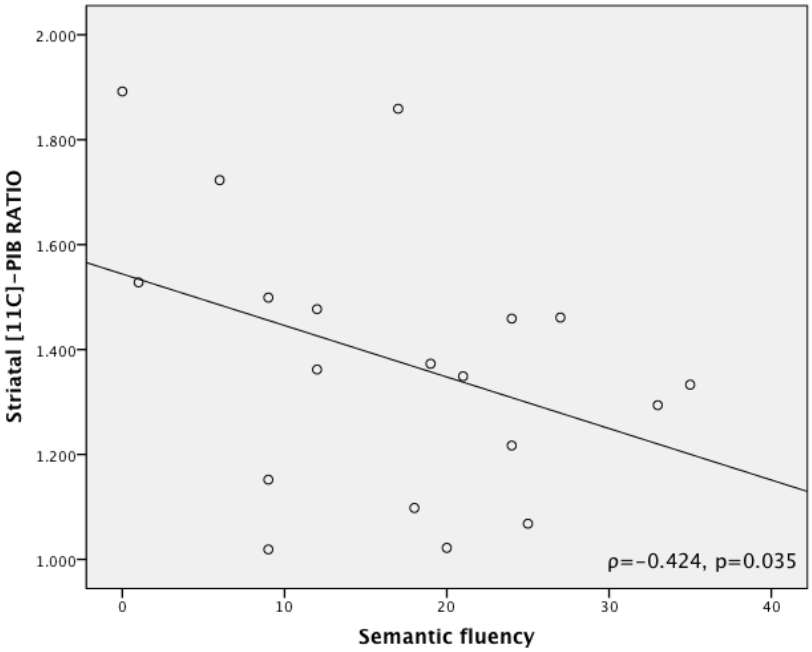


Figure 4.8. Correlation between striatal [^{11}C]-PIB RATIO and semantic fluency scores

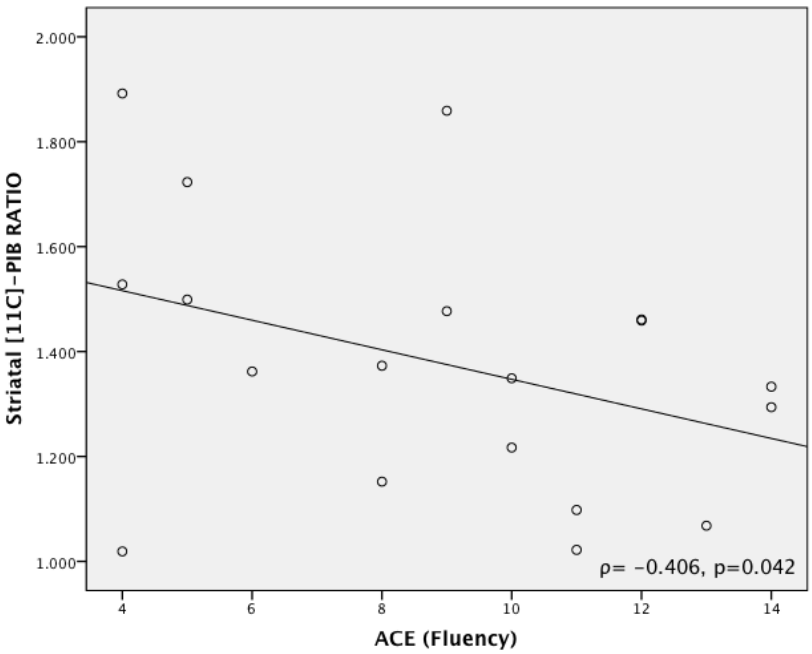


Figure 4.9. Correlation between striatal [^{11}C]-PIB RATIO and ACE verbal fluency scores

4.5.11 Follow up ROI analysis: depression

Greater subject-rated depression, assessed with the GDS-15, correlated with temporal lobe [^{11}C]-PIB uptake (ρ=0.434, p=0.036; figure 4.10).

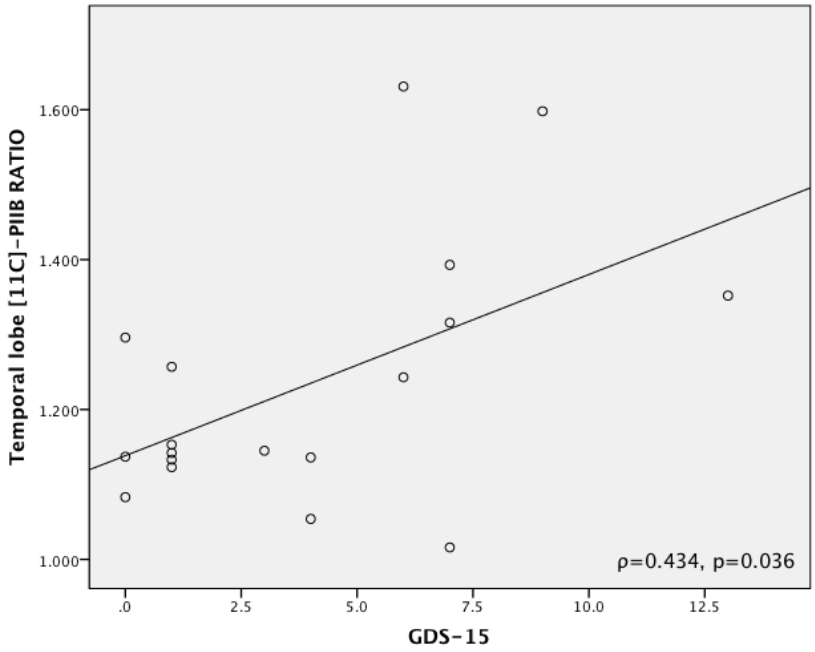


Figure 4.10. Correlation between temporal lobe [^{11}C]-PIB RATIO and GDS-15 scores

Voxel-based analysis: statistical parametric mapping (SPM)

Follow up SPM analysis: clinical correlation

4.5.12 Follow up SPM analysis: verbal fluency

Frontal lobe [^{11}C]-PIB uptake correlated with impaired verbal fluency, assessed using the ACE (figure 4.11, table 4.5) and the FAS letter task (figure 4.12, table 4.6).

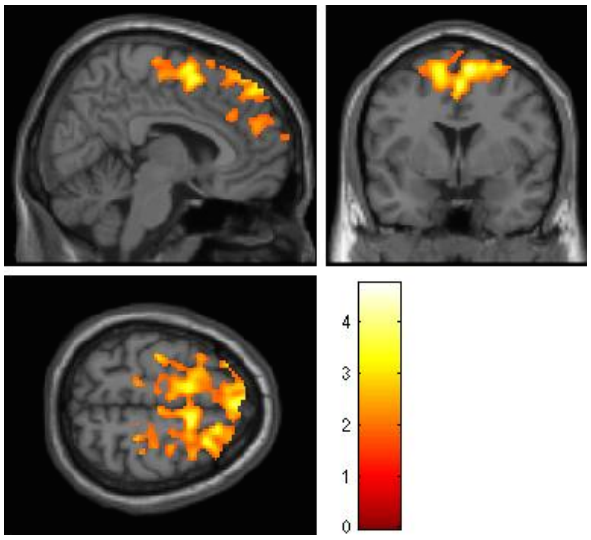


Figure 4.11. Inverse correlation between [^{11}C]-PIB uptake and the verbal fluency sub-score of the Addenbrooke's Cognitive Examination (ACE). Statistical parametric map (SPM) showing bilateral frontal lobe [^{11}C]-PIB signal correlates with greater impairment in verbal fluency (voxel threshold p=0.05; cluster significance p<0.001, corrected). The colour stripe indicates Z score.

Table 4.5. Areas of inverse correlation between [^{11}C]-PIB and the ACE verbal fluency sub-score.

Z score	MNI coordinates			Area
	x	*y*	*z*	
3.74	2	4	54	Right premotor cortex
3.57	8	4	64	Right supplementary motor area
3.47	-10	-4	68	Left superior frontal gyrus
3.41	-32	-16	54	Left precentral gyrus
3.22	-36	16	48	Left middle frontal gyrus
3.10	18	44	54	Right superior frontal gyrus
3.09	26	16	60	Right middle frontal gyrus
3.07	-12	2	62	Left premotor cortex
3.03	26	14	64	Right superior frontal gyrus
2.95	28	4	66	Right middle frontal gyrus

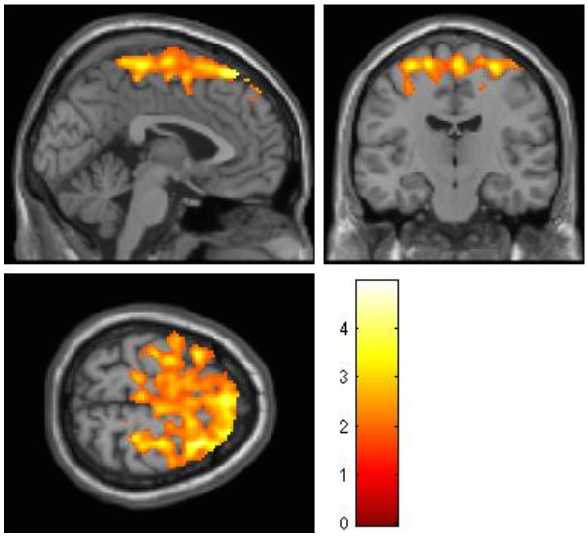


Figure 4.12. Inverse correlation between [^{11}C]-PIB uptake and phonemic fluency (FAS letter task). Statistical parametric map (SPM) showing bilateral frontal lobe [^{11}C]-PIB signal correlates with greater impairment in phonemic fluency (voxel threshold p=0.05; cluster significance p<0.001, corrected). The colour stripe indicates Z score.

Table 4.6. Areas of inverse correlation between [^{11}C]-PIB uptake and phonemic fluency (FAS letter task) scores.

	MNI coordinates			
Z score	*x*	*y*	*z*	Area
3.85	30	18	60	Right premotor cortex
3.62	0	36	60	Left supplementary motor area
3.59	2	52	52	Right superior frontal gyrus
3.46	-36	-6	50	Left premotor cortex
3.35	28	-14	66	Right middle frontal gyrus
3.32	-36	-22	68	Left precentral gyrus
3.26	2	-21	68	Right medial frontal gyrus

4.5.13 Follow up SPM analysis: depression

Greater depression scores correlated with [^{11}C]-PIB uptake in frontal and temporal cortices (figure 4.13, table 4.7).

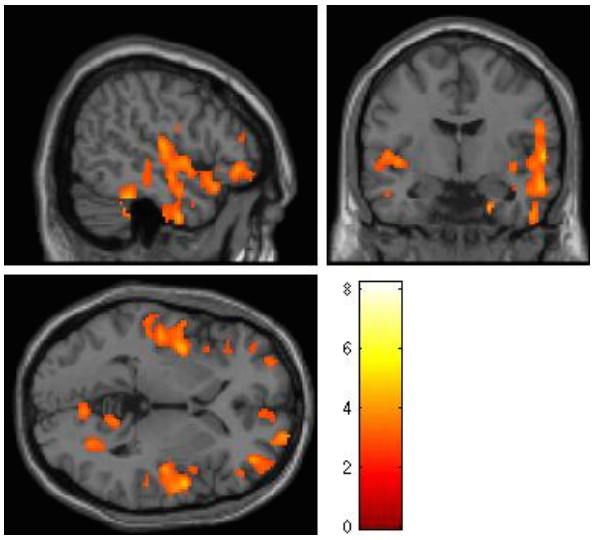


Figure 4.13. Positive correlation between [^{11}C]-PIB uptake and subject-rated depression (GDS-15) scores. Statistical parametric map (SPM) showing [^{11}C]-PIB signal correlates with greater impairment depression scores predominantly in the temporal lobes (voxel threshold p=0.05; cluster significance p<0.001, corrected). The colour stripe indicates Z score.

Table 4.7. Areas of positive correlation between [^{11}C]-PIB and depression (GDS-15) scores.

	MNI coordinates			
Z score	*x*	*y*	*z*	Area
5.07	32	36	-22	Right orbitofrontal cortex
4.22	-58	-14	14	Left postcentral gyrus
4.18	-6	16	50	Left superior frontal gyrus
4.16	48	34	-8	Right inferior frontal gyrus
3.90	58	-8	-18	Right middle temporal gyrus
3.83	-14	14	46	Cingulate
3.74	42	-46	-16	Right fusiform gyrus

4.5.14 Follow up SPM analysis: PDQ-39 communication domain

Subjective communication impairment, rated with the communication domain of the PDQ-39, correlated with frontal lobe [^{11}C]-PIB uptake (figure 4.14, table 4.8).

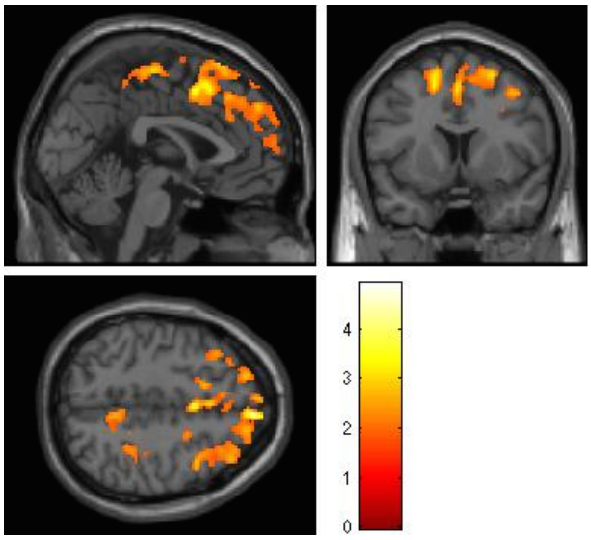


Figure 4.14. Positive correlation between [^{11}C]-PIB uptake and subjective communication impairment (PDQ-39 communication domain). Statistical parametric map (SPM) showing [^{11}C]-PIB signal in the frontal lobes correlates with greater subjective communication impairment (voxel threshold p=0.05; cluster significance p<0.001, corrected). The colour stripe indicates Z score.

Table 4.8. Areas of positive correlation between [^{11}C]-PIB and the communication impairment domain of the PDQ-39.

	MNI coordinates			
Z score	*x*	*y*	*z*	Area
3.69	8	48	50	Right superior frontal gyrus
3.45	20	-34	58	Right primary sensory cortex
3.29	-10	34	60	Left superior frontal gyrus
3.25	-8	30	62	Left premotor cortex
3.16	26	-14	62	Right premotor cortex
3.15	-4	-26	62	Left medial frontal gyrus
3.10	28	56	6	Right anterior prefrontal cortex

4.5.15 Follow up SPM analysis: PDQ-39 mobility domain

Subjective mobility impairment correlated with frontal, insular and putamenal [^{11}C]-PIB uptake (figure 4.15, table 4.9).

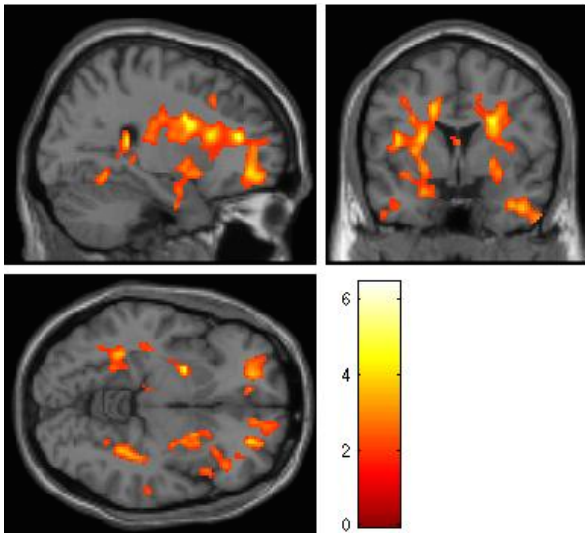


Figure 4.15. Positive correlation between [^{11}C]-PIB uptake and subjective mobility impairment (PDQ-39 mobility domain). Statistical parametric map (SPM) showing [^{11}C]-PIB signal in the frontal lobes, insulae and putamena correlates with greater subjective mobility impairment (voxel threshold p=0.05; cluster significance p<0.001, corrected). The colour stripe indicates Z score.

Table 4.9. Areas of positive correlation between [^{11}C]-PIB and the PDQ-39 mobility impairment scores.

Z score	MNI coordinates			Area
	x	*y*	*z*	
4.33	-24	48	16	Left middle frontal gyrus
4.17	-32	-28	10	Left superior temporal gyrus
3.91	-26	6	20	Left inferior frontal gyrus
3.61	-24	0	-6	Left putamen
3.60	-16	6	32	Cingulate
3.20	-44	6	10	Left precentral gyrus
3.19	-40	2	16	Left insula
3.13	-8	-22	6	Right thalamus
3.89	32	-20	14	Right insula
3.88	26	38	16	Right superior frontal gyrus
3.47	28	48	-10	Right middle frontal gyrus
3.39	38	36	2	Right inferior frontal gyrus
3.12	38	4	-32	Right superior temporal gyrus
3.06	36	20	-36	Right temperopolar cortex

2.97	46	2	-34	Right middle temporal gyrus

Correlation between amyloid deposition and glucose metabolism

4.5.16 Baseline [^{11}C]-PIB v [^{18}F]-FDG

In the non-demented PD group at baseline, an inverse relationship was seen between occipital lobe [^{18}F]-FDG and striatal [^{11}C]-PIB uptake (ρ = -0.398, p=0.041; figure 4.16).

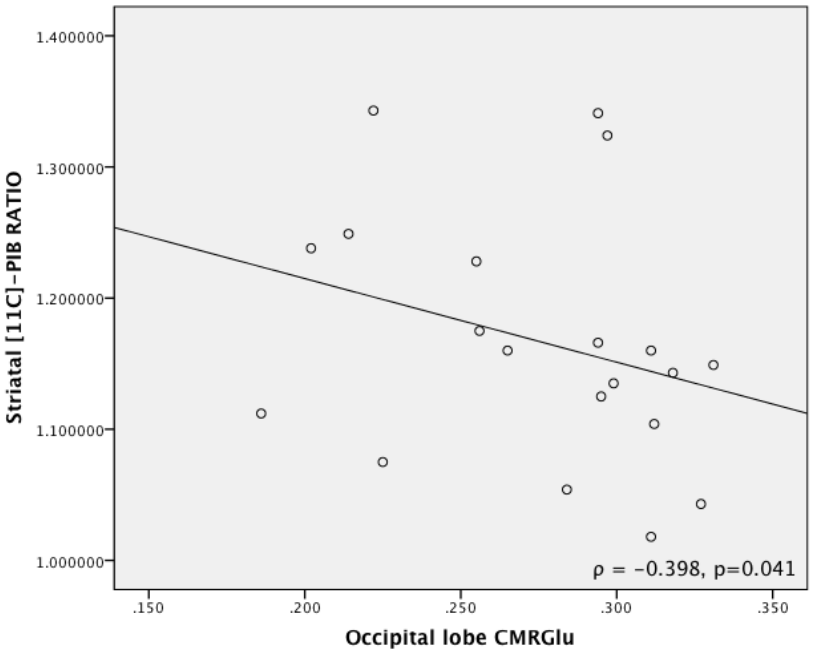


Figure 4.16. Correlation between striatal [^{11}C]-PIB RATIO and occipital lobe CMRGlu

When the demented and non-demented PD subjects were analysed as a single group, striatal [^{11}C]-PIB RATIO correlated inversely with CMRGlu at whole brain level, and in the striatum, thalamus, anterior and posterior cingulate, insula, frontal, temporal, parietal and occipital cortex (table 4.10; Appendix, figures B1-10).

Table 4.10. Correlation between striatal [^{11}C]-PIB RATIO and regional CMRGlu

	Correlation Coefficient (Spearman Rho)	p value
Whole brain	-0.373	0.028
Striatum	-0.376	0.027
Thalamus	-0.523	0.003
Anterior cingulate	-0.461	0.008
Posterior cingulate	-0.412	0.016
Insula	-0.487	0.005
Frontal lobe	-0.433	0.012
Temporal lobe	-0.396	0.020
Parietal lobe	-0.410	0.017
Occipital lobe	-0.432	0.012

4.5.17 Follow up [^{11}C]-PIB v [^{18}F]-FDG

At follow up imaging, [^{11}C]-(R)-PK11195 BP_{ND} and [^{11}C]-PIB uptake exhibited significant correlation in the anterior cingulate (ρ=0.401, p=0.044; figure 4.17) and frontal lobes (ρ=0.402, p=0.044; figure 4.18).

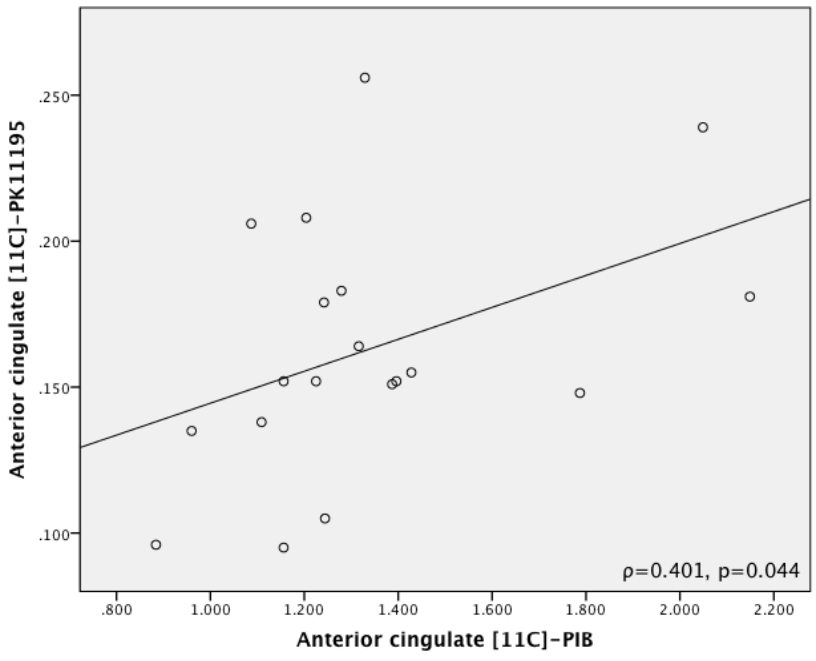


Figure 4.17. Correlation between [^{11}C]-PIB RATIO and CMRGlu in anterior cingulate

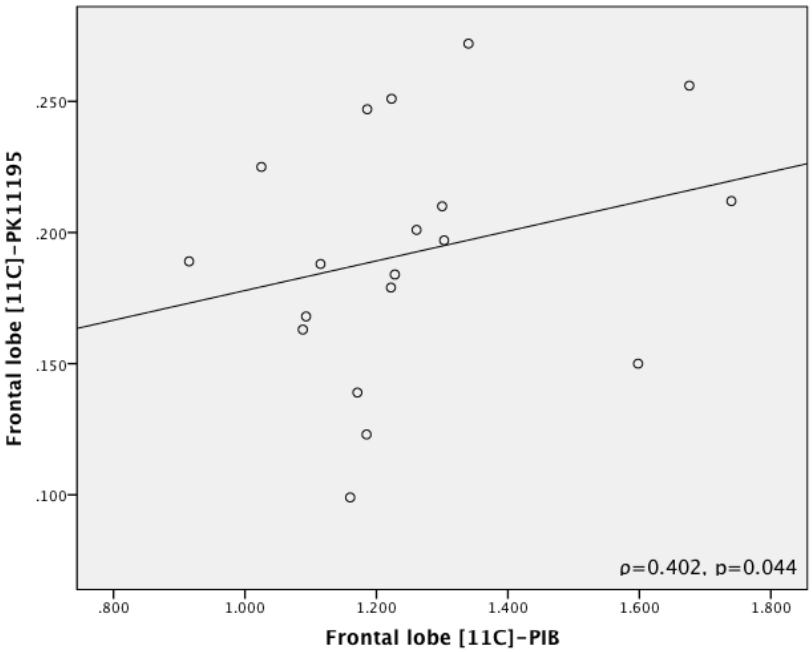


Figure 4.18. Correlation between [^{11}C]-PIB RATIO and CMRGlu in frontal cortex

4.6 Discussion

Region of interest analysis showed raised amyloid in non-demented PD subjects compared to controls in the striatum and throughout the neocortex. The effect magnitude was greater for posterior cortical structures (occipital, parietal and temporal lobes) compared to anterior (frontal and insula) regions. This predilection for amyloid deposition in posterior cortical areas was supported by the voxel-wise SPM analysis, which localised greater [^{11}C]-PIB signal in parietal and occipital lobes in non-demented PD subjects compared to controls. [^{11}C]-PIB uptake was higher in all cortical and subcortical regions in demented compared to non-demented PD subjects, but this was statistically significant only in posterior cingulate, thalamus, striatum, putamen and insula. SPM by contrast localised relatively greater frontal lobe [^{11}C]-PIB in the PD dementia group. Together, these data indicate that the evolution of amyloid deposition in PD reflects - and may in part drive - the rostral pattern of progression of cerebral dysfunction and atrophy reported in [^{18}F]-FDG PET and MRI studies (Jokinen et al., 2010; Bohnen et al. 2011).

There has been debate in the literature regarding the role of striatal amyloid in Lewy body disorders. Striatal amyloid has been consistently demonstrated in autopsy series only in DLB, with conflicting data in PDD (Jellinger and Attems 2008b; Halliday et al., 2011; Kalaitzakis et al. 2011). These histologic studies report the absence of striatal amyloid in non-demented PD, although since dementia is the usual end phenotype in PD (Hely et al., 2008), cases coming to autopsy without a history of dementia may be atypically benign, or else premature death may have occur for a reason unrelated to PD. [^{11}C]-PIB PET studies to date have supported these neuropathologic data: Edison et al. (2008) found significantly elevated [^{11}C]-PIB in the striatum in DLB cases, but not in PD with or without dementia; and Maetzler et al. (2008) reported elevated striatal [^{11}C]-PIB in only 2/10 PDD subjects. The present study by contrast detected significantly elevated [^{11}C]-PIB in the striatum of non-demented PD subjects at baseline compared to controls, whilst striatal [^{11}C]-PIB uptake in PDD was higher than in non-demented PD subjects at baseline. The number of non-demented PD subjects in the current study was twice that of Edison et al., which may have accounted for the failure to detect striatal amyloid in the latter. Alternatively, the groups may have differed biologically in the degree of striatal amyloid pathology. Striatal [^{11}C]-PIB retention was also shown to increase in the non-demented subjects at interval scanning. Whilst the neuropathologic, CSF and previous imaging data presented above provide circumstantial evidence for the role of amyloid in the transition from PD to PDD, the present study provides the first direct objective evidence for the accumulation of amyloid within the brains of non-demented PD subjects within a clinically relevant two year timescale.

Striatal [^{11}C]-PIB binding in non-demented PD subjects correlated inversely with semantic fluency and with the verbal fluency domain of the ACE. Impaired semantic fluency at baseline was a key predictor of conversion to dementia in the largest prospective study of incident PD to date (Williams-Gray et al. 2007; 2009). In the present study, striatal [^{11}C]-PIB binding in the non-demented PD group correlated inversely with glucose metabolism in occipital cortex, consistent with previous [^{18}F]-FDG PET studies demonstrating the early involvement of posterior cortical hypometabolism in PD [refs]. When PD subjects with and without dementia were analysed together, striatal [^{11}C]-PIB uptake correlated with hypometabolism in the striatum, thalamus and throughout the neocortex. These data suggest that striatal

amyloid deposition may be a biomarker predicting cognitive decline leading to dementia in PD. Whilst striatal metabolism is usually normal or even elevated in non-demented PD (Antonini et al., 1997), it is reduced in PDD (Bohnen et al., 2011). A direct effect of striatal amyloid on cognition is possible. This is supported by non-human primate experiments (Alexander et al., 1990; Hoover and Strick, 1993) and human functional imaging studies (Lehéricy et al., 2004; Di Martino et al., 2008), which have demonstrated a functional partitioning of the striatum into motor, affective and cognitive areas. Dopamine depletion in the ventral striatum in particular has been shown to be associated with cognitive impairment in PD subjects (Rinne et al., 2000; Brück et al., 2001; Niethammer et al., 2013). Further support for a role for striatal amyloid in PD comes from a recent PET study demonstrating an inverse relationship between striatal serotonin transporter availability (measured using [^{11}C]-DASB) and striatal [^{11}C]-PIB uptake (Kotagal et al., 2012). Whilst this could be explained by a toxic effect of amyloid on striatal serotoninergic projections, there is evidence that serotonin may have an inhibitory effect on amyloid deposition: *in vitro* and mouse model data indicate that selective serotonin reuptake inhibitors (SSRIs), commonly used to treat depression clinically, attenuate amyloid accumulation (Nelson et al. 2007; Cirrito et al., 2011). Since serotoninergic neuron loss is known to occur in PD (see Chapter 1, paragraph 1.5.3), an effect of serotonin on amyloid deposition may be another component in the multifaceted pathology of the disease. Evidence also exists for similar effect of cholinergic neurotransmission on amyloid pathology (Nitsch et al. 2000; Davis et al. 2010).

The lack of correlation between clinical status and [^{11}C]-PIB uptake at baseline in the voxel-wise analysis might be due to a diffuse but relatively low density distribution of amyloid pathology in non-demented PD. Significant SPM correlations were observed at follow up, possibly due to the demonstrable increase in amyloid deposition in the interval between scans.

Global cognitive performance, assessed with the MoCA was inversely correlated with [^{11}C]-PIB uptake in the thalamus. Cognitive disorders have traditionally been understood in terms of the specialized modular functions of cortical regions. Recent research, however, has shown cognitive function to be distributed across large cortical networks (Sepulcre et al., 2012). Much of this cortical connectivity is routed through

the thalamus, the integrity of which is essential for normal cognition (Exner et al., 2001; Piras et al., 2010; Saalmann et al., 2012). Greater subject-reported depression at follow up (assessed with the GDS-15) correlated with temporal lobe [^{11}C]-PIB uptake in the region of interest analysis, and with frontal and temporal lobe [^{11}C]-PIB signal with the SPM method. Depression in PD is associated with structural abnormalities in the frontal lobes (Benoit and Robert, 2011) with reduced activity in frontal and temporal lobes in functional MRI experiments (Wen et al., 2013).

At baseline, SPM revealed that [^{11}C]-PIB uptake in the insula correlated with greater subjective motor disability, rated with part 2 of the UPDRS. At follow up, subject-rated mobility impairment (assessed with the mobility domain of the PDQ39) correlated with [^{11}C]-PIB binding in the frontal lobes, insula and putamen in the SPM analysis. This pattern is similar to that observed for [^{11}C]-(R)-PK11195 uptake and subjective and objective motor disability (assessed with parts 2 and 3 of the UPDRS; chapter 4, paragraphs 4.5.4 and 4.5.5). An inverse relationship was found between phonemic fluency and frontal [^{11}C]-PIB signal, which is again in agreement with the negative correlation between phonemic fluency scores and frontal lobe [^{11}C]-(R)-PK11195 uptake reported in Chapter 4 (paragraph 4.5.13). At follow up SPM analysis, frontal lobe [^{11}C]-PIB uptake correlated with phonemic fluency, as well as the verbal fluency subscale of the ACE, and with subjective communication problems, assessed with the PDQ39 communication domain. At follow up assessment, [^{11}C]-(R)-PK11195 and [^{11}C]-PIB uptake were positively correlated in the frontal lobes and anterior cingulate, consistent with the rostral progression of both pathologies. This evidence suggests that inflammatory and amyloid pathologies may contribute to frontal lobe dysfunction in PD.

In summary, this study provides the first direct evidence for the accumulation of amyloid in the brains of PD subjects before the onset of dementia. Cross sectional evidence suggests this process continues in PDD. The distribution of amyloid deposition in non-demented PD has a posterior cortical predominance, with rostral extension in PD dementia, which mirrors the evolution of cerebral dysfunction reported in [^{18}F]-FDG PET studies. Striatal amyloid accumulation begins in PD before dementia, and may be a marker of or directly contribute to subsequent cognitive decline. Amyloid deposition in the frontal lobes correlates with subjective

motor disability and impaired verbal fluency, which suggests amyloid may contribute to the clinical expression of frontal lobe dysfunction in PD.

Chapter 5

Brain glucose metabolism and gait dysfunction in Parkinson's disease

5.1 Objectives

1. To study brain metabolism in a large cohort of subjects with early symptomatic Parkinson's disease, using [^{18}F]-FDG PET.
2. To correlate [^{18}F]-FDG uptake with objective clinical measures of gait disorder in Parkinson's disease subjects

5.2 Summary

Brain metabolic deficits detected with [^{18}F]-FDG PET correlated with three gait domains: pace, variability and asymmetry. Abnormalities of gait pace were associated with hypometabolism in the brainstem, putamen, globus pallidus, cingulate and anterior neocortex. The pattern of metabolic derangement related to gait variability was very similar, but did not affect the brainstem. This may be because brainstem structures, including the mesencephalic locomotor centre and pontomedullary reticular formation, contribute to pace, a more rudimentary component of gait function, whilst excess variability is a consequence of impaired supratentorial control of brainstem locomotion structures. Excess gait variability in PD may thereby represent failure of compensatory mechanisms localising to the basal ganglia and anterior neocortex, due to progressive intrinsic PD pathology in these structures.

5.3 Introduction

5.3.1 Neural basis of normal gait function

Axial sectioning experiments in cats have robustly demonstrated the existence of a spinal central pattern generator (CPG) that is able to produce the basic gait cycle reflexly. The CPG is, however, under supraspinal control: the mesencephalic locomotor region (MLR) projects to the pontomedullary reticular formation (RF), which in turn activates the CPG (Whelan et al., 1996). The MLR itself receives extensive connections from the basal ganglia, cerebellum, and cortex (Martinez-Gonzalez et al, 2011). The existence of this hierarchical neuroanatomical arrangement is now accepted in humans (Duysens et al., 1998; Takakusaki et al., 2008).

5.3.2 Cognition and gait dysfunction in normal elderly subjects

There is a reciprocal relationship between cognitive impairment and gait disorder in the elderly. The risk of falling in those over 75 years of age is elevated 5 fold in the presence of cognitive impairment (Tinetti et al., 1988). In a large epidemiological study of subjects over 65 years of age with no history of neurological disease, poor performance on a formal test of attention and executive function (Trail Making Test) was associated with reduced gait speed on an obstacle course, but not on a simple timed walk, suggesting that walking in more challenging environments (eg on uneven terrain), makes greater demands on frontal lobe function (Ble et al., 2005). In a later study of 256 community dwelling elderly subjects, poor performance on attention and executive tests predicted a high risk of falls within 5 years (Mirelman et al., 2012).

Dual-task studies have been used to evaluate the relationship between cognition and gait in normal elderly subjects and in those with neuropathology. The increased attentional demand imposed by simultaneous cognitive tasks may lead to impairment in a walking task due to the need for intact executive function and attention in voluntary ambulation. A quotidian clinical sign, “stops talking when walking”, is an example of this phenomenon and predicts a higher risk of falls in elderly nursing home residents (Lundin-Olsson et al., 1997). In a study of 186 cognitively normal elderly subjects, levels of attention and memory predicted gait velocity in a dual task interference condition (Holtzer et al., 2006). Increased gait variability in the dual-task condition occurred only in those with a history of falls, suggesting that impairment in attention mediates gait destabilisation in fallers (Springer et al., 2006).

5.3.3 Cognition and gait dysfunction in the presence of brain pathology

Gait dysfunction is associated with underling structural and functional brain abnormalities. Rosano et al. (2006) found a correlation between reduced step length and gait velocity and otherwise asymptomatic brain infarcts and central white matter disease among high-functioning elderly subjects. The same group also reported an association between cortical atrophy and gait dysfunction (Rosano et al., 2008; 2012). In a study of 429 individuals aged 50-85 years, MRI white matter lesion load correlated with lower gait velocity, shorter step length and wider gait (De Laat et al., 2011), whilst in a more recent study of 225 subjects aged 60-86 years, white and gray matter atrophy as well white matter lesions were associated with gait dysfunction (Callisaya et al., 2013). Further, the presence of frontal lobe grey matter atrophy predicts a high risk of falls over 12 months (Makizako et al., 2013). In addition to these structural abnormalities, a recent fMRI study reported changes in functional network connectivity in fallers compared to non-fallers. The fallers showed increased connectivity between the fronto-parietal and default mode networks, but reduced connectivity between fronto-parietal and primary motor sensory networks. This pattern also predicted decline in mobility and cognition over 12 months (Hsu et al., 2014).

5.3.4 Cognition and gait dysfunction in Parkinson's disease

Reduced gait velocity with a compensatory increase in cadence ("festination") is the hallmark of ambulatory dysfunction in PD. Falls and freezing of gait in particular are associated with physical and psychosocial disability (Bloem et al., 2004). 40-50% of PD patients have a history of falls (Hausdorff et al., 2001; Pickering et al. 2007; Kerr et al., 2010). The presence of postural instability or gait disorder in PD is also of prognostic significance, as it is associated with increased risk of dementia (Alves et al., 2006; Burn et al., 2006). Furthermore, gait dysfunction in PD is often refractory to dopaminergic medication, suggesting it has a non-dopaminergic aetiology.

In addition to the classical changes in pace and rhythm, gait variability is increased in PD (Hausdorff et al., 1998; Baltadjieva et al., 2006), is an independent risk factor for falls, and is only partially responsive to levodopa (Schaafsma et al., 2003). Asymptomatic LRRK2 (G2019S) mutation carriers display greater gait variability than non-carriers, demonstrating that gait abnormalities occur early in subjects at elevated genetic risk of PD, even before classical motor symptoms (Mirelman et al., 2011). In a study of 122 subjects with recent onset sporadic PD, those with depressive symptoms had lower gait velocity and greater variability than those without depression (Lord et al., 2013a). In a recent study of 25 PD subjects and 27 elderly controls, test-retest reliability of gait variability did not differ between the groups, confirming that assessments of gait variability are robust in the presence of PD pathology (Galna et al., 2013).

Gait velocity is further reduced in PD during cognitive interference tasks (Rochester et al., 2004). In a study of 29 PD subjects "off" dopaminergic medication walking at home whilst wearing an accelerometer, assessed under single and dual task interference conditions, motor function, attention and executive cognition in combination accounted for 66% of the variance in gait interference, showing that all three contribute to gait performance in a "real world" environment (Lord et al., 2010).

5.3.5 Functional imaging studies of gait dysfunction in Parkinson's disease

Most functional imaging studies examining gait disorder in PD have measured cerebral metabolism or blood flow using SPECT, [^{18}F]-FDG PET or fMRI. A minority has assessed dopaminergic and non-dopaminergic neurotransmission. Fabre et al. (1998) used ^{133}Xe SPECT to assess regional cerebral blood flow in controls, PD, PSP, and "isolated gait ignition failure", but detected frontal hyoperfusion only in the PSP group. Mito et al., (2006) reported reduced cerebral perfusion in the anterior cingulate cortex and primary visual cortex of PD subjects with the PIGD phenotype, whilst no difference in perfusion was found between tremor-dominant PD cases and controls.

Several studies have focused on freezing of gait (FoG) in PD. Matsui et al. (2005) reported reduced orbitofrontal perfusion, assessed using N-isopropyl-p-^{123}I iodoamphetamine SPECT, in PD subjects with freezing of gait compared to those without. In a PET study of 10 PD subjects with freezing of gait, using [^{18}F]-DOPA and [^{18}F]-FDG to assess dopamine and glucose metabolism respectively, a relative reduction in [^{18}F]-DOPA and [^{18}F]-FDG uptake in the caudate was seen compared to 7 PD cases without freezing of gait, whilst the putamen showed reduced [^{18}F]-DOPA but elevated [^{18}F]-FDG uptake (Bartels et al., 2006). Subjects with FOG also had reduced glucose metabolism in the parietal cortex.

Since gait dysfunction in PD is often refractory to dopaminergic treatment, the use of functional imaging to probe non-dopaminergic systems in PD with a gait disorder is rational. The cholinergic system has been studied in this context. Bohnen et al. (2009) scanned PD subjects with and without a history of falls using the PET radiotracers [^{11}C]methyl-4-piperidinyl propionate (PMP), and [^{11}C]dihydrotetrabenazine (DTBZ), markers of cholinergic and dopaminergic function, respectively: fallers had reduced thalamic cholinergic activity, reflecting loss of pedunculopontine nucleus (PPN) input, but there was no difference between groups in dopaminergic function. In a larger study, the same group later demonstrated reduced cholinergic activity in PD subjects with slower gait velocity, whilst those with intact cholinergic innervation had normal gait speed (Bohnen et al., 2013). Cholinergic function has also been investigated indirectly using a neurophysiological approach: if the median nerve is electrically stimulated a fraction of a second before transcranial magnetic stimulation of the motor cortex, the resulting motor evoked potential is suppressed, a phenomenon termed short latency afferent inhibition (SAI; Di Lazzaro et al., 2000; 2002). This effect appears to depend on intact cholinergic function, since it is abolished by pharmacological blockade of muscarinic receptors (Di Lazzaro et al., 2000). A recent study of 22 early PD subjects (disease duration < 3 years) showed that reduced SAI correlated with clinical measures of gait dysfunction (Rochester et al., 2012).

5.4 Subjects and methods

5.4.1 Source of subjects & ethics

Subjects were recruited from the Incidence of Cognitive Impairment in Cohorts with Longitudinal Evaluation–PD (ICICLE-PD) study. This study recruited newly diagnosed PD subjects from community and outpatient clinics in Newcastle upon Tyne/Gateshead and Cambridgeshire between June 2009 and December 2011, and was approved by the Newcastle and North Tyneside Research Ethics Committee.

5.4.2 Subjects

219 subjects with newly diagnosed PD (UK Brain Bank criteria; Hughes et al., 1992) were recruited into the ICICLE-PD study. Of these, gait analysis data, [^{18}F]-FDG PET and MRI were available for 47 subjects, constituting the dataset for present study.

5.4.3 Gait assessment

Gait assessment was performed in Newcastle. Subjects were asked to walk at a comfortable pace around a 25m circuit (figure 5.1). Gait parameters were repeatedly measured as the subject walked across the 7m Gaitrite mat. Subjects were tested 1 hour after taking PD medication.

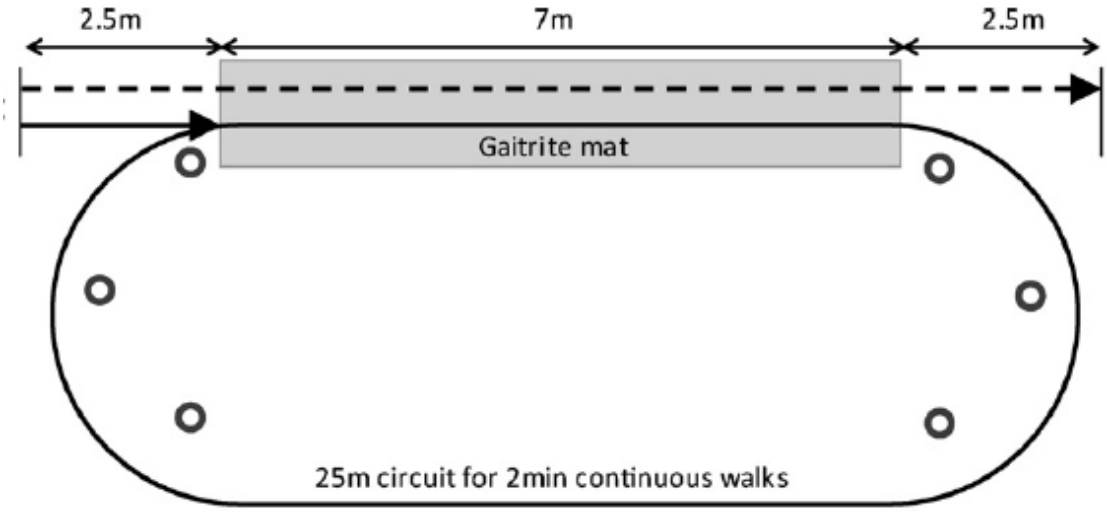


Figure 5.1. Laboratory arrangement for gait analysis. Reproduced from Galna et al. (2013).

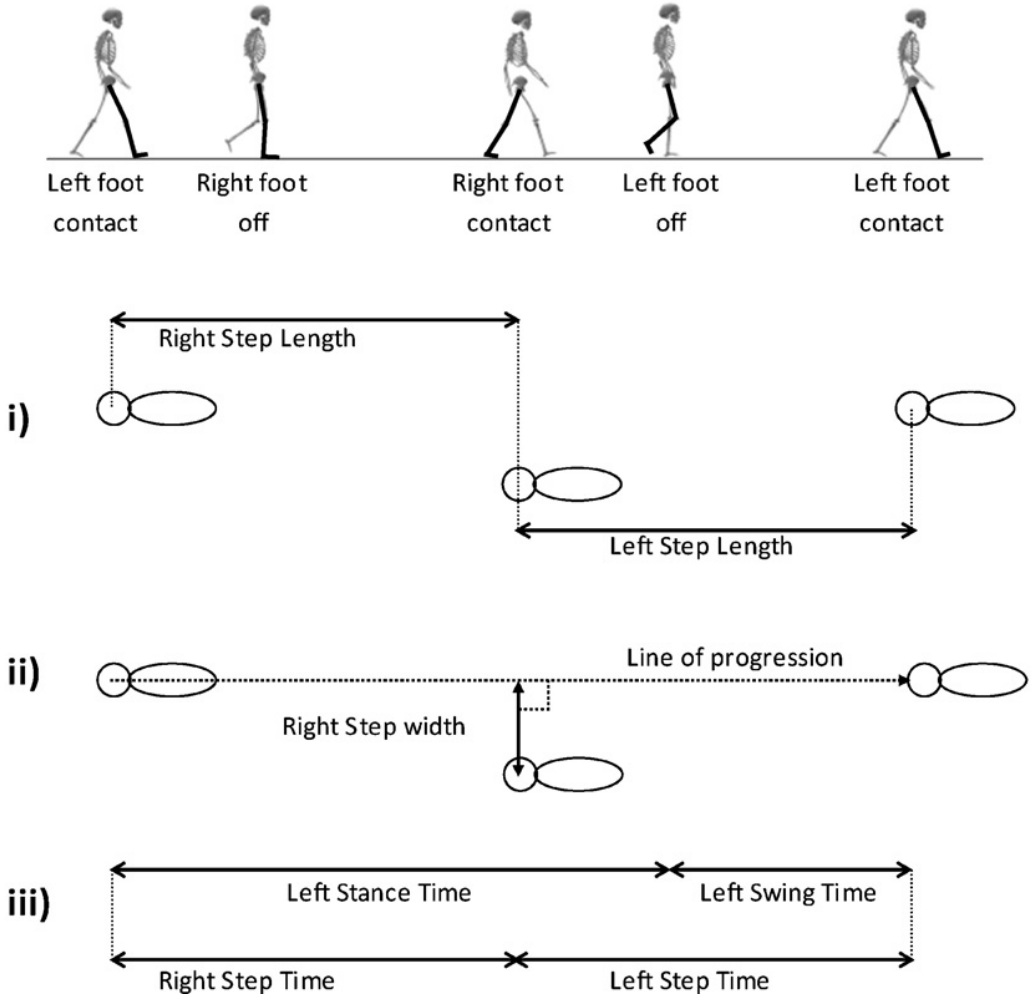


Figure 5.2. Illustration of gait parameters assessed: (i) length, (ii) width and (iii) timing. Reproduced from Galna et al. (2013).

5.4.4 Equipment

Gait was assessed using the Gaitrite instrumented walkway (CIR systems, USA). The Gaitrite system has a spatial resolution of 1.27 cm and a temporal resolution of 4.17 ms, and has been shown to be a valid and reliable method for the assessment of spatiotemporal gait parameters (Menz et al., 2004).

5.4.5 Gait characteristics

Table 5.1 shows the gait parameters derived from the above methodology (Galna et al, 2013; Lord et al. 2013). Figure 5.2 illustrates the definition of the terms used. Gait variability was calculated as the square root of the mean variance of left and right steps. Asymmetry was the difference between left and right steps.

5.4.6 Scans

T1-weighted MRI scans were acquired using a 3T Philips Intera Achieva scanner with a magnetization-prepared rapid gradient echo sequence (MPRAGE). [^{18}F]-FDG PET scans were acquired using a Siemens Biograph 40 scanner.

Table 5.1. Gait characteristics
Mean spatiotemporal characteristics
Step velocity (m/s)
Step length (m)
Step width (m)
Step time (ms)
Step swing time (ms)
Step stance time (ms)
Variability characteristics (SD)
Step velocity (m/s)
Step length (m)
Step width (m)
Step time (ms)
Step swing time (ms)
Step stance time (ms)
Asymmetry characteristics
Step length (m)
Step time (ms)
Step stance (ms)
Step swing time (ms)
Step velocity (m/s)
Step length (m)

5.4.7 Image analysis

Spatial normalisation of [^{18}F]-FDG and MR images into standard MNI stereotaxic space was performed using SPM8 implemented in Matlab 7. Subject-specific object maps for region of interest analysis were generated in ANALYZE (Mayo Clinic, Rochester, MN) as described in Chapter 2 (paragraph 2.9.4).

5.4.8 Region of interest data sampling

The subject-specific object map was laid over the spatially normalized [^{18}F]-FDG PET image in ANALYZE, followed by systematic sampling of the regions of interest (Chapter 2, paragraph 2.9.5).

5.4.9 Voxel-based analysis: statistical parametric mapping (SPM)

Correlations between [^{18}F]-FDG uptake at a voxel level and gait parameters were performed using SPM8 (Wellcome Trust Centre for Neuroimaging, UCL, London) as described in Chapter 2.

5.4.10 Statistical analysis

Statistical analysis was performed with SPSS 21.0 (IBM, NY). Normality of data distributions was interrogated with the Kolmogorov-Smirnov test. Correlations between variables were analysed with the Spearman Rank correlation test.

5.5 Results

The majority of variables failed the Kolmogorov-Smirnov test of normality. Non-parametric tests were therefore used throughout.

Region of interest analysis

5.5.1 ROI analysis: step velocity

Step velocity in PD correlated positively with [^{18}F]-FDG uptake in the putamen (ρ = 0.277, p = 0.030; figure 5.3).

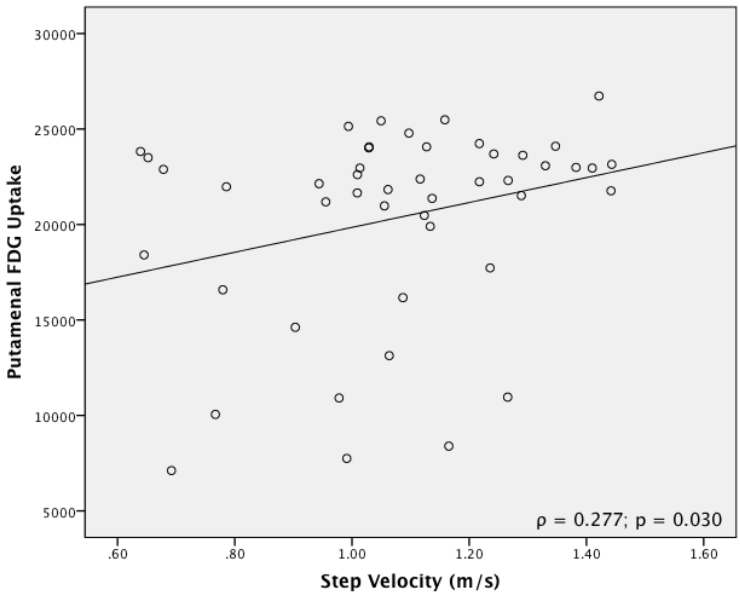


Figure 5.3. Correlation between putamenal [^{18}F]-FDG uptake and step velocity

5.5.2 ROI analysis: step velocity variability

Step velocity variability correlated inversely with [^{18}F]-FDG uptake in the anterior cingulate (ρ = -0. 284, p = 0.027; figure 5.4) and posterior cingulate (ρ = -0.428, p = 0.001; figure 5.5).

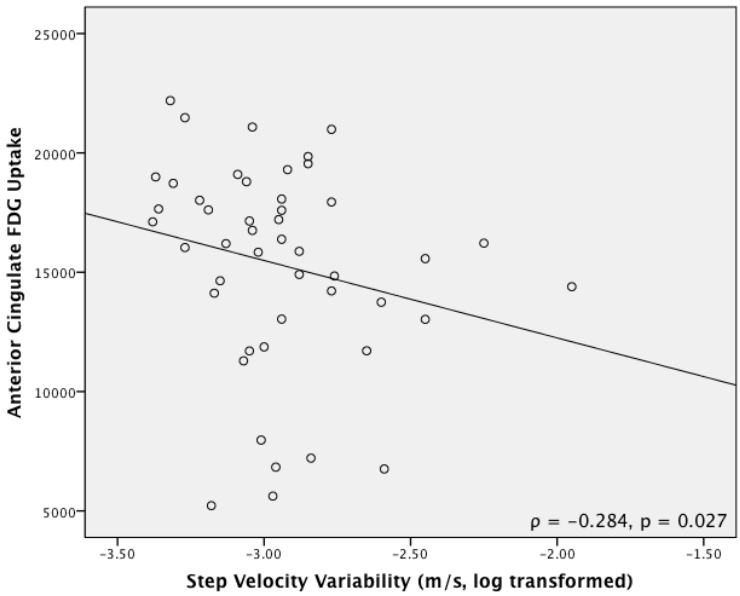


Figure 5.4. Correlation between anterior cingulate [^{18}F]-FDG uptake and step

velocity variability

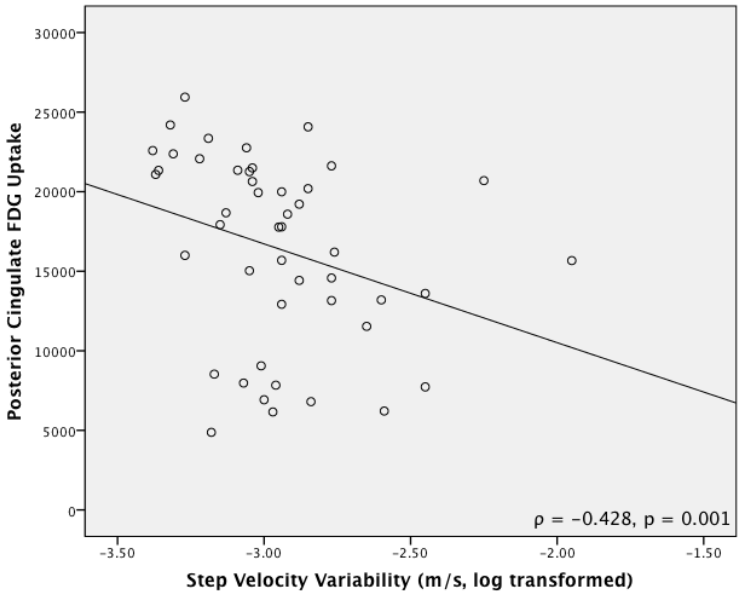


Figure 5.5. Correlation between posterior cingulate [^{18}F]-FDG uptake and step velocity variability

5.5.3 ROI analysis: step time

An inverse correlation was found between step time and [^{18}F]-FDG uptake at whole brain level, and in the brainstem, putamen, globus pallidus, anterior and posterior cingulate, insula, and in frontal and temporal lobes (table 5.2; Appendix, figures C1-9).

Table 5.2. Correlation between mean regional [^{18}F]-FDG uptake and step time.

	Correlation Coefficient (Spearman Rho)	**p value**
Whole brain	-0.271	0.032
Brainstem	-0.296	0.022
Putamen	-0.365	0.006
Globus pallidus	-0.380	0.004
Anterior cingulate	-0.253	0.043
Posterior cingulate	-0.278	0.029

Insula	-0.278	0.029
Frontal lobe	-0.271	0.033
Temporal lobe	-0.294	0.023

5.5.4 ROI analysis: step time variability

An inverse correlation was found between step time variability and [^{18}F]-FDG uptake at whole brain level, and in the brainstem, putamen, globus pallidus, anterior and posterior cingulate, insula, and in frontal and temporal lobes (table 5.3; Appendix, figures C10-17).

Table 5.3. Correlation between mean regional [^{18}F]-FDG uptake and step time variability.

	Correlation Coefficient (Spearman Rho)	**p value**
Whole brain	-0.291	0.024
Putamen	-0.403	0.003
Globus pallidus	-0.380	0.004
Anterior cingulate	-0.322	0.014
Posterior cingulate	-0.373	0.005
Insula	-0.314	0.016
Frontal lobe	-0.317	0.015
Temporal lobe	-0.322	0.014

5.5.5 ROI analysis: stance time

An inverse correlation between stance time and [^{18}F]-FDG uptake was found in the brainstem, putamen, globus pallidus, posterior cingulate, insula, and in frontal and temporal lobes (table 5.4; Appendix, figures C18-24).

Table 5.4. Correlation between mean regional [^{18}F]-FDG uptake and stance time.

	Correlation Coefficient (Spearman Rho)	**p value**
Brainstem	-0.263	0.037
Putamen	-0.302	0.012
Globus pallidus	-0.333	0.011
Posterior cingulate	-0.250	0.045
Insula	-0.247	0.047
Frontal lobe	-0.248	0.047
Temporal lobe	-0.264	0.037

5.5.6 ROI analysis: stance time variability

Stance time variability correlated inversely with [^{18}F]-FDG uptake at the whole brain level, and in the putamen, globus pallidus, anterior and posterior cingulate, insula, and in frontal and temporal lobes (table 5.5; Appendix C25-32).

Table 5.5. Correlation between mean regional [^{18}F]-FDG uptake and stance time variability.

	Correlation Coefficient (Spearman Rho)	**p value**
Whole brain	-0.256	0.041
Putamen	-0.326	0.013
Globus pallidus	-0.270	0.033
Anterior cingulate	-0.274	0.031
Posterior cingulate	-0.356	0.007
Insula	-0.257	0.041
Frontal lobe	-0.299	0.021
Temporal lobe	-0.276	0.030

5.5.7 ROI analysis: step length asymmetry

Step length asymmetry correlated inversely with [^{18}F]-FDG uptake in the caudate (ρ = -0.290, p = 0.024; Appendix, figure C33), and putamen (ρ = -0.281, p = 0.028; Appendix, figure C34).

5.5.8 ROI analysis: step length variability

An inverse correlation was found between step length variability and [^{18}F]-FDG uptake in the caudate, putamen, globus pallidus, anterior and posterior cingulate, insula, and in frontal and temporal lobes (table 5.6; Appendix, figure C35-42).

Table 5.6. Correlation between mean regional [^{18}F]-FDG uptake and step length variability.

	Correlation Coefficient (Spearman Rho)	**p value**
Caudate	-0.355	0.007
Putamen	-0.304	0.019
Globus pallidus	-0.248	0.047
Anterior cingulate	-0.347	0.008
Posterior cingulate	-0.452	0.001
Insula	-0.288	0.025
Frontal lobe	-0.253	0.043
Temporal lobe	-0.249	0.046

5.5.9 ROI analysis: step width variability

An inverse correlation was found between step width variability and [^{18}F]-FDG uptake in the striatum (ρ = -0.270, p=0.033; Appendix, figure C43).

5.5.10 ROI analysis: swing time

Swing time correlated inversely with [^{18}F]-FDG uptake at whole brain level, and in the brainstem, putamen, globus pallidus, posterior cingulate, and in frontal, temporal, parietal and occipital cortex (table 5.7; Appendix, figures C44-52).

Table 5.7. Correlation between mean regional [^{18}F]-FDG uptake and swing time.

	Correlation Coefficient (Spearman Rho)	**p value**
Whole brain	-0.296	0.022
Brainstem	-0.302	0.020
Putamen	-0.284	0.027
Globus pallidus	-0.339	0.010
Posterior cingulate	-0.251	0.045
Frontal lobe	-0.274	0.031
Temporal lobe	-0.298	0.021
Parietal lobe	-0.248	0.046
Occipital lobe	-0.247	0.047

5.5.11 ROI analysis: swing time variability

An inverse correlation was found between swing time variability and [^{18}F]-FDG uptake in the putamen, globus pallidus, cingulate, insula, and in frontal and temporal cortex (table 5.8; Appendix, figures C53-58).

Table 5.8. Correlation between mean regional [^{18}F]-FDG uptake and swing time variability.

	Correlation Coefficient (Spearman Rho)	**p value**
Putamen	-0.375	0.005
Globus pallidus	-0.303	0.019
Anterior cingulate	-0.279	0.029
Posterior cingulate	-0.341	0.009
Insula	-0.269	0.034
Frontal lobe	-0.251	0.045

Temporal lobe	-0.269	0.034

Voxel-based analysis: statistical parametric mapping (SPM)

5.5.12 SPM analysis: step time variability

Greater step time variability was associated with hypometabolism in the frontal lobes, and in the right striatum, insula and temporal lobe (figure 5.6, table 5.9).

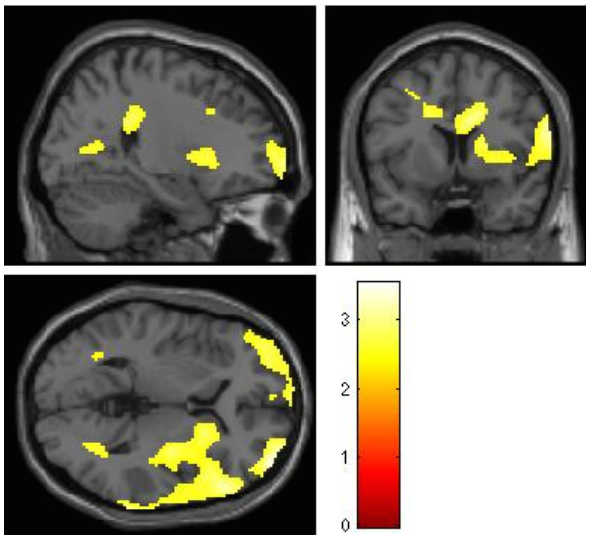


Figure 5.6. Negative correlation between [^{18}F]-FDG uptake and step time variability. Statistical parametric map (SPM) showing step time variability correlated inversely with [^{18}F]-FDG uptake in the frontal lobes, right striatum, insula and temporal cortex (voxel threshold p=0.01; cluster significance p<0.05, corrected). The colour stripe indicates Z score.

Table 5.9. Areas of inverse correlation between [^{18}F]-FDG uptake and step time variability.

	MNI coordinates			Area
Z score	*x*	*y*	*z*	
3.31	-12	67	-10	Left superior frontal gyrus
3.21	68	-18	20	Right postcentral gyrus
3.20	40	60	8	Right anterior prefrontal cortex

3.17	-12	-26	32	Posterior cingulate
3.16	14	63	-18	Right superior frontal gyrus
3.15	15	18	8	Right caudate
3.01	6	68	-24	Right medial frontal gyrus
2.96	23	11	8	Right putamen
2.95	69	-24	-4	Right middle temporal gyrus
2.95	58	28	4	Right inferior frontal gyrus
2.95	58	28	4	Right inferior frontal gyrus

5.5.13 SPM analysis: stance time

Longer stance time correlated with hypometabolism predominantly in the striatum, and fronto-temporal cortex (figure 5.7, table 5.10).

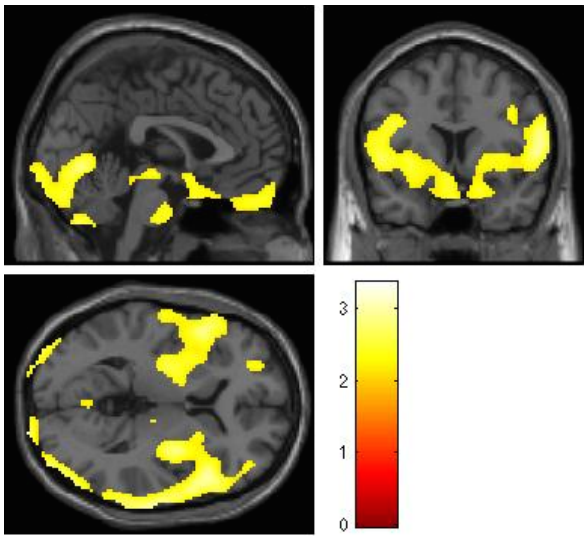


Figure 5.7. Negative correlation between [^{18}F]-FDG uptake and stance time. Statistical parametric map (SPM) showing stance time correlated inversely with [^{18}F]-FDG uptake predominantly in the putamen, frontal, temporal and insula cortex (voxel threshold p=0.02; cluster significance p<0.05, corrected). The colour stripe indicates Z score.

Table 5.10. Areas of inverse correlation between [^{18}F]-FDG uptake and stance time.

MNI coordinates			Area

Z score	*x*	*y*	*z*	
3.09	72	-22	-16	Right middle temporal gyrus
2.93	66	-8	16	Right postcentral gyrus
2.90	39	-8	-8	Right insula
2.88	-54	3	1	Left superior temporal gyrus
2.84	14	-24	-36	Pons
2.84	-54	18	2	Left inferior frontal gyrus
2.82	56	12	8	Right precentral gyrus
2.81	62	-60	28	Right angular gyrus
2.81	-34	-94	-18	Left secondary visual cortex
2.79	26	3	0	Right putamen
2.78	-40	7	2	Left insula
2.75	-24	-1	2	Left putamen

5.5.14 SPM analysis: stance time variability

Greater variability in stance time was associated with hypometabolism in the frontal lobes, posterior cingulate, and in the right striatum and insula (figure 5.8, table 5.11).

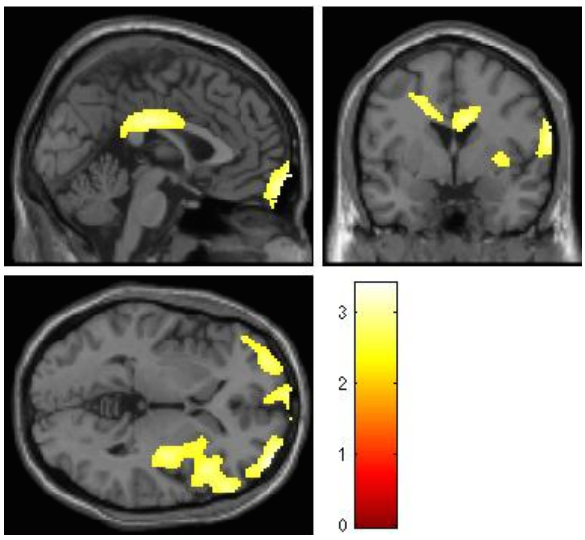


Figure 5.8. Negative correlation between [^{18}F]-FDG uptake and stance time variability. Statistical parametric map (SPM) showing stance time variability correlated inversely with [^{18}F]-FDG uptake in the frontal lobes, posterior cingulate,

right putamen and insula (voxel threshold p=0.01; cluster significance p<0.05, corrected). The colour stripe indicates Z score.

Table 5.11. Areas of inverse correlation between [^{18}F]-FDG uptake and stance time variability.

Z score	MNI coordinates			Area
	x	*y*	*z*	
3.19	-32	52	30	Left superior frontal gyrus
3.17	40	60	6	Right anterior prefrontal cortex
3.07	13	70	-10	Right medial frontal cortex
2.98	-12	-20	34	Cingulate
2.97	-10	-26	32	Posterior cingulate
2.94	68	-4	16	Right postcentral gyrus
2.93	27	-2	-2	Right putamen
2.91	41	12	-3	Right insula
2.91	6	68	-24	Right superior frontal gyrus
2.91	-40	54	14	Left middle frontal gyrus
2.90	-6	74	-6	Left medial frontal gyrus
2.90	64	10	20	Right inferior frontal gyrus
2.80	68	2	24	Right precentral gyrus

5.5.15 SPM analysis: step length asymmetry

Greater step length asymmetry correlated with hypometabolism in the striatum bilaterally and the right insula (figure 5.9, table 5.12).

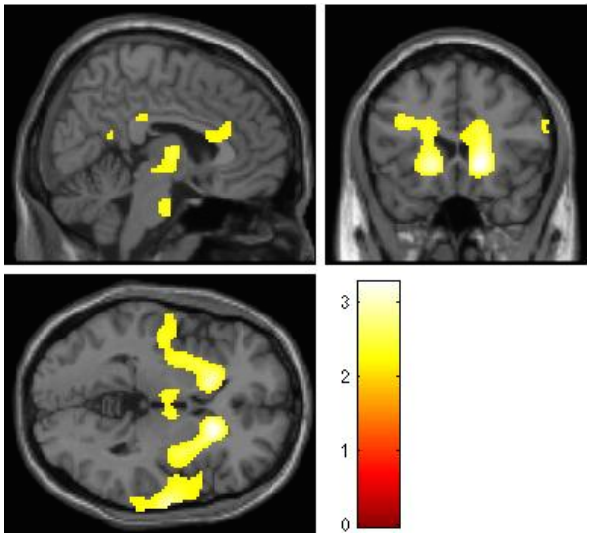


Figure 5.9. Negative correlation between [^{18}F]-FDG uptake and step length asymmetry. Statistical parametric map (SPM) showing step length asymmetry correlated inversely with [^{18}F]-FDG uptake in the striatum, thalamus, and right insula (voxel threshold p=0.02; uncorrected). The colour stripe indicates Z score.

Table 5.12. Areas of inverse correlation between [^{18}F]-FDG uptake and step length asymmetry.

	MNI coordinates			
Z score	*x*	*y*	*z*	Area
3.08	18	20	-2	Right caudate
2.88	68	-14	6	Right superior temporal gyrus
2.83	-16	18	-2	Left caudate
2.69	14	-6	10	Right thalamus
2.67	-44	-54	30	Left supramarginal gyrus
2.65	48	4	-40	Right middle temporal gyrus
2.60	40	-2	2	Right insula
2.54	-20	-38	30	Posterior cingulate
2.53	-24	-10	-32	Left parahippocampal gyrus
2.50	-18	4	34	Anterior cingulate
2.49	-12	-6	8	Left thalamus
2.46	28	6	-2	Right putamen
2.45	-52	-14	2	Left superior temporal gyrus
2.44	-27	5	2	Right putamen

5.5.16 SPM analysis: step length variability

Higher variability in step length was associated with hypometabolism in the striatum, posterior cingulate, frontal and temporal lobes (figure 5.10, table 5.13).

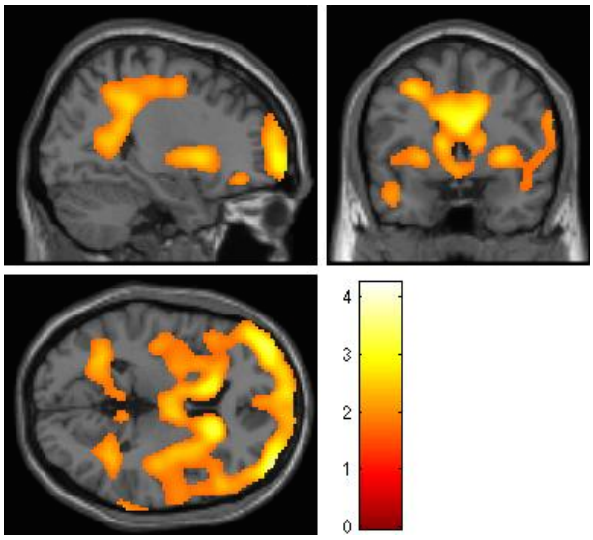


Figure 5.10. Negative correlation between [^{18}F]-FDG uptake and step length variability. Statistical parametric map (SPM) showing step length variability correlated inversely with [^{18}F]-FDG uptake in the striatum, posterior cingulate, and frontal and temporal cortex (voxel threshold p=0.05; uncorrected). The colour stripe indicates Z score.

Table 5.13. Areas of inverse correlation between [^{18}F]-FDG uptake and step length variability.

Z score	MNI coordinates			Area
	x	*y*	*z*	
3.87	-4	-28	28	Posterior cingulate
3.30	40	60	6	Right anterior prefrontal cortex
3.19	-42	54	10	Left middle frontal gyrus
3.07	16	20	6	Right caudate
3.02	-12	18	2	Left caudate
2.94	-20	66	18	Left anterior prefrontal cortex
2.85	-8	70	-14	Left superior frontal gyrus
2.82	-19	-3	6	Left putamen
2.74	14	66	26	Right superior frontal gyrus

2.64	54	36	24	Right middle frontal gyrus
2.53	27	3	2	Right putamen
2.49	-30	2	48	Left premotor cortex

5.5.17 SPM analysis: swing time variability

Swing time variability correlated with widespread cortical and subcortical hypometabolism, especially in the frontal and temporal lobes, insula, cingulate and striatum (figure 5.11, table 5.14).

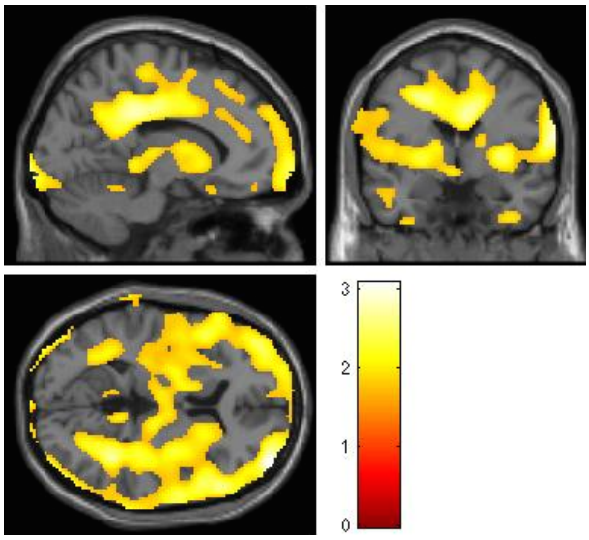


Figure 5.11. Negative correlation between [^{18}F]-FDG uptake and swing time variability. Statistical parametric map (SPM) showing swing time variability correlated inversely with [^{18}F]-FDG uptake predominantly in the striatum, insula, cingulate, frontal and temporal cortex (voxel threshold p=0.05; cluster significance p<0.05, corrected). The colour stripe indicates Z score.

Table 5.14. Areas of inverse correlation between [^{18}F]-FDG uptake and swing time variability.

	MNI coordinates			Area
Z score	*x*	*y*	*z*	
2.92	40	60	8	Right anterior prefrontal cortex
2.82	8	-22	32	Posterior cingulate
2.79	46	-44	12	Right superior temporal gyrus

2.71	68	-4	18	Right postcentral gyrus
2.69	-24	-1	-3	Left putamen
2.65	32	66	2	Right superior frontal gyrus
2.61	29	-19	-2	Right globus pallidus
2.56	16	20	30	Anterior cingulate
2.53	-25	-11	-3	Left globus pallidus
2.52	-26	-52	22	Left angular gyrus
2.52	28	3	2	Right putamen
2.52	56	26	6	Right inferior frontal gyrus
2.52	72	-24	-8	Right middle temporal gyrus
2.49	-28	28	-2	Left inferior frontal gyrus

5.6 Discussion

Metabolic deficits were detected that correlated with three gait domains: pace, variability and asymmetry. Abnormalities of gait pace and variability were associated with consistent patterns of regional brain hypometabolism. Three pace variables (step time, stance time and swing time), which together describe the complete gait cycle, correlated with hypometabolism in the brainstem, putamen, globus pallidus, cingulate and anterior neocortex. The pattern of metabolic derangement associated with gait variability parameters was very similar, with the notable absence of brainstem hypometabolism. These findings are discussed in the context of published data on normal gait physiology and ambulatory dysfunction in PD.

Several brainstem structures contribute to gait function. Although the precise extent of the MLR in humans is controversial (Alam et al., 2011), the complex is currently defined as the pedunculopontine nucleus (PPN), plus the adjacent cuneiform and subcuneiform nuclei (Garcia-Rill, 1991). The PPN contains cholinergic, glutamatergic, and GABAergic neurons (Martinez-Gonzalez et al, 2011). Loss of cholinergic neurons in the PPN accompanies that of dopaminergic neurons in the substantia nigra para compacta (SNc; Hirsch et al., 1987). The PPN has extensive connections throughout the neuraxis: it receives descending projections from the motor cortex and the output nuclei of the basal ganglia – the globus pallidus pars

interna (GPi) and the substantia nigra pars reticularis (SNr) and sends ascending efferent tracts to the basal ganglia (thalamus, GPi and SNc) and descending efferent projections to the pontomedullary RF which in turn projects to the spinal CPG (Martinez-Gonzalez et al, 2011; Bennaroch, 2013). Due to its role in the putative human MLR, the PPN has recently emerged as target for deep brain stimulation to relieve levodopa-refractory gait dysfunction, including FoG and falls (Alam et al., 2011). The usual explanation for a beneficial effect of dopamine on gait is via its action on established basal ganglia circuits: the nigrostriatal dopaminergic projections exert a prokinetic effect on the striatum (the input nuclei of the basal ganglia) by reducing the activity of inhibitory GABAergic neurons in the GPi and SNr (the basal ganglia output nuclei) which in turn project back to the brainstem MLR facilitating locomotion (Takakusaki et al., 2003; Ménard et al., 2007; Le Ray et al., 2011). There is, however, also evidence for direct dopaminergic innervation of the PPN by the SNc (Rolland et al., 2009; Ryczko et al., 2013).

Brainstem pathology may also influence gait via non-dopaminergic intrinsic brainstem structures (MLR and RF) and remote connections (glutamatergic and GABAergic), in addition to the dopaminergic pathology in the mesencephalic SNc. The present study found an association of brainstem hypometabolism with gait pace, but not variability. This may be because brainstem structures contribute to pace, a more rudimentary component of gait function, whilst excess variability is a consequence of impaired supratentorial control of brainstem locomotion structures, discussed below.

In functional MRI (fMRI) studies on healthy young adults, the premotor cortex (PMC) and supplementary area (SMA) are recruited in preparation for foot movement, consistent with the known role of these areas in motor planning (Sahyoun et al., 2004). Data from normal elderly subjects show that limb movements are associated with the recruitment of additional cortical regions. The anatomical extent of this differential activation increases with task difficulty, maximally encompassing the PMC, SMA, insula, anterior cingulate, and dorsal parietal and superior temporal lobes (Heuninckx et al., 2005). Thus movement is associated with increased cognitive demand as a function of normal aging.

Due to obvious logistic constraints, fMRI cannot be performed during walking tasks. Motor imagery, in which the subject imagines performing a specific motor task, has emerged as a proxy for real movement. Normal subjects imagining performing a gait task whilst undergoing fMRI scanning demonstrate activation of the primary motor cortex, PMC, SMA and cingulate (Wang et al., 2008). Based on similar physiological principles as fMRI, functional near-infrared spectroscopic topography (fNIRS) exploits the differential absorption spectra of oxyhaemoglobin and deoxyhaemoglobin to near-infrared light (which penetrates bone and soft tissue) to infer changes in cerebral blood flow, which are in turn driven by local neural activity (neurovascular coupling). Critically, the technique does not require the subject to lie supine in a fixed scanner, and the experimental apparatus is light enough to allow the real-time study of cortical activation during ambulation. Using fNIRS, Miyai et al. (2001) reported increases in activity of medial primary sensorimotor cortex (SMC) and SMA during ambulation in healthy adults, whilst increasing gait velocity resulted in greater activation of prefrontal cortex (PFC) and SMA (Suzuki et al., 2004). In normal elderly subjects, activation of SMC, SMA and PFC correlated with gait velocity, with greater activation of the PFC in subjects with low gait capacity, which may be a compensatory response to gait impairment (Harada et al., 2009). Imaging techniques such as fMRI and fNIRS have the temporal resolution to study cortical activation changes at the level of intra-stride kinematics. Using high density surface electroencephalography (EEG) and a sophisticated movement artifact subtraction algorithm, Gwin et al. (2011) have recorded cortical activity with intra-stride temporal resolution in the SMC, anterior cingulate and posterior parietal lobes. During an imagined gait task, Snijders et al. (2001) found reduced fMRI activation in medial frontal and posterior parietal cortex. The present study reports a correlation between gait pace and a pattern of cortical hypometabolism in PD subjects that includes the SMA, PFC, PMC and cingulate, regions implicated above in gait pace in normal subjects.

Increased gait variability is a well-recognised feature of PD (Blin et al., 1990; Hausdorff et al., 1998; Roemmich et al., 2012), and is detectable clinimetrically in recent-onset drug naïve patients, even in the absence of observable gait disorder (Baltadjieva et al., 2006). Moreover, gait variability is more common in PD subjects with a history of falls, and is predictive of a higher falls risk, independent of classical

motor symptoms (Hausdorff et al., 2001; Schaafsma et al., 2003). Although stride variability improves to some extent on dopaminergic therapy, it remains higher in fallers compared to non-fallers, implicating non-dopaminergic mechanisms (Schaafsma et al., 2003; Hausdorff et al., 2009).

Gait variability did not correlate with levels of brainstem hypometabolism in the present study, but variability in all gait parameters correlated with hypometabolism of the putamen, globus pallidus, cingulate, and anterior neocortex. This suggests that gait variability arises from a combination of cortical and basal ganglia dysfunction, whilst pace and rhythm may also be directly influenced by infratentorial pathology.
Gait variability in PD may in part be a consequence of an elevated cognitive load associated with ambulation, which may in turn be a compensatory response to subcortical (brainstem and basal ganglia) pathology. Yogev et al. (2005; 2007) showed that gait variability increases in a dual task condition in PD subjects but not in controls. Impairment on executive testing correlated with gait variability only in the dual task condition, in which elevated executive and attentional demand may exceed cognitive reserve, leading to gait decompensation (Yogev et al., 2005).

The SMA may be involved in making anticipatory postural adjustments, which are impaired in PD (Jacobs et al., 2009). Exaggerated gait variability may in part be a consequence of the failure to make normal anticipatory adjustments during ambulation. PD subjects with freezing of gait (FoG) exhibit reduced structural connectivity between the PPN and the frontal lobes (Fling et al., 2013), but have greater functional connectivity between the SMA and the MLR/PPN, compared to both PD subjects without FoG and controls, with the degree of excess connectivity correlating with objective measures of FoG (Fling et al., 2014). The authors interpreted this as an inadequate compensatory mechanism, arising in response either to loss of dopaminergic projections to the SMA, or to impaired basal ganglia control of gait, or both. During imagined gait tasks, PD subjects with FoG had lower fMRI activation in the globus pallidus, with a trend toward reduced activity in the SMA and MLR that may represent incipient failure of this compensatory response (Peterson et al., 2014).

Gait asymmetry is present in *de novo* PD patients and persists into advanced disease (Baltadjieva et al., 2006). This may be due to underlying asymmetry of pathology (Lord et al., 2013b), since nigral dopaminergic neuron loss is an asymmetric process (Fearnley and Lees, 1991). Nevertheless, gait asymmetry does not correlate with asymmetry of classical PD motor signs (Yogev et al., 2007). It has been suggested that gait asymmetry is causally related to FoG in PD (Plotnik et al., 2005), although this has recently been challenged (Danoudis et al., 2012; Boonstra et al., 2014). The present study reports a correlation between gait asymmetry and hypometabolism predominantly in the striatum, with less involvement of cortical structures than for gait variability parameters. This is consistent with a predominantly subcortical origin for gait asymmetry.

The above data are consistent with a model in which progressive brainstem and basal ganglia pathology in PD leads to increasing demand for cortical compensatory mechanisms beyond that seen in normal aging. When these cortical structures are themselves affected pathologically (Braak stages 5 and 6) these mechanisms will ultimately fail, leading to gait decompensation and disability.

Chapter 6

Summary of findings and conclusions

6.1 Activated microglia in Parkinson's disease

This is the first study to demonstrate that levels of microglial activation correlate with a wide range of motor and cognitive and other non-motor markers of phenotypic severity in a group of non-demented PD subjects with a broad range of disease duration, suggesting that neuroinflammation is relevant to the clinical phenotypic expression from early disease onwards. It confirms the widespread distribution of activated microglia in non-demented PD, involving brainstem, basal ganglia and neocortex. This implies that early patients already have advanced cortical (Braak stage 5 and 6) pathology well before the onset of dementia. The presence of activated microglia on PET imaging appears to be a valid biomarker of disease activity.

Motor disability (assessed with the UPDRS) correlated with [^{11}C]-(R)-PK11195 uptake in the putamen, globus pallidus and fronto-temporal cortex, regions involved in planning and execution of movement. Subject-reported depression scores correlated with widespread cortical [^{11}C]-(R)-PK11195 signal, suggesting that supratentorial pathology contributes to depression in PD, which may explain the failure of previous studies to find a consistent pattern of neurotransmitters imbalance in depressed PD subjects. Somnolence scores were also associated with diffuse cortical [^{11}C]-(R)-PK11195 uptake. Impaired performance on visuospatial cognitive tasks correlated with [^{11}C]-(R)-PK11195 signal in the dorsal parietal lobe which mediates visuospatial processing in normal subjects. Bilateral frontal lobe [^{11}C]-(R)-PK11195 uptake was associated with phonemic and semantic fluency deficits, tasks that depend on frontal lobe function. Impaired quality of life rated with the PDQ-39 scale correlated with extensive cortical and subcortical [^{11}C]-(R)-PK11195 uptake at baseline and follow up. Subject-rated non-motor symptom burden correlated with raised fronto-temporal and right putamenal [^{11}C]-(R)-PK11195 signal.

In the voxel-level analysis, shorter disease duration correlated with higher [^{11}C]-(R)-PK11195 uptake in the putamen and medial basal forebrain. The latter region contains the anterior olfactory nuclei, which is the first cortical structure affected according to Braak staging. Region of interest analysis showed a correlation between disease duration and brainstem [^{11}C]-(R)-PK11195 uptake at baseline, and striatal [^{11}C]-(R)-PK11195 uptake at follow-up. These findings again are in line with Braak staging, with initial accumulation of activated microglia in brainstem followed by striatum with disease progression. No statistically significant change in [^{11}C]-(R)-PK11195 uptake was found at a 2 year follow up assessment. This could reflect plateauing of inflammation in established disease or may be due to a lack of statistical power, or reflect a difference in sensitivity between the PET scanners used for baseline and follow-up imaging.

PD subjects at a higher risk of conversion to dementia due to an akinetic–rigid rather than tremulous phenotype showed raised [^{11}C]-(R)-PK11195 binding predominantly in the dorsal parietal and frontal cortex compared to lower risk subjects. If infiltration by activated microglia is an early phenomenon, and is quantitatively stable thereafter, the degree of microglial activation at baseline in early disease may determine subsequent rates of clinical deterioration, in which case the assessment of early pathological load could be prognostic. If activated microglia continue to accumulate with advancing disease, they may be a biomarker of disease progression, and consequently could be used to monitor the response to putative disease modifying treatments. These hypotheses are not mutually exclusive but to date imaging evidence supports a ceiling to levels of microglial activity.

Second-generation TSPO tracers ([^{11}C]-PBR28, [^{11}C]-DAA1106, [^{11}C]-PBR111 and [^{18}F]-FEPPA) have higher affinity than [^{11}C]-(R)-PK11195 and would be expected to provide a higher signal-to-noise ratio. However, they are affected by the polymorphism of TSPO expressed by subjects leading to heterogeneous pharmacodynamics at a population level whereas [^{11}C]-(R)-PK11195 is free of this problem. There are no published studies in PD to date using any of the second-generation tracers, though two studies have been reported in AD (using [^{11}C]-DAA1106 and [^{11}C]-PBR28) and the signal to noise did not seem improved though uptake was more confluent. In the present study it was not possible to demonstrate

robust changes in [^{11}C]-PK11195 binding in individual subjects over a two year interval to justify its use in monitoring the effect of putative disease-modifying therapies. It remains possible that [^{11}C]-(R)-PK11195 might provide prognostic information in individual patients, but the signal-to-noise ratio of this tracer is low. Further, PET using ^{11}C radiotracers is not practical for clinical use, since the short half-life of ^{11}C (20 minutes) necessitates on-site synthesis in a particle accelerator, limiting it to a research setting. ^{18}F based ligands, with a half-life of 110 minutes, may be sourced externally, and their routine use in clinical scenarios is therefore feasible. The conditions for a satisfactory TSPO tracer for clinical deployment would therefore be: a high signal-to-noise ratio; pharmacodynamic homogeneity; and a longer half-life.

6.2 Amyloid deposition in Parkinson's disease

Increased [^{11}C]-PIB uptake was found throughout the neocortex and striatum in non-demented PD cases compared to controls, with a posterior cortical predilection. Further accumulation of amyloid in this group was demonstrated by repeat scanning at two years. This is the first time amyloid accumulation in individual PD subjects has been demonstrated with PET. [^{11}C]-PIB uptake in the PD dementia group was higher than in the non-demented group, with greater anterior cortical involvement. Striatal [^{11}C]-PIB binding was elevated in the non-demented PD group and levels correlated inversely with verbal fluency. Subjective motor disability, impaired verbal fluency, and communication difficulties were all associated with raised frontal lobe [^{11}C]-PIB uptake, suggesting that amyloid may contribute to frontal lobe dysfunction in PD. When the PD and PDD subjects were analysed as a unified group, striatal [^{11}C]-PIB retention correlated with widespread cortical hypometabolism, suggesting that striatal amyloid accompanies generalised cortical dysfunction, notwithstanding a potential direct effect of striatal amyloid on cognition.

[^{11}C]-PIB PET has been used extensively in the AD literature, but remains a research tool due to the short half-life of ^{11}C. The development of ^{18}F based amyloid-specific tracers for clinical use is more advanced than for TSPO ligands: florbetapir, flutemetamol and florbetaben are now approved for the diagnostic evaluation of

patients with suspected AD in the United States and Europe. As with the presence of activated microglia, a raised amyloid load in PD may predict cognitive decline and prove to have prognostic utility. Anti-amyloid immunotherapy trials for AD, however, have generally been disappointing (Counts and Lahiri, 2014). One reason for this may be that much of the amyloid deposition in AD occurs in the pre-symptomatic stage, and hence anti-amyloid therapies given to patients with symptomatic disease may be too late to affect clinical status, despite a demonstrable reduction in brain amyloid load, measured with [^{11}C]-PIB PET (Rinne et al., 2010; Rosenberg, 2011; Salloway et al., 2014). Furthermore, current anti-amyloid monoclonal antibody treatments have toxicity issues, especially meningo-encephalitis and vasogenic oedema (Lambracht-Washington and Rosenberg, 2013). Since amyloid deposition in PD may well occur later than in AD, it may be more responsive to therapeutic intervention during symptomatic disease, especially if a less toxic small molecule drug were available.

6.3 Brain glucose metabolism and gait dysfunction in Parkinson's disease

[^{18}F]-FDG PET revealed a correlation of brain hypometabolism with gait dysfunction in three domains: pace, variability and asymmetry. Reduced gait velocity was associated with hypometabolism in the brainstem, putamen, globus pallidus, cingulate and anterior cortical structures. Increased gait variability correlated with a very similar pattern of anterior cortical and basal ganglia metabolic dysfunction, but did not affect the brainstem. The basic gait cycle is produced by descending control of a spinal pattern generator by brainstem structures, including the mesencephalic locomotor centre and pontomedullary reticular formation. Gait velocity is a rudimentary component of gait function, hence may be affected by intrinsic brainstem pathology. Excess gait variability is thought to be due to impaired supratentorial regulation of brainstem locomotion structures. Gait dysfunction in early PD is likely due to brainstem and basal ganglia pathology, with increased demand for cortical compensation. In advanced PD, intrinsic neocortical pathology will affect the capacity of these compensatory mechanisms, which, combined with progression of subcortical pathology, manifests as increased gait variability and locomotor instability. Whilst this work has predominantly been an investigation into the pathologic basis of gait dysfunction in PD, in clinical practice, imaging cortical metabolic activity with [^{18}F]-

FDG or [^{99m}Tc]-HMPAO (hexamethylpropylene amine oxime) SPECT may identify subjects at risk of falling.

Chapter 7
Appendix

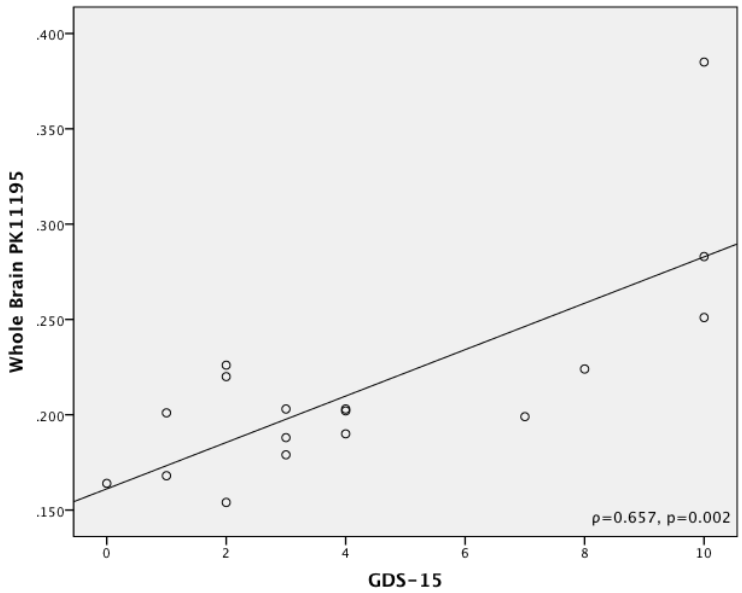


Figure A1. Correlation between whole brain [^{11}C]-(R)-PK11195 BP_{ND} and GDS-15

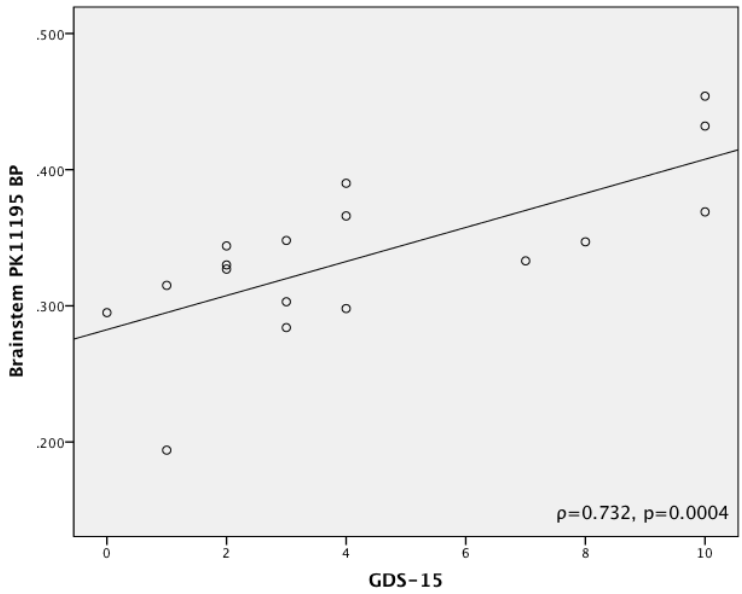


Figure A2. Correlation between brainstem [^{11}C]-(R)-PK11195 BP_{ND} and GDS-15

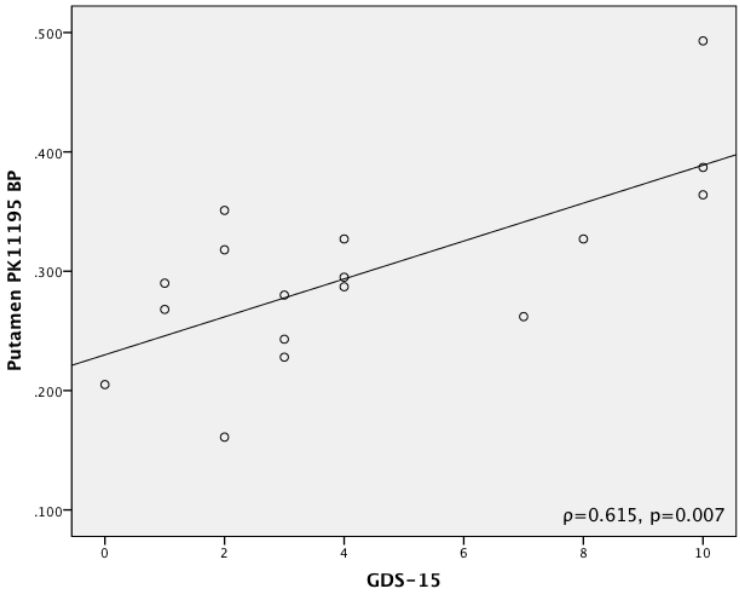


Figure A3. Correlation between putamenal [^{11}C]-(R)-PK11195 BP_{ND} and GDS-15

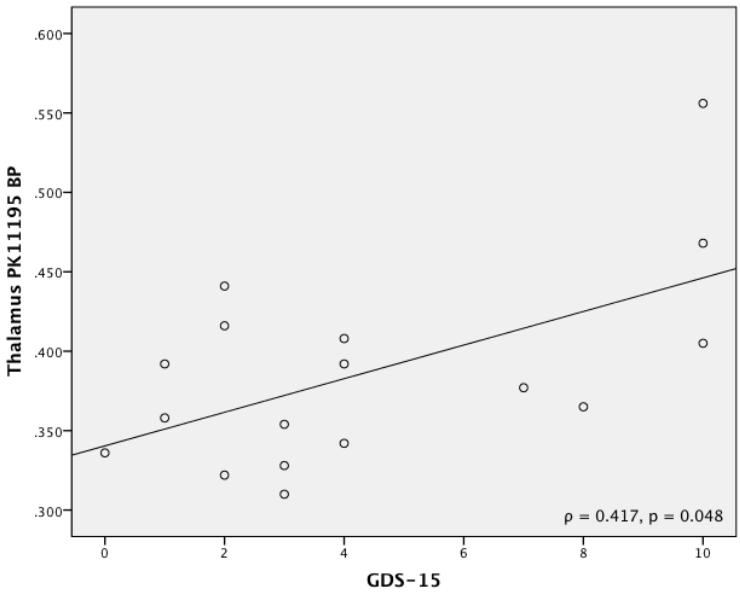


Figure A4. Correlation between thalamic [^{11}C]-(R)-PK11195 BP_{ND} and GDS-15

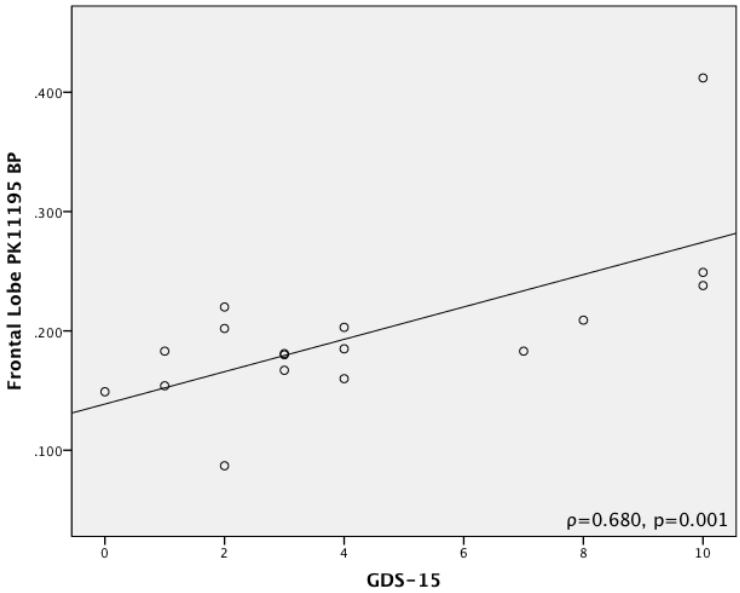


Figure A5 Correlation between frontal lobe [^{11}C]-(R)-PK11195 BP_{ND} and GDS-15

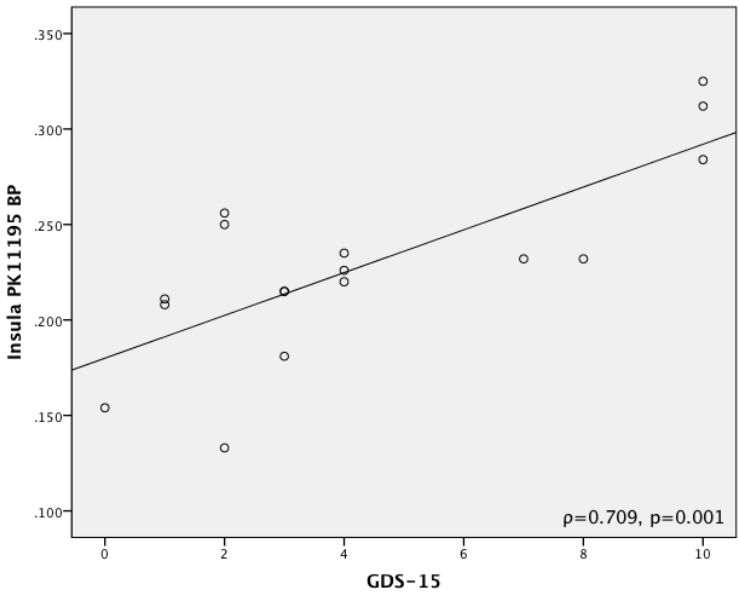


Figure A6. Correlation between insula [^{11}C]-(R)-PK11195 BP_{ND} and GDS-15

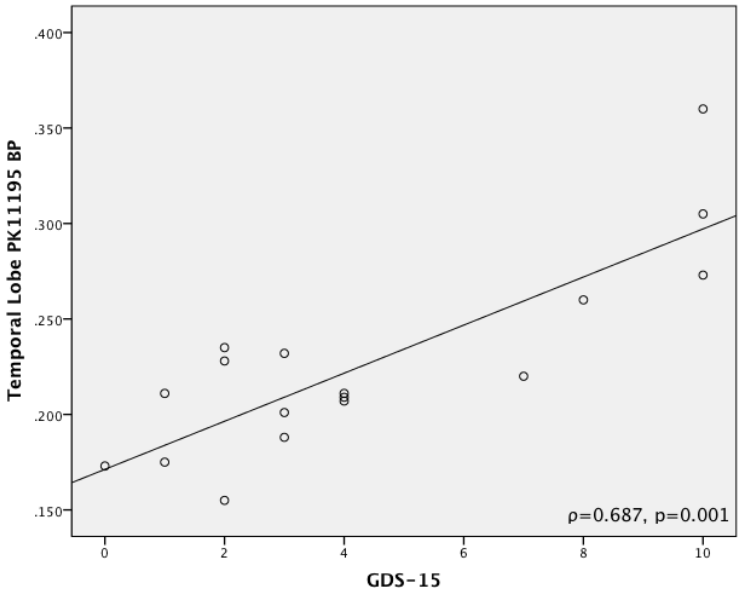


Figure A7. Correlation between temporal lobe [^{11}C]-(R)-PK11195 BP_{ND} and GDS-15

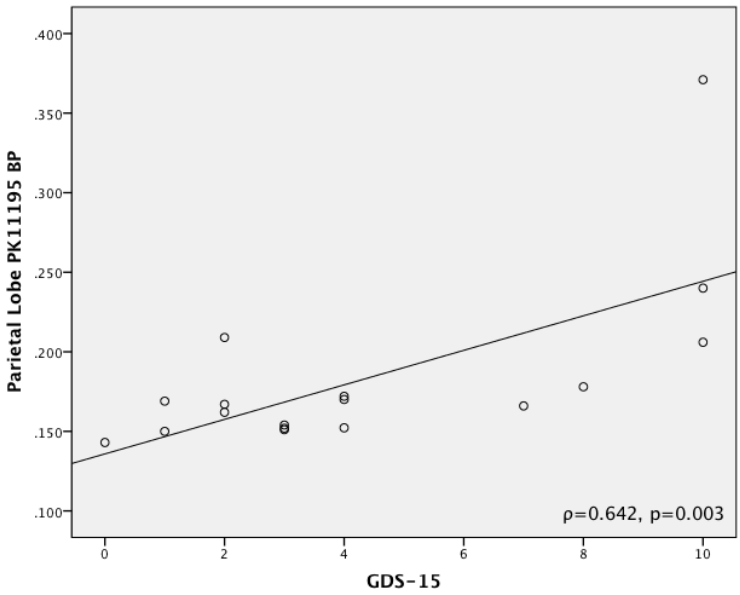


Figure A8. Correlation between parietal lobe [^{11}C]-(R)-PK11195 BP_{ND} and GDS-15

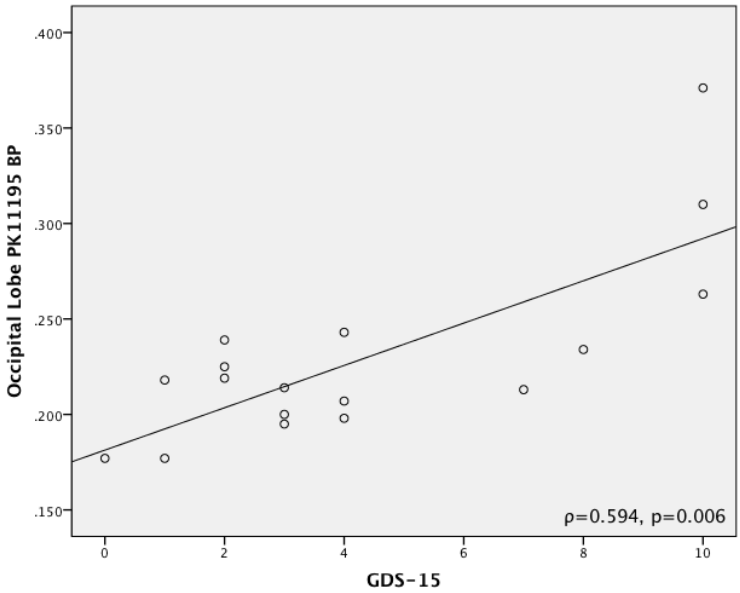


Figure A9. Correlation between occipital lobe [^{11}C]-(R)-PK11195 BP_{ND} and GDS-15

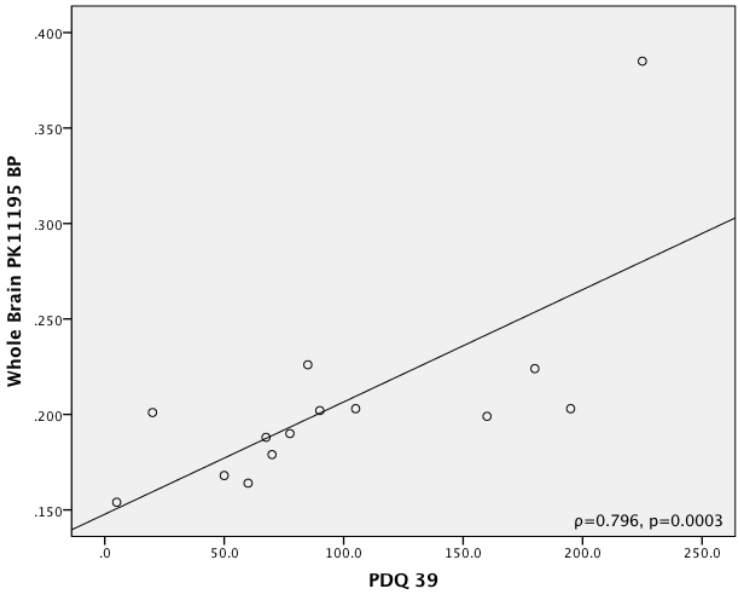


Figure A10. Correlation between whole brain [^{11}C]-(R)-PK11195 BP_{ND} and PDQ 39 at baseline

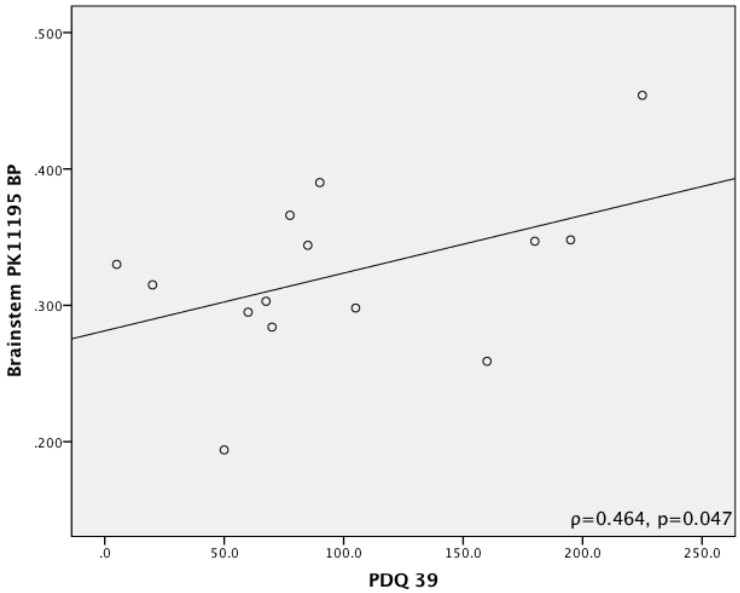


Figure A11. Correlation between brainstem [^{11}C]-(R)-PK11195 BP_{ND} and PDQ 39 at baseline

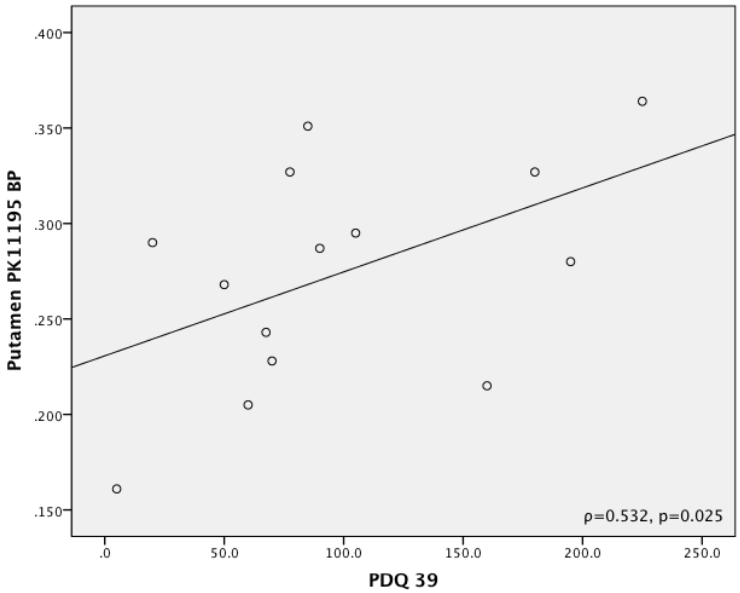


Figure A12. Correlation between putamenal [^{11}C]-(R)-PK11195 BP_{ND} and PDQ 39 at baseline

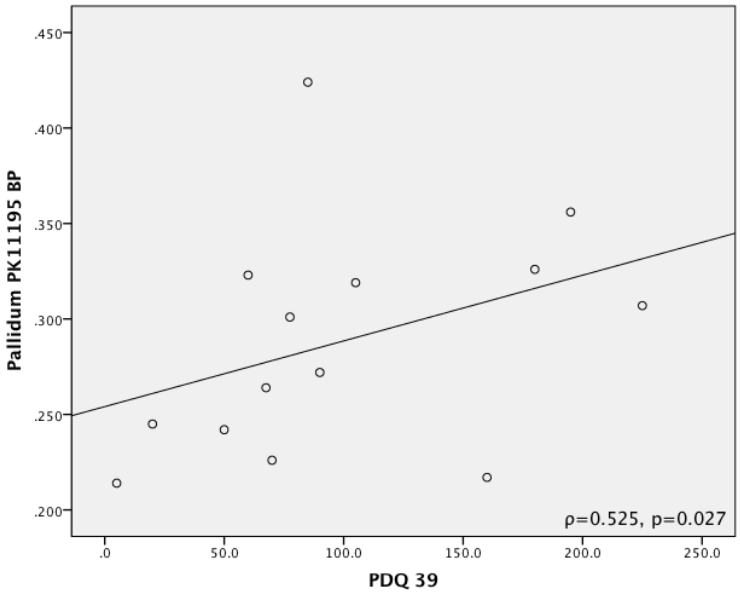


Figure A13. Correlation between globus pallidus [^{11}C]-(R)-PK11195 BP_{ND} and PDQ 39 at baseline

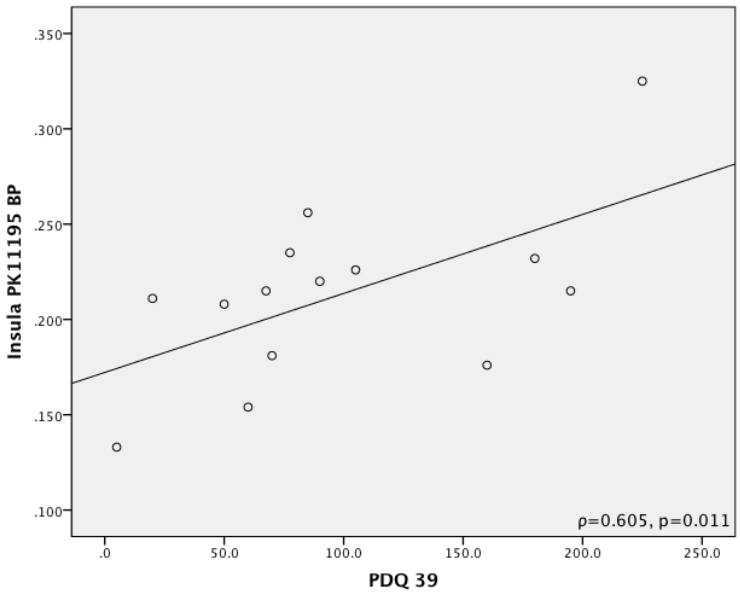


Figure A14. Correlation between insula [^{11}C]-(R)-PK11195 BP_{ND} and PDQ 39 at baseline

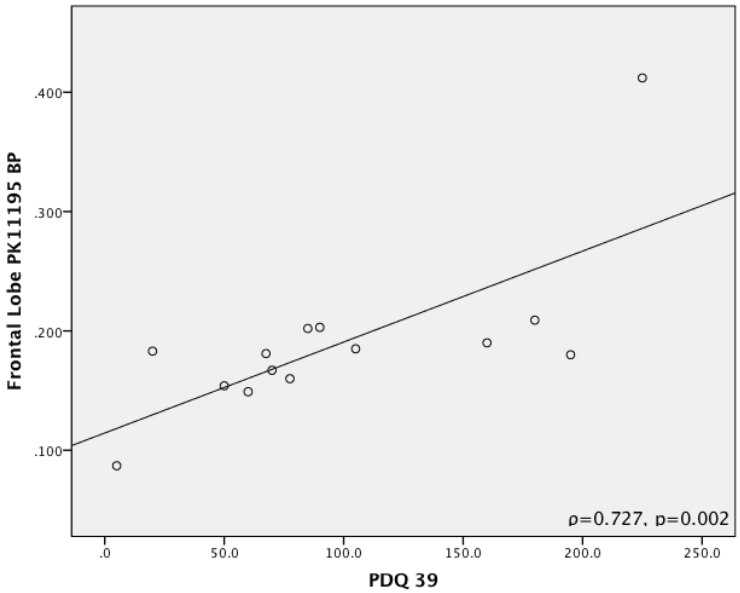


Figure A15. Correlation between frontal lobe [^{11}C]-(R)-PK11195 BP_{ND} and PDQ 39 at baseline

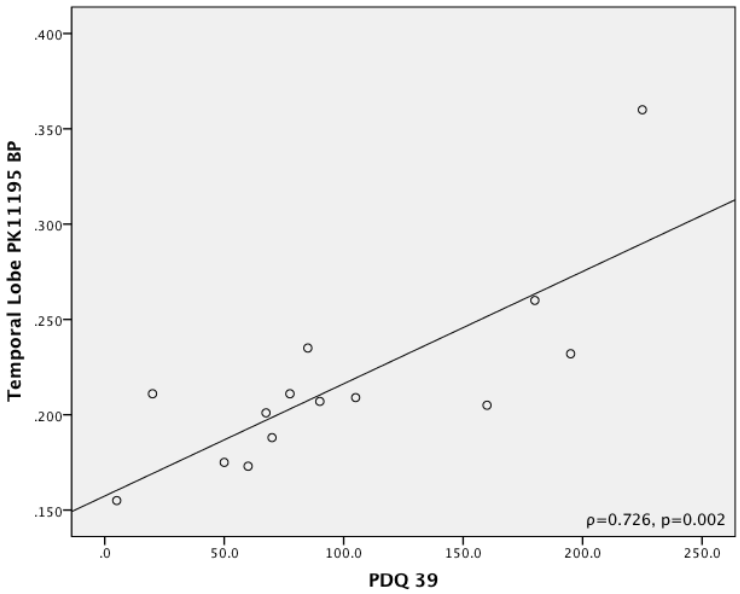


Figure A16. Correlation between temporal lobe [^{11}C]-(R)-PK11195 BP_{ND} and PDQ 39 at baseline

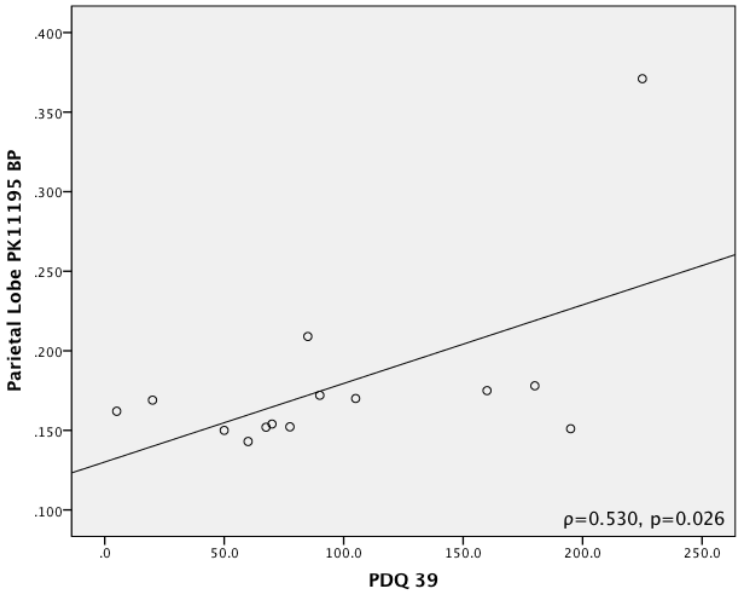


Figure A17. Correlation between parietal lobe [^{11}C]-(R)-PK11195 BP_{ND} and PDQ 39 at baseline

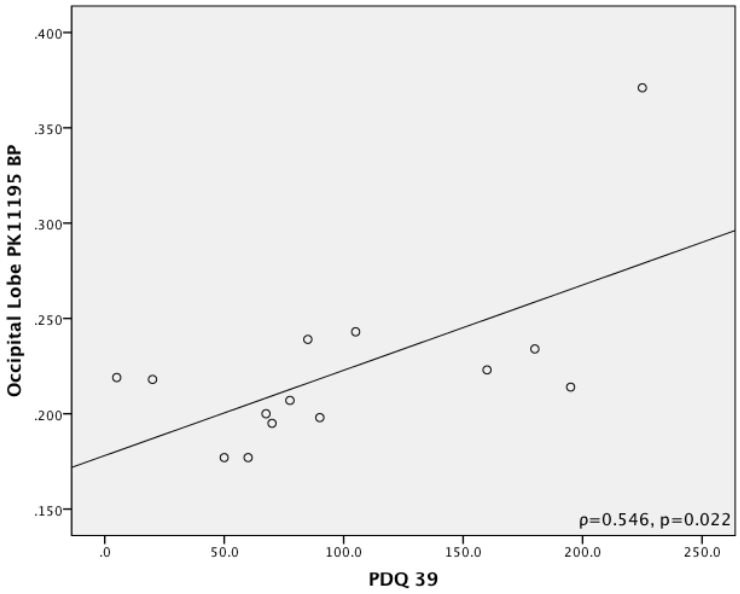


Figure A18. Correlation between occipital lobe [^{11}C]-(R)-PK11195 BP_{ND} and PDQ 39 at baseline

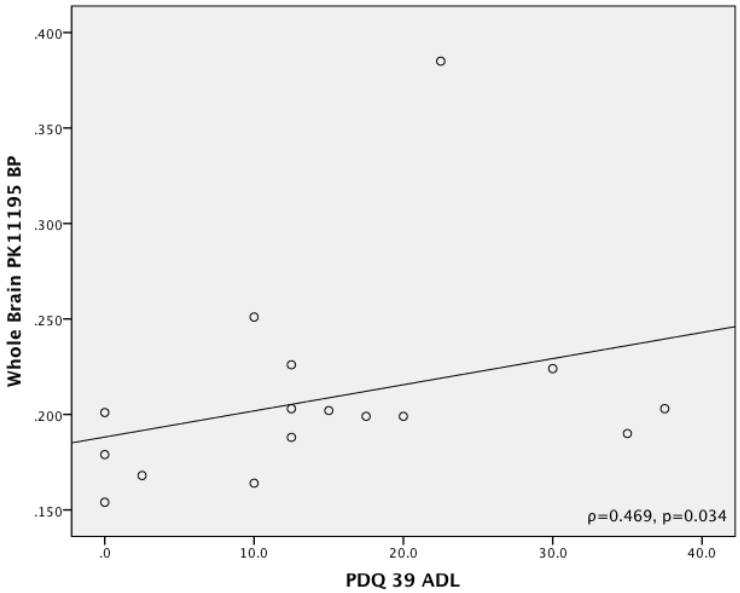


Figure A19. Correlation between whole brain [^{11}C]-(R)-PK11195 BP_{ND} and PDQ 39 ADL domain at baseline

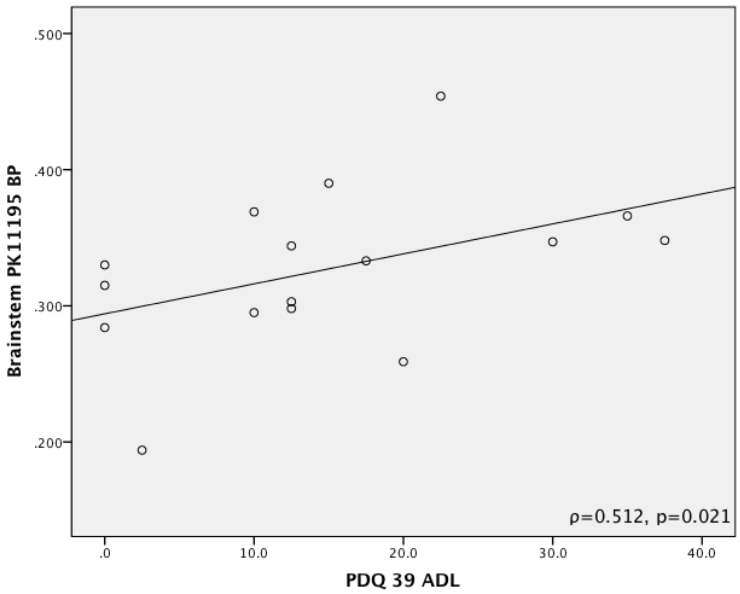


Figure A20. Correlation between brainstem [^{11}C]-(R)-PK11195 BP_{ND} and PDQ 39 ADL domain at baseline

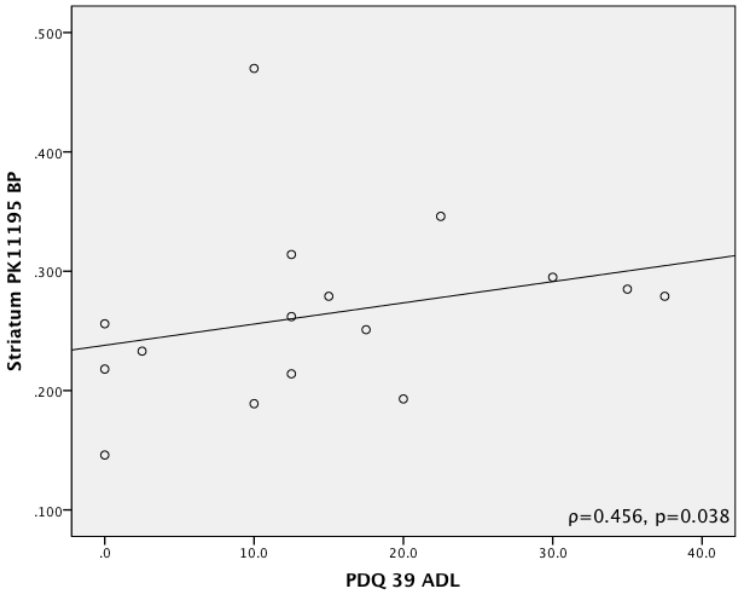


Figure A21. Correlation between striatal [^{11}C]-(R)-PK11195 BP_{ND} and PDQ 39 ADL domain at baseline

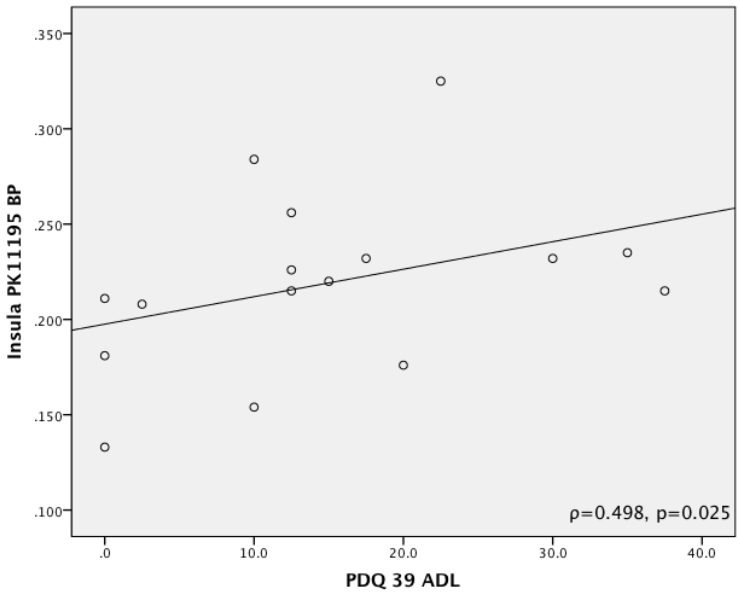


Figure A22. Correlation between insula [^{11}C]-(R)-PK11195 BP_{ND} and PDQ 39 ADL domain at baseline

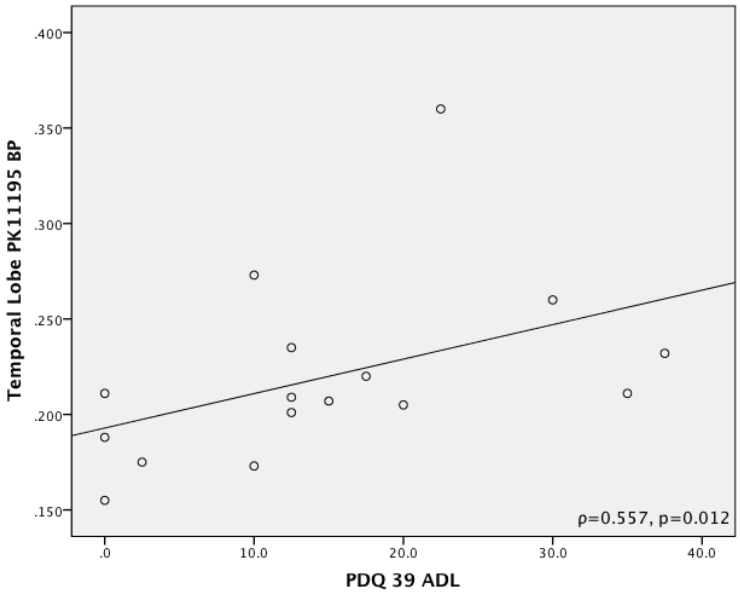


Figure A23. Correlation between temporal lobe [^{11}C]-(R)-PK11195 BP_{ND} and PDQ 39 ADL domain at baseline

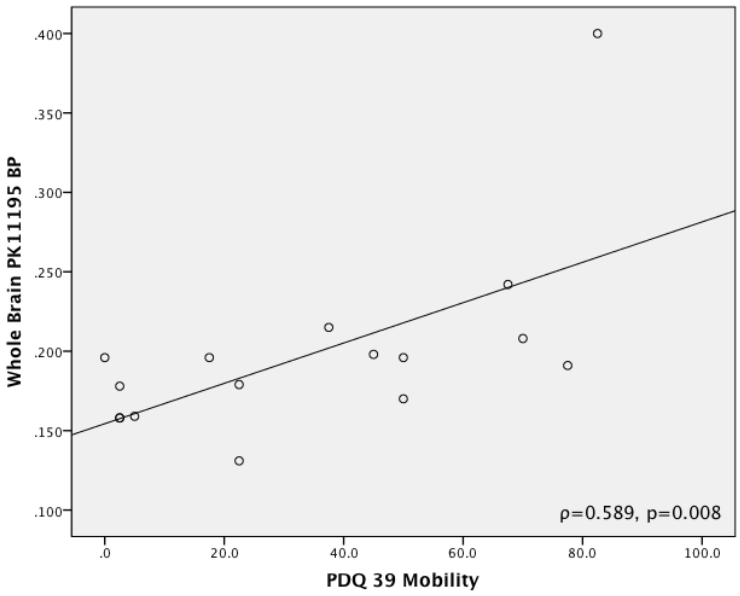


Figure A24. Correlation between whole brain [^{11}C]-(R)-PK11195 BP_{ND} and PDQ 39 Mobility domain at baseline

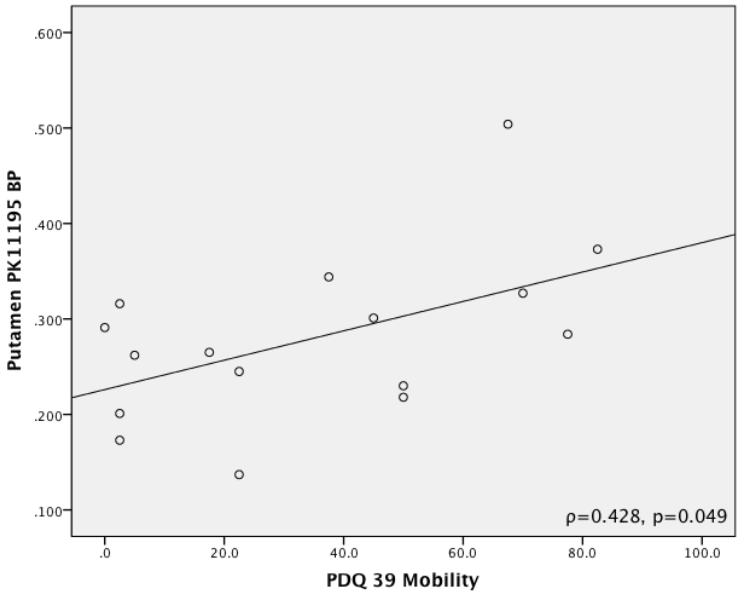


Figure A25. Correlation between putamenal [^{11}C]-(R)-PK11195 BP_{ND} and PDQ 39 Mobility domain at baseline

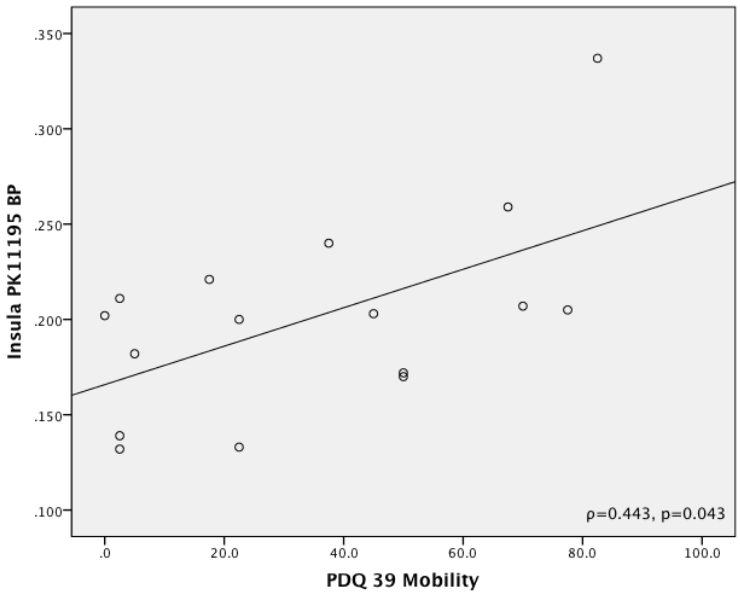


Figure A26. Correlation between insula [^{11}C]-(R)-PK11195 BP_{ND} and PDQ 39 Mobility domain at baseline

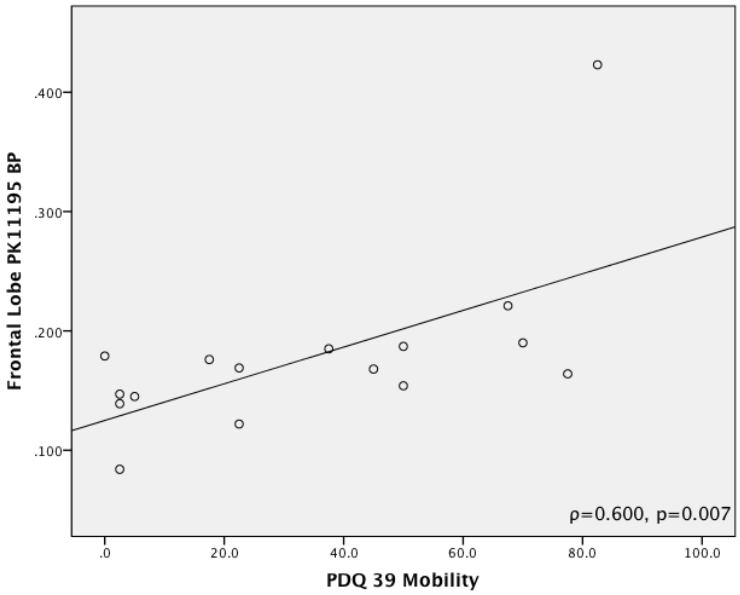


Figure A27. Correlation between frontal lobe [^{11}C]-(R)-PK11195 BP_{ND} and PDQ 39 Mobility domain at baseline

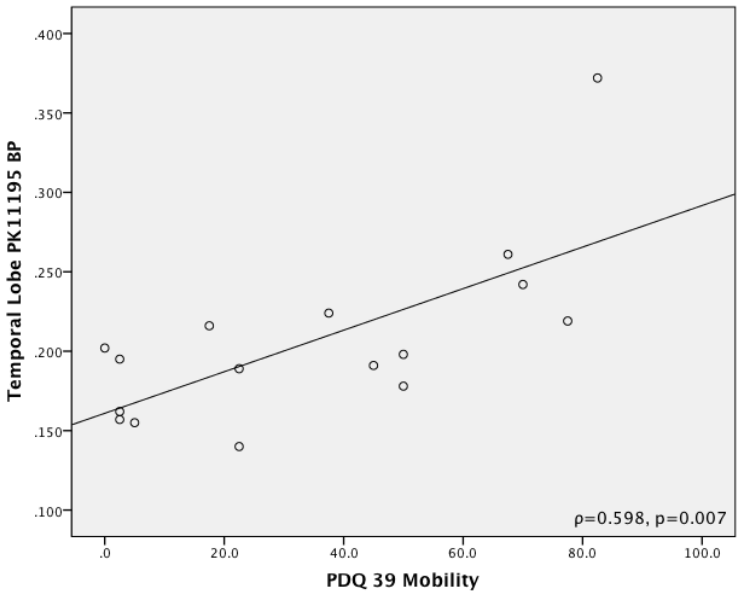


Figure A28. Correlation between temporal lobe [^{11}C]-(R)-PK11195 BP_{ND} and PDQ 39 Mobility domain at baseline

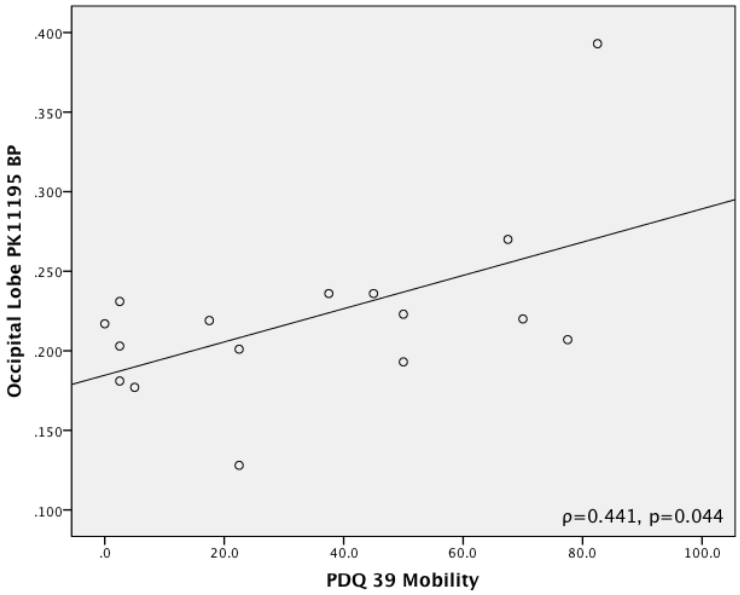


Figure A29. Correlation between occipital lobe [^{11}C]-(R)-PK11195 BP_{ND} and PDQ 39 Mobility domain at baseline

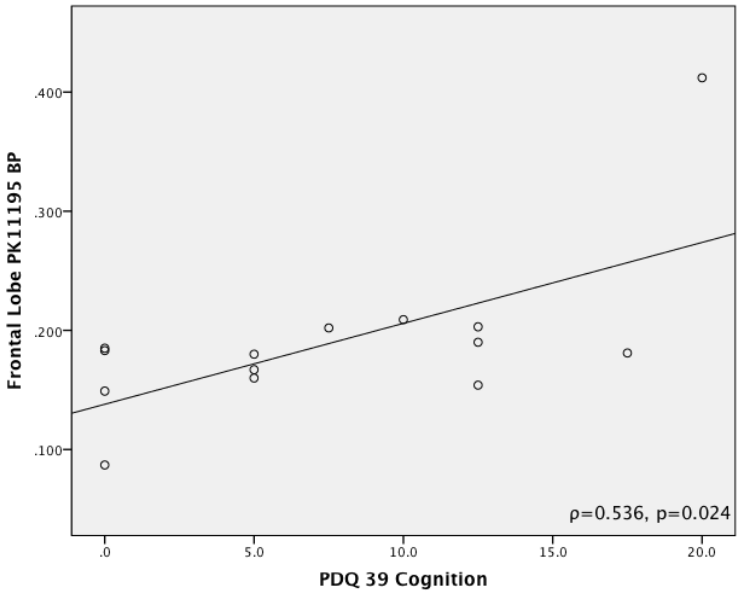


Figure A30. Correlation between frontal lobe [^{11}C]-(R)-PK11195 BP_{ND} and PDQ 39 Cognition domain at baseline

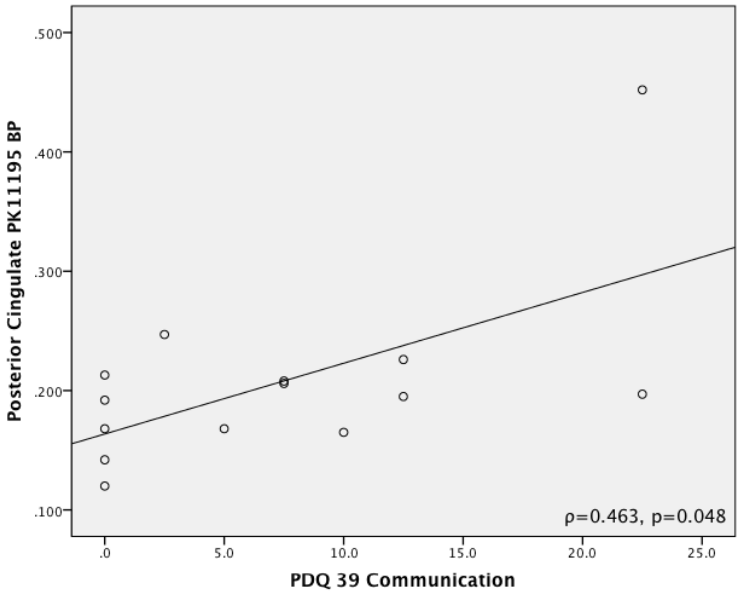


Figure A31. Correlation between posterior cingulate [^{11}C]-(R)-PK11195 BP_{ND} and PDQ 39 Communication domain at baseline

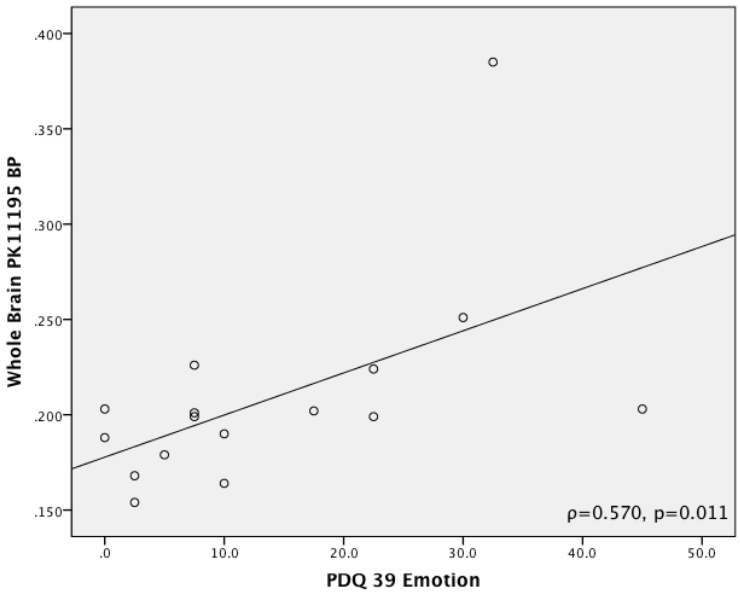


Figure A32. Correlation between whole brain [^{11}C]-(R)-PK11195 BP_{ND} and PDQ 39 Emotional Wellbeing domain at baseline

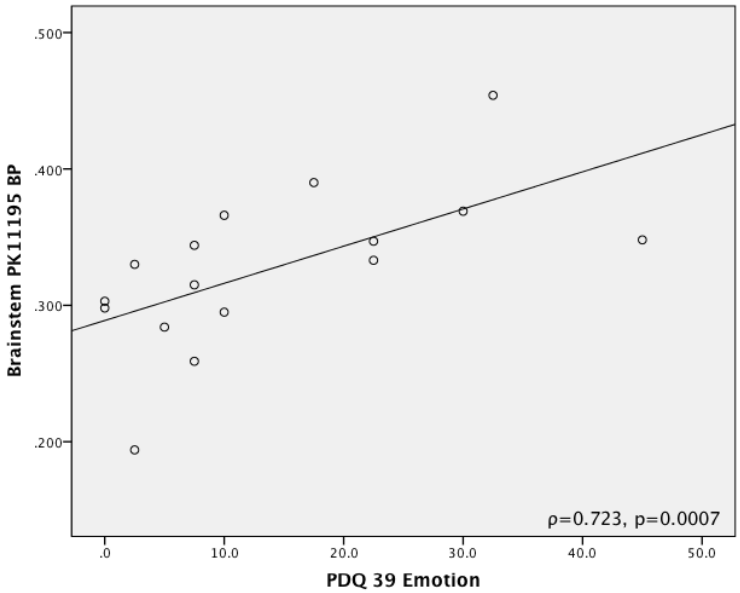


Figure A33. Correlation between brainstem [^{11}C]-(R)-PK11195 BP_{ND} and PDQ 39 Emotional Wellbeing domain at baseline

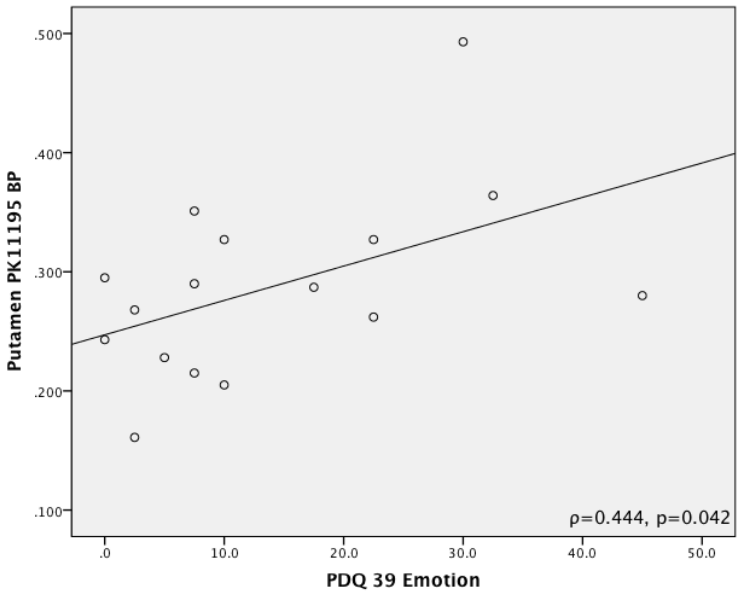


Figure A34. Correlation between putamenal [^{11}C]-(R)-PK11195 BP_{ND} and PDQ 39 Emotional Wellbeing domain at baseline

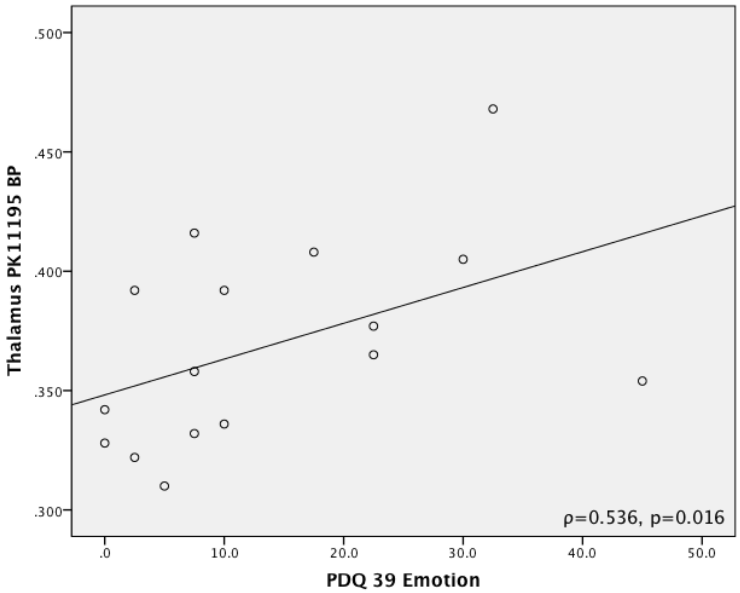


Figure A35. Correlation between thalamic [^{11}C]-(R)-PK11195 BP_{ND} and PDQ 39 Emotional Wellbeing domain at baseline

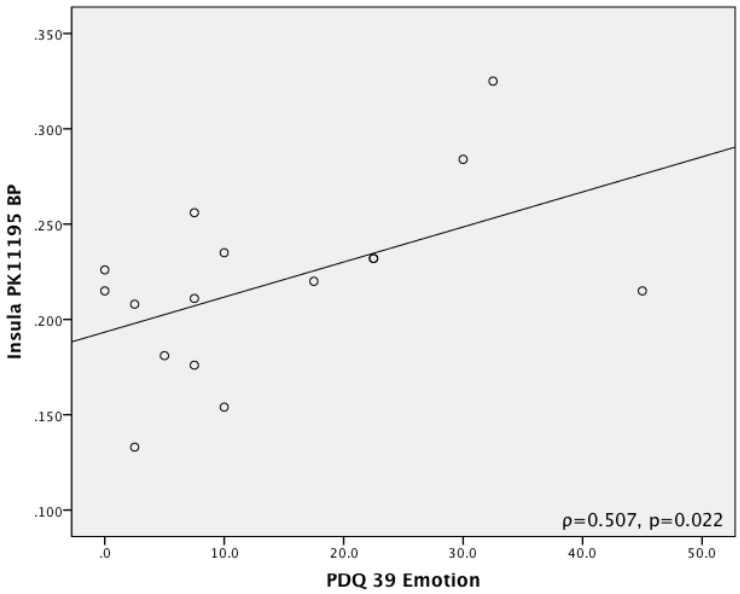


Figure A36. Correlation between insula [^{11}C]-(R)-PK11195 BP_{ND} and PDQ 39 Emotional Wellbeing domain at baseline

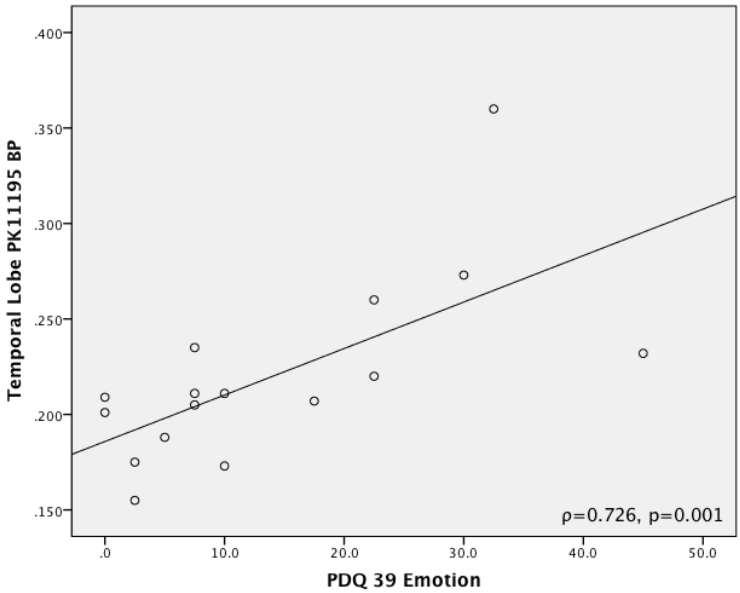


Figure A37. Correlation between temporal lobe [^{11}C]-(R)-PK11195 BP_{ND} and PDQ 39 Emotional Wellbeing domain at baseline

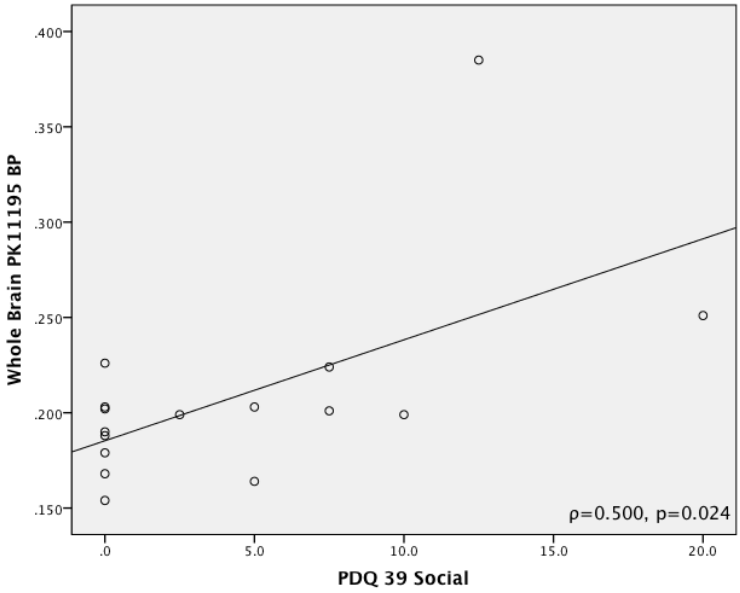


Figure A38. Correlation between whole brain [^{11}C]-(R)-PK11195 BP_{ND} and PDQ 39 Social domain at baseline

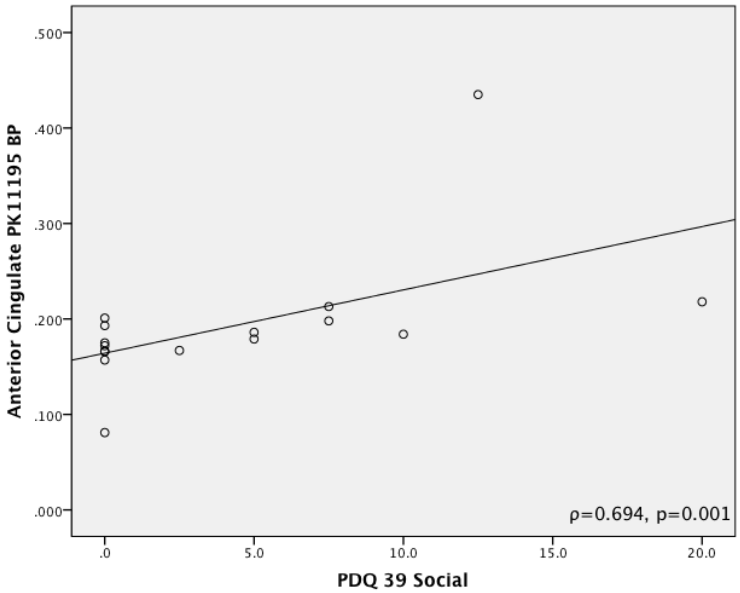


Figure A39. Correlation between anterior cingulate [^{11}C]-(R)-PK11195 BP_{ND} and PDQ 39 Social domain at baseline

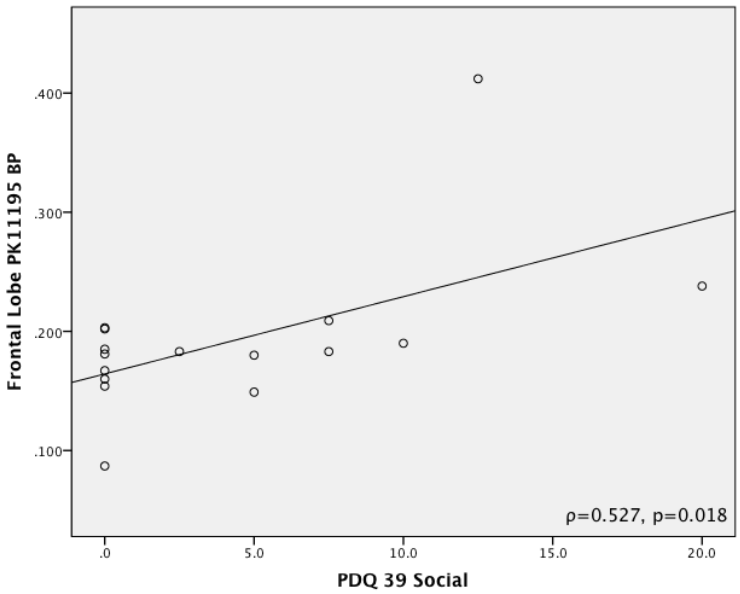


Figure A40. Correlation between frontal lobe [^{11}C]-(R)-PK11195 BP_{ND} and PDQ 39 Social domain at baseline

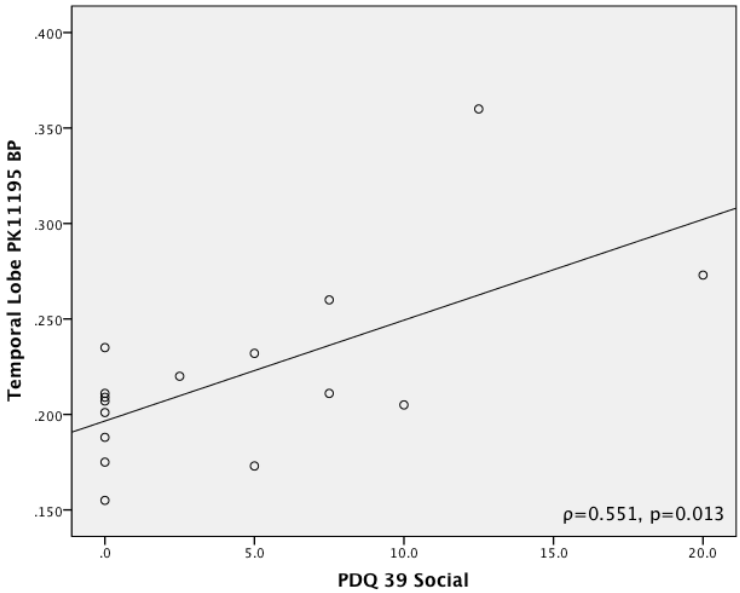


Figure A41. Correlation between temporal lobe [^{11}C]-(R)-PK11195 BP_{ND} and PDQ 39 Social domain at baseline

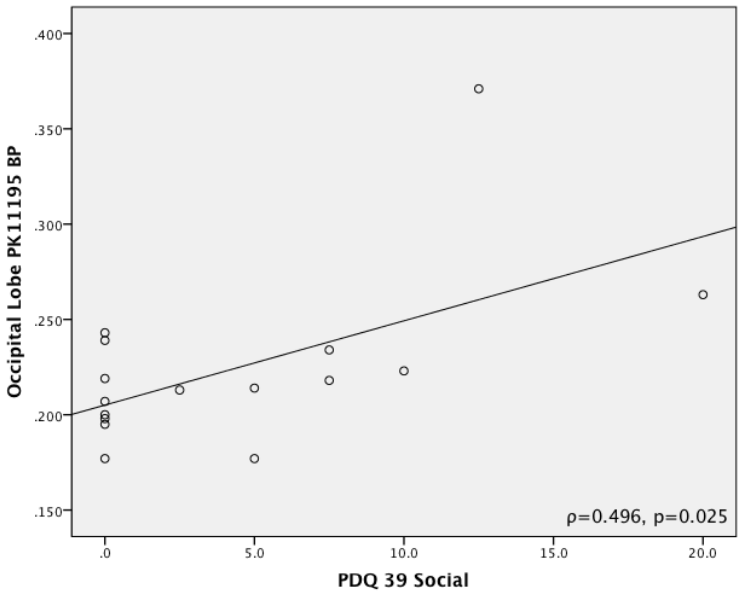


Figure A42. Correlation between occipital lobe [^{11}C]-(R)-PK11195 BP_{ND} and PDQ 39 Social domain at baseline

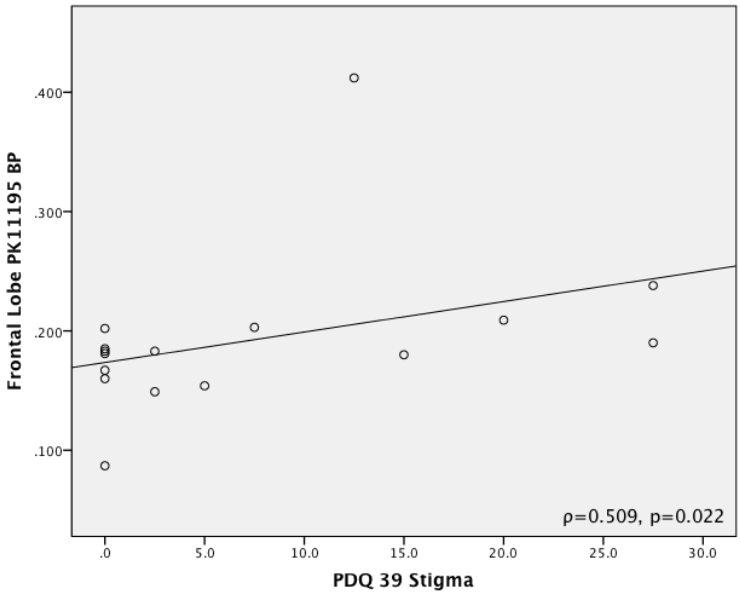


Figure A43. Correlation between whole brain [^{11}C]-(R)-PK11195 BP_{ND} and PDQ 39 Stigmatisation domain at baseline

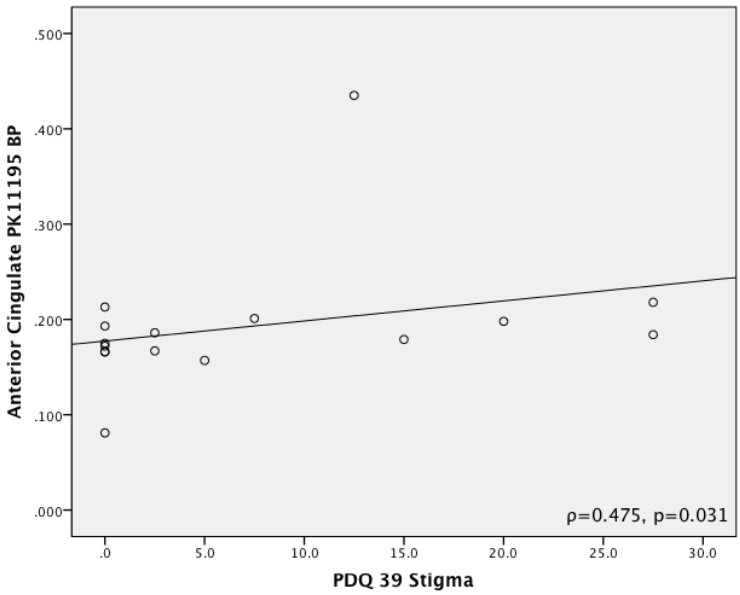


Figure A44. Correlation between anterior cingulate [^{11}C]-(R)-PK11195 BP_{ND} and PDQ 39 Stigmatisation domain at baseline

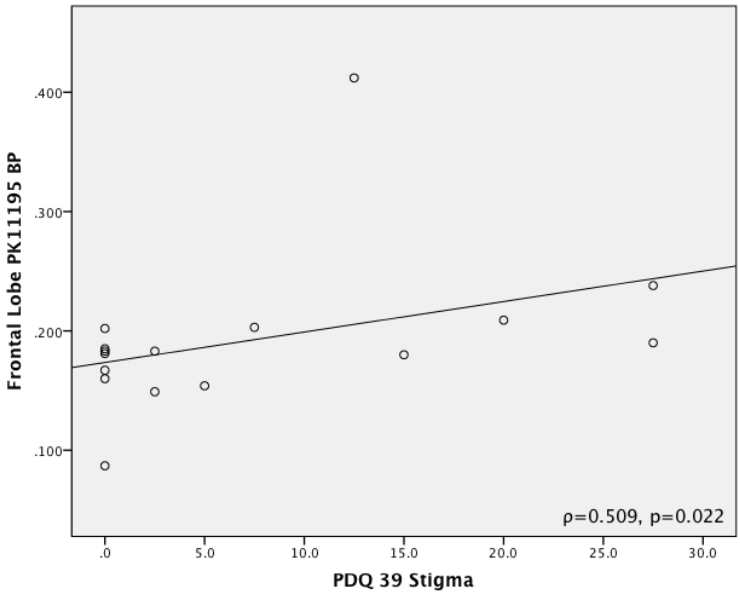


Figure A45. Correlation between frontal lobe [^{11}C]-(R)-PK11195 BP_{ND} and PDQ 39 Stigmatisation domain at baseline

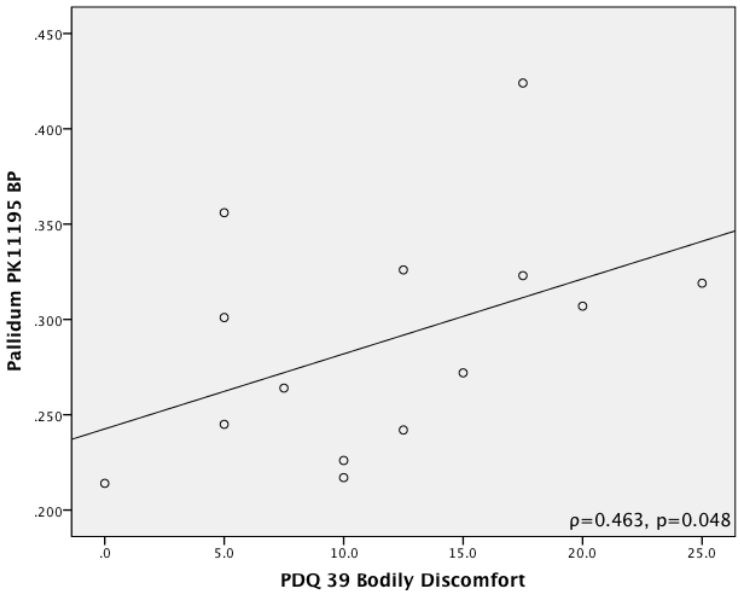


Figure A46. Correlation between globus pallidus [^{11}C]-(R)-PK11195 BP_{ND} and PDQ 39 bodily discomfort domain at baseline

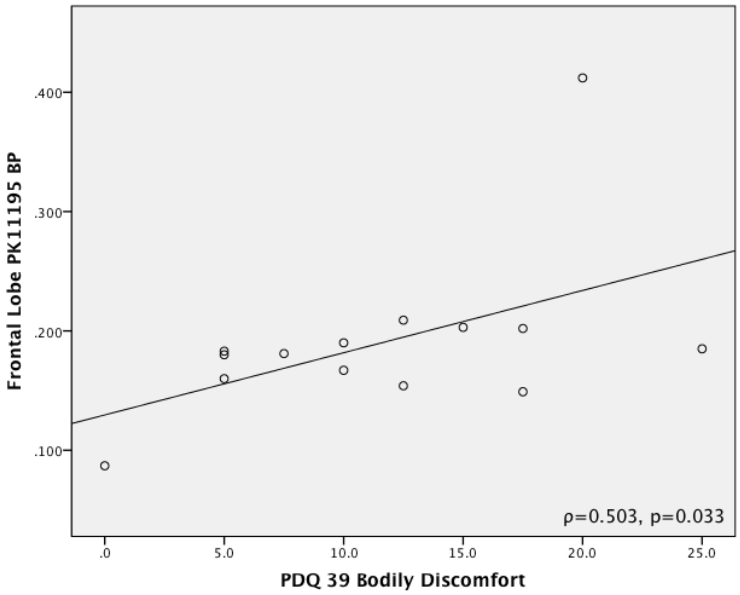


Figure A47. Correlation between frontal lobe [^{11}C]-(R)-PK11195 BP_{ND} and PDQ 39 Bodily Discomfort domain at baseline

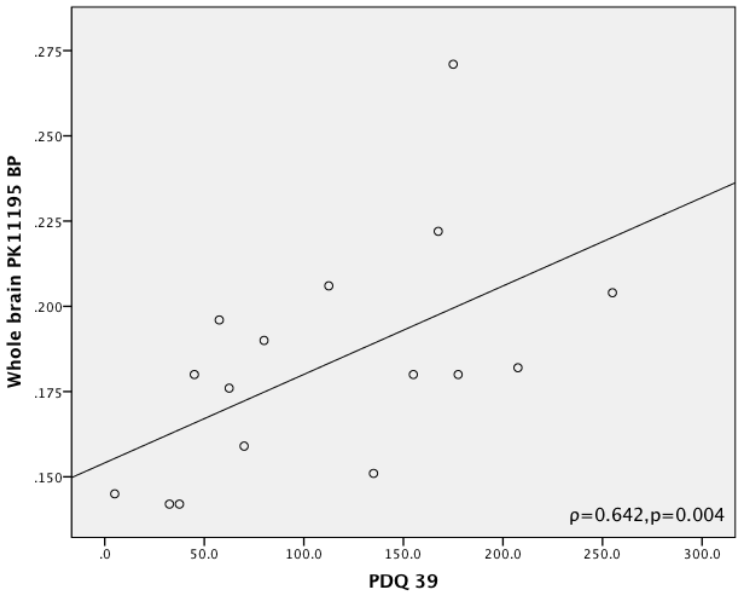


Figure A48. Correlation between whole brain [^{11}C]-(R)-PK11195 BP_{ND} and PDQ 39 at follow up

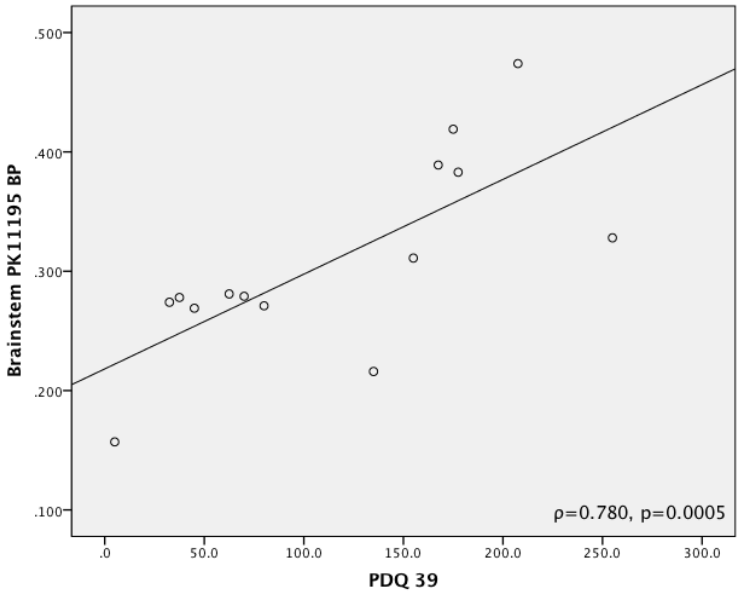


Figure A49. Correlation between brainstem [^{11}C]-(R)-PK11195 BP_{ND} and PDQ 39 at follow up

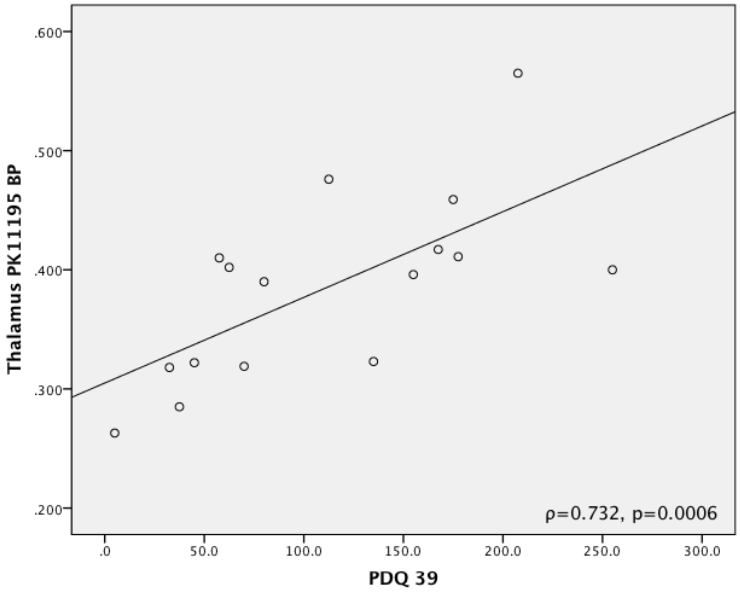


Figure A50. Correlation between thalamic [^{11}C]-(R)-PK11195 BP_{ND} and PDQ 39 at follow up

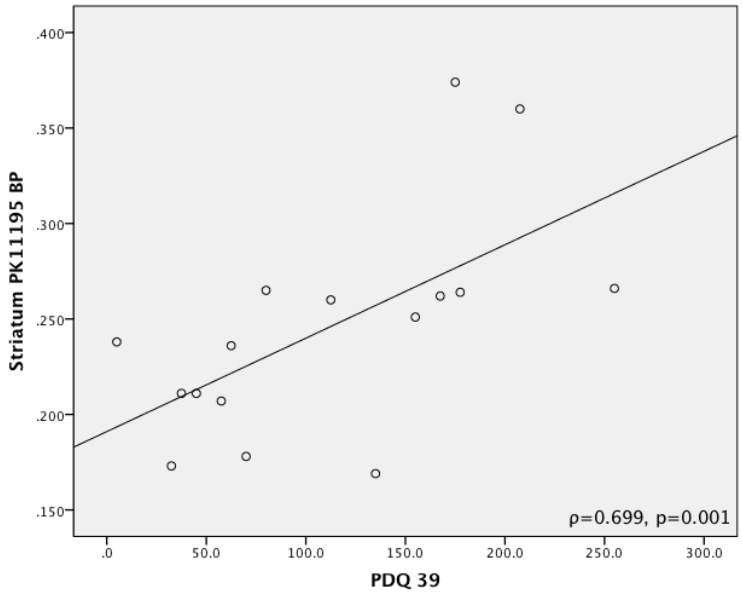


Figure A51. Correlation between striatal [^{11}C]-(R)-PK11195 BP_{ND} and PDQ 39 at follow up

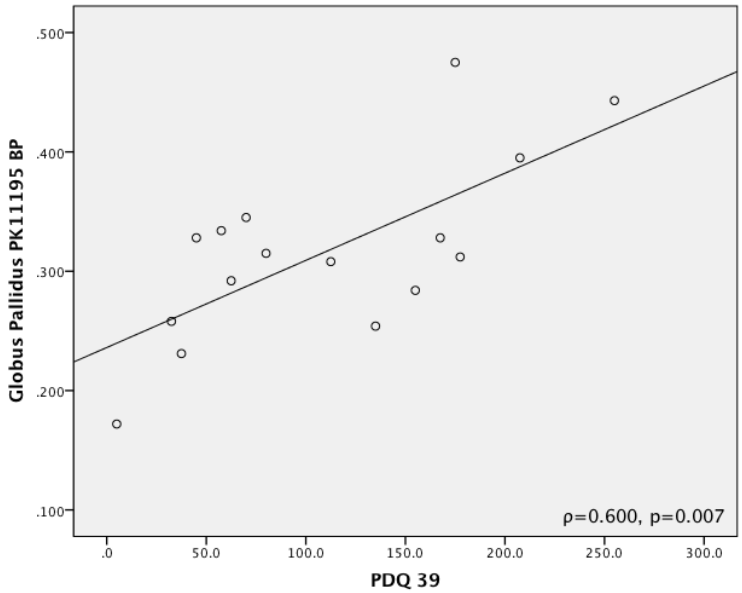


Figure A52. Correlation between globus pallidus [^{11}C]-(R)-PK11195 BP_{ND} and PDQ 39 at follow up

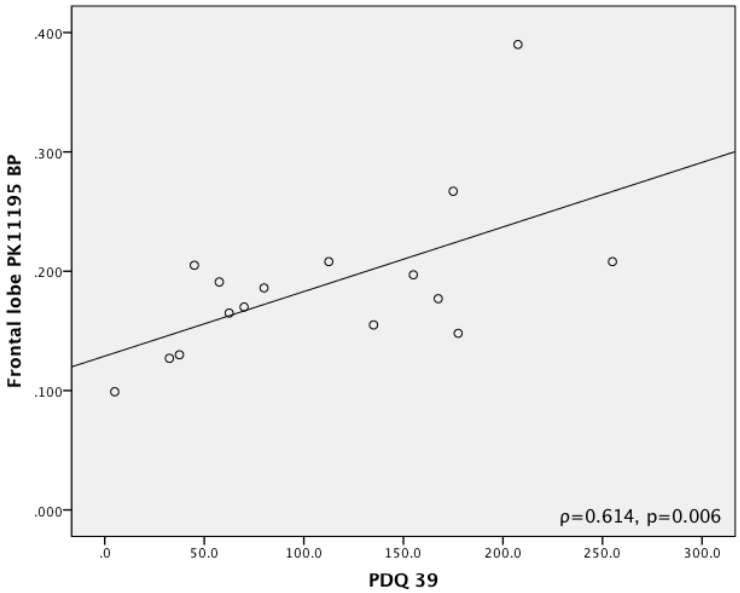


Figure A53. Correlation between frontal lobe [^{11}C]-(R)-PK11195 BP_{ND} and PDQ 39 at follow up

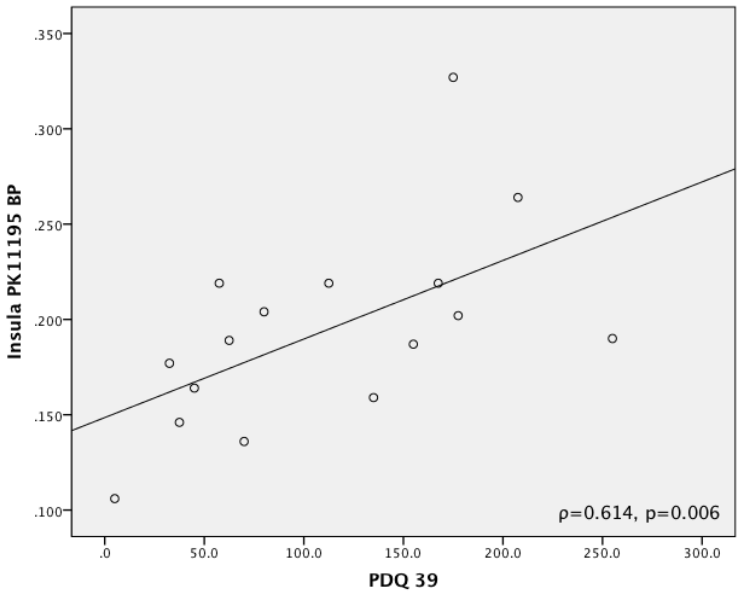


Figure A54. Correlation between insula [^{11}C]-(R)-PK11195 BP_{ND} and PDQ 39 at follow up

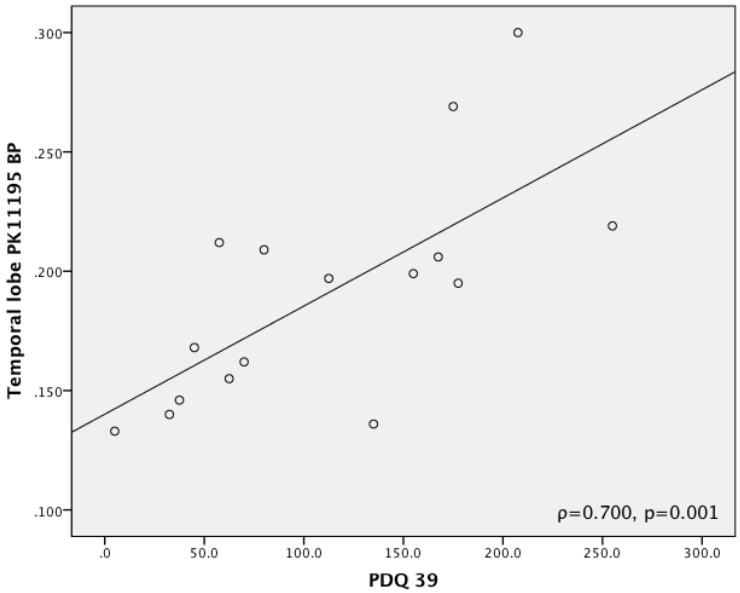


Figure A55. Correlation between temporal lobe [^{11}C]-(R)-PK11195 BP_{ND} and PDQ 39 at follow up

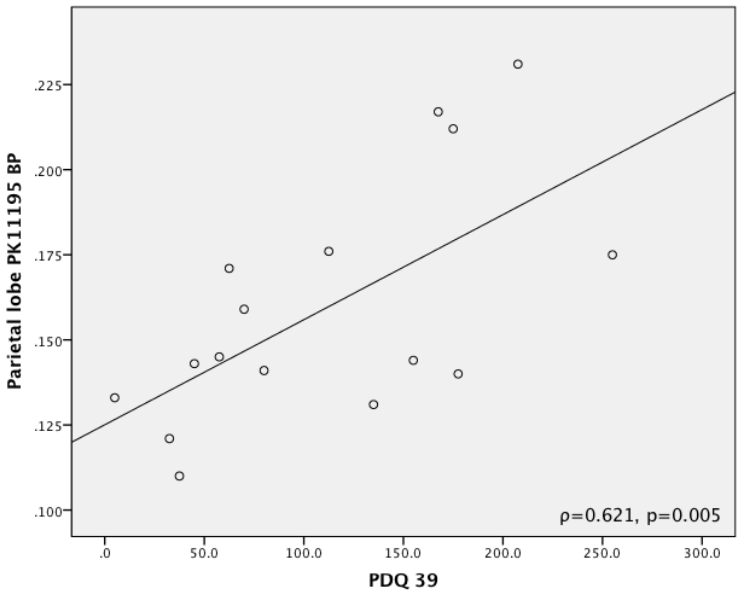


Figure A56. Correlation between parietal lobe [^{11}C]-(R)-PK11195 BP_{ND} and PDQ 39 at follow up

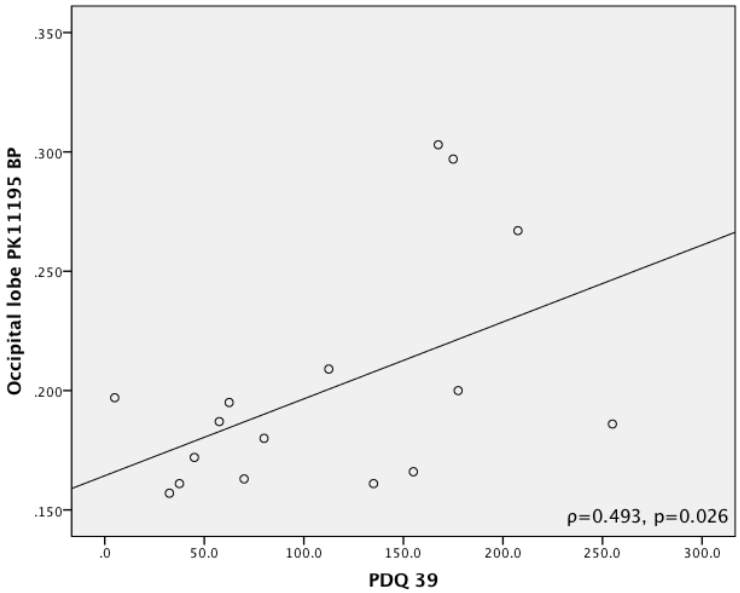


Figure A57. Correlation between occipital lobe [^{11}C]-(R)-PK11195 BP_{ND} and PDQ 39 at follow up

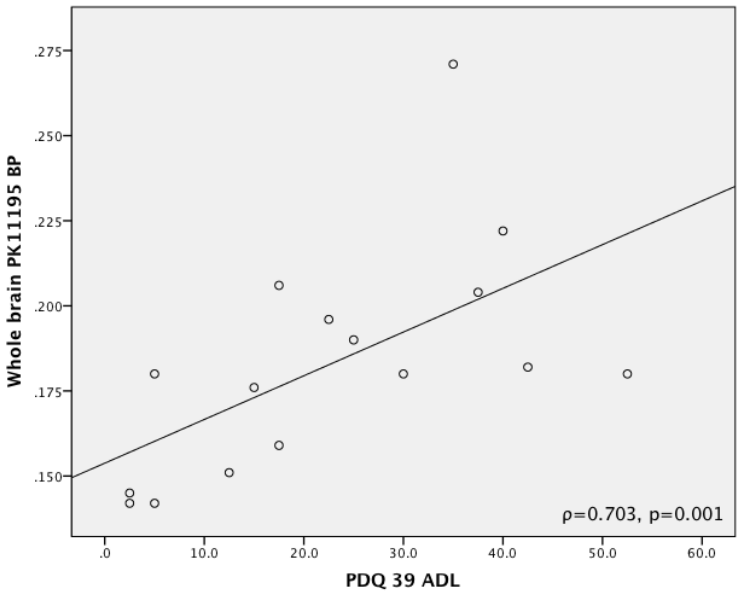


Figure A58. Correlation between whole brain [^{11}C]-(R)-PK11195 BP_{ND} and PDQ 39 ADL domain at follow up

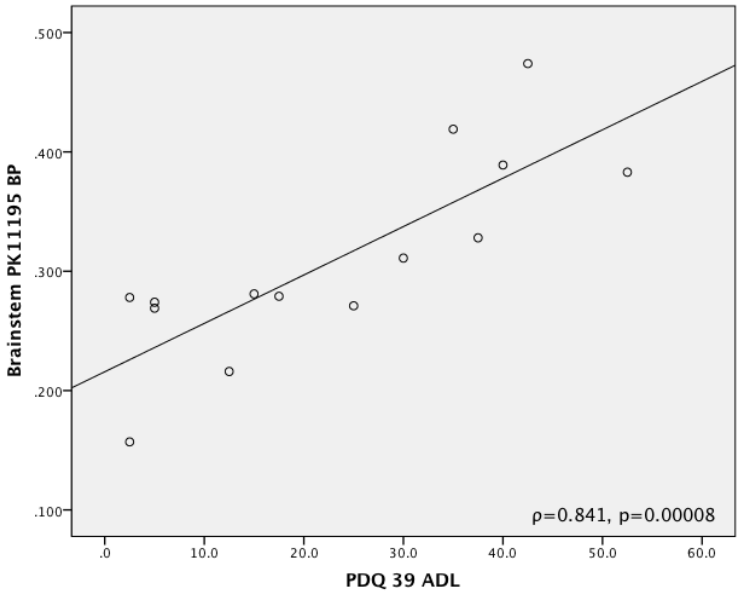


Figure A59. Correlation between brainstem [^{11}C]-(R)-PK11195 BP_{ND} and PDQ 39 ADL domain at follow up

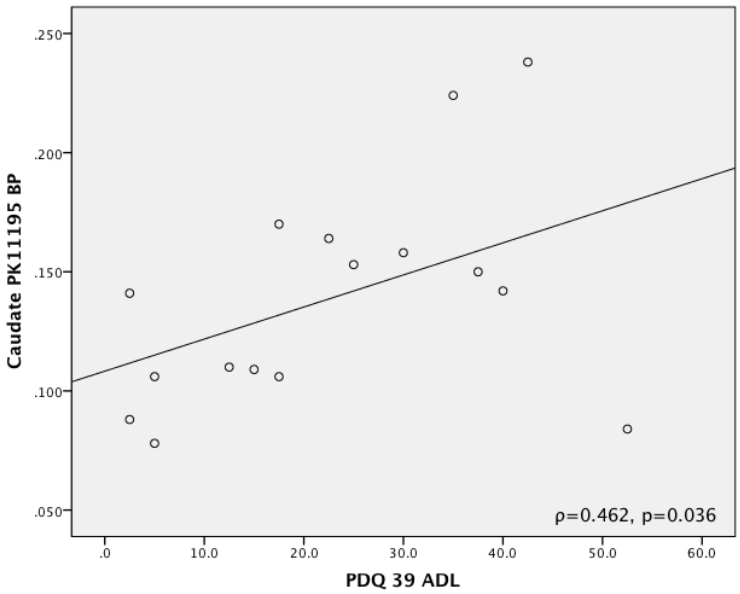


Figure A60. Correlation between caudate [^{11}C]-(R)-PK11195 BP_{ND} and PDQ 39 ADL domain at follow up

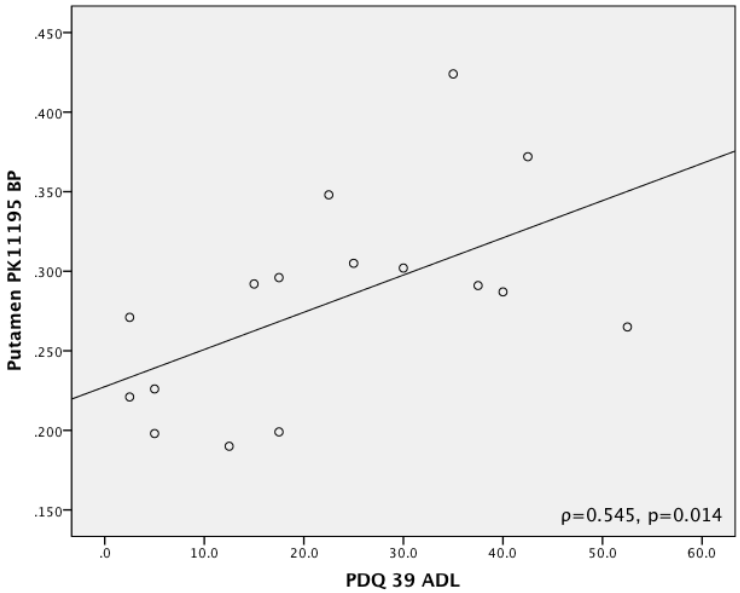


Figure A61. Correlation between putamenal [^{11}C]-(R)-PK11195 BP_{ND} and PDQ 39 ADL domain at follow up

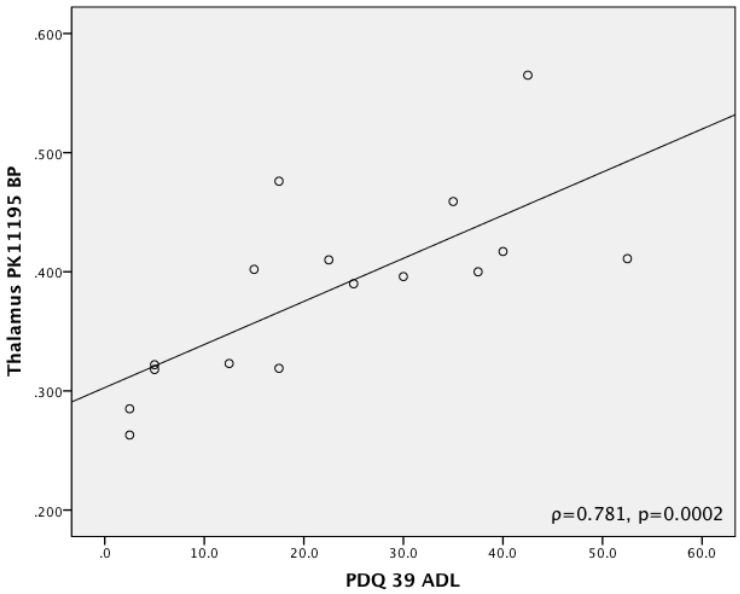


Figure A62. Correlation between thalamic [^{11}C]-(R)-PK11195 BP_{ND} and PDQ 39 ADL domain at follow up

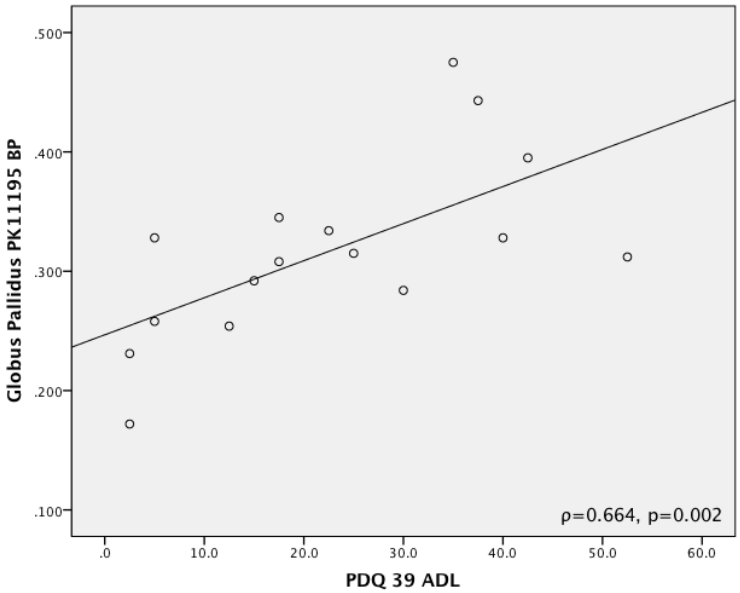


Figure A63. Correlation between globus pallidus [^{11}C]-(R)-PK11195 BP_{ND} and PDQ 39 ADL domain at follow up

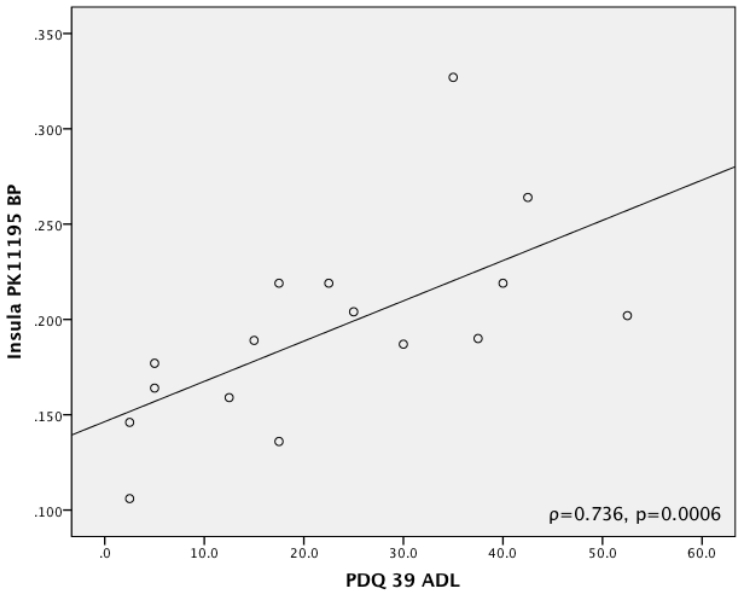


Figure A64. Correlation between insula [^{11}C]-(R)-PK11195 BP_{ND} and PDQ 39 ADL domain at follow up

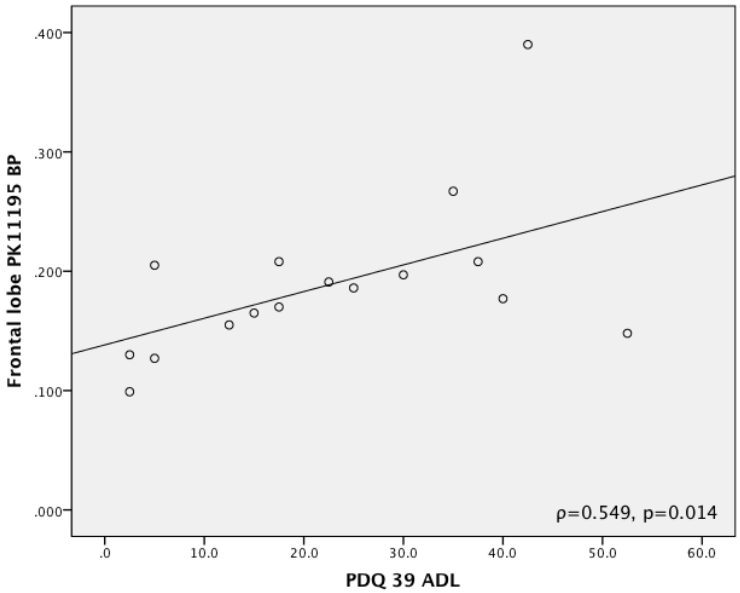


Figure A65. Correlation between frontal lobe [^{11}C]-(R)-PK11195 BP_{ND} and PDQ 39 ADL domain at follow up

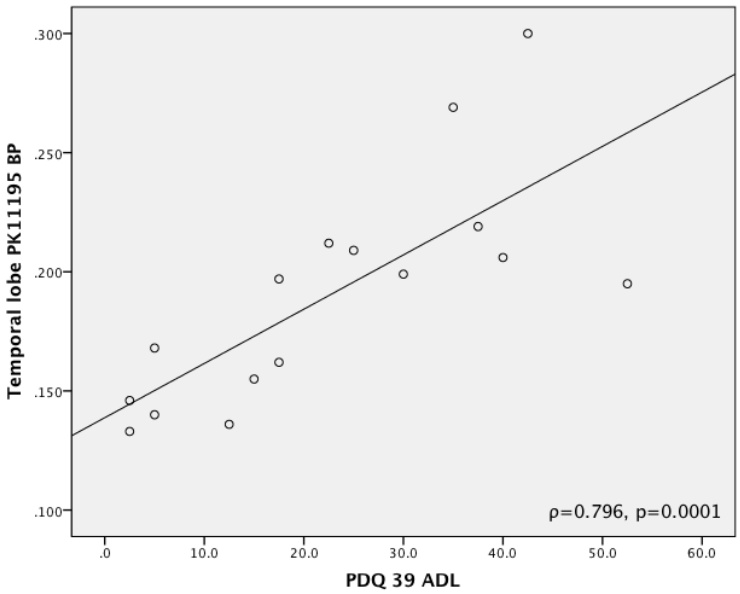


Figure A66. Correlation between temporal lobe [^{11}C]-(R)-PK11195 BP_{ND} and PDQ 39 ADL domain at follow up

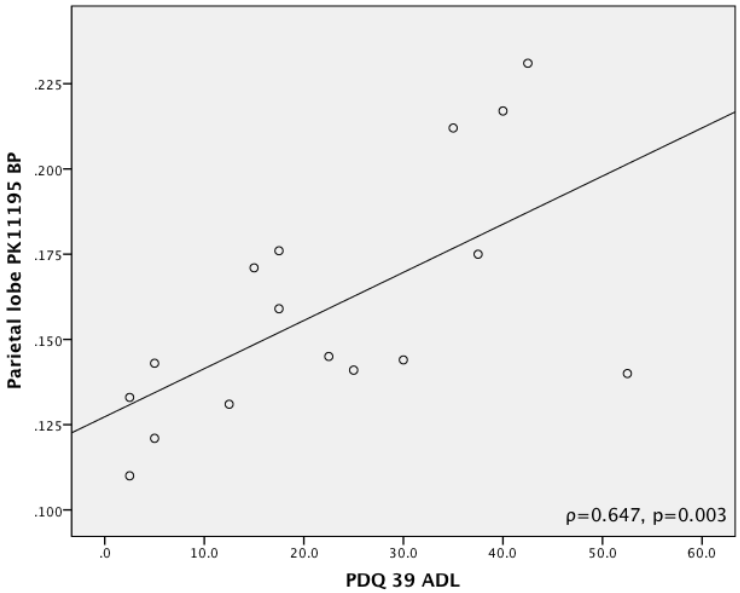


Figure A67. Correlation between parietal lobe [^{11}C]-(R)-PK11195 BP_{ND} and PDQ 39 ADL domain at follow up

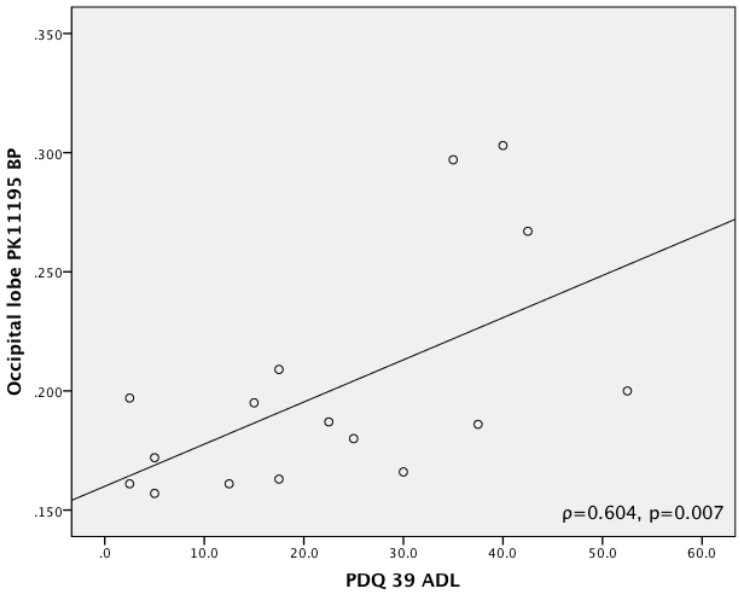


Figure A68. Correlation between occipital lobe [^{11}C]-(R)-PK11195 BP_{ND} and PDQ 39 ADL domain at follow up

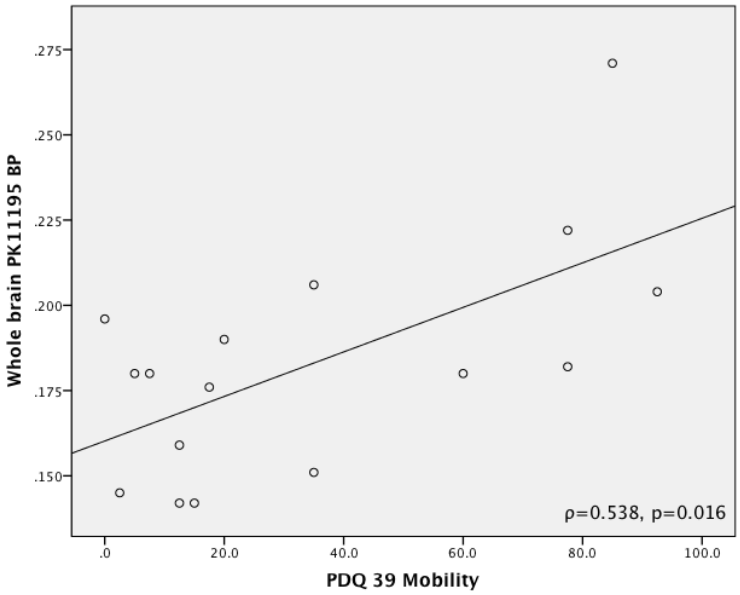


Figure A69. Correlation between whole brain [^{11}C]-(R)-PK11195 BP_{ND} and PDQ 39 Mobility domain at follow up

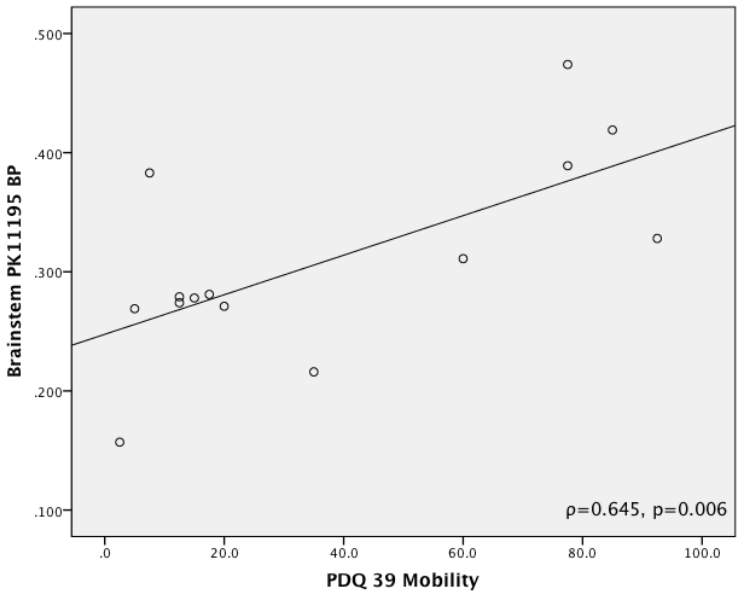


Figure A70. Correlation between brainstem [^{11}C]-(R)-PK11195 BP_{ND} and PDQ 39 Mobility domain at follow up

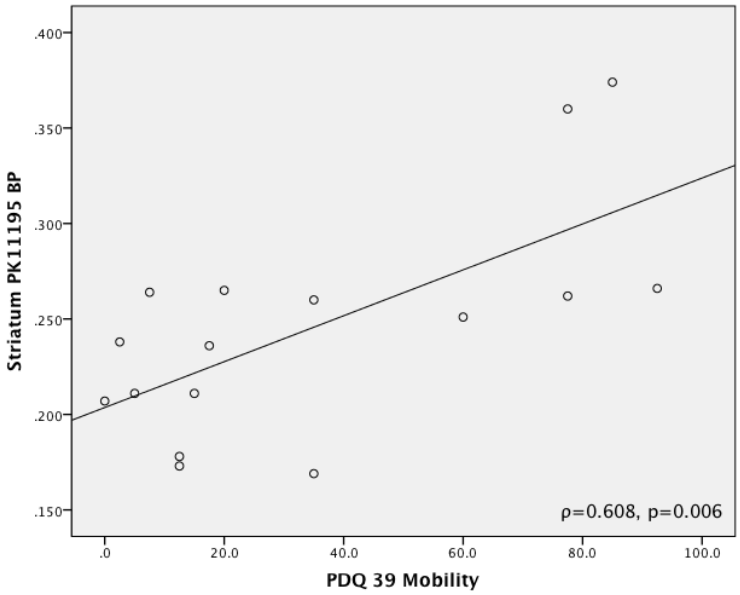


Figure A71. Correlation between striatal [^{11}C]-(R)-PK11195 BP_{ND} and PDQ 39 Mobility domain at follow up

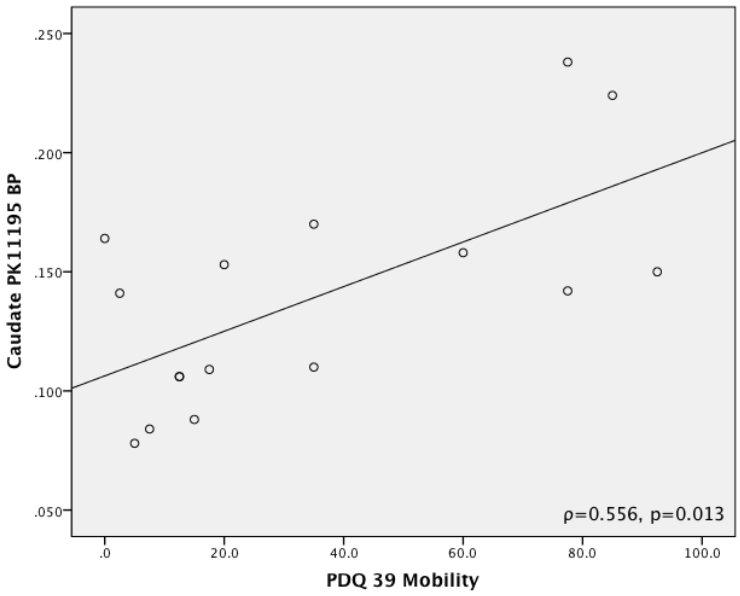


Figure A72. Correlation between caudate [^{11}C]-(R)-PK11195 BP_{ND} and PDQ 39 Mobility domain at follow up

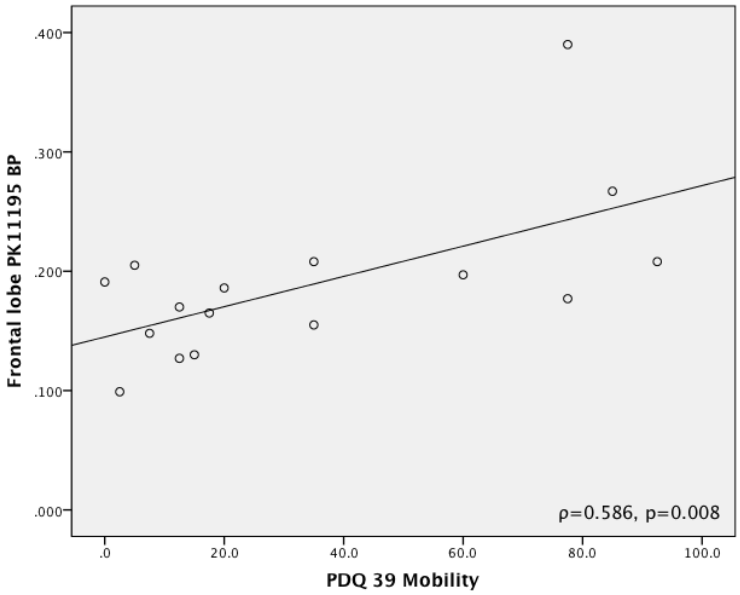


Figure A72. Correlation between frontal lobe [^{11}C]-(R)-PK11195 BP_{ND} and PDQ 39 Mobility domain at follow up

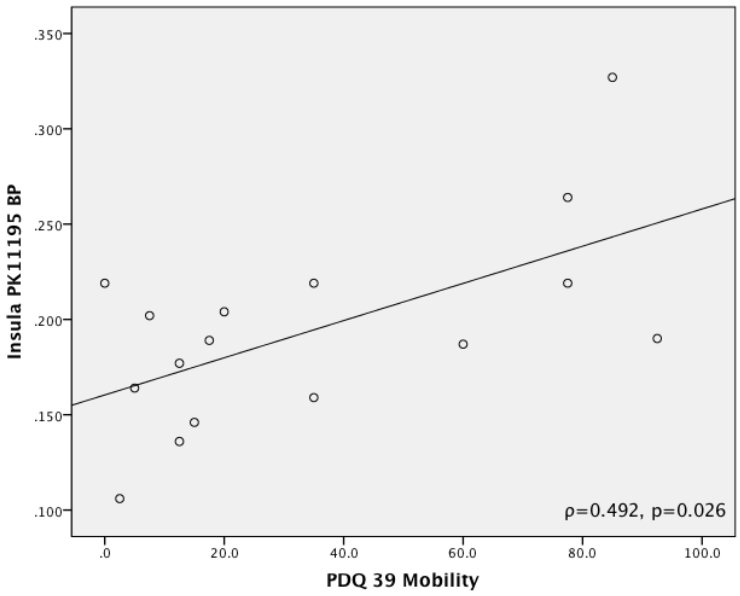


Figure A73. Correlation between insula [^{11}C]-(R)-PK11195 BP_{ND} and PDQ 39 Mobility domain at follow up

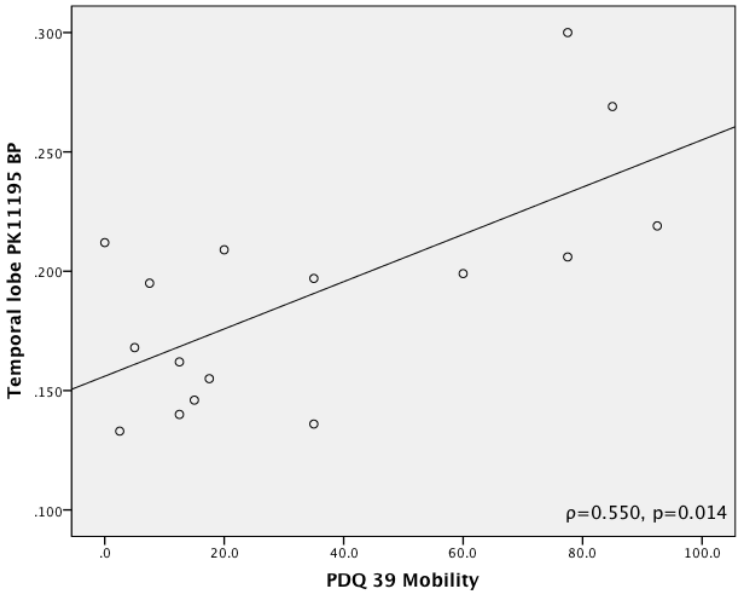


Figure A74. Correlation between temporal lobe [^{11}C]-(R)-PK11195 BP_{ND} and PDQ 39 Mobility domain at follow up

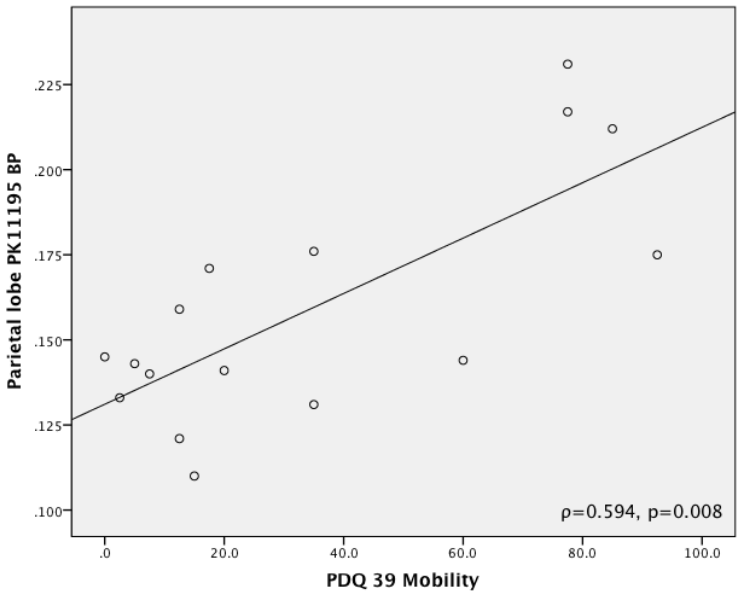


Figure A75. Correlation between parietal lobe [^{11}C]-(R)-PK11195 BP_{ND} and PDQ 39 Mobility domain at follow up

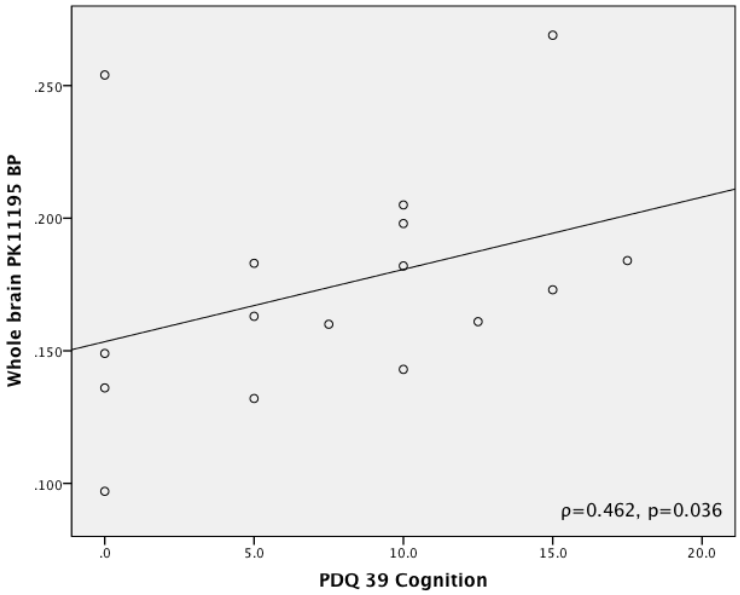


Figure A76. Correlation between whole brain [^{11}C]-(R)-PK11195 BP_{ND} and PDQ 39 Cognition domain at follow up

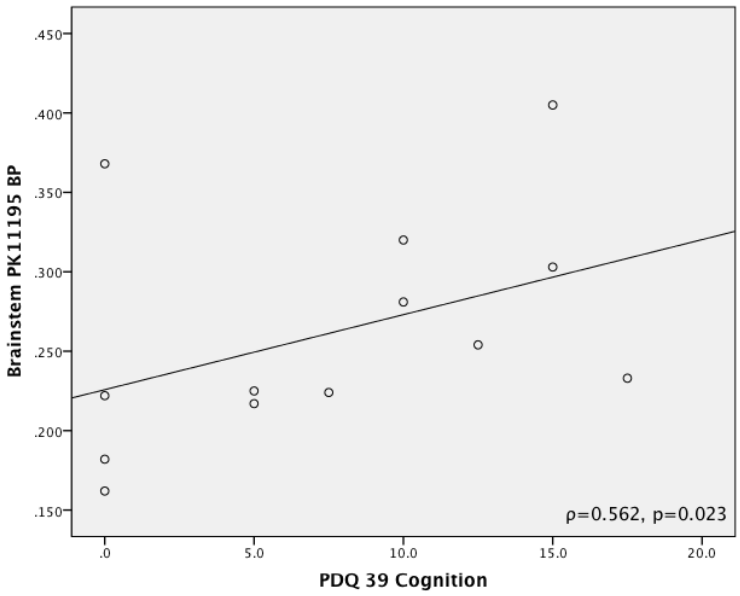


Figure A77. Correlation between brainstem [^{11}C]-(R)-PK11195 BP_{ND} and PDQ 39 Cognition domain at follow up

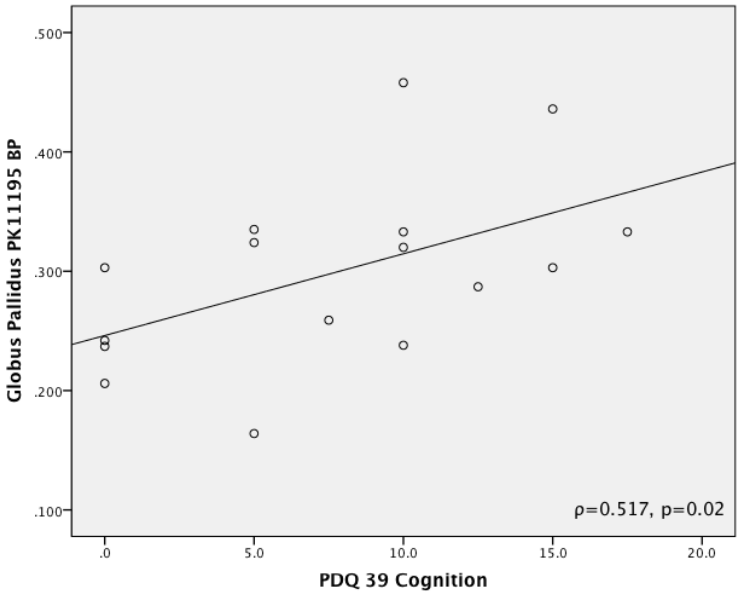


Figure A78. Correlation between globus pallidus [^{11}C]-(R)-PK11195 BP_{ND} and PDQ 39 Cognition domain at follow up

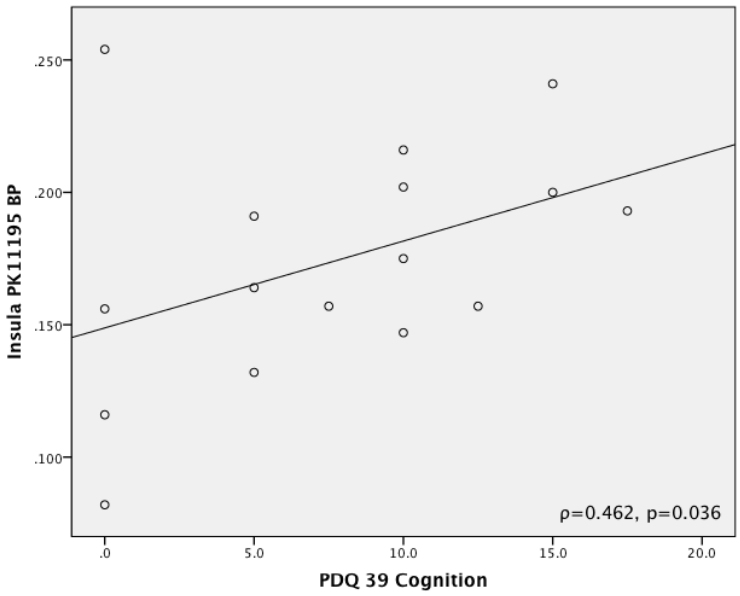


Figure A79. Correlation between insula [^{11}C]-(R)-PK11195 BP_{ND} and PDQ 39 Cognition domain at follow up

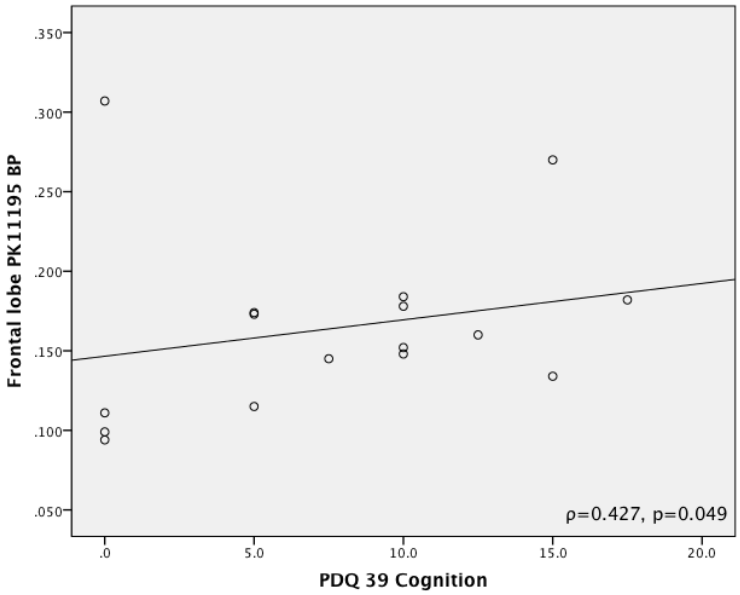


Figure A80. Correlation between frontal lobe [^{11}C]-(R)-PK11195 BP_{ND} and PDQ 39 Cognition domain at follow up

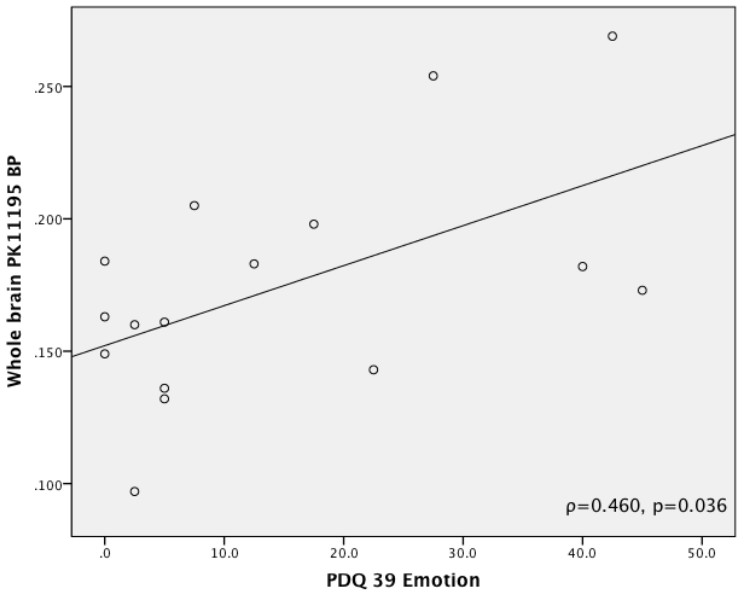


Figure A81. Correlation between whole brain [^{11}C]-(R)-PK11195 BP_{ND} and PDQ 39 Emotional Wellbeing domain at follow up

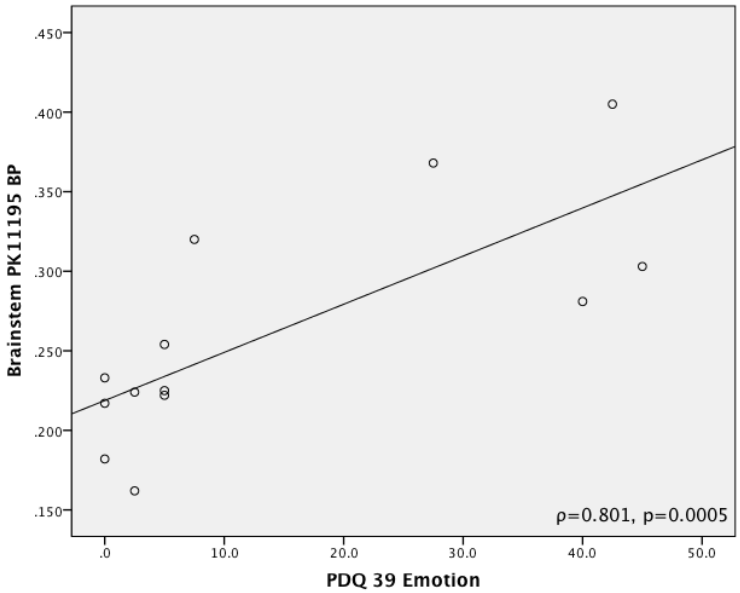


Figure A82. Correlation between brainstem [^{11}C]-(R)-PK11195 BP_{ND} and PDQ 39 Emotional Wellbeing domain at follow up

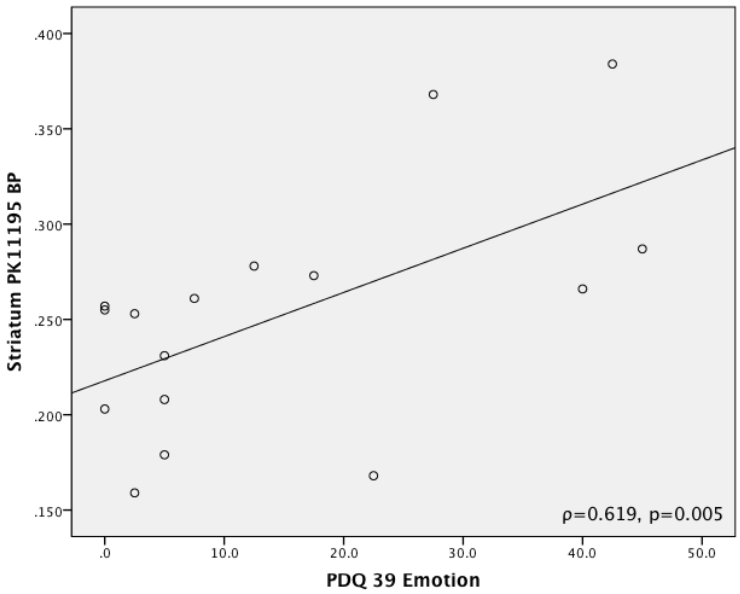


Figure A83. Correlation between striatal [^{11}C]-(R)-PK11195 BP_{ND} and PDQ 39 Emotional Wellbeing domain at follow up

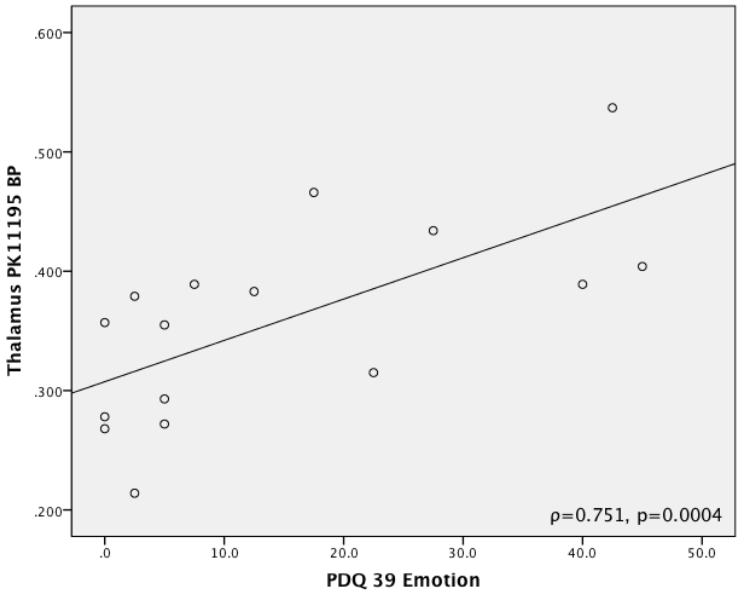


Figure A84. Correlation between thalamic [^{11}C]-(R)-PK11195 BP_{ND} and PDQ 39 Emotional Wellbeing domain at follow up

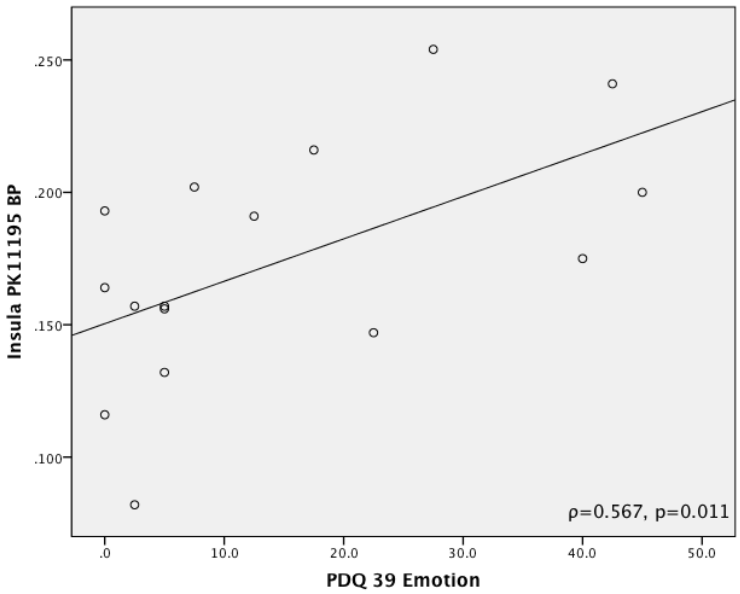


Figure A85. Correlation between insula [^{11}C]-(R)-PK11195 BP_{ND} and PDQ 39 Emotional Wellbeing domain at follow up

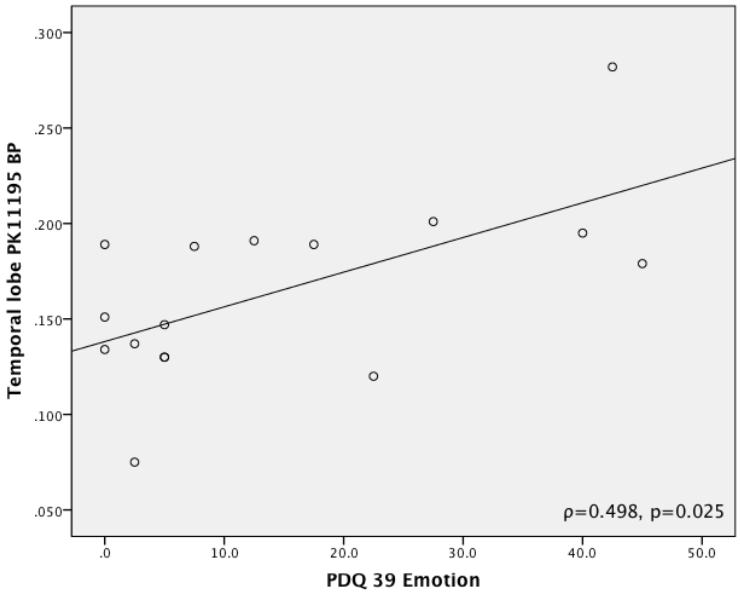


Figure A86. Correlation between temporal lobe [^{11}C]-(R)-PK11195 BP_{ND} and PDQ 39 Emotional Wellbeing domain at follow up

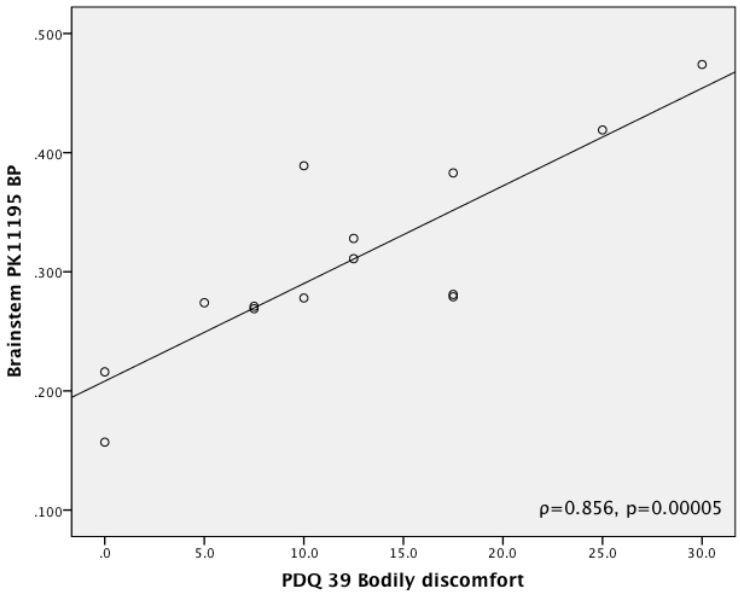


Figure A87. Correlation between brainstem [^{11}C]-(R)-PK11195 BP_{ND} and PDQ 39 Bodily Discomfort domain at follow up

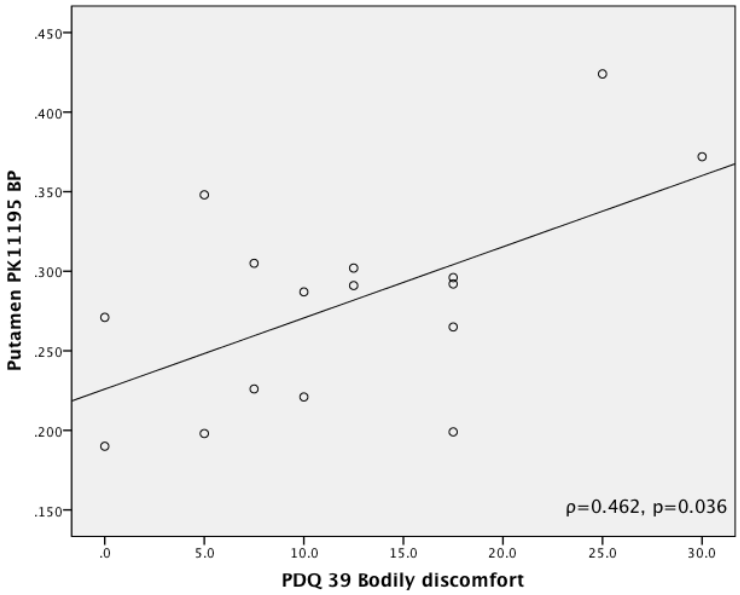


Figure A88. Correlation between putamenal [^{11}C]-(R)-PK11195 BP_{ND} and PDQ 39 Bodily Discomfort domain at follow up

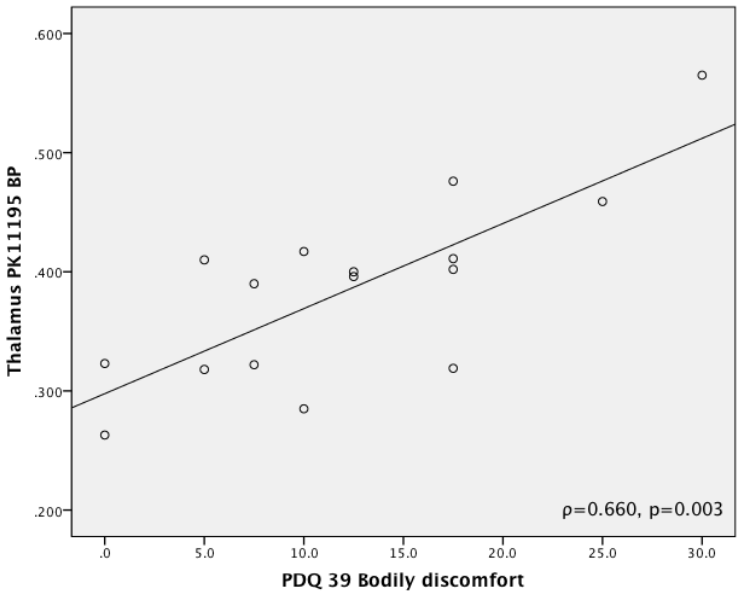


Figure A89. Correlation between thalamic [^{11}C]-(R)-PK11195 BP_{ND} and PDQ 39 Bodily Discomfort domain at follow up

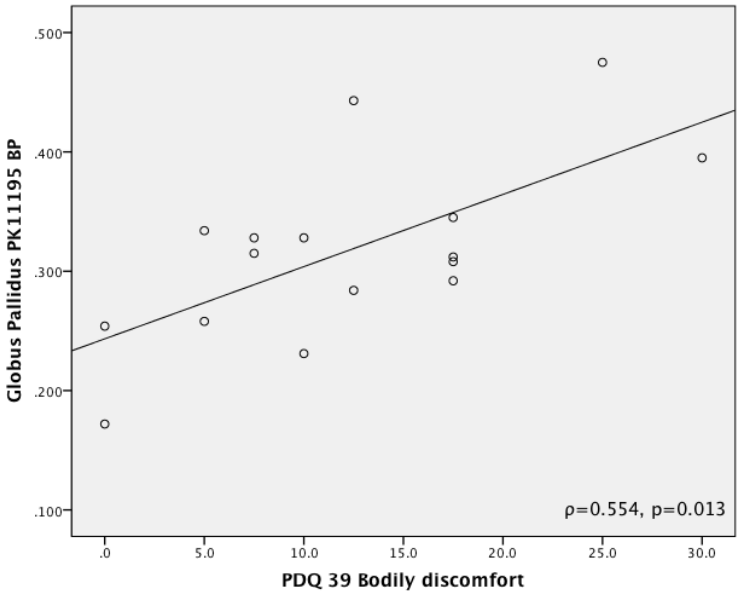


Figure A90. Correlation between globus pallidus [^{11}C]-(R)-PK11195 BP_{ND} and PDQ 39 Bodily Discomfort domain at follow up

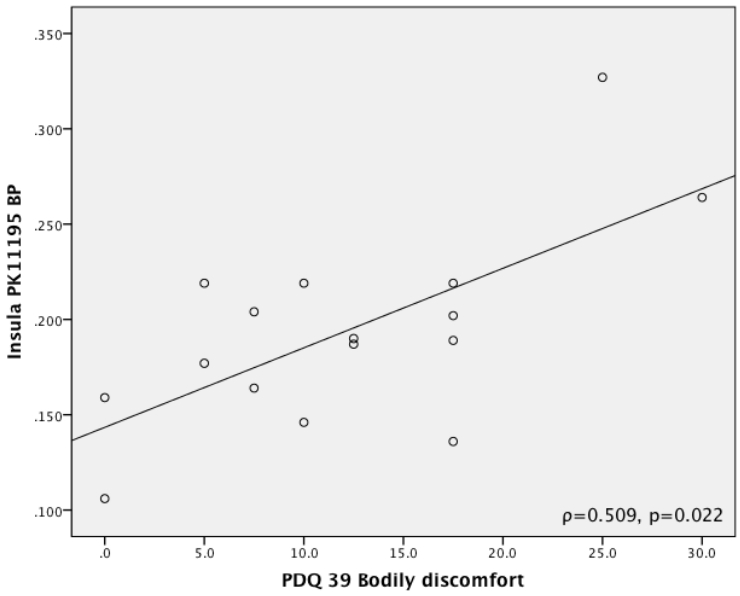


Figure A91. Correlation between insula [^{11}C]-(R)-PK11195 BP_{ND} and PDQ 39 Bodily Discomfort domain at follow up

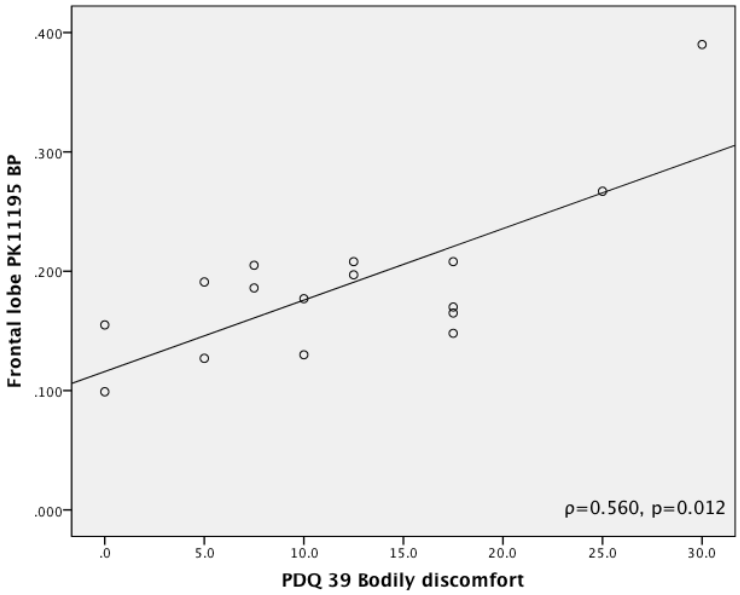


Figure A92 Correlation between frontal lobe [^{11}C]-(R)-PK11195 BP_{ND} and PDQ 39 Bodily Discomfort domain at follow up

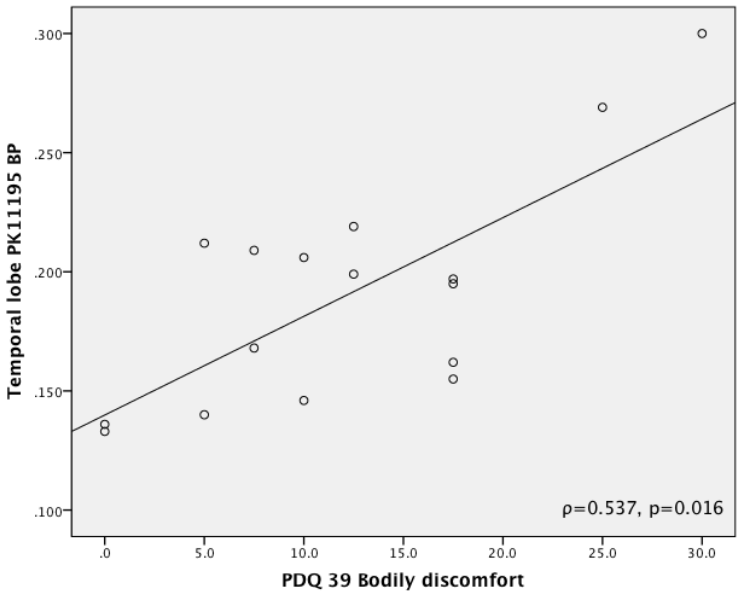


Figure A93. Correlation between temporal lobe [^{11}C]-(R)-PK11195 BP_{ND} and PDQ 39 Bodily Discomfort domain at follow up

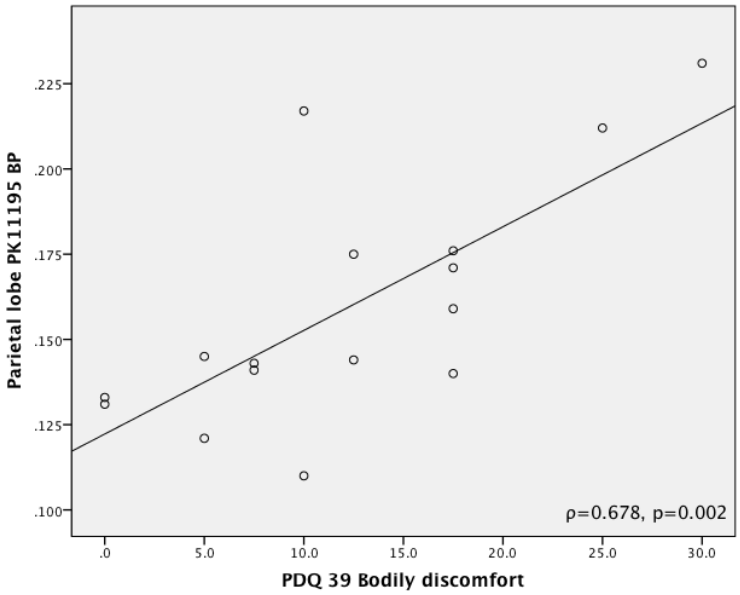


Figure A94. Correlation between parietal lobe [^{11}C]-(R)-PK11195 BP_{ND} and PDQ 39 Bodily Discomfort domain at follow up

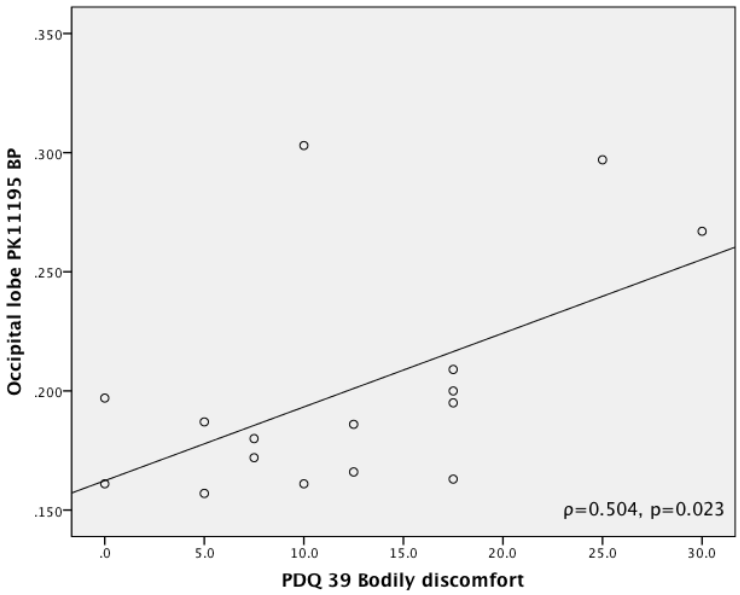


Figure A95. Correlation between occipital [^{11}C]-(R)-PK11195 BP_{ND} and PDQ 39 Bodily Discomfort domain at follow up

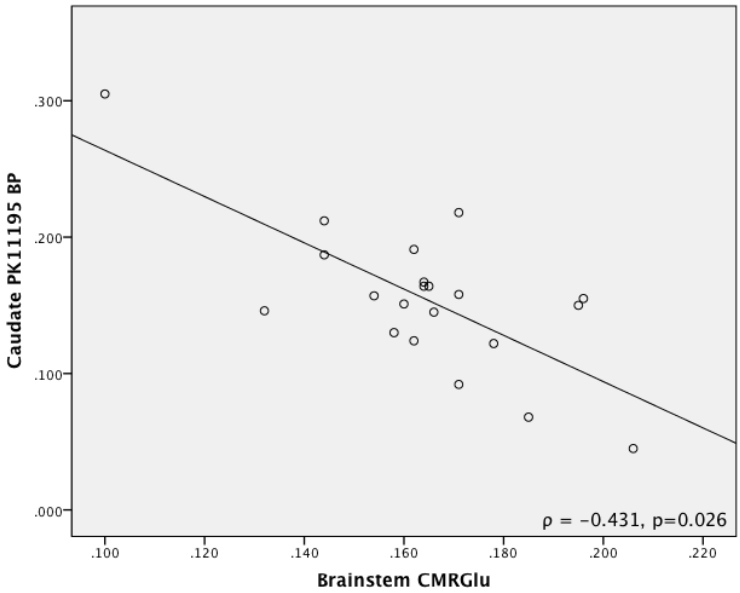


Figure A96. Correlation between caudate [^{11}C]-(R)-PK11195 BP_{ND} and brainstem CMRGlu at baseline

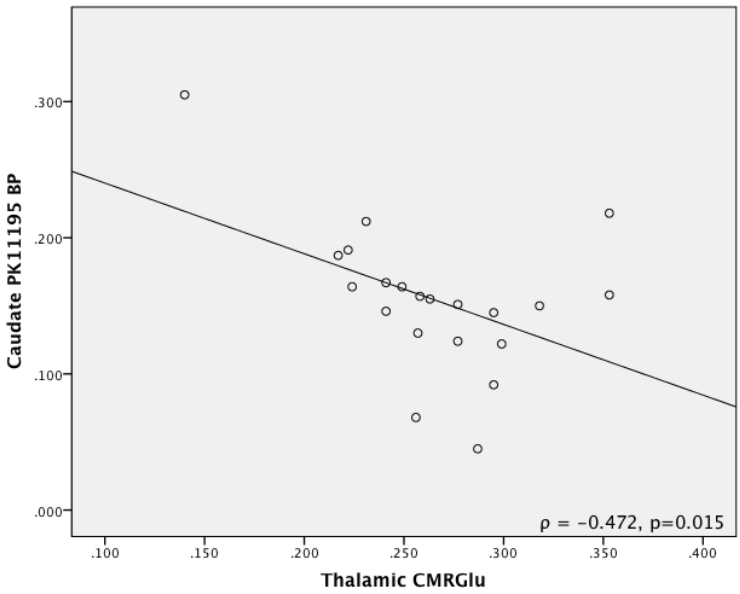


Figure A97. Correlation between caudate [^{11}C]-(R)-PK11195 BP_{ND} and thalamic CMRGlu at baseline

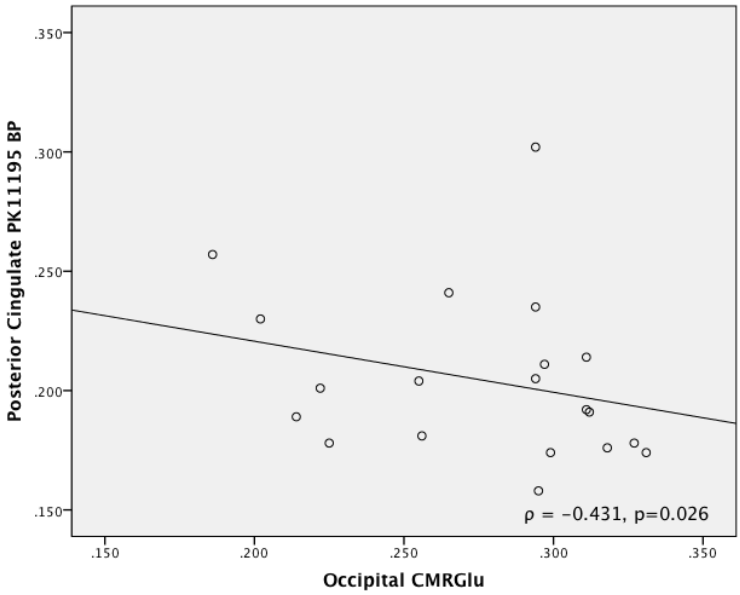


Figure A98. Correlation between posterior cingulate [^{11}C]-(R)-PK11195 BP_{ND} and occipital lobe CMRGlu at baseline

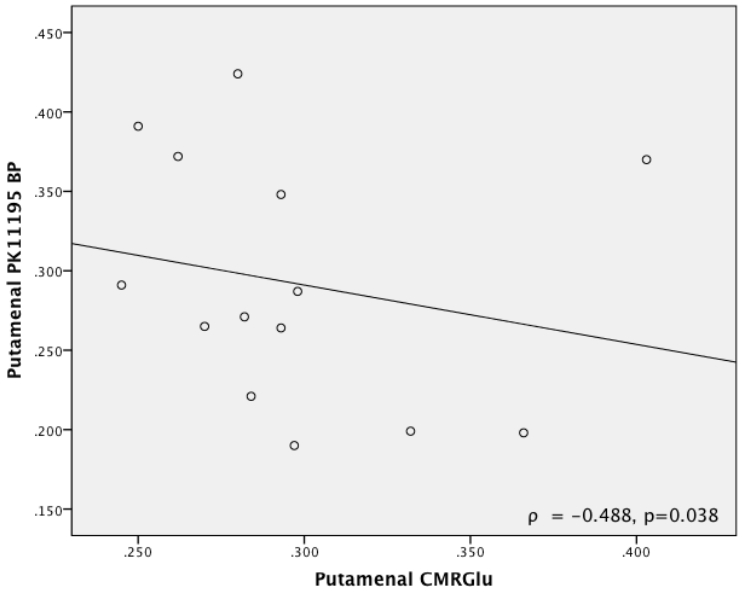


Figure A99. Correlation between putamenal [^{11}C]-(R)-PK11195 BP_{ND} and putamenal CMRGlu at follow up

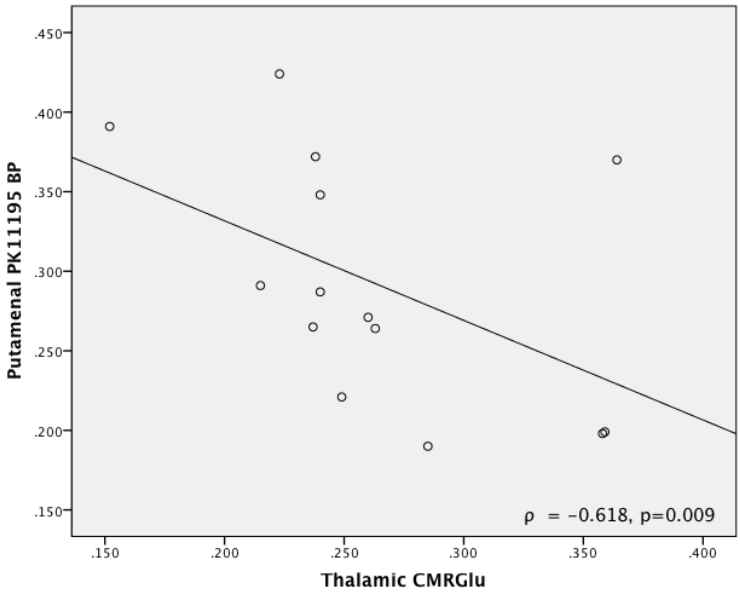


Figure A100. Correlation between putamenal [^{11}C]-(R)-PK11195 BP_{ND} and thalamic CMRGlu at follow up

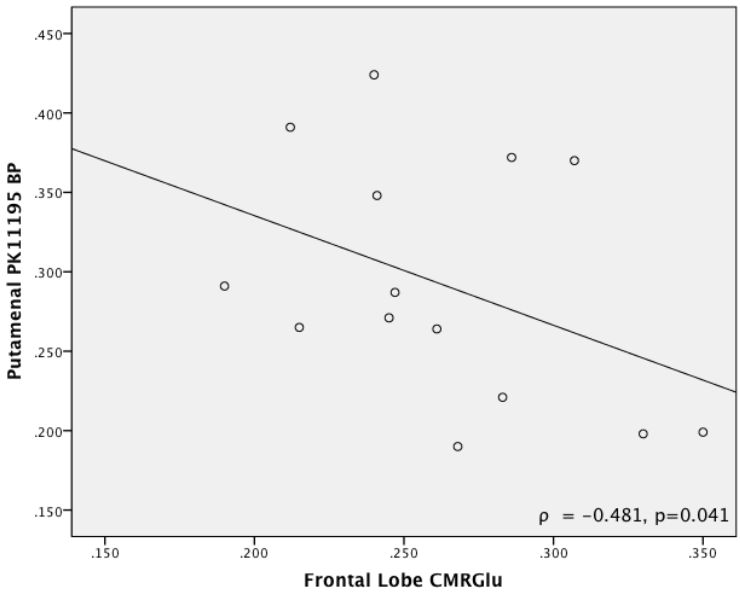


Figure A101. Correlation between putamenal [^{11}C]-(R)-PK11195 BP_{ND} and frontal lobe CMRGlu at follow up

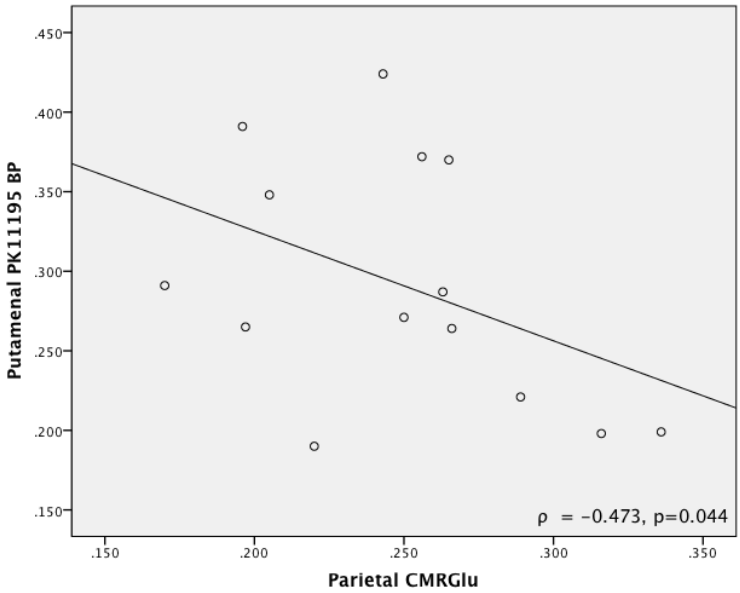


Figure A102. Correlation between putamenal [^{11}C]-(R)-PK11195 BP_{ND} and parietal lobe CMRGlu at follow up

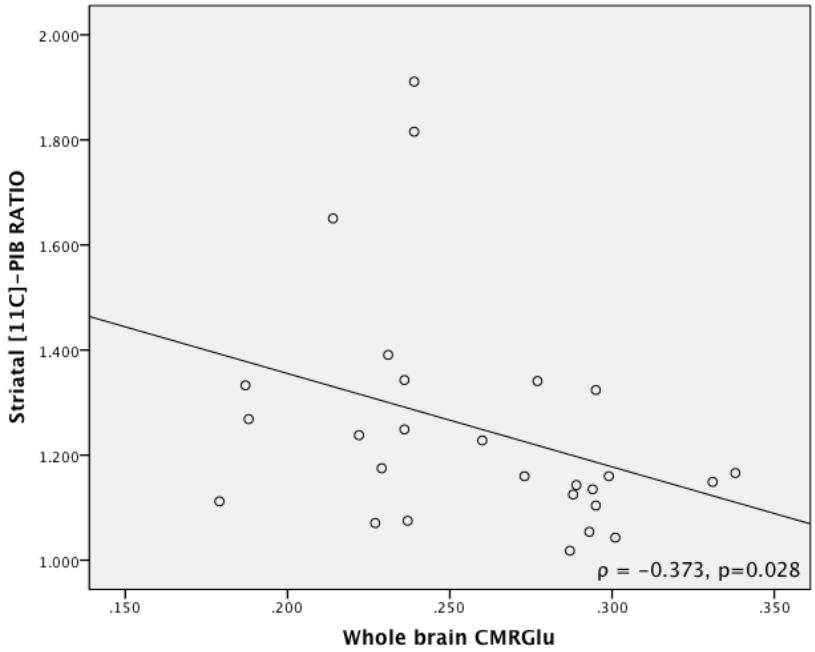


Figure B1. Correlation between striatal [^{11}C]-PIB RATIO and whole brain CMRGlu

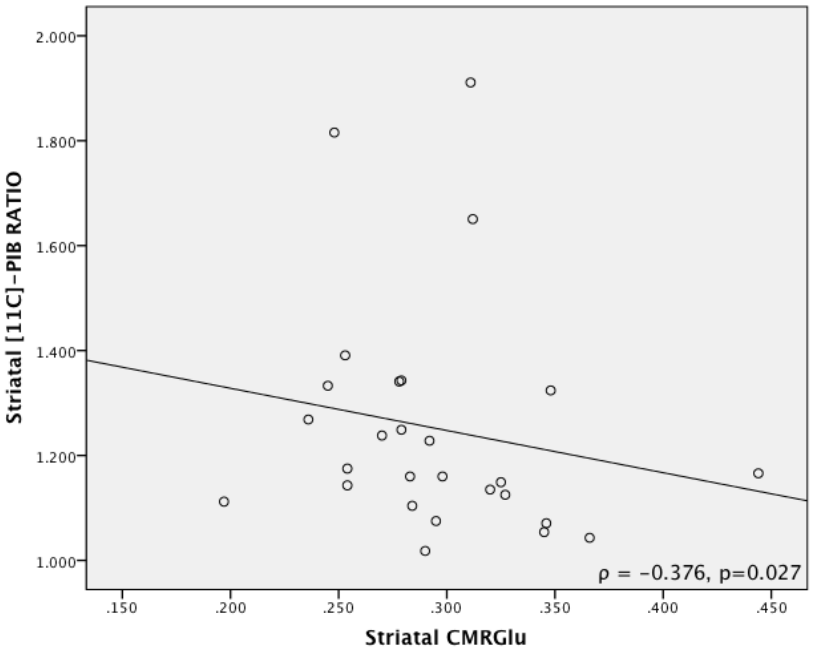


Figure B2. Correlation between striatal [^{11}C]-PIB RATIO and striatal CMRGlu

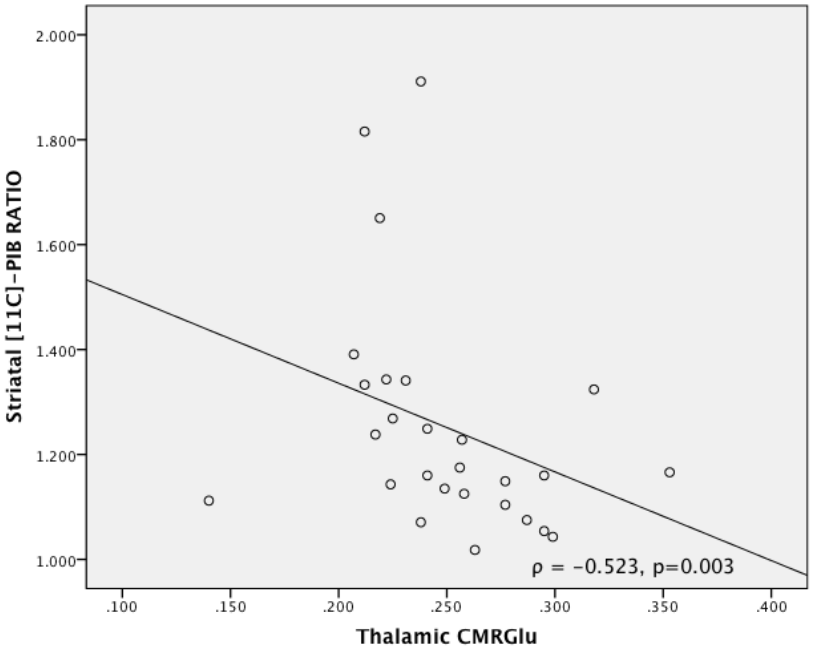


Figure B3. Correlation between striatal [^{11}C]-PIB RATIO and thalamic CMRGlu

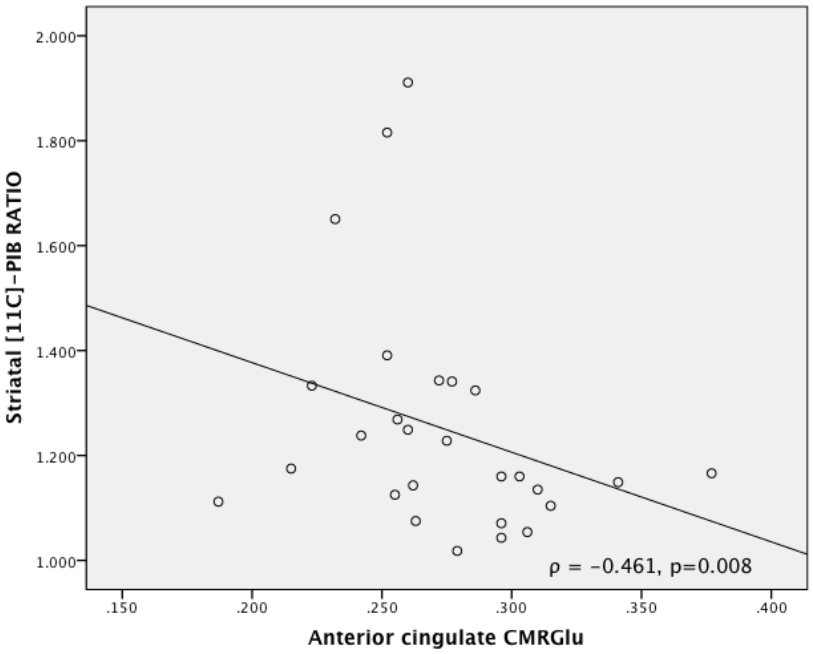


Figure B4. Correlation between striatal [^{11}C]-PIB RATIO and anterior cingulate CMRGlu

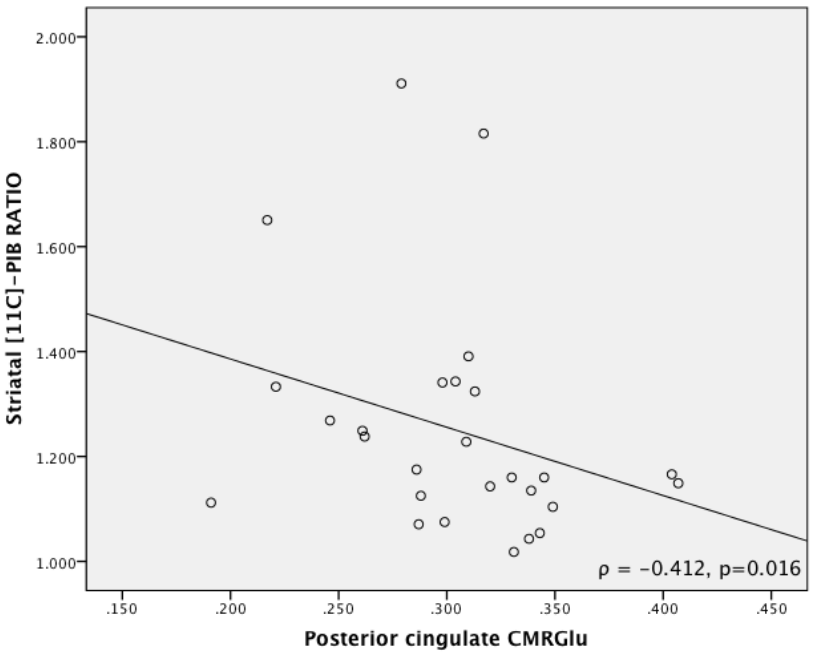


Figure B5. Correlation between striatal [^{11}C]-PIB RATIO and posterior cingulate CMRGlu

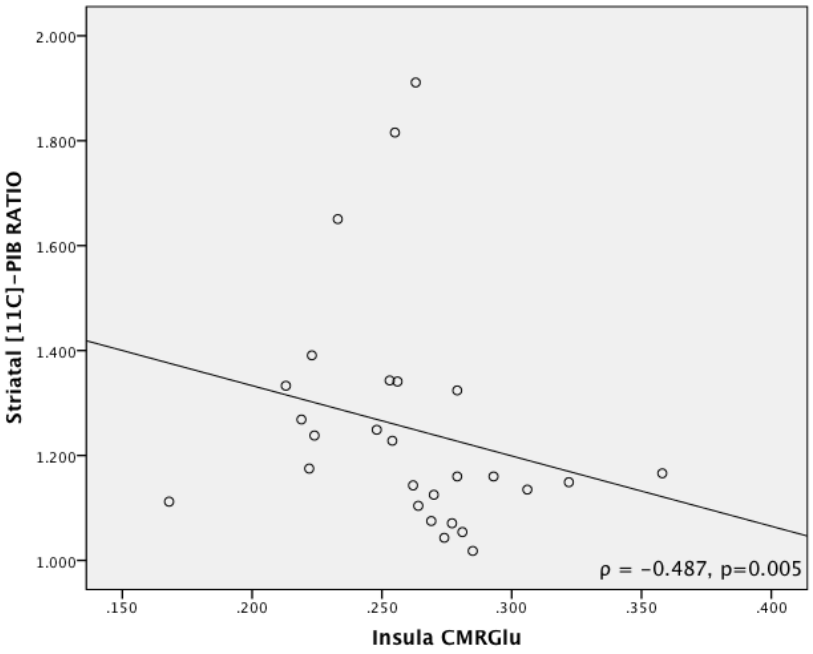


Figure B6. Correlation between striatal [^{11}C]-PIB RATIO and insula CMRGlu

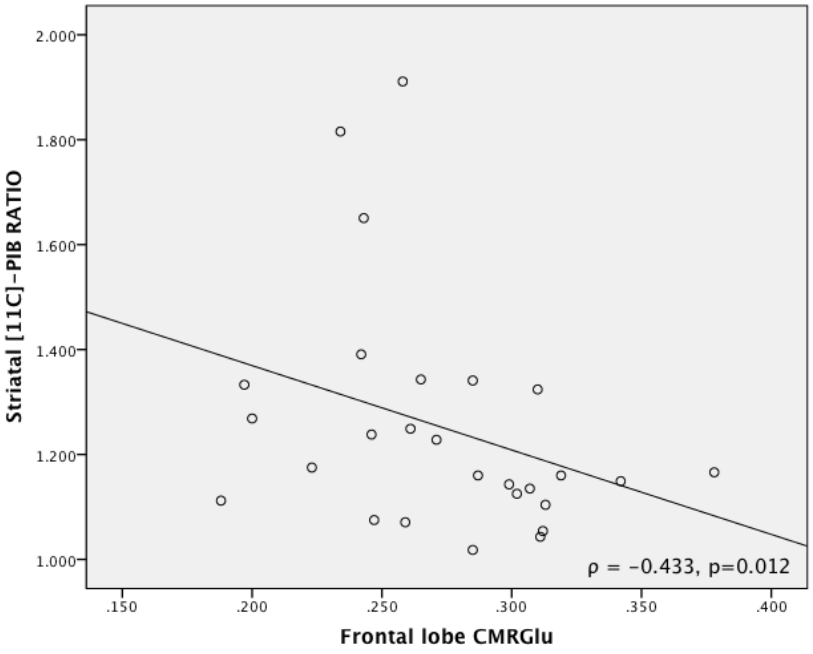


Figure B7. Correlation between striatal [^{11}C]-PIB RATIO and frontal lobe CMRGlu

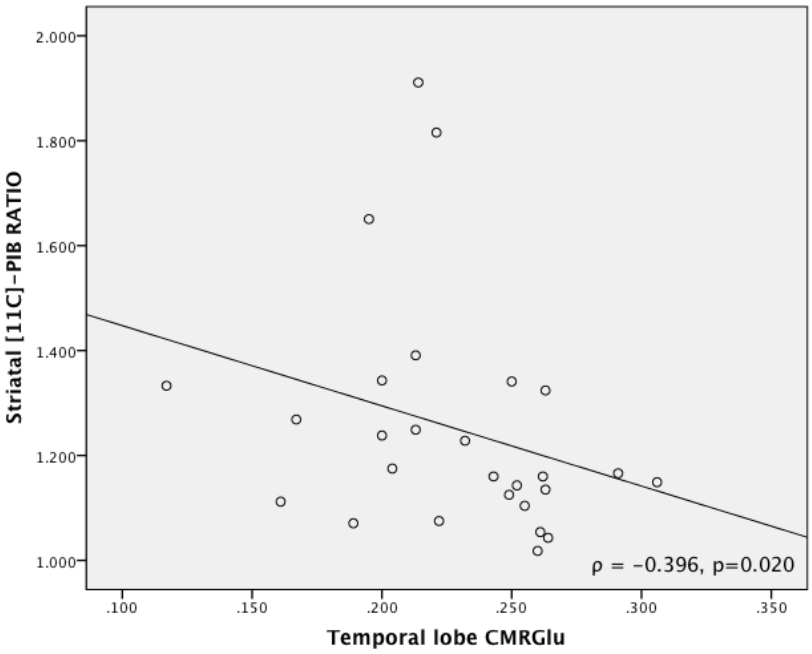


Figure B8. Correlation between striatal [^{11}C]-PIB RATIO and temporal lobe CMRGlu

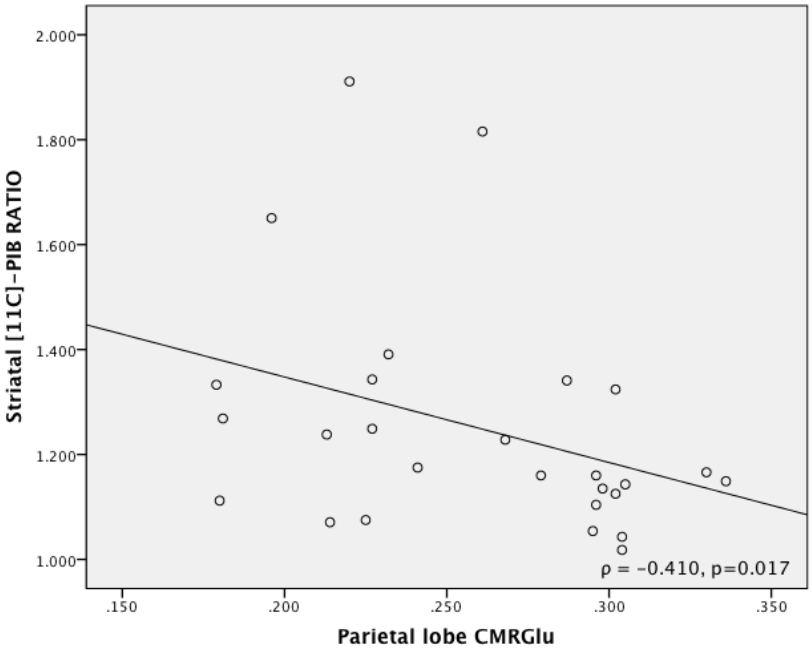


Figure B9. Correlation between striatal [^{11}C]-PIB RATIO and parietal lobe CMRGlu

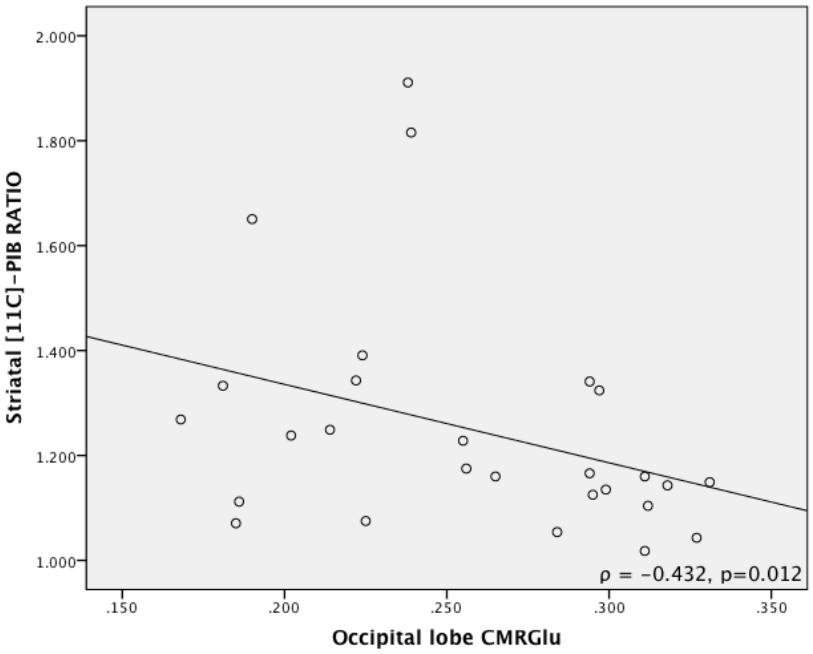


Figure B10. Correlation between striatal [^{11}C]-PIB RATIO and occipital lobe CMRGlu

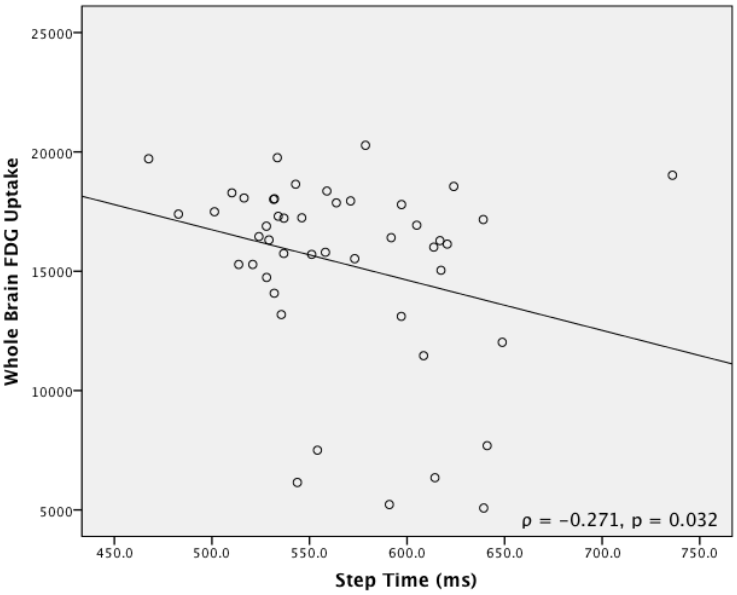


Figure C1. Correlation between whole brain [^{18}F]-FDG uptake and step time

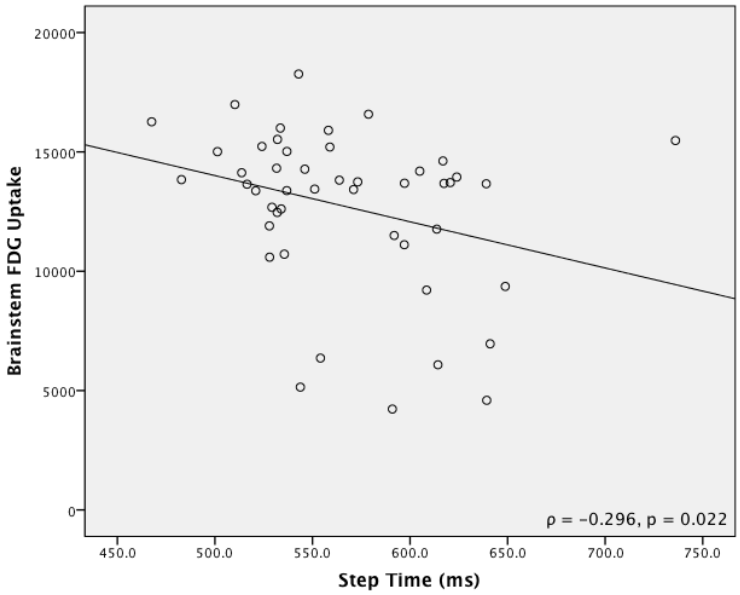


Figure C2. Correlation between brainstem [^{18}F]-FDG uptake and step time

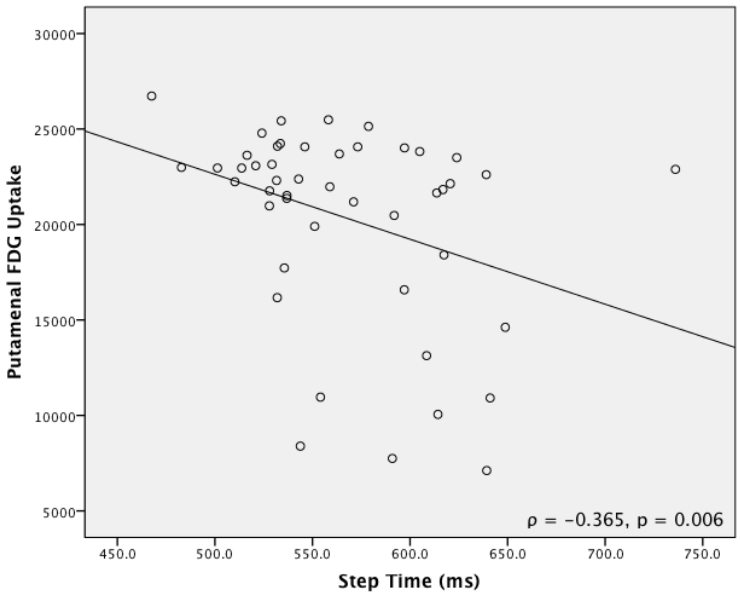


Figure C3. Correlation between putamenal [^{18}F]-FDG uptake and step time

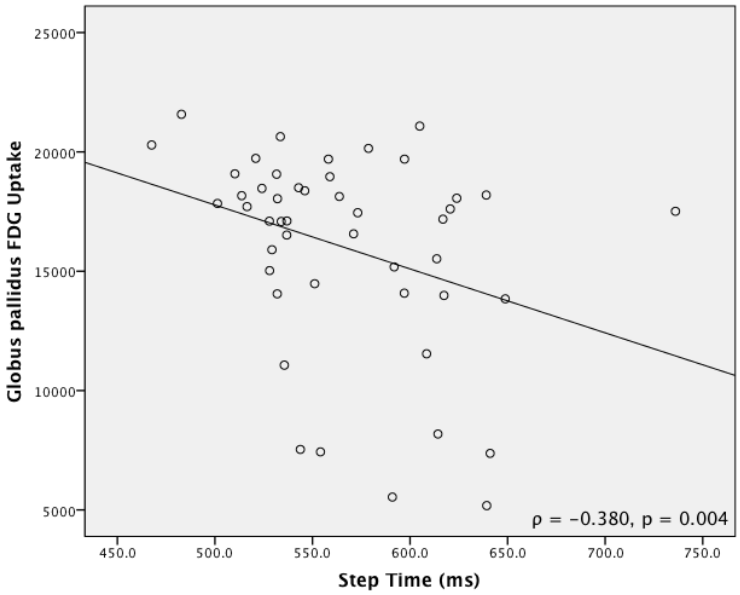


Figure C4. Correlation between globus pallidus [^{18}F]-FDG uptake and step time

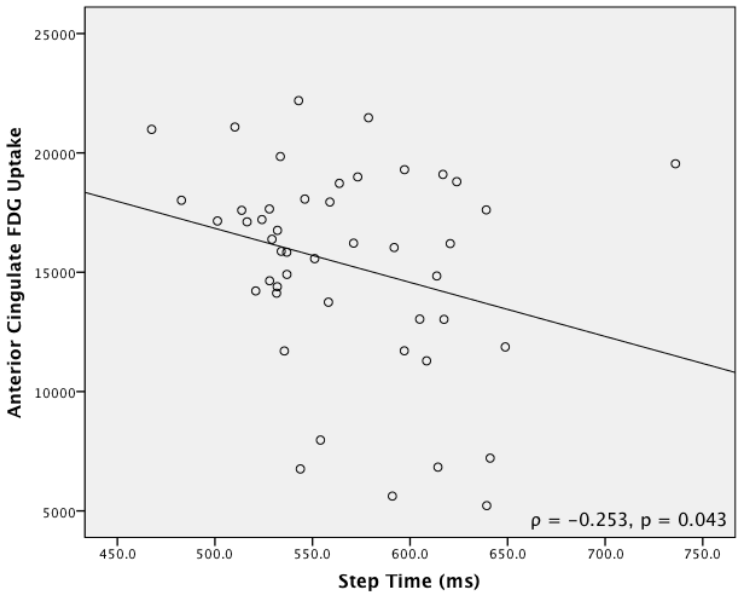


Figure C5. Correlation between anterior cingulate [^{18}F]-FDG uptake and step time

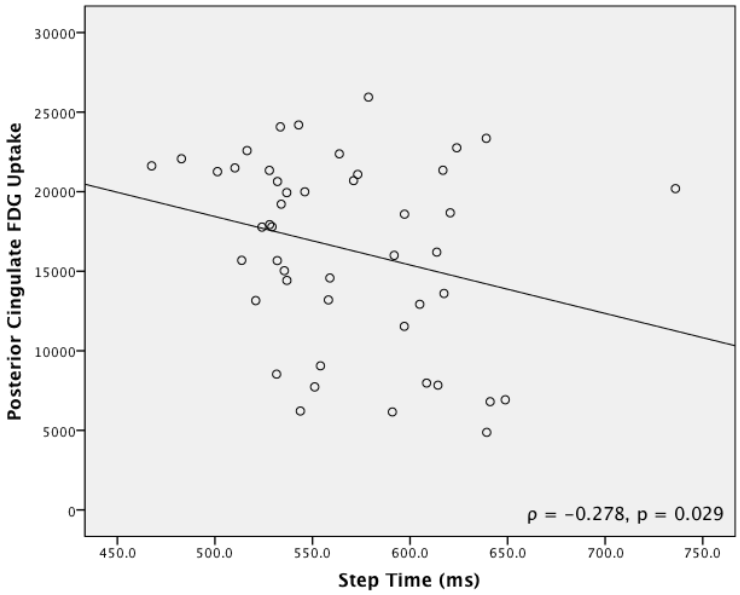


Figure C6. Correlation between posterior cingulate [^{18}F]-FDG uptake and step time

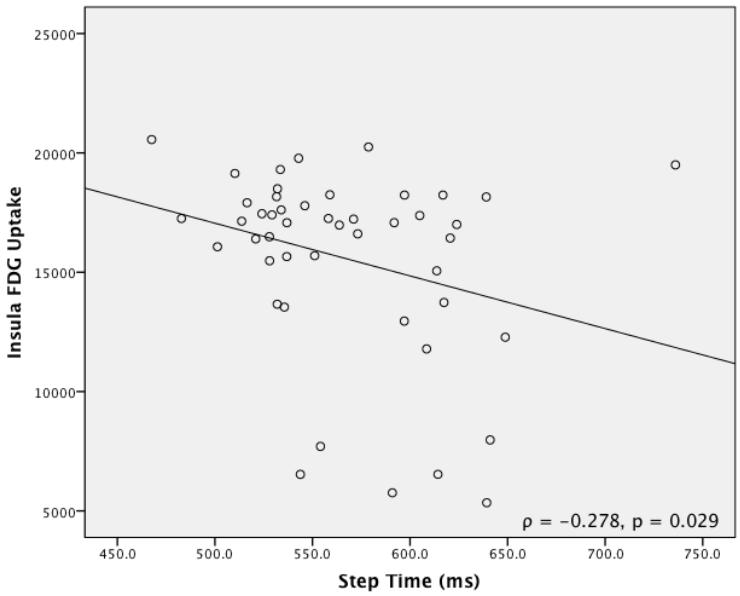


Figure C7. Correlation between insula [^{18}F]-FDG uptake and step time

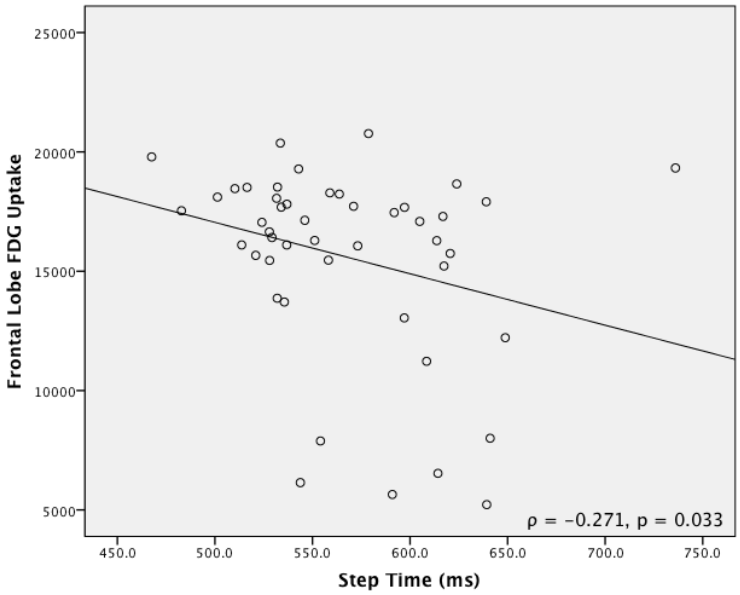


Figure C8. Correlation between frontal lobe [^{18}F]-FDG uptake and step time

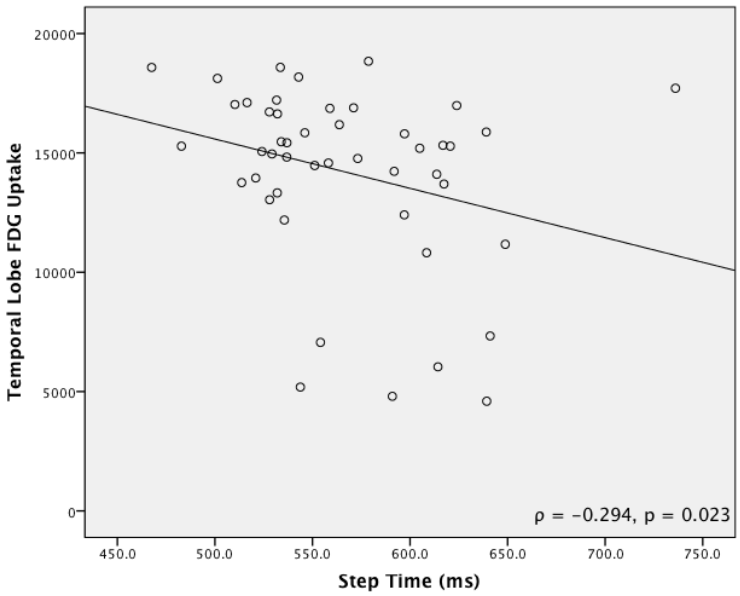


Figure C9. Correlation between temporal lobe [^{18}F]-FDG uptake and step time

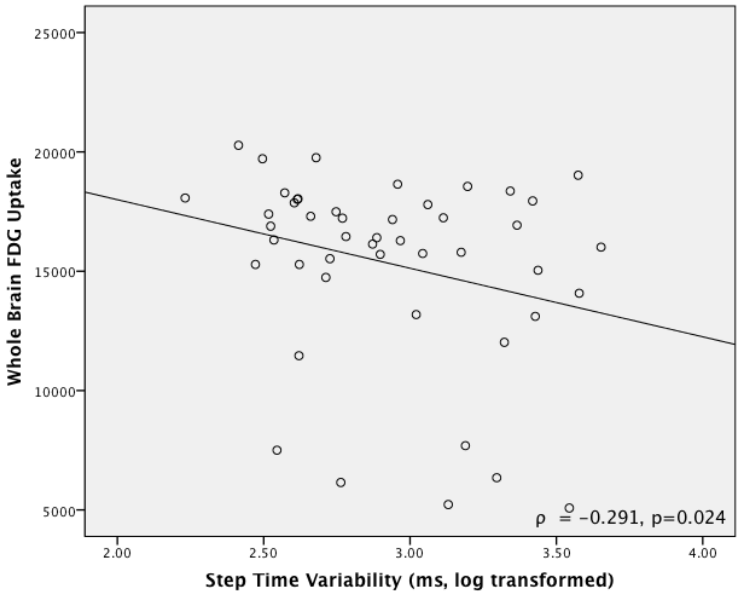


Figure C10. Correlation between whole brain [^{18}F]-FDG uptake and step time variability

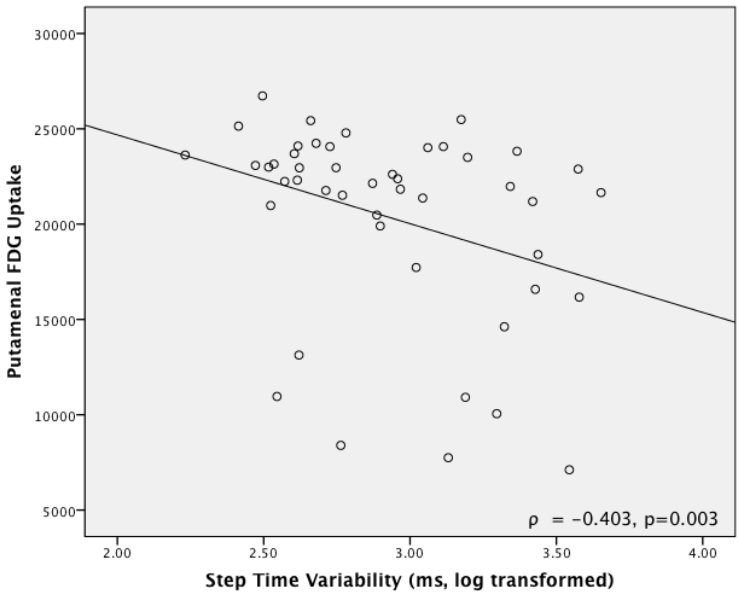


Figure C11. Correlation between putamenal [^{18}F]-FDG uptake and step time variability

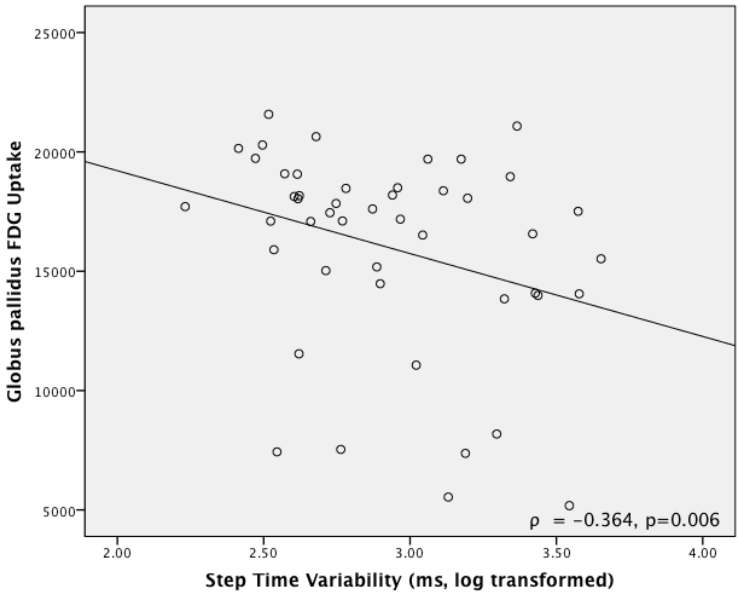


Figure C12. Correlation between globus pallidus [^{18}F]-FDG uptake and step time variability

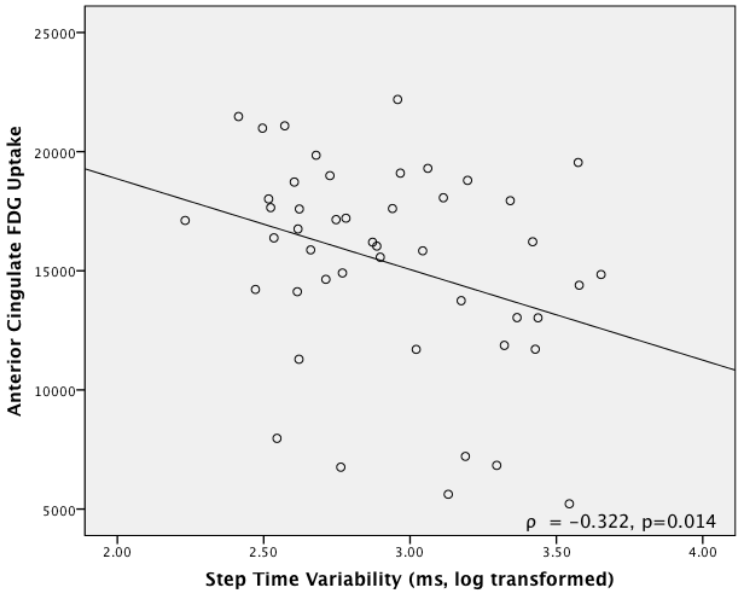


Figure C13. Correlation between anterior cingulate [^{18}F]-FDG uptake and step time variability

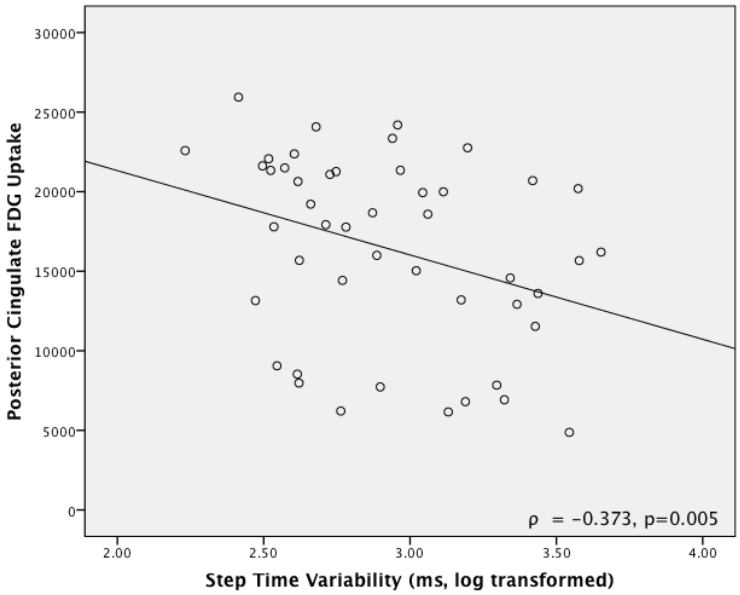


Figure C14. Correlation between posterior cingulate [^{18}F]-FDG uptake and step time variability

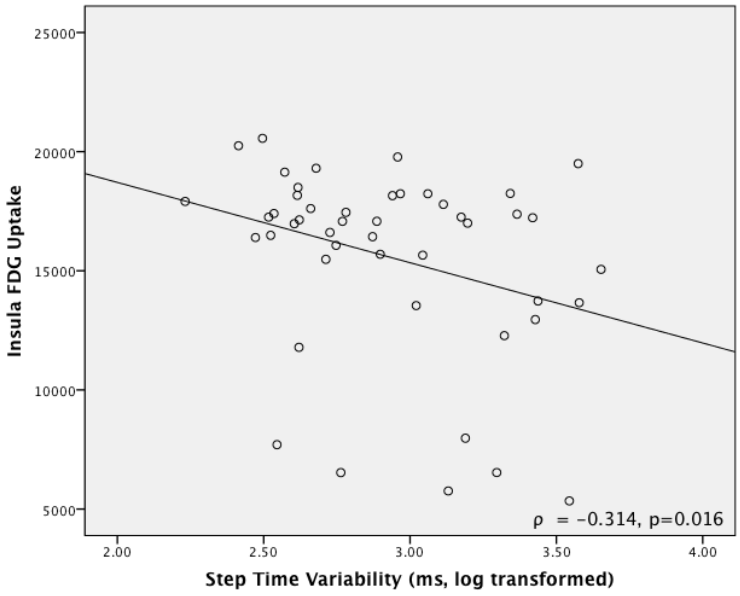


Figure C15. Correlation between insula [^{18}F]-FDG uptake and step time variability

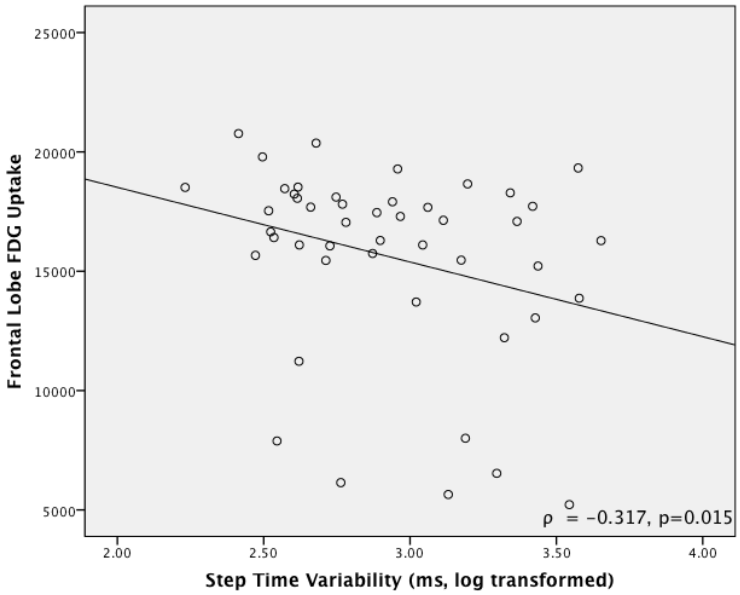


Figure C16. Correlation between frontal lobe [^{18}F]-FDG uptake and step time variability

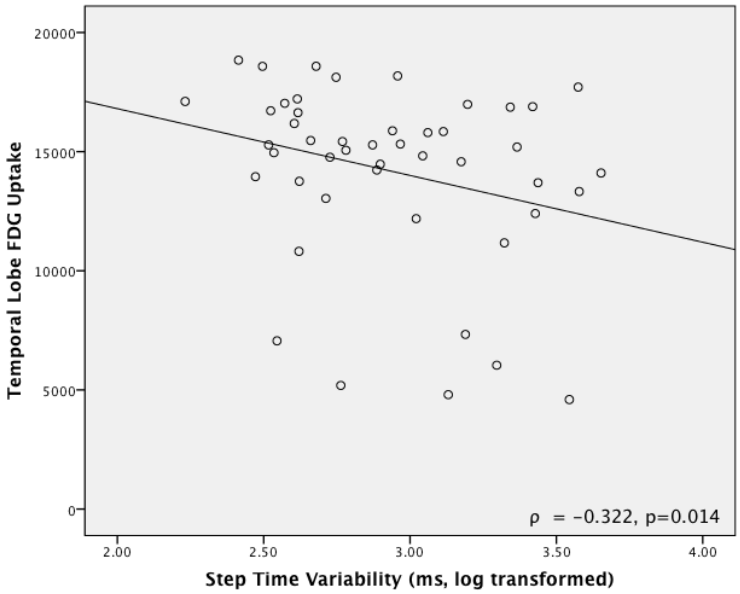


Figure C17. Correlation between temporal lobe [^{18}F]-FDG uptake and step time variability

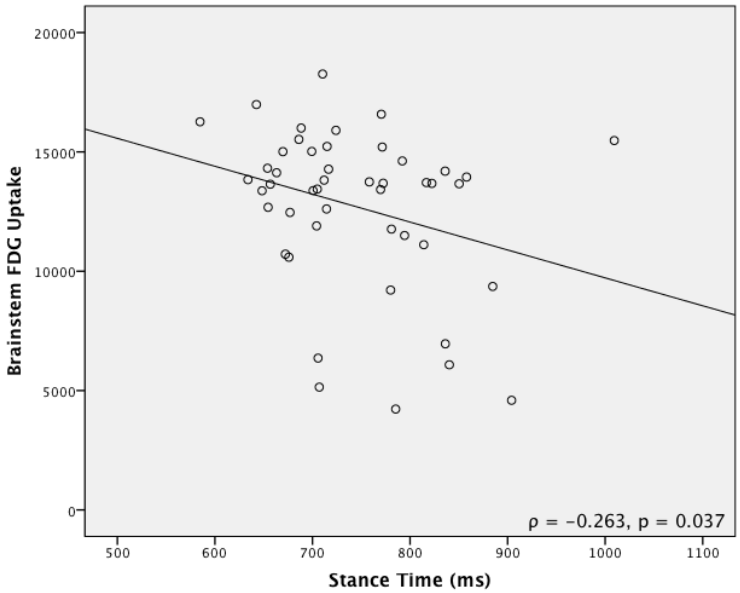


Figure C18. Correlation between brainstem [^{18}F]-FDG uptake and stance time

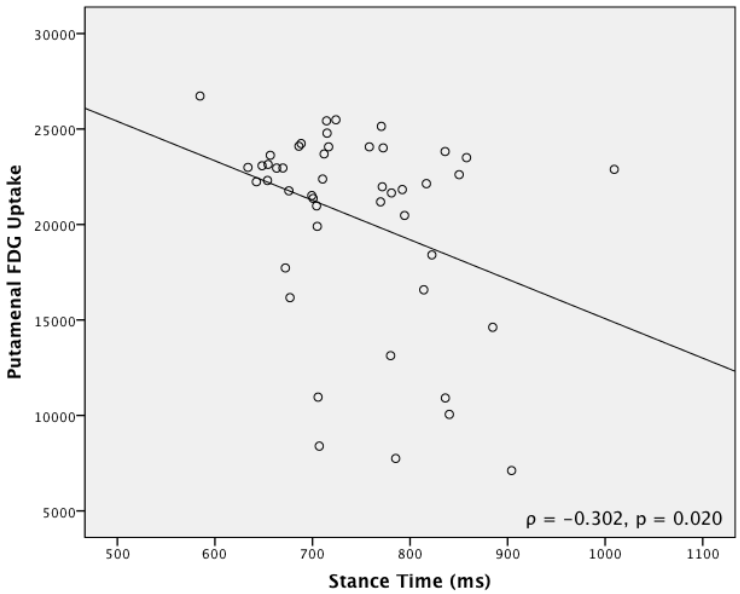


Figure C19. Correlation between putamneal [^{18}F]-FDG uptake and stance time

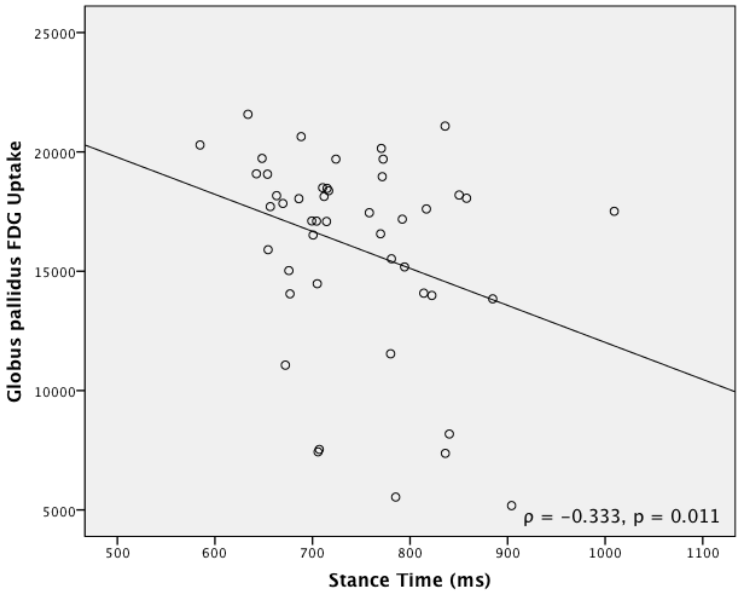


Figure C20. Correlation between globus pallidus [^{18}F]-FDG uptake and stance time

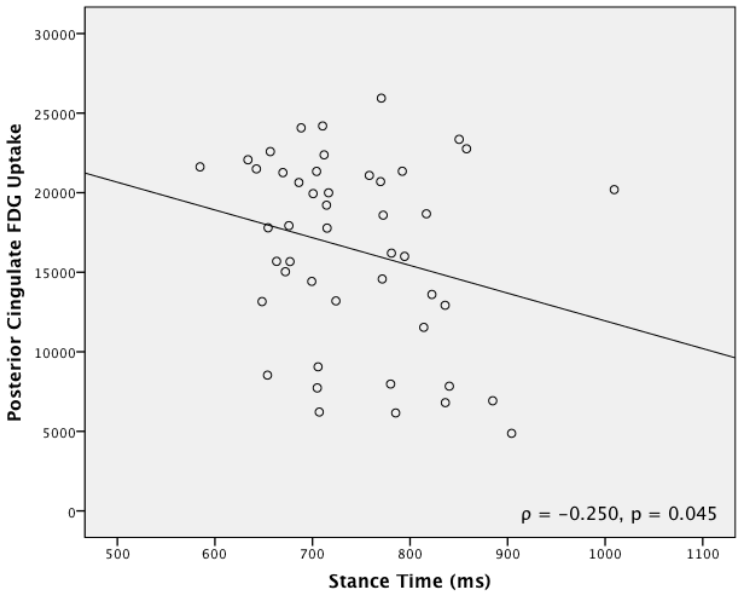


Figure C21. Correlation between posterior cingulate [^{18}F]-FDG uptake and stance time

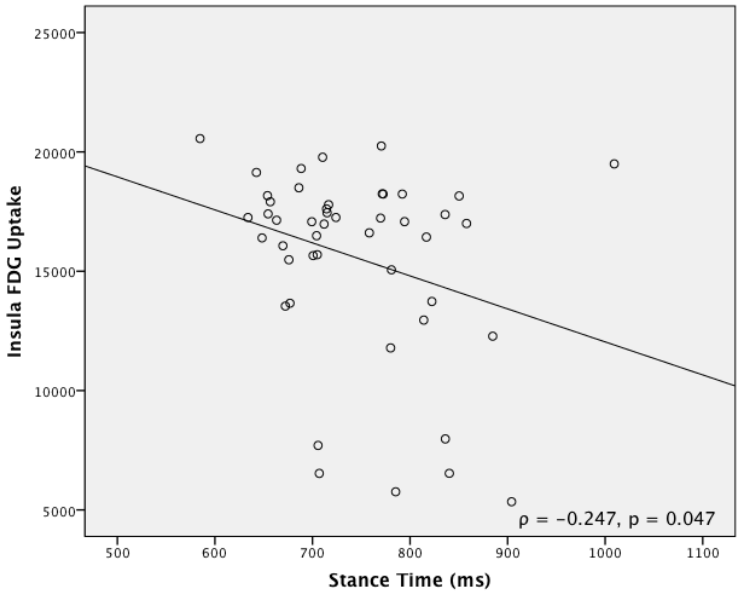


Figure C22. Correlation between insula [^{18}F]-FDG uptake and stance time

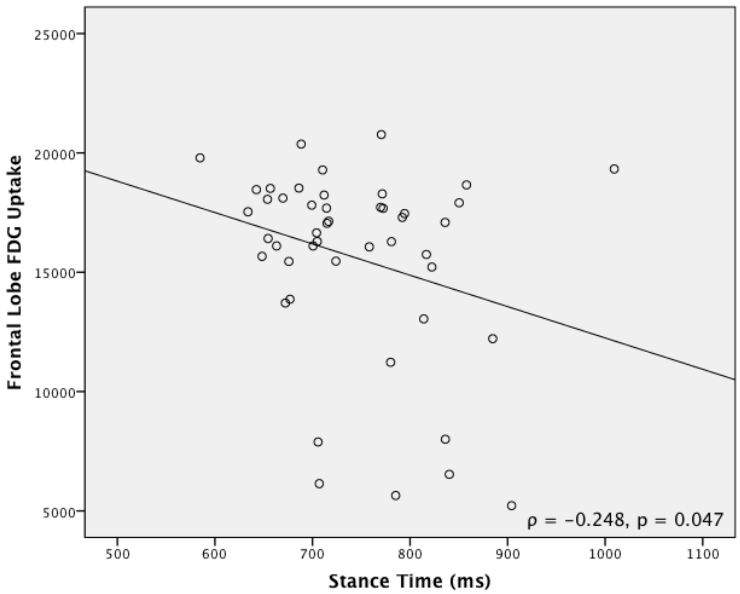


Figure C23. Correlation between frontal lobe [^{18}F]-FDG uptake and stance time

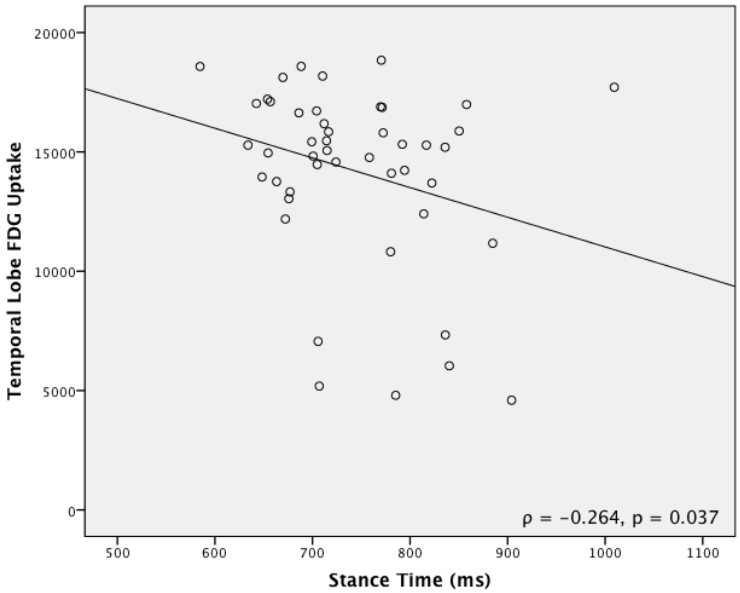


Figure C24. Correlation between temporal lobe [^{18}F]-FDG uptake and stance time

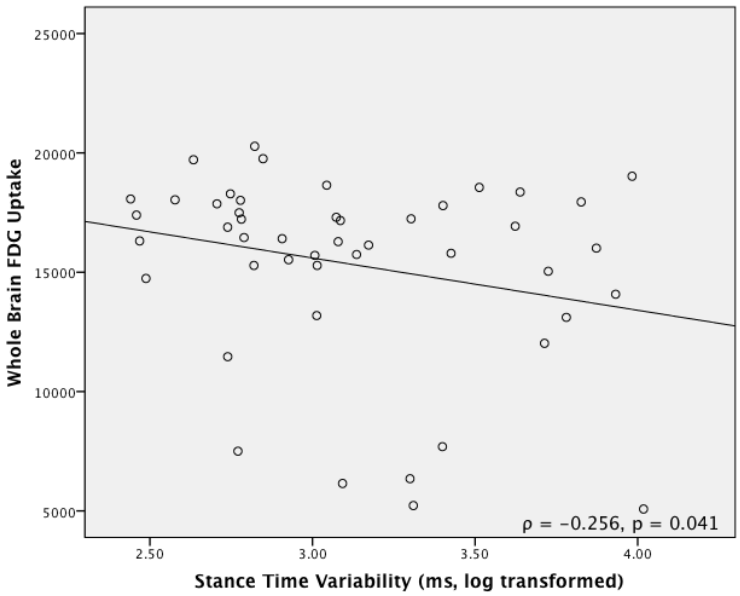


Figure C25. Correlation between whole brain [^{18}F]-FDG uptake and stance time variability

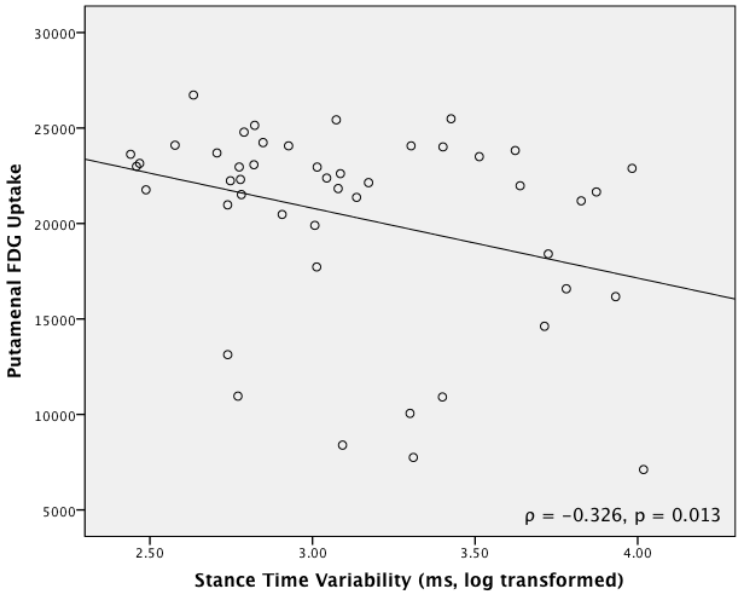


Figure C26. Correlation between putamenal [^{18}F]-FDG uptake and stance time variability

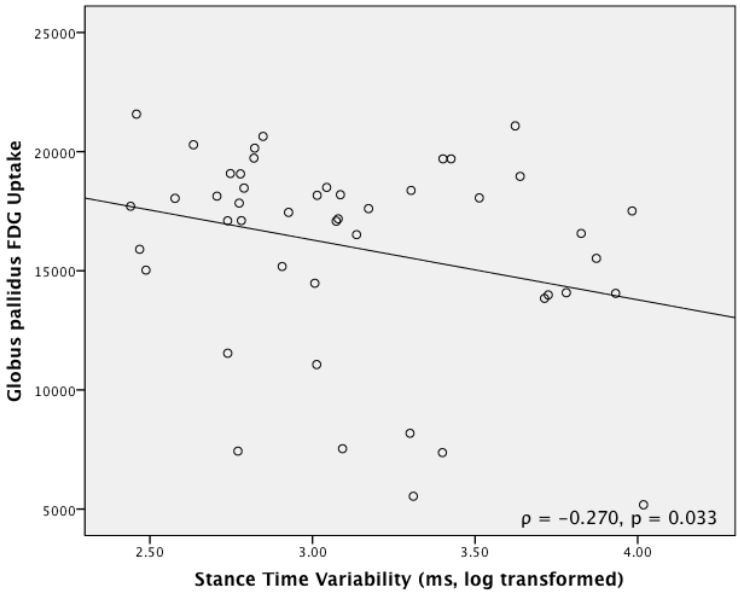


Figure C27. Correlation between globus pallidus [^{18}F]-FDG uptake and stance time variability

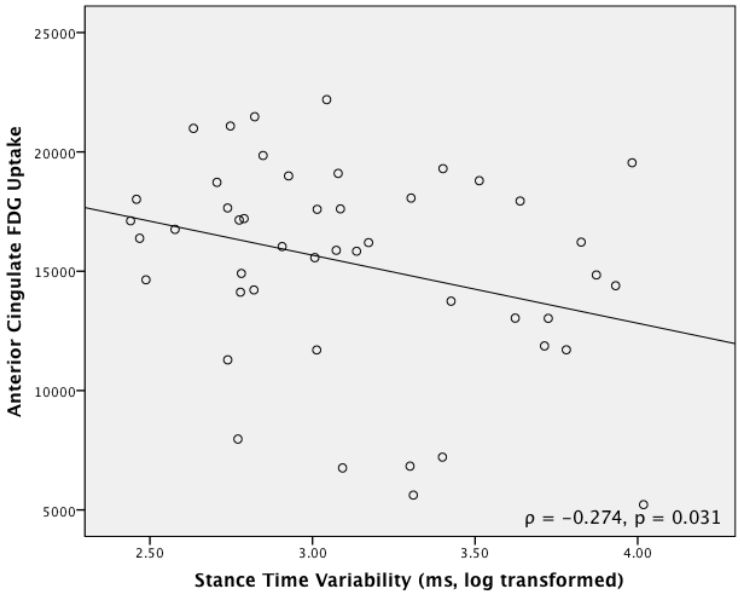


Figure C28. Correlation between anterior cingulate [^{18}F]-FDG uptake and stance time variability

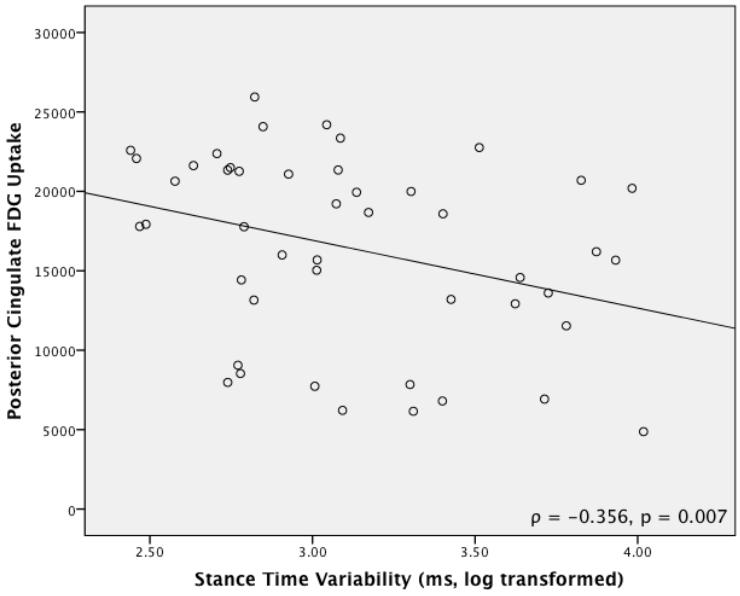


Figure C29. Correlation between posterior cingulate [^{18}F]-FDG uptake and stance time variability

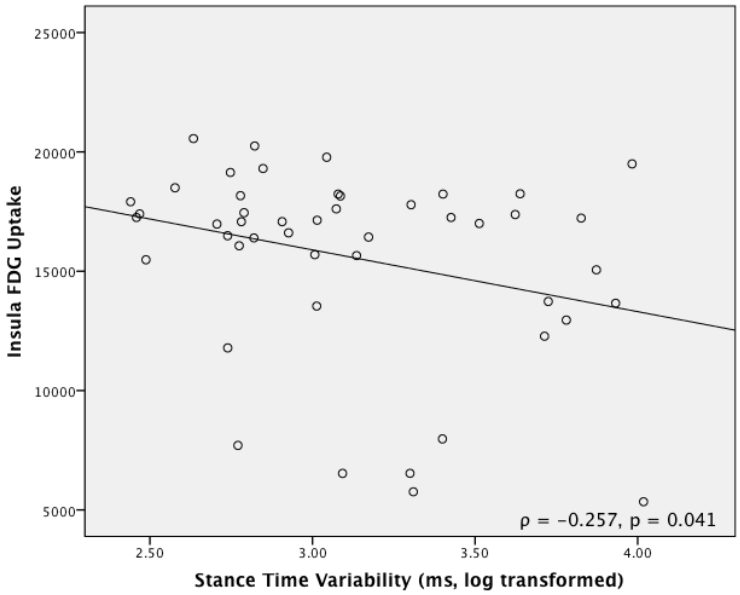


Figure C30. Correlation between insula [^{18}F]-FDG uptake and stance time variability

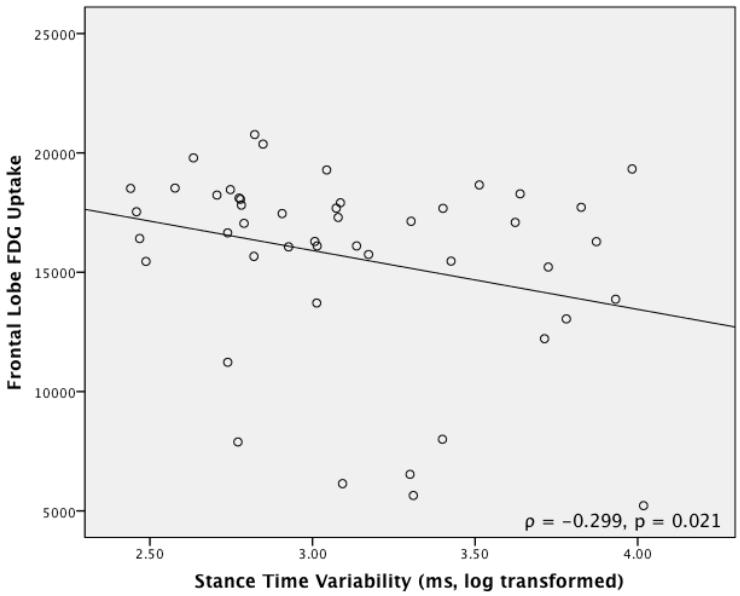


Figure C31. Correlation between frontal lobe [^{18}F]-FDG uptake and stance time variability

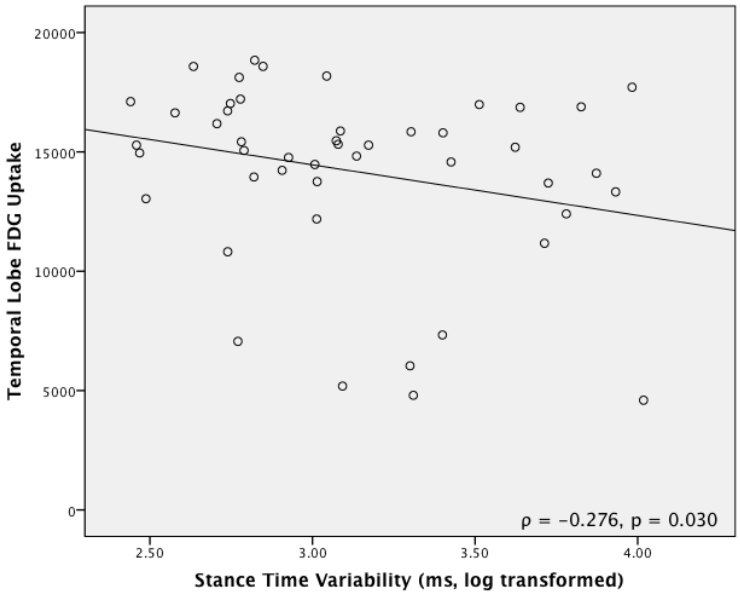


Figure C32. Correlation between temporal lobe [^{18}F]-FDG uptake and stance time variability

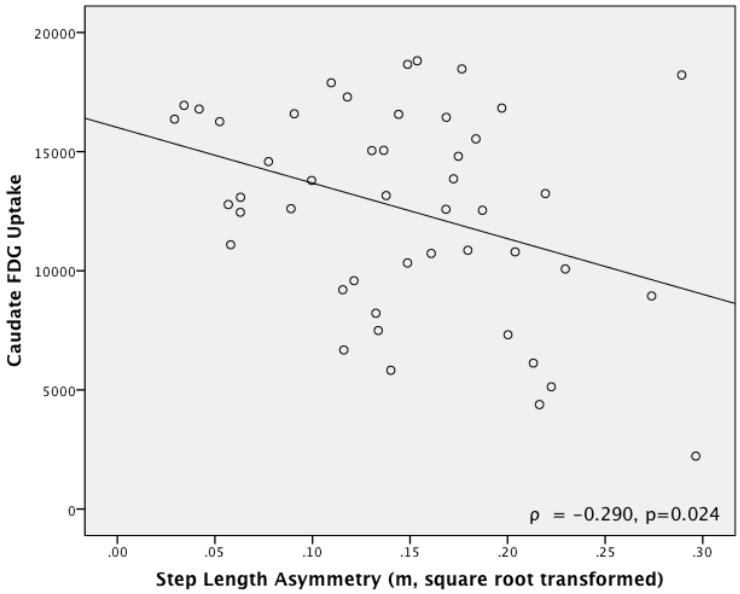


Figure C33. Correlation between caudate [^{18}F]-FDG uptake and step length asymmetry

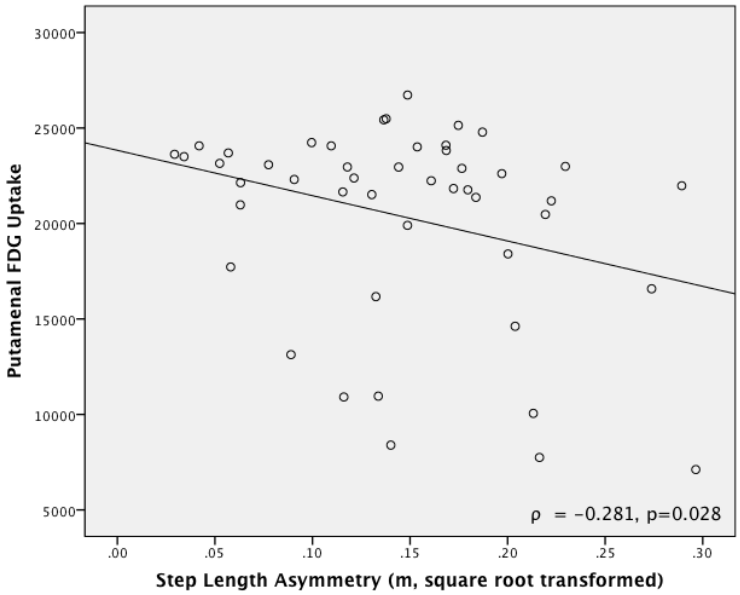


Figure C34. Correlation between putamen [^{18}F]-FDG uptake and step length asymmetry

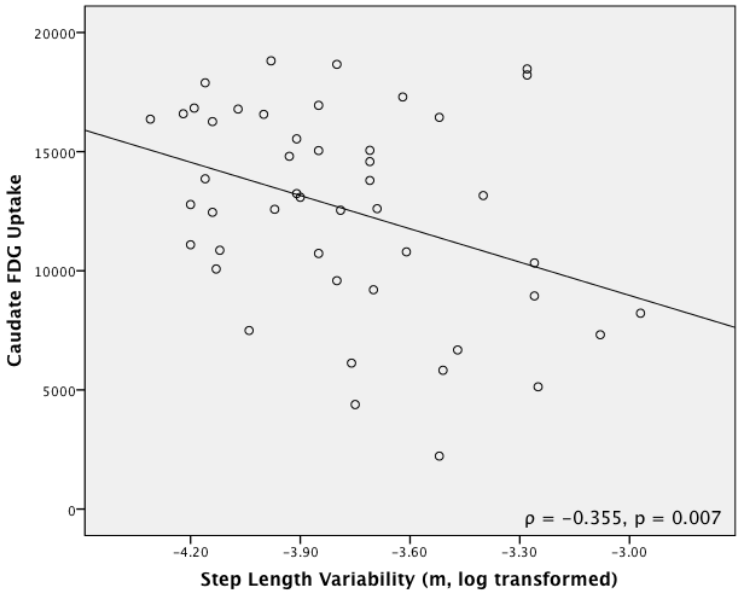


Figure C35. Correlation between caudate [^{18}F]-FDG uptake and step length variability

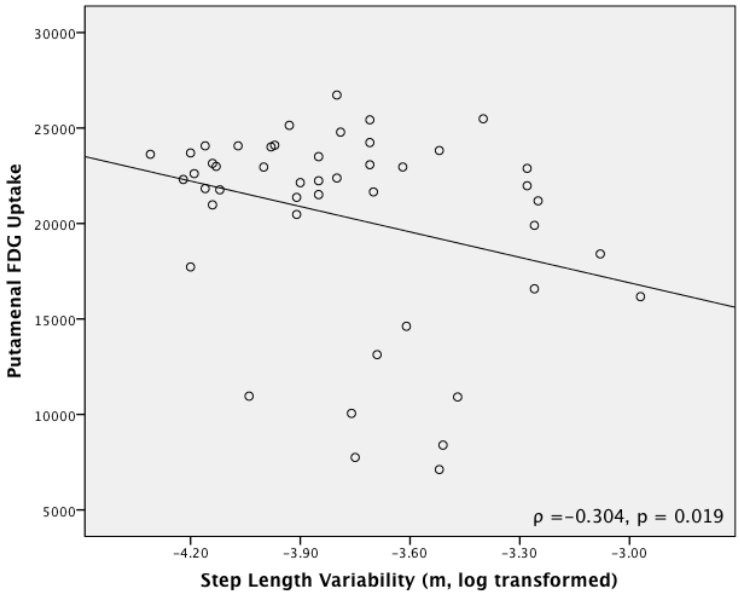


Figure C36. Correlation between putamenal [^{18}F]-FDG uptake and step length variability

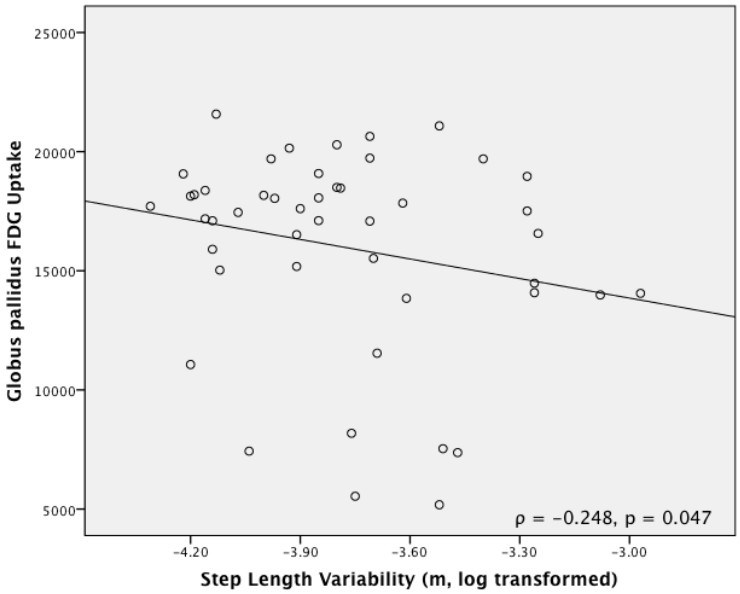


Figure C37. Correlation between globus pallidus [^{18}F]-FDG uptake and step length variability

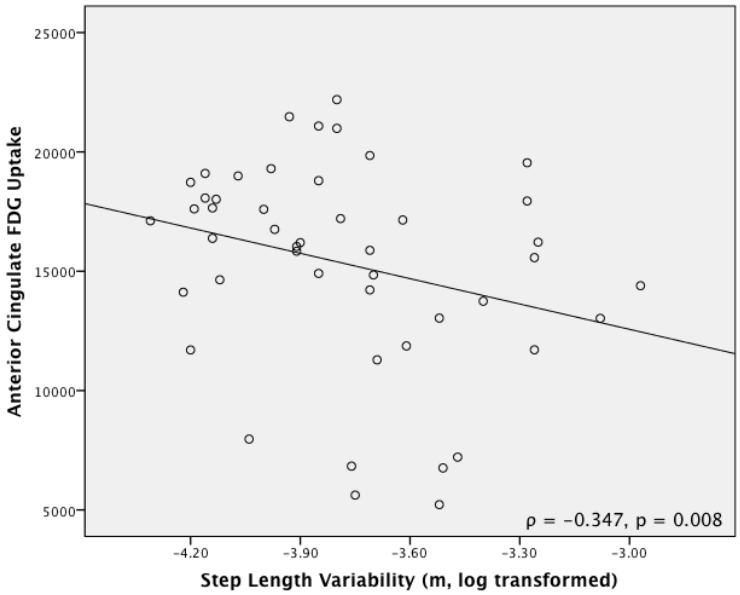


Figure C38. Correlation between anterior cingulate [^{18}F]-FDG uptake and step length variability

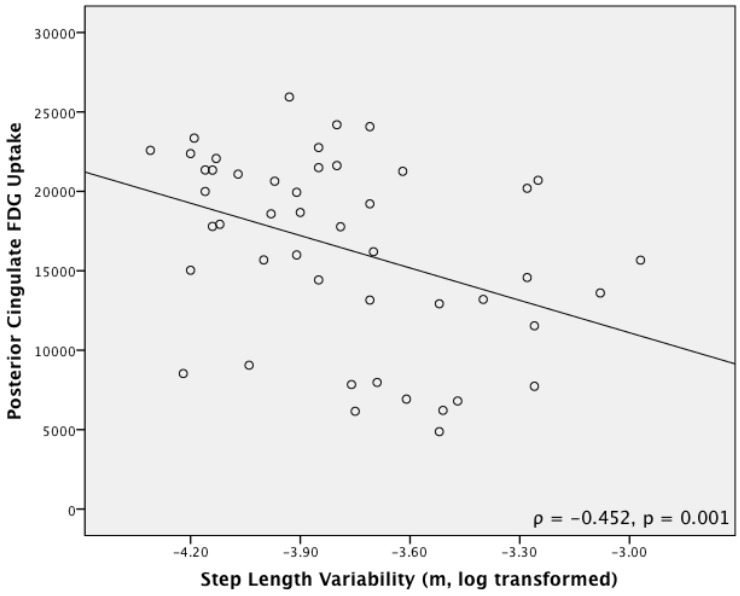


Figure C39. Correlation between posterior cingulate [^{18}F]-FDG uptake and step length variability

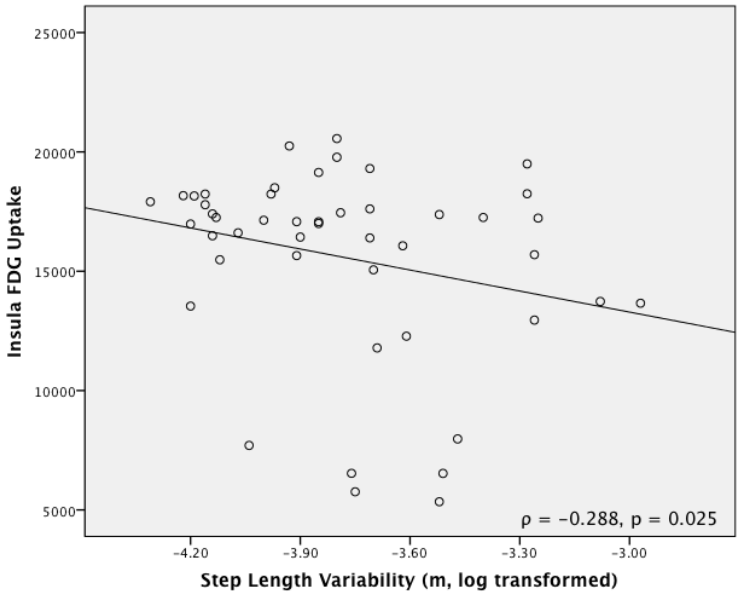


Figure C40. Correlation between insula [^{18}F]-FDG uptake and step length variability

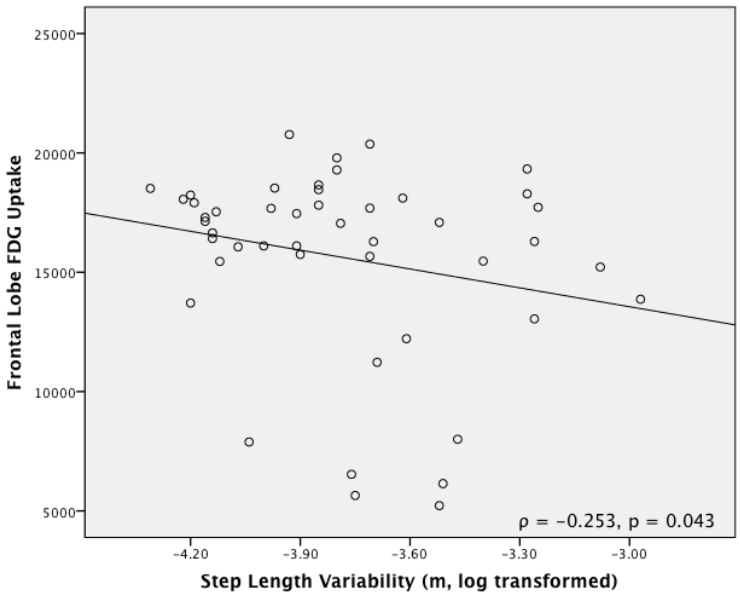


Figure C41. Correlation between frontal lobe [^{18}F]-FDG uptake and step length variability

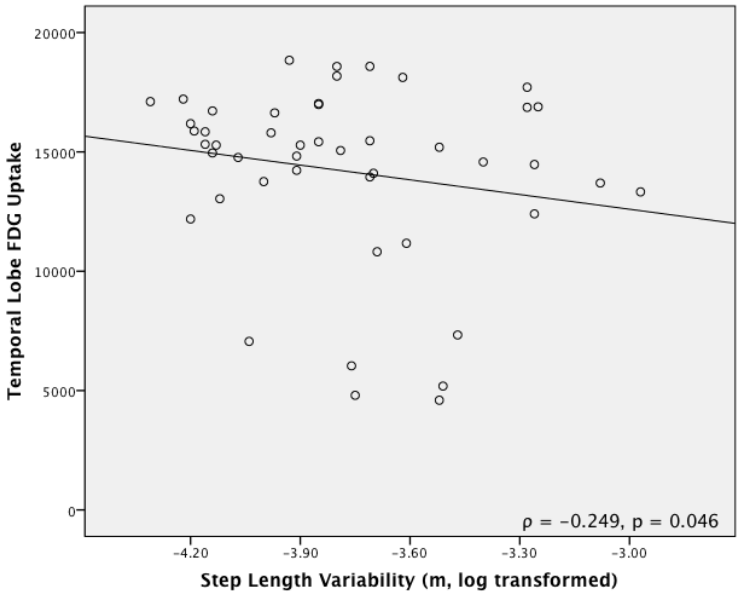


Figure C42. Correlation between temporal lobe [^{18}F]-FDG uptake and step length variability

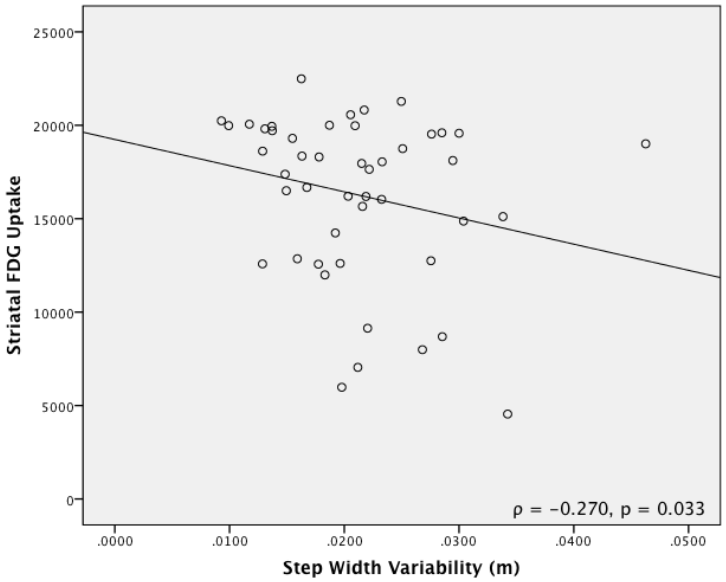


Figure C43. Correlation between striatal [^{18}F]-FDG uptake and step width variability

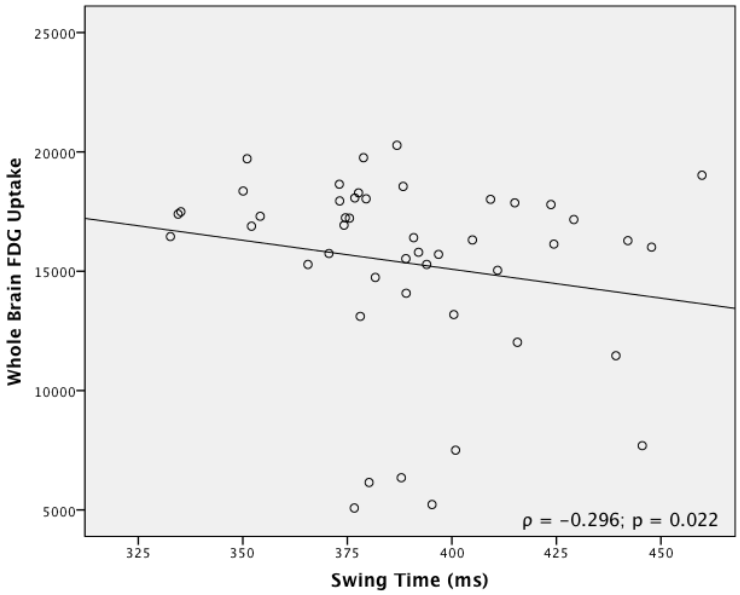


Figure C44. Correlation between whole brain [^{18}F]-FDG uptake and swing time

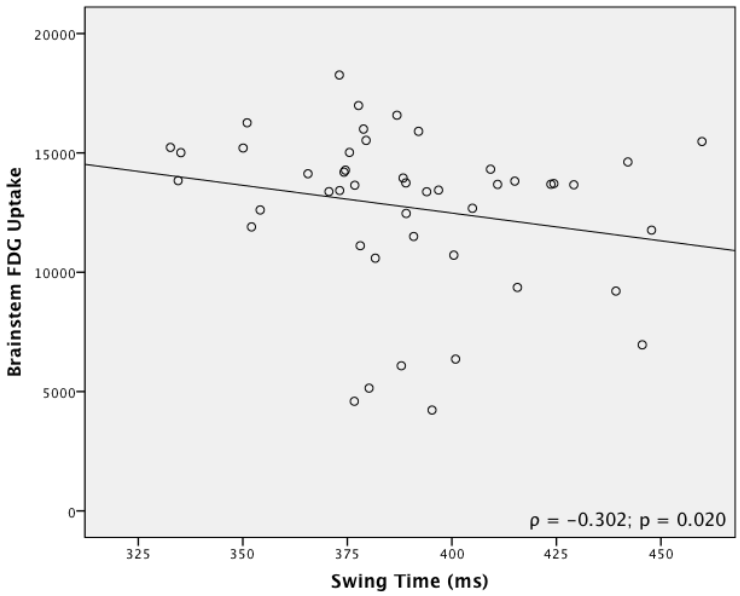


Figure C45. Correlation between brainstem [^{18}F]-FDG uptake and swing time

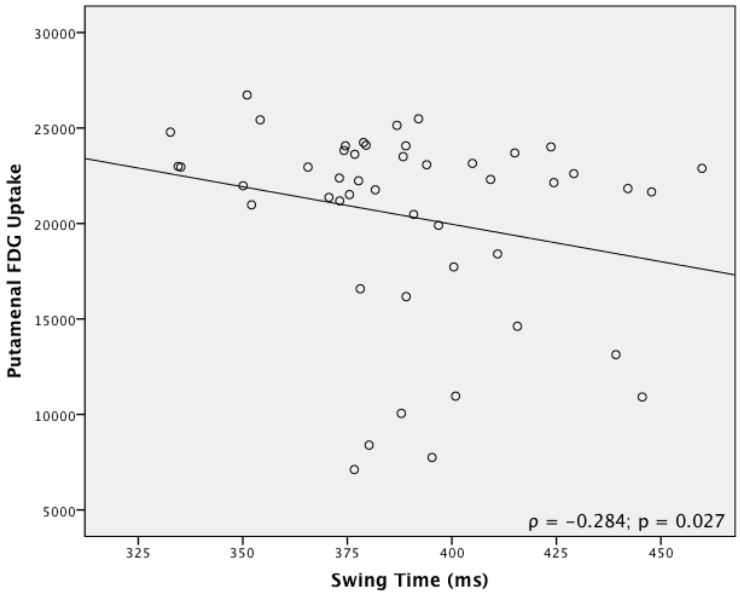


Figure C46. Correlation between putamenal [^{18}F]-FDG uptake and swing time

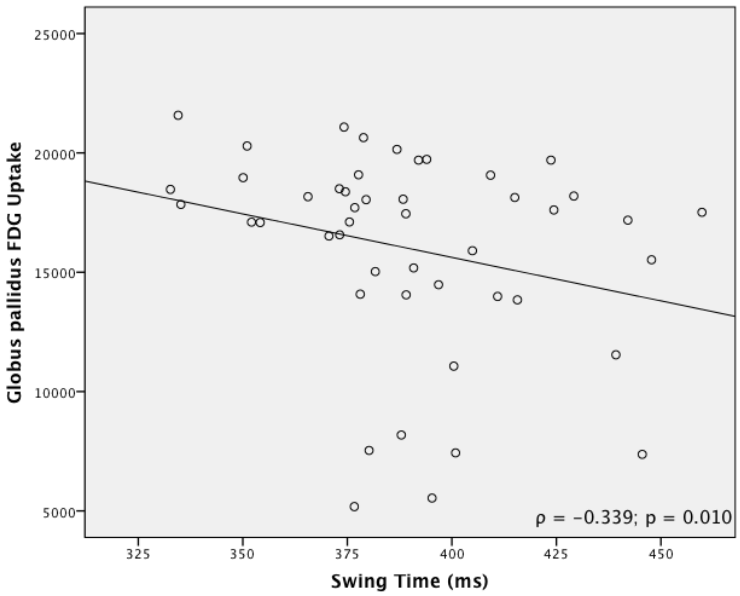


Figure C47. Correlation between globus pallidus [^{18}F]-FDG uptake and swing time

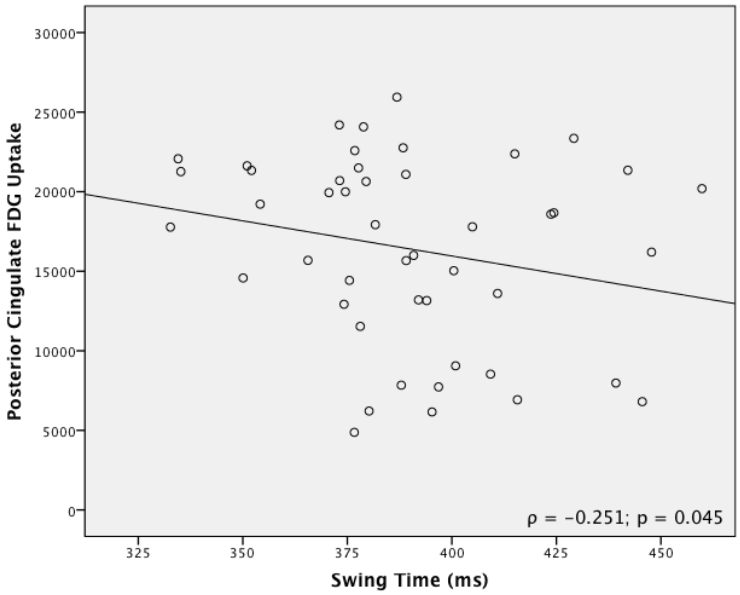


Figure C48. Correlation between posterior cingulate [^{18}F]-FDG uptake and swing time

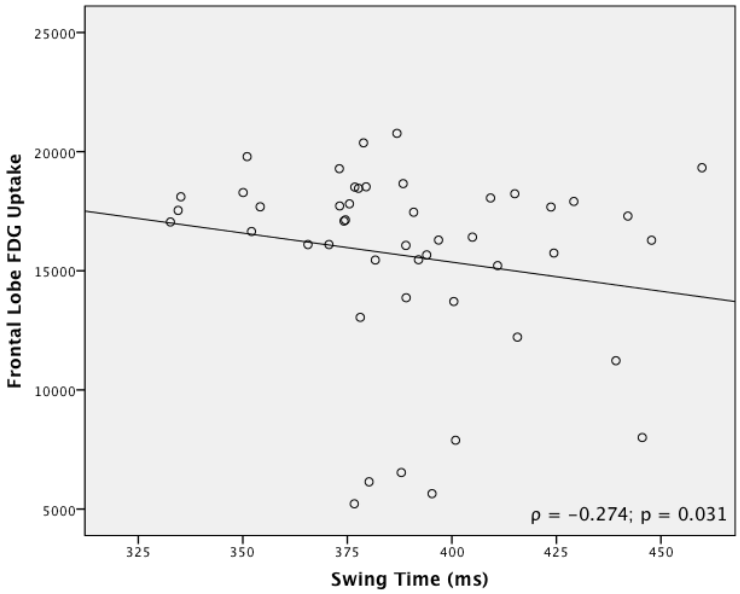


Figure C49. Correlation between frontal lobe [^{18}F]-FDG uptake and swing time

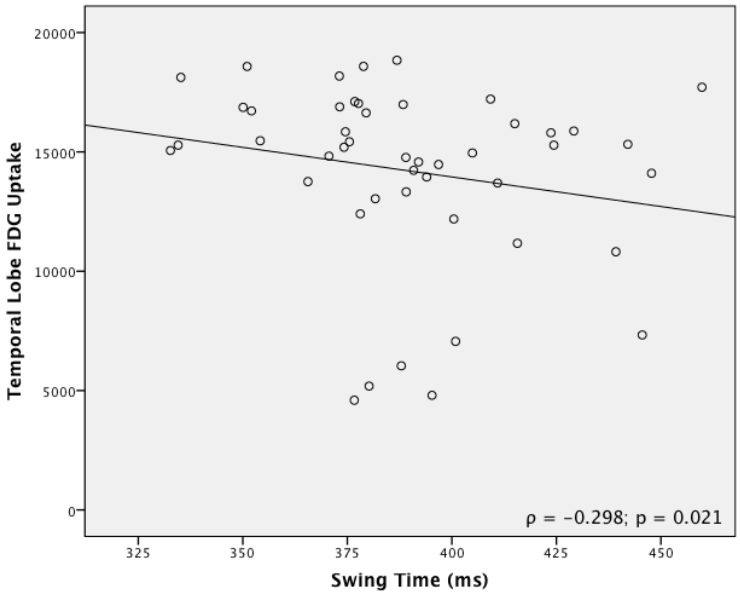


Figure C50. Correlation between temporal lobe [^{18}F]-FDG uptake and swing time

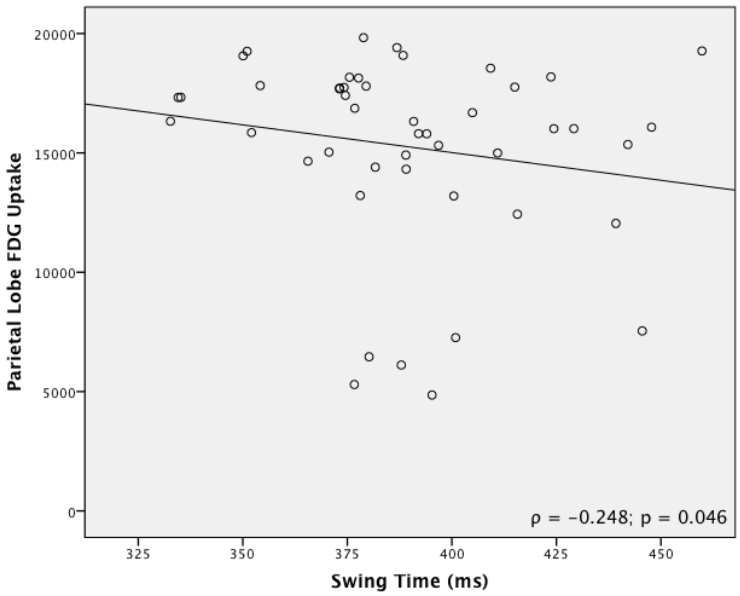


Figure C51. Correlation between parietal lobe [^{18}F]-FDG uptake and swing time

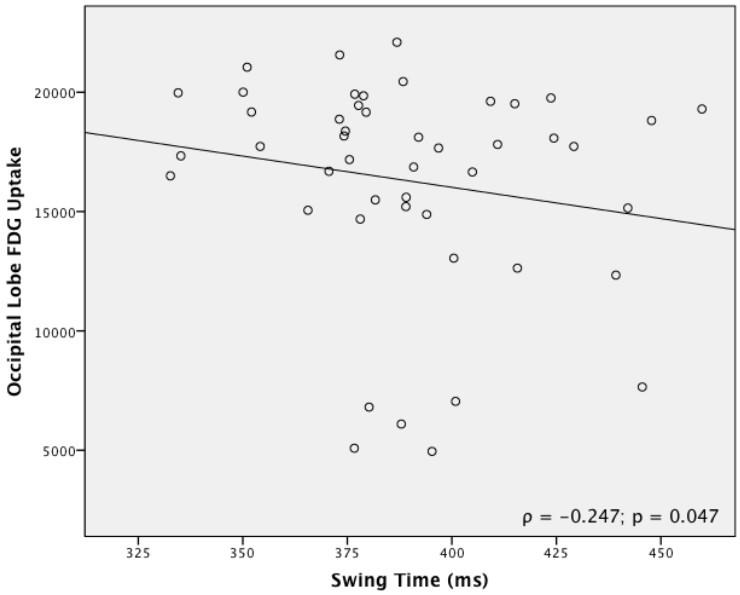


Figure C52. Correlation between occipital lobe [^{18}F]-FDG uptake and swing time

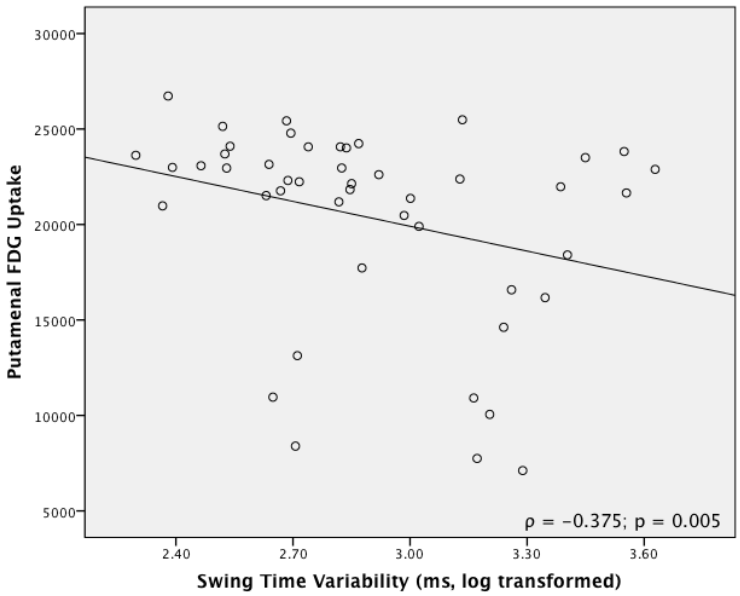


Figure C53. Correlation between putamenal [^{18}F]-FDG uptake and swing time variability

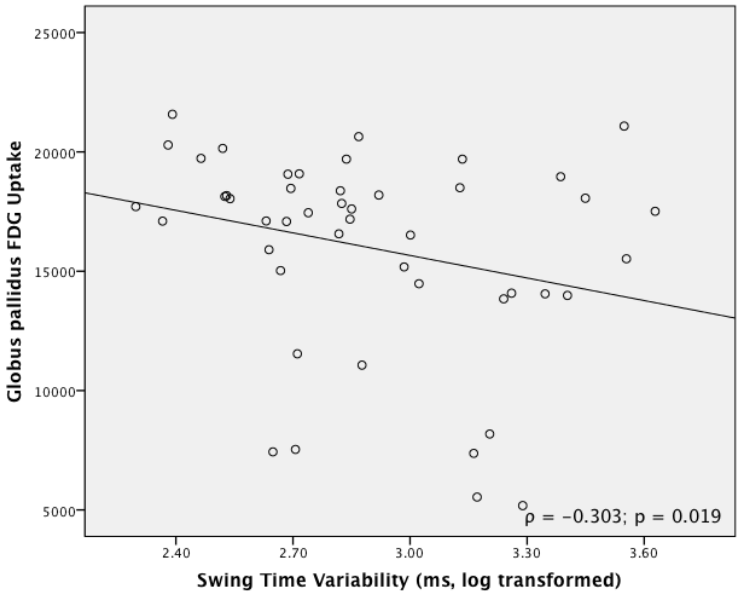


Figure C54. Correlation between globus pallidus [^{18}F]-FDG uptake and swing time variability

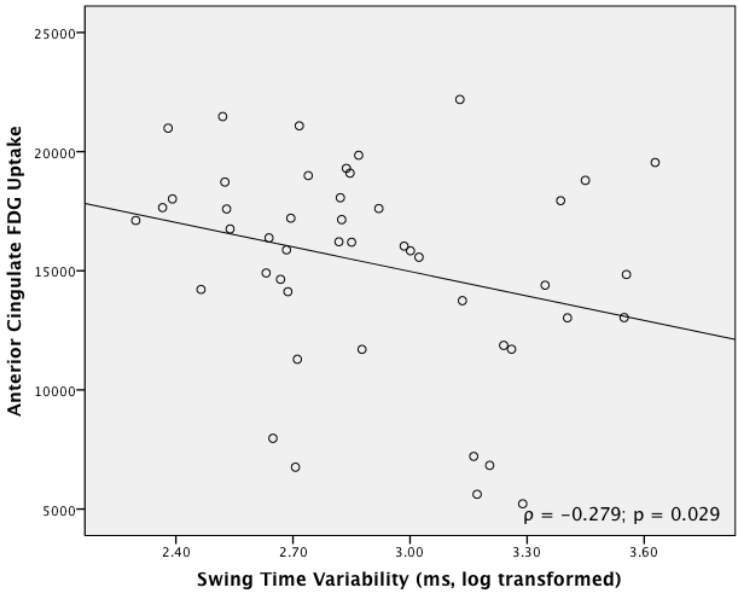


Figure C55. Correlation between anterior cingulate [^{18}F]-FDG uptake and swing time variability

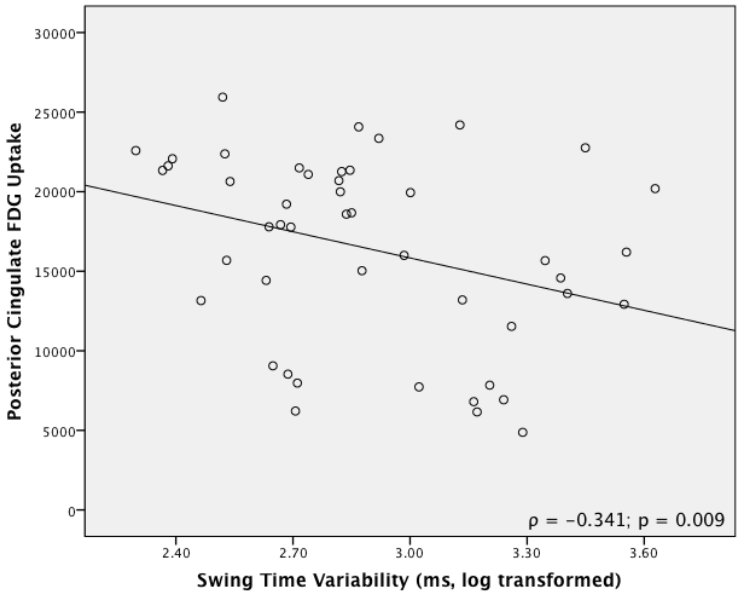


Figure C56. Correlation between posterior cingulate [^{18}F]-FDG uptake and swing time variability

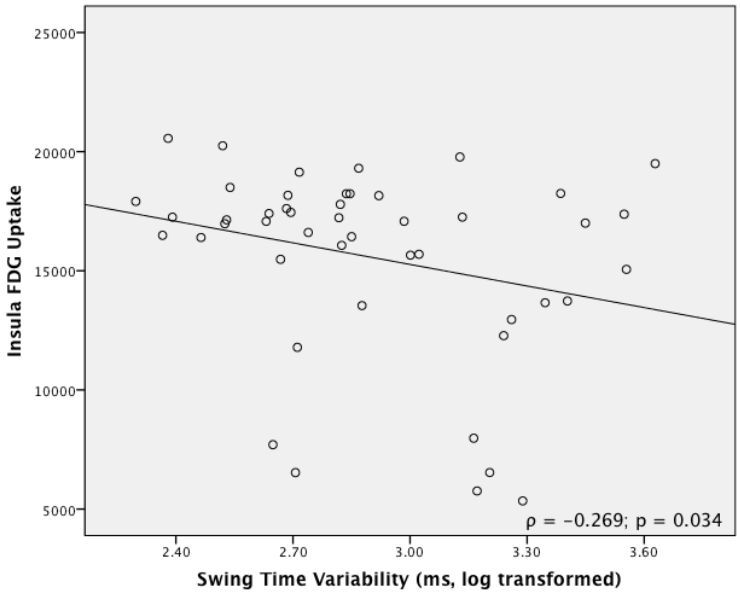


Figure C56. Correlation between insula [^{18}F]-FDG uptake and swing time variability

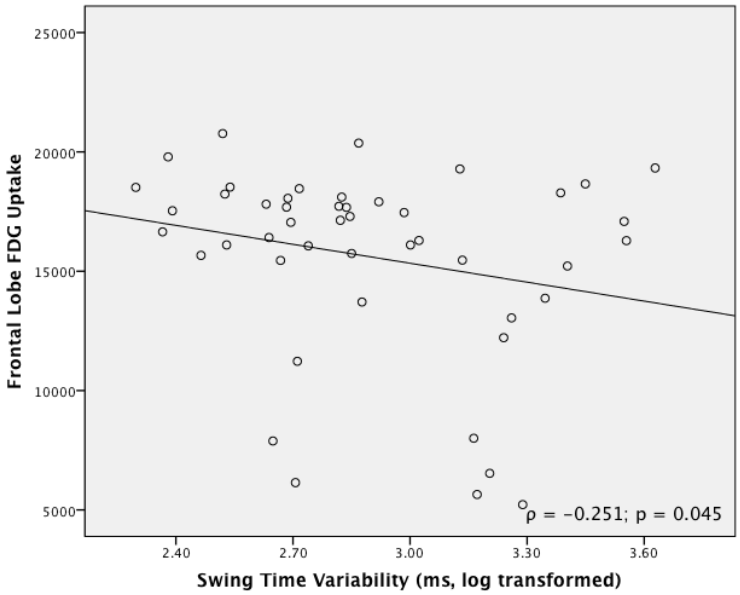


Figure C57. Correlation between frontal lobe [^{18}F]-FDG uptake and swing time variability

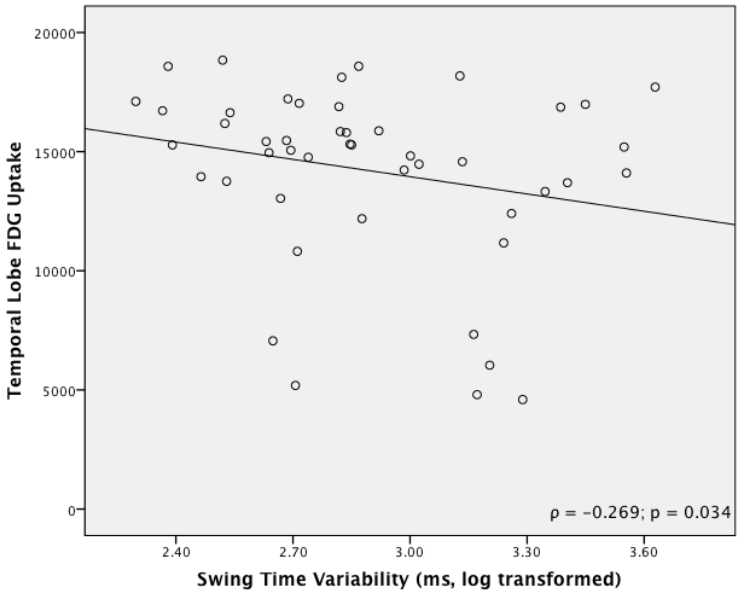


Figure C58. Correlation between temporal lobe [^{18}F]-FDG uptake and swing time variability

Chapter 8

References

Aarsland D, Larsen JP, Lim NG, Janvin C, Karlsen K, Tandberg E, Cummings JL. J Neurol Neurosurg Psychiatry. 1999; 67:492-496. Range of neuropsychiatric disturbances in patients with Parkinson's disease.

Aarsland D, Perry R, Brown A, Larsen JP, Ballard C. Neuropathology of dementia in Parkinson's disease: a prospective, community-based study. Ann Neurol 2005; 58:773-776.

Aarsland D, Brønnick K, Larsen JP, Tysnes OB, Alves G. Norwegian ParkWest Study Group. Cognitive impairment in incident, untreated Parkinson disease: the Norwegian ParkWest study. Neurology. 2009; 72:1121-6.

Aarsland D, Bronnick K, Williams-Gray C, et al. Mild cognitive impairment in Parkinson disease: a multicenter pooled analysis. Neurology. 2010; 75:1062-1069.

Aasly JO, Shi M, Sossi V, et al. Cerebrospinal fluid amyloid β and tau in LRRK2 mutation carriers. Neurology. 2012; 78:55-61.

Adams JR, van Netten H, Schulzer M, et al. PET in LRRK2 mutations: comparison to sporadic Parkinson's disease and evidence for presymptomatic compensation. Brain. 2005; 128:2777–2785.

Aharon-Peretz J, Badarny S, Rosenbaum H, Gershoni-Baruch R. Mutations in the glucocerebrosidase gene and Parkinson disease: phenotype-genotype correlation. Neurology. 2005; 65:1460-1461.

Aharon-Peretz J, Rosenbaum H, Gershoni-Baruch R. Mutations in the glucocerebrosidase gene and Parkinson's disease in Ashkenazi Jews. N Engl J Med. 2004; 351:1972-1977.

Ahlskog JE. Beating a dead horse: dopamine and Parkinson disease. Neurology. 2007; 69:1701-1711.

Ahlskog JE. Parkin and PINK1 parkinsonism may represent nigral mitochondrial cytopathies distinct from Lewy body Parkinson's disease. Parkinsonism Relat Disord 2009; 15:721-727.

Alam M, Schwabe K, Krauss JK. The pedunculopontine nucleus area: critical evaluation of interspecies differences relevant for its use as a target for deep brain stimulation. Brain. 2011; 134:11-23.

Albert MS, DeKosky ST, Dickson D, et al. The diagnosis of mild cognitive impairment due to Alzheimer's disease: recommendations from the National Institute

on Aging-Alzheimer's Association workgroups on diagnostic guidelines for Alzheimer's disease. Alzheimers Dement. 2011; 7:270-279.

Albert PR, Vahid-Ansari F, Luckhart C. Serotonin-prefrontal cortical circuitry in anxiety and depression phenotypes: pivotal role of pre- and post-synaptic 5-HT1A receptor expression. Front Behav Neurosci. 2014; 8:199.

Alcalay RN, Dinur T, Quinn T, et al. Comparison of Parkinson risk in Ashkenazi Jewish patients with Gaucher disease and GBA heterozygotes. JAMA Neurol. 2014; 71:752-757.

Alexander GE, Crutcher MD, DeLong MR. Basal ganglia-thalamocortical circuits: parallel substrates for motor, oculomotor, "prefrontal" and "limbic" functions. Prog Brain Res. 1990; 85:119–146.

Allam MF, Del Castillo AS, Navajas RF-C. Parkinson's disease, smoking and family history: meta-analysis. Eur J Neurol. 2003; 10:59–62.

Alvarez-Erviti L, Couch Y, Richardson J, Cooper JM, Wood MJ. Alpha-synuclein release by neurons activates the inflammatory response in a microglial cell line. Neurosci Res. 2011; 69:
337–342.

Alves G, Lange J, Blennow K, et al. CSF Aβ42 predicts early-onset dementia in Parkinson disease. Neurology. 2014; 82:1784-1790.

Alves G, Larsen JP, Emre M, Wentzel-Larsen T, Aarsland D. Changes in motor subtype and risk for incident dementia in Parkinson's disease. Mov Disord 2006; 21:1123–1130.

Andlin-Sobocki P, Jönsson B, Wittchen HU, Olesen J. Cost of disorders of the brain in Europe. Eur J Neurol. 2005; Suppl 1:1-27.

Angot E, Steiner JA, Hansen C, Li JY, Brundin P. Are synucleinopathies prion-like disorders? Lancet Neurol. 2010; 9:1128-1138.

Antonini A, Leenders KL, Vontobel P, Maguire RP, Missimer J, Psylla M, Günter I Complementary PET studies of striatal neuronal function in the differential diagnosis between multiple system atrophy and Parkinson's disease. Brain 1997; 120:2187-2195.

Apaydin H, Ahlskog JE, Parisi JE, et al. Parkinson disease neuropathology: later-developing dementia and loss of the levodopa response. Arch Neurol 2002; 59:102–112.

Arai H, Furuya T, Yasuda T, Miura M, Mizuno Y, Mochizuki H. Neurotoxic effects of lipopolysaccharide on nigral dopaminergic neurons are mediated by microglial activation, interleukin-1beta, and expression of caspase-11 in mice. J Biol Chem. 2004; 279:51647-51653.

Arendt T, Bigl V, Arendt A, Tennstedt A. Loss of neurons in the nucleus basalis of Meynert in Alzheimer's disease, paralysis agitans and Korsakoff's Disease. Acta Neuropathol. 1983; 61:101-108.

Awerbuch GI, Sandyk R. Autonomic functions in the early stages of Parkinson's disease. Int J Neurosci. 1994; 74:9-16.

Bacskai BJ, Hickey GA, Skoch J, et al. Four-dimensional multiphoton imaging of brain entry, amyloid binding, and clearance of an amyloid-beta ligand in transgenic mice. Proc Natl Acad Sci U S A. 2003; 100:12462-12467.

Bacskai BJ, Frosch MP, Freeman SH, et al. Molecular imaging with Pittsburgh Compound B confirmed at autopsy: a case report. Arch Neurol. 2007; 64:431-434.

Ballard C, Ziabreva I, Perry R et al. Differences in neuropathologic characteristics across the Lewy body dementia spectrum. Neurology 2006; 67:1931–1934.

Baltadjieva R, Giladi N, Gruendlinger L, Peretz C, Hausdorff JM. Marked alterations in the gait timing and rhythmicity of patients with de novo Parkinson's disease. Eur J Neurosci. 2006; 24:1815-1820.

Banati RB, Myers R, Kreutzberg GW. PK (‘peripheral benzodiazepine’)-binding sites in the CNS indicate early and discrete brain lesions: microautoradiographic detection of [3H]PK11195 binding to activated microglia. J Neurocytol 1997; 26:77–82.

Banati RB, Goerres GW, Myers R, et al. [11C](R)-PK11195 positron emission tomography imaging of activated microglia in vivo in Rasmussen's encephalitis. Neurology. 1999; 53:2199-2203.

Banati RB, Newcombe J, Gunn RN, et al. The peripheral benzodiazepine binding site in the brain in multiple sclerosis: quantitative in vivo imaging of microglia as a measure of disease activity. Brain. 2000; 123:2321-2337.

Banati RB. Visualising microglial activation in vivo. Glia. 2002; 40:206–217.

Barcia C, Ros CM, Ros-Bernal F, et al. Persistent phagocytic characteristics of microglia in the substantia nigra of long-term Parkinsonian macaques. J Neuroimmunol. 2013; 261:60-66.

Bartels AL, Willemsen AT, Doorduin J, et al. [11C]-PK11195 PET: quantification of neuroinflammation and a monitor of anti-inflammatory treatment in Parkinson's disease? Parkinsonism Relat Disord. 2010; 16:57-59.

Bartels AL, de Jong BM, Giladi N, Schaafsma JD, Maguire RP, Veenma L, Pruim J, Balash Y, Youdim MB, Leenders KL. Striatal dopa and glucose metabolism in PD patients with freezing of gait. Mov Disord. 2006; 21:1326-1332.

Bassett DS, Bullmore ET. Human brain networks in health and disease. Curr Opin Neurol. 2006; 22:340-347.

Bate C, Gentleman S, Williams A. alpha-synuclein induced synapse damage is enhanced by amyloid-beta1–42. Mol Neurodegener. 2010; 5:55.

Beach TG, Adler CH, Sue LI, et al. Reduced striatal tyrosine hydroxylase in incidental Lewy body disease. Acta Neuropathol. 2008; 115:445–451.

Beach TG, Adler CH, Lue L, et al. Unified staging system for Lewy body disorders: correlation with nigrostriatal degeneration, cognitive impairment and motor dysfunction. Acta Neuropathol. 2009; 117:613–634.

Beach TG, Adler CH, Sue LI, et al. Multi-organ distribution of phosphorylated alpha-synuclein histopathology in subjects with Lewy body disorders. Acta Neuropathol 2009;119:689 –702.

Benamer HTS, Patterson J, Wyper DJ, et al. Correlation of Parkinson's disease severity and duration with I-123-FP-CIT SPECT striatal uptake. Mov Disord. 2000; 15:692–698.

Benarroch EE. Pedunculopontine nucleus: functional organization and clinical implications. Neurology. 2013; 80:1148-1155.

Benoit M, Robert PH. Imaging correlates of apathy and depression in Parkinson's disease. J Neurol Sci. 2011; 310:58-60.

Beppu T. The Role of MR Imaging in Assessment of Brain Damage from Carbon Monoxide Poisoning: A Review of the Literature. AJNR Am J Neuroradiol. 2013; 35:625-631.

Berardelli A, Conte A, Fabbrini G, et al. Pathophysiology of pain and fatigue in Parkinson's disease. Parkinsonism Relat Disord. 2012; 18:Suppl 1:S226-228.

Bergstrom DA, Walters JR. Dopamine attenuates the effects of GABA on single unit activity in the globus pallidus. Brain Res 1984; 310:23-33.

Beyer MK, Alves G, Hwang KS, et al. Cerebrospinal fluid Aβ levels correlate with structural brain changes in Parkinson's disease. Mov Disord. 2013; 28:302-310.

Birkmayer W, Hornykiewicz O. [The L-3,4-dioxyphenylalanine (DOPA)-effect in Parkinson-akinesia]. Wien Klin Wochenschr. 1961; 73:787-788.

Ble A, Volpato S, Zuliani G, et al. Executive function correlates with walking speed in older persons: the InCHIANTI study. J Am Geriatr Soc. 2005; 53:410-415.

Blin O, Ferrandez AM, Serratrice G. Quantitative analysis of gait in Parkinson patients: increased variability of stride length. J Neurol Sci. 1990; 98:91-97.

Bloch A, Probst A, Bissig H, Adams H, Tolnay M. Alpha-synuclein pathology of the spinal and peripheral autonomic nervous system in neurologically unimpaired elderly subjects. Neuropathol Appl Neurobiol. 2006; 32:284-295.

Block ML, Zecca L, Hong JS. Microglia-mediated neurotoxicity: uncovering the molecular mechanisms. Nat Rev Neurosci. 2007; 8:57-69.

Bloem BR, Hausdorff JM, Visser JE, Giladi N. Falls and freezing of gait in Parkinson's disease: a review of two interconnected, episodic phenomena. Mov Disord. 2004; 19:871-884.

Bohnen NI, Minoshima S, Giordani B, et al. Motor correlates of occipital glucose hypometabolism in Parkinson's disease without dementia. Neurology 1999; 52:541–546.

Bohnen NI, Albin RL. Cholinergic denervation occurs early in Parkinson disease. Neurology 2009; 73: 256–257.

Bohnen NI, Frey KA, Studenski S, et al. Gait speed in Parkinson disease correlates with cholinergic degeneration. Neurology. 2013; 81:1611-1616.

Bohnen NI, Muller ML, Koeppe RA, et al. History of falls in Parkinson disease is associated with reduced cholinergic activity. Neurology. 2009; 73:1670–1676.

Bohnen NI, Koeppe RA, Minoshima S, Giordani B, Albin RL, Frey KA, Kuhl DE. Cerebral glucose metabolic features of Parkinson disease and incident dementia: longitudinal study. J Nucl Med. 2011; 52:848-855.

Boonstra TA, van Vugt JP, van der Kooij H, Bloem BR. Balance asymmetry in Parkinson's disease and its contribution to freezing of gait. PLoS One. 2014; 9:e102493.

Bonifati V, Rizzu P, van Baren MJ, et al. Mutations in the DJ-1 gene associated with autosomal recessive early-onset parkinsonism. Science 2003; 299:256-259.

Braak H, Del Tredici K, Rüb U, et al. Staging of brain pathology related to sporadic Parkinson's disease. Neurobiol Aging. 2003; 24:197-211.

Braak H, Rub U, Jansen Steur EN, Del Tredici K, de Vos RA. Cognitive status correlates with neuropathologic stage in Parkinson disease. Neurology. 2005; 64:1404–1410.

Braak H, Rüb U, Gai WP, et al. Idiopathic Parkinson's disease: possible routes by which vulnerable neuronal types may be subject to neuroinvasion by an unknown pathogen. Neural Transm. 2003; 110:517-536.

Braak H, Sandmann-Keil D, Gai W, Braak E. Extensive axonal Lewy neurites in Parkinson's disease: a novel pathological feature revealed by alpha-synuclein immunocytochemistry. Neurosci Lett. 1999; 265:67–69.

Braak H, Sastre M, Del Tredici K. Development of alpha-synuclein immunoreactive astrocytes in the forebrain parallels stages of intraneuronal pathology in sporadic Parkinson's disease. Acta Neuropathol 2004; 114:231–241.

Braak H, Rüb U, Jansen-Steur E, et al. Cognitive status correlates with neuropathologic stage in Parkinson disease. Neurology 2005; 64: 1404–1410.

Broeders M, de Bie RM, Velseboer DC, Speelman JD, Muslimovic D, Schmand B. Evolution of mild cognitive impairment in Parkinson disease. Neurology. 2013; 81:346-352.

Brooks DJ, Ibanez V, Sawle GV, et al. Differing patterns of striatal 18F-dopa uptake in Parkinson's disease, multiple system atrophy, and progressive supranuclear palsy. Ann Neurol. 1990; 28:547-555.

Brooks DJ, Ibanez V, Sawle GV, et al. Striatal D2 receptor status in patients with Parkinson's disease, striatonigral degeneration, and progressive supranuclear palsy, measured with 11C-raclopride and positron emission tomography. Ann Neurol. 1992; 31:184-192.

Brooks DJ, Salmon EP, Mathias CJ, et al. The relationship between locomotor disability, autonomic dysfunction, and the integrity of the striatal dopaminergic system in patients with multiple system atrophy, pure autonomic failure, and Parkinson's disease, studied with PET. Brain. 1990; 113:1539-1552.

Brooks DJ. Imaging amyloid in Parkinson's disease dementia and dementia with Lewy bodies with positron emission tomography. Mov Disord. 2009; 24 Suppl 2:S742-747.

Brooks DJ. Examining Braak's hypothesis by imaging Parkinson's disease. Mov Disord. 2010; 25 Suppl 1:S83-8.

Brück A, Portin R, Lindell A, et al. Positron emission tomography shows that impaired frontal lobe functioning in Parkinson's disease is related to dopaminergic hypofunction in the caudate nucleus. Neurosci Lett. 2001; 311:81-84.

Burack MA, Hartlein J, Flores HP, et al. In vivo amyloid imaging in autopsy-confirmed Parkinson disease with dementia. Neurology 2010; 74:77-84.

Burn DJ, Rowan EN, Allan LM, Molloy S, O'Brien JT, McKeith IG. Motor subtype and cognitive decline in Parkinson's disease, Parkinson's disease with dementia, and dementia with Lewy bodies. J Neurol Neurosurg Psychiatry 2006; 77: 585–589.

Burns RS, Chiueh CC, Markey SP, Ebert MH, Jacobowitz DM, Kopin IJ. A primate model of parkinsonism: selective destruction of dopaminergic neurons in the pars compacta of the substantia nigra by N-methyl-4-phenyl-1,2,3,6-tetrahydropyridine. Proc Natl Acad Sci U S A. 1983; 80:4546-4550.

Cagnin A, Brooks DJ, Kennedy AM, et al. In-vivo measurement of activated microglia in dementia. Lancet. 2001; 358:461-467.

Cagnin A, Rossor M, Sampson EL, Mackinnon T, Banati RB. In vivo detection of microglial activation in frontotemporal dementia. Ann Neurol. 2004; 56:894-897.

Callisaya ML, Beare R, Phan TG, Blizzard L, Thrift AG, Chen J, Srikanth VK. Brain structural change and gait decline: a longitudinal population-based study. J Am Geriatr Soc. 2013 61:1074-1079.

Calne DB, Chu NS, Huang CC, Lu CS, Olanow W. Manganism and idiopathic parkinsonism: similarities and differences. Neurology. 1994; 44:1583-1586.

Campbell MC, Markham J, Flores H, et al. Principal component analysis of PiB distribution in Parkinson and Alzheimer diseases. Neurology. 2013; 81:520-527.

Candy JM, Perry RH, Perry EK, et al. Pathological changes in the nucleus of Meynert in Alzheimer's and Parkinson's diseases. J Neurol Sci. 1983; 59:277-289.

Carlsson A, Lindqvist M, Magnusson T, Waldeck B. 3,4-dihydroxy-phenylalanine and 5-hydroxytryptophan as reserpine antagonists. Nature 1957; 180:1200.

Carta AR, Frau L, Pisanu A, Wardas J, Spiga S, Carboni E. Rosiglitazone decreases peroxisome proliferator receptor-γ levels in microglia and inhibits TNF-α production: new evidences on neuroprotection in a progressive Parkinson's disease model. Neuroscience. 2011;194:250-261.

Caughey B, Lansbury PT. Protofibrils, pores, fibrils, and neurodegeneration: separating the responsible protein aggregates from the innocent bystanders. Annu Rev Neurosci. 2003; 26:267-298.

Chapados C, Petrides M. Impairment only on the fluency subtest of the Frontal Assessment Battery after prefrontal lesions. Brain. 2013; 136:2966-2978.

Chartier-Harlin MC, Kachergus J, Roumier C, et al. Alpha-synuclein locus duplication as a cause of familial Parkinson's disease. Lancet. 2004; 364:1167-1169.

Chartier-Harlin MC, Dachsel JC, Vilarino-Guell C, et al. Translation initiator EIF4G1 mutations in familial Parkinson disease. Am J Hum Genet 2011; 89:398-406.

Chaudhuri KR, Healy DG, Schapira AH; National Institute for Clinical Excellence. Non-motor symptoms of Parkinson's disease: diagnosis and management. Lancet Neurol. 2006; 5:235-245.

Chauveau F, Boutin H, Van Camp N, Dollé F, Tavitian B. Nuclear imaging of neuroinflammation: a comprehensive review of [11C]PK11195 challengers. Eur J Nucl Med Mol Imaging. 2008; 35:2304-2319.

Chen H, Zhang SM, Hernan MA, et al. Nonsteroidal antiinflammatory drugs and the risk of Parkinson disease. Arch Neurol 2003; 60:1059 –1064.

Chen H, Jacobs E, Schwarzschild MA, et al. Nonsteroidal antiinflammatory drug use and the risk for Parkinson’s disease. Ann Neurol 2005; 58:963–967.

Chen J, Lipska BK, Halim N, Ma QD, Matsumoto M, Melhem S, Kolachana BS, Hyde TM, Herman MM, Apud J, Egan MF, Kleinman JE, Weinberger DR.

Functional analysis of genetic variation in catechol-O-methyltransferase (COMT): effects on mRNA, protein, and enzyme activity in postmortem human brain. Am J Hum Genet. 2004; 75:807-821.

Chen H, O'Reilly EJ, Schwarzschild MA, Ascherio A. Peripheral inflammatory biomarkers and risk of Parkinson's disease. Am J Epidemiol. 2008; 167:90-95.

Cheng HC, Ulane CM, Burke RE. Clinical progression in Parkinson disease and the neurobiology of axons. Ann Neurol. 2010; 67:715–725.

Choi DY, Liu M, Hunter RL, Cass WA, Pandya JD, Sullivan PG, Shin EJ, Kim HC, Gash DM, Bing G. Striatal neuroinflammation promotes Parkinsonism in rats. PLoS One. 2009; 4:e5482.

Choi EY, Yeo BT, Buckner RL. The organization of the human striatum estimated by intrinsic functional connectivity. J Neurophysiol. 2012; 108:2242-2263.

Choi HB, Khoo C, Ryu JK, van Breemen E, Kim SU, McLarnon JG. Inhibition of lipopolysaccharide-induced cyclooxygenase-2, tumor necrosis factor-alpha and [Ca2+]i responses in human microglia by the peripheral benzodiazepine receptor ligand PK11195. J Neurochem. 2002; 83:546-555.

Cirrito JR, Disabato BM, Restivo JL, et al. Serotonin signaling is associated with lower amyloid-β levels and plaques in transgenic mice and humans. Proc Natl Acad Sci U S A. 2011; 108:14968-14973.

Claassen DO, Josephs KA, Ahlskog JE, et al. REM sleep behavior disorder preceding other aspects of synucleinopathies by up to half a century. Neurology. 2010; 75:494–499.

Clinton LK, Blurton-Jones M, Myczek K, Trojanowski JQ, LaFerla FM. Synergistic Interactions between Abeta, tau, and alpha-synuclein: acceleration of neuropathology and cognitive decline. J Neurosci. 2010; 30:7281-7289.

Colom-Cadena M, Gelpi E, Charif S, et al. Confluence of α-synuclein, tau, and β-amyloid pathologies in dementia with Lewy bodies. J Neuropathol Exp Neurol. 2013; 72:1203-1212.

Colosimo C, Hughes AJ, Kilford L, et al. Lewy body cortical involvement may not always predict dementia in Parkinson’s disease. J Neurol Neurosurg Psych 2003; 74:852–856.

Compta Y, Martí MJ, Ibarretxe-Bilbao N, et al. Cerebrospinal tau, phospho-tau, and beta-amyloid and neuropsychological functions in Parkinson's disease. Mov Disord. 2009; 24:2203-2210.

Compta Y, Parkkinen L, O'Sullivan SS, et al. Lewy- and Alzheimer-type pathologies in Parkinson's disease dementia: which is more important? Brain. 2011; 134:1493-1505.

Conway KA, Lee SJ, Rochet JC, Ding TT, Williamson RE, Lansbury PT Jr. Acceleration of oligomerization, not fibrillization, is a shared property of both alpha-synuclein mutations linked to early-onset Parkinson's disease: implications for pathogenesis and therapy. Proc Natl Acad Sci U S A. 2000; 97:571-576.

Cook DG, Fahn S, Brait KA. Chronic manganese intoxication. Arch Neurol. 1974; 30:59-64.

Cools R, Miyakawa A, Sheridan M, D'Esposito M. Enhanced frontal function in Parkinson's disease. Brain. 2010; 133:225-233.

Corder EH, Saunders AM, Strittmatter WJ, et al. Gene dose of apolipoprotein E type 4 allele and the risk of Alzheimer's disease in late onset families. Science. 1993; 261:921-923.

Cotzias GC, Van Woert MH, Schiffer LM. Aromatic amino acids and modification of parkinsonism. N Engl J Med. 1967; 276:374-379.

Counts SE, Lahiri DK. Overview of Immunotherapy in Alzheimer's Disease (AD) and Mechanisms of IVIG Neuroprotection in Preclinical Models of AD. Curr Alzheimer Res. 2014; 11:623-625.

Couper J. On the effects of black oxide or manganese when inhaled into the lungs. Br Ann Med Pharm 1837; 1:41–42.

Criswell SR, Perlmutter JS, Videen TO, et al. Reduced uptake of [18F]FDOPA PET in asymptomatic welders with occupational manganese exposure. Neurology. 2011; 76:1296-1301.

Crofts HS, Dalley JW, Collins P, et al. Differential effects of 6-OHDA lesions of the frontal cortex and caudate nucleus on the ability to acquire an attentional set. Cereb Cortex. 2001; 11:1015-1026.

Cunningham VJ, Jones T. Spectral analysis of dynamic PET studies. J Cereb Blood Flow Metab. 1993; 13:15-23.

Członkowska A, Kurkowska-Jastrzebska I, Członkowski A. Inflammatory changes in the substantia nigra and striatum following MPTP intoxication. Ann Neurol. 2000;48:127.

Damier P, Hirsch EC, Agid Y, Graybiel AM. The substantia nigra of the human brain. II. Patterns of loss of dopamine-containing neurons in Parkinson's disease. Brain. 1999; 122:1437-1448.

Daniel SE, Hawkes CH: Preliminary diagnosis of Parkinson's disease by olfactory bulb pathology. Lancet 1992, 340:186–186.

Danoudis M, Iansek R, Simpson P. Freezing of gait in Parkinson's disease: further insights into pathophysiological mechanisms. Parkinsonism Relat Disord. 2012; 18:543-547.

Danzer KM, Haasen D, Karow AR, et al. Different species of alpha-synuclein oligomers induce calcium influx and seeding. J Neurosci. 2007; 27:9220-9232.

Davis AA, Fritz JJ, Wess J, Lah JJ, Levey AI. Deletion of M1 muscarinic acetylcholine receptors increases amyloid pathology in vitro and in vivo. J Neurosci. 2010; 30:4190-4196.

Davis GC, Williams AC, Markey SP, et al. Chronic Parkinsonism secondary to intravenous injection of meperidine analogues. Psychiatry Res. 1979; 1:249-54.

Defazio G, Tinazzi M, Berardelli A. How pain arises in Parkinson's disease? Eur J Neurol. 2013; 20:1517-1523.

de Laat KF, Tuladhar AM, van Norden AG, Norris DG, Zwiers MP, de Leeuw FE. Loss of white matter integrity is associated with gait disorders in cerebral small vessel disease. Brain. 2011; 134:73-83.

de la Fuente-Fernández R, Sossi V, Huang Z, et al. Levodopa-induced changes in synaptic dopamine levels increase with progression of Parkinson's disease: implications for dyskinesias. Brain. 2004; 127:2747-2754.

de la Fuente-Fernández R, Schulzer M, Mak E, Sossi V. Trials of neuroprotective therapies for Parkinson's disease: problems and limitations. Parkinsonism Relat Disord. 2010; 16:365-369.

de Rijk MC, Launer LJ, Berger K, Breteler MM, Dartigues JF, Baldereschi M, Fratiglioni L, Lobo A, Martinez-Lage J, Trenkwalder C, Hofman A. Prevalence of Parkinson's disease in Europe: A collaborative study of population-based cohorts, Neurologic Diseases in the Elderly Research Group. Neurology. 2000; 54 Suppl 5:S21-S23.

Dickson DW, Fujishiro H, DelleDonne A, et al. Evidence that incidental Lewy body disease is pre-symptomatic Parkinson's disease. Acta Neuropathol. 2008; 115:437-444.

Di Lazzaro V, Oliviero A, Profice P, et al. Muscarinic receptor blockade has differential effects on the excitability of intracortical circuits in the human motor cortex. Exp Brain Res 2000; 135:455–461.

Di Lazzaro V, Oliviero A, Tonali P, Marra C, Daniele A, Profice P, et al. Noninvasive in vivo assessment of cholinergic cortical circuits in AD using transcranial magnetic stimulation. Neurology 2002; 13: 392–397.

Di Martino A, Scheres A, Margulies DS, et al. Functional connectivity of human striatum: a resting state fMRI study. Cereb Cortex 2008; 18:2735–2747.

Doble A, Malgouris C, Daniel M, et al. Labelling of peripheral-type benzodiazepine binding sites in human brain with [3H]PK 11195: anatomical and subcellular distribution. Brain Res Bull 1987; 18:49–61.

Doder M, Rabiner EA, Turjanski N, Lees AJ, Brooks DJ. Brain serotonin HT1A receptors in Parkinson's disease with and without depression measured by positron emission tomography and 11C-WAY100635. Mov Disord. 2000; 15(suppl 3):213.

Doder M, Rabiner EA, Turjanski N, Lees AJ, Brooks DJ. Tremor in Parkinson's disease and serotinergic dysfunction: an 11C-WAY100635 PET study. Neurology 2003; 60:601-605.

Doorn KJ, Goudriaan A, Blits-Huizinga C, et al. Increased amoeboid microglial density in the olfactory bulb of Parkinson's and Alzheimer's patients. Brain Pathol. 2014; 24:152-165.

Dorsey ER, Constantinescu R, Thompson JP, et al. Projected number of people with Parkinson disease in the most populous nations, 2005 through 2030. Neurology. 2007; 68:384-386.

Driver JA, Logroscino G, Gaziano JM, Kurth T. Incidence and remaining lifetime risk of Parkinson disease in advanced age. Neurology 2009; 72:432–438.

Driver JA, Logroscino G, Lu L, Gaziano JM, et al. Use of non-steroidal anti-inflammatory drugs and risk of Parkinson's disease: nested case-control study. BMJ 2011; 342:198.

Dubois B, Burn D, Goetz C, et al. Diagnostic procedures for Parkinson's disease dementia: recommendations from the movement disorder society task force. Mov Disord. 2007; 22:2314-2324.

Duda JE, Giasson BI, Mabon ME, Lee VM, Trojanowski JQ. Novel antibodies to synuclein show abundant striatal pathology in Lewy body diseases. Ann Neurol. 2002; 52:205-210.

Duda JE. Olfactory system pathology as a model of Lewy neurodegenerative disease. J Neurol Sci. 2010; 289:49–54.

Duncan GW, Khoo TK, Yarnall AJ, et al. Health-related quality of life in early Parkinson's disease: the impact of nonmotor symptoms. Mov Disord. 2014; 29:195-202.

Duysens J, Van de Crommert HW. Neural control of locomotion; The central pattern generator from cats to humans. Gait Posture. 1998 7:131-141.

Dyson NA. The annihilation coincidence method of localizing positron-emitting isotopes, and a comparison with parallel counting. Phys Med Biol.1960; 4:376-390.

Edison P, Rowe CC, Rinne JO, et al. Amyloid load in Parkinson's disease dementia and Lewy body dementia measured with [11C]PIB-PET. J Neurol Neurosurg Psych. 2008; 79:1331–1338.

Edison P, Archer HA, Gerhard A, et al. Microglia, amyloid, and cognition in Alzheimer's disease: An [11C](R)PK11195-PET and [11C]PIB-PET study. Neurobiol Dis. 2008; 32:412-419.

Edison P, Ahmed I, Fan Z, et al. Microglia, amyloid, and glucose metabolism in Parkinson's disease with and without dementia. Neuropsychopharmacology. 2013; 38:938-949.

Ehringer H, Hornykiewicz O. Distribution of noradrenaline and dopamine (3-hydroxytyramine) in the human brain and their behaviour in diseases of the extrapyramidal system. Klin Wochenschr 1960; 38:1236-1239.

Eidelberg D, Moeller JR, Dhawan V, et al. The metabolic topography of parkinsonism. J Cereb Blood Flow Metab. 1994; 14:783–801.

Eisensehr I, Linke R, Noachtar S, Schwarz J, Gildehaus FJ, Tatsch K. Reduced striatal dopamine transporters in idiopathic rapid eye movement sleep behaviour disorder: comparison with Parkinson's disease and controls. Brain 2000; 123:1155–1160.

Elbaz A, Ross OA, Ioannidis JP, et al. Independent and joint effects of the MAPT and SNCA genes in Parkinson disease. Ann Neurol 2011; 69:778–792.

Elstner M, Morris CM, Heim K, et al. Expression analysis of dopaminergic neurons in Parkinson's disease and aging links transcriptional dysregulation of energy metabolism to cell death. Acta Neuropathol 2011; 122:75–86.

Emmanouilidou E, Elenis D, Papasilekas T, et al. Assessment of α-synuclein secretion in mouse and human brain parenchyma. PLoS One. 2011; 6:e22225.

Emmrich JV, Hornik TC, Neher JJ, Brown GC. Rotenone induces neuronal death by microglial phagocytosis of neurons. FEBS J. 2013; 280:5030-5038.

Exner C, Weniger G, Irle E. Implicit and explicit memory after focal thalamic lesions. Neurology. 2001; 57:2054-2063.

Fabbrini G, Barbanti P, Aurilia C, Vanacore N, Pauletti C, Meco G. Excessive daytime sleepiness in de novo and treated Parkinson's disease. Mov Disord. 2002; 17:1026-1030.

Fabre N, Brefel C, Sabatini U, et al. Normal frontal perfusion in patients with frozen gait. Mov Disord. 1998; 13:677-683.

Fallon SJ, Hampshire A, Williams-Gray CH, Barker RA, Owen AM. Putative cortical dopamine levels affect cortical recruitment during planning. Neuropsychologia. 2013; 51:2194-2201.

Farrer LA, Cupples LA, Haines JL, et al. Effects of age, sex, and ethnicity on the association between apolipoprotein E genotype and Alzheimer disease. A meta-

analysis. APOE and Alzheimer Disease Meta Analysis Consortium. JAMA. 1997; 278:1349-1356.

Farrer M, Stone J, Mata IF, et al. LRRK2 mutations in Parkinson disease. Neurology 2005; 65: 738–740.

Faucheux BA, Martin ME, Beaumont C, Hauw JJ, Agid Y, Hirsch EC. Neuromelanin associated redox-active iron is increased in the substantia nigra of patients with Parkinson's disease. J Neurochem. 2003; 86:1142–1148.

Fearnley JM, Lees AJ. Ageing and Parkinson's disease: substantia nigra regional selectivity. Brain 1991; 114:2283-2301.

Feigin A, Fukuda M, Dhawan V, et al. Metabolic correlates of levodopa response in Parkinson's disease. Neurology. 2001; 57:2083–2088.

Fénelon G, Mahieux F, Huon R, Ziégler M. Hallucinations in Parkinson's disease: prevalence, phenomenology and risk factors. Brain. 2000; 123:733-745.

Fénelon G, Goetz CG, Karenberg A. Hallucinations in Parkinson disease in the prelevodopa era. Neurology. 2006; 66:93-98.

Ferman TJ, Smith GE, Boeve BF, et al. DLB fluctuations: specific features that reliably differentiate DLB from AD and normal aging. Neurology 2004; 62:181-187.

Ferman TJ, Smith GE, Kantarci K, et al. Nonamnestic mild cognitive impairment progresses to dementia with Lewy bodies. Neurology. 2013; 81:2032-2038.

Ferrara J, Jankovic J. Acquired hepatocerebral degeneration. J Neurol. 2009; 256:320–322.

Ferrer I, Martinez A, Blanco R, Dalfo E, Carmona M. Neuropathology of sporadic Parkinson disease before the appearance of parkinsonism: preclinical Parkinson disease. J Neural Transm. 2011; 118:821–839.

Finn JT, Weil M, Archer F, et al. Evidence that Wallerian degeneration and localized axon
degeneration induced by local neurotrophin deprivation do not involve caspases. J Neurosci. 2000; 20:1333–1341.

Fling BW, Cohen RG, Mancini M, Nutt JG, Fair DA, Horak FB. Asymmetric pedunculopontine network connectivity in parkinsonian patients with freezing of gait. Brain. 2013; 136:2405-2418.

Fling BW, Cohen RG, Mancini M, et al. Functional reorganization of the locomotor network in Parkinson patients with freezing of gait. PLoS One. 2014; 9:e100291.

Foley D, Monjan A, Masaki K, et al. Daytime sleepiness is associated with 3-year incident dementia and cognitive decline in older Japanese-American men. J Am Geriatr Soc. 2001; 49:1628-1632.

Foltynie T, Goldberg TE, Lewis SG, et al. Planning ability in Parkinson's disease is influenced by the COMT val158met polymorphism. Mov Disord. 2004; 19:885-891.

Fookes CJ, Pham TQ, Mattner F, et al. Synthesis and biological evaluation of substituted [18F]imidazo[1,2-a]pyridines and [18F]pyrazolo[1,5-a]pyrimidines for the study of the peripheral benzodiazepine receptor using positron emission tomography. J Med Chem. 2008; 51:3700-3712.

Foster ER, Campbell MC, Burack MA, et al. Amyloid imaging of Lewy body-associated disorders. Mov Disord. 2010; 25:2516-2523.

Freundt EC, Maynard N, Clancy EK, et al. Neuron-to-neuron transmission of alphasynuclein
fibrils through axonal transport. Ann Neurol. 2012; 72:517–524.

Friston KJ, Holmes AP, Worsley KJ, Poline J-B, Frith CD, Frackowiak RSJ. Statistical Parametric Maps in functional imaging: A general linear approach. Human Brain Mapping 1995; 2:189-210.

Fujishiro H, Tsuboi Y, Lin WL, Uchikado H, Dickson DW. Colocalization of tau and alpha-synuclein in the olfactory bulb in Alzheimer’s disease with amygdala Lewy bodies. Acta Neuropathol. 2008; 116:17–24.

Fujishiro H, Iseki E, Higashi S, et al. Distribution of cerebral amyloid deposition and its relevance to clinical phenotype in Lewy body dementia. Neurosci Lett. 2010; 486:19-23.

Fujita M, Ichise M, Zoghbi SS, et al. Widespread decrease of nicotinic acetylcholine receptors in Parkinson’s disease. Ann Neurol. 2006; 59:174–177.

Fujita M, Imaizumi M, Zoghbi SS, et al. Kinetic analysis in healthy humans of a novel positron emission tomography radioligand to image the peripheral benzodiazepine receptor, a potential biomarker for inflammation. Neuroimage. 2008; 40:43-52.

Fujiwara H, Hasegawa M, Dohmae N, et al. alpha-Synuclein is phosphorylated in synucleinopathy lesions. Nat Cell Biol. 2002; 4:160–164.

Gagne JJ, Power MC. Anti-inflammatory drugs and risk of Parkinson disease: a meta-analysis. Neurology. 2010; 74:995-1002.

Galasko D, Saitoh T, Xia Y, et al. The apolipoprotein E allele epsilon 4 is overrepresented in patients with the Lewy body variant of Alzheimer's disease. Neurology. 1994; 44:1950-1951.

Galna B, Lord S, Rochester L. Is gait variability reliable in older adults and Parkinson's disease? Towards an optimal testing protocol. Gait Posture. 2013; 37:580-585.

Galvin JE, Uryu K, Lee VM, et al. Axon pathology in Parkinson's disease and Lewy body
dementia hippocampus contains alpha-, beta-, and gamma-synuclein. Proc Natl Acad Sci U S A. 1999; 96:13450–13455.

Gao HM, Kotzbauer PT, Uryu K, Leight S, Trojanowski JQ, Lee VM. Neuroinflammation and oxidation/nitration of alpha-synuclein linked to dopaminergic neurodegeneration. J Neurosci. 2008; 28:7687-7698.

Gao X, Chen H, Schwarzschild MA, et al. Use of ibuprofen and risk of Parkinson disease. Neurology. 2011; 76:863-869.

Garcia-Rill E. The pedunculopontine nucleus. Prog Neurobiol 1991; 36:363–389.

Gerhard A, Watts J, Trender-Gerhard I, et al. In vivo imaging of microglial activation with [11C](R)-PK11195 PET in corticobasal degeneration. Mov Disord. 2004; 19:1221-1226.

Gerhard A, Pavese N, Hotton G, Turkheimer F, et al. In vivo imaging of microglial activation with [11C](R)-PK11195 PET in idiopathic Parkinson's disease. Neurobiol Dis. 2006; 21:404-412.

Gerhard A, Trender-Gerhard I, Turkheimer F, Quinn NP, Bhatia KP, Brooks DJ. In vivo imaging of microglial activation with [11C](R)-PK11195 PET in progressive supranuclear palsy. Mov Disord. 2006; 21:89-93.

German DC, Manaye KF, White CL 3rd, Woodward DJ, McIntire DD, Smith WK, Kalaria RN, Mann DM. Disease-specific patterns of locus coeruleus cell loss. Ann Neurol. 1992; 32:667-676.

Giasson BI, Duda JE, Quinn SM, Zhang B, Trojanowski JQ, Lee VM. Neuronal alpha-synucleinopathy with severe movement disorder in mice expressing A53T human alpha-synuclein. Neuron 2002; 34:521–533.

Giasson BI, Forman MS, Higuchi M, et al. Initiation and synergistic fibrillization of tau and alpha-synuclein. Science 2003; 300:636–640.

Gillardon F, Schmid R, Draheim H. Parkinson's disease-linked leucine-rich repeat kinase 2(R1441G) mutation increases proinflammatory cytokine release from activated primary microglial cells and resultant neurotoxicity. Neuroscience. 2012; 208:41-48.

Gilman S, Koeppe RA, Nan B, et al. Cerebral cortical and subcortical cholinergic deficits in parkinsonian syndromes. Neurology. 2010; 74:1416-1423.

Gilks WP, Abou-Sleiman PM, Gandhi S, , et al. A common LRRK2 mutation in idiopathic Parkinson’s disease. Lancet 2005; 365:415–416.

Gjerstad MD, Alves G, Wentzel-Larsen T, Aarsland D, Larsen JP. Excessive daytime sleepiness in Parkinson disease: is it the drugs or the disease? Neurology 2006; 67:853–858.

Goker-Alpan O, Stubblefield BK, Giasson BI, Sidransky E. Glucocerebrosidase is present in α-synuclein inclusions in Lewy body disorders. Acta Neuropathol. 2010; 120:641-649.

Golbe LI, Di Iorio G, Sanges G, et al. Clinical genetic analysis of Parkinson's disease in the Contursi kindred. Ann Neurol 1996; 40:767-775.

Goldman JG, Williams-Gray C, Barker RA, Duda JE, Galvin JE. The spectrum of cognitive impairment in Lewy body diseases. Mov Disord. 2014; 29:608-621.

Gomperts SN, Rentz DM, Moran E, et al. Imaging amyloid deposition in Lewy body diseases. Neurology 2008; 71:903–910.

Gomperts SN, Locascio JJ, Rentz D, et al. Amyloid is linked to cognitive decline in patients with Parkinson disease without dementia. Neurology. 2013; 80:85-91.

Gorell JM, Johnson CC, Rybicki BA, Peterson EL, Richardson RJ. The risk of Parkinson's disease with exposure to pesticides, farming, well water, and rural living. Neurology. 1998; 50:1346-1350.

Goris A, Williams-Gray CH, Clark GR, et al. Tau and alpha-synuclein in susceptibility to, and dementia in Parkinson's disease. Ann Neurol 2007; 62:145–153.

Greffard S, Verny M, Bonnet AM, et al. Motor score of the Unified Parkinson Disease Rating Scale as a good predictor of Lewy body-associated neuronal loss in the substantia nigra. Arch Neurol. 2006; 63:584–588.

Greffard S, Verny M, Bonnet AM, Seilhean D, Hauw JJ, Duyckaerts C. A stable proportion of Lewy body bearing neurons in the substantia nigra suggests a model in which the Lewy body causes neuronal death. Neurobiol Aging. 2008; 31:99–103.

Grimmer T, Henriksen G, Wester HJ, et al. Clinical severity of Alzheimer's disease is associated with PIB uptake in PET. Neurobiol Aging 2009; 30:1902–1909.

Grootoonk S, Spinks TJ, Sashin D, Spyrou NM, Jones T. Correction for scatter in 3D brain PET using a dual energy window method. Phys Med Biol. 1996; 41:2757-2774.

Gu XL, Long CX, Sun L, Xie C, Lin X, Cai H. Astrocytic expression of Parkinson's disease-related A53T alpha-synuclein causes neurodegeneration in mice. Mol Brain 2010; 3:12.

Gunn RN, Lammertsma AA, Hume SP, Cunningham VJ. Parametric imaging of ligand-receptor binding in PET using a simplified reference region model. Neuroimage. 1997; 6:279-287.

Gustavsson A, Svensson M, Jacobi F, et al; CDBE2010 Study Group. Cost of disorders of the brain in Europe 2010. Eur Neuropsychopharmacol. 2011; 21:718-779.

Guttman M, Boileau I, Warsh J, et al. Brain serotonin transporter binding in non-depressed patients with Parkinson's disease. Eur J Neurol. 2007; 14:523-528.

Gwin JT, Gramann K, Makeig S, Ferris DP. Electrocortical activity is coupled to gait cycle phase during treadmill walking. Neuroimage. 2011; 54:1289-1296.

Halliday GM, Ophof A, Broe M, et al. Alpha-synuclein redistributes to neuromelanin lipid in the substantia nigra early in Parkinson's disease. Brain. 2005; 128:2654–2664.

Halliday GM, Del Tredici K, Braak H. Critical appraisal of brain pathology staging related to presymptomatic and symptomatic cases of sporadic Parkinson's disease. J Neural Transm Suppl. 2006; 70:99–103.

Halliday G, Hely M, Reid W, Morris J. The progression of pathology in longitudinally followed patients with Parkinson's disease. Acta Neuropathol. 2008; 115:409–415.

Halliday G, Stevens C. Glia: Initiators and Progressors of Pathology in Parkinson's Disease. Mov Disord. 2011; 26:6-17.

Halliday GM, Song YJ, Harding AJ. Striatal β-amyloid in dementia with Lewy bodies but not Parkinson's disease. J Neural Transm. 2011; 118:713–719.

Hamilton RL Lewy bodies in Alzheimer's disease: a neuropathological review of 145 cases using alpha-synuclein immunohistochemistry. Brain Pathol 2000; 10:378–384.

Hammers A, Allom R, Koepp MJ, et al. Three-dimensional maximum probability atlas of the human brain, with particular reference to the temporal lobe. Hum Brain Mapp 2003; 19:224–247.

Hamza TH, Zabetian CP, Tenesa A, et al. Common genetic variation in the HLA region is associated with late-onset sporadic Parkinson's disease. Nat Genet. 2010; 42:781-785.

Hansen L, Salmon D, Galasko D, et al. The Lewy body variant of Alzheimer's disease: a clinical and pathologic entity. Neurology 1990; 40:1-8.

Harada A, Oguchi K, Okabe S, et al. Altered microtubule organization in small-calibre axons of mice lacking tau protein. Nature. 1994; 369:488-491.

Harada T, Miyai I, Suzuki M, Kubota K. Gait capacity affects cortical activation patterns related to speed control in the elderly. Exp Brain Res. 2009; 193:445-454.

Hardy J, Allsop D. Amyloid deposition as the central event in the aetiology of Alzheimer's disease. Trends Pharmacol Sci. 1991; 12:383-388.

Harmon-Jones E, Winkielman P. Social Neuroscience: Integrating Biological and Psychological Explanations of Social Behavior. Guilford Press. 2007. ISBN 978-1-59385-404-1.

Hartlage-Rübsamen M, Lemke R, Schliebs R. Interleukin-1beta, inducible nitric oxide synthase, and nuclear factor-kappaB are induced in morphologically distinct microglia after rat hippocampal lipopolysaccharide/interferon-gamma injection. J Neurosci Res. 1999; 57:388-398.

Hausdorff JM. Gait dynamics in Parkinson's disease: common and distinct behavior among stride length, gait variability, and fractal-like scaling. Chaos. 2009; 19:026113.

Hausdorff JM, Cudkowicz ME, Firtion R, Wei JY, Goldberger AL. Gait variability and basal ganglia disorders: stride-to-stride variations of gait cycle timing in Parkinson's disease and Huntington's disease. Mov Disord. 1998; 13:428-437.

Hausdorff JM, Rios DA, Edelberg HK. Gait variability and fall risk in community-living older adults: a 1-year prospective study. Arch Phys Med Rehabil. 2001; 82:1050-1056.

Hellwig S, Amtage F, Kreft A, et al. [^{18}F]FDG-PET is superior to [^{123}I]IBZM-SPECT for the differential diagnosis of parkinsonism Neurology 2012; 79:1314-1322.

Hely MA, Reid WG, Adena MA, et al. The Sydney multicenter study of Parkinson's disease: the inevitability of dementia at 20 years. Mov Disord. 2008; 23:837-844.

Hernan MA, Takkouche B, Caamano-Isorna F, Gestal-Otero JJ. A meta-analysis of coffee drinking, cigarette smoking, and the risk of Parkinson’s disease. Ann Neurol 2002; 52:276–284.

Hernan MA, Logroscino G, García Rodríguez LA. Nonsteroidal anti-inflammatory drugs and the incidence of Parkinson disease. Neurology 2006; 66:1097–1099.

Hernandes MS, Santos GD, Café-Mendes CC, et al. Microglial cells are involved in the susceptibility of NADPH oxidase knockout mice to 6-hydroxy-dopamine-induced neurodegeneration. PLoS One. 2013; 8:e75532.

Herva ME, Zibaee S, Fraser G, Barker RA, Goedert M, Spillantini MG. Anti-amyloid Compounds Inhibit α-Synuclein Aggregation Induced by Protein Misfolding Cyclic Amplification (PMCA). J Biol Chem. 2014; 289:11897-11905.

Hilker R, Thomas AV, Klein JC, et al. Dementia in Parkinson disease: functional imaging of cholinergic and dopaminergic pathways. Neurology 2005; 65:1716-1722.

Hilton D, Stephens M, Kirk L, et al. Accumulation of α-synuclein in the bowel of patients in the pre-clinical phase of Parkinson's disease. Acta Neuropathol. 2014; 127:235-241.

Hirano A, Malamud N, Kurland LT. Parkinsonism-dementia complex, an endemic disease on the island of Guam: II. Pathological Features. Brain. 1961; 84:662–679.

Hirsch E, Graybiel AM, Agid YA. Melanized dopaminergic neurons are differentially susceptible to generation in Parkinson's disease. Nature 1988; 334:345-348.

Hirsch EC, Graybiel AM, Duyckaerts C, Javoy-Agid F. Neuronal loss in the pedunculopontine tegmental nucleus in Parkinson disease and in progressive supranuclear palsy. Proc Natl Acad Sci U S A. 1987; 84:5976-5980.

Hirsch EC, Hunot S. Neuroinflammation in Parkinson's disease: a target for neuroprotection? Lancet Neurol 2009; 8:382–397.

Hoffman JM, Welsh-Bohmer KA, Hanson M, et al. FDG PET imaging in patients with pathologically verified dementia. J Nucl Med. 2000; 41:1920–1928.

Holtzer R, Verghese J, Xue X, Lipton RB. Cognitive processes related to gait velocity: results from the Einstein Aging Study. Neuropsychology. 2006; 20:215-223.

Hoover JE, Strick PL. Multiple output channels in the basal ganglia. Science. 1993; 259:819-821.

Hornykiewicz O. Biochemical aspects of Parkinson's disease. Neurology. 1998; 51:Suppl 2:S2-9.

Hsu CL, Voss MW, Handy TC, et al. Disruptions in brain networks of older fallers are associated with subsequent cognitive decline: a 12-month prospective exploratory study. PLoS One. 2014; 9:e93673.

Hu MT, Taylor-Robinson SD, Chaudhuri KR, et al. Cortical dysfunction in non-demented Parkinson's disease patients: a combined 31Phosphorus MRS and 18FDG PET study. Brain 2000; 123:340–352.

Huang C, Mattis P, Perrine K, Brown N, Dhawan V, Eidelberg D. Metabolic abnormalities associated with mild cognitive impairment in Parkinson disease. Neurology 2008; 70:1470-1477.

Hughes AJ, Daniel SE, Kilford L, et al. Accuracy of clinical diagnosis of idiopathic Parkinson's disease: a clinico-pathological study of 100 cases. J Neurol Neurosurg Psychiatry. 1992; 55:181-184.

Hughes AJ, Daniel SE, Lees AJ. Improved accuracy of clinical diagnosis of Lewy body Parkinson's disease. Neurology 2001; 57:1497-1499.

Hurtig HI, Trojanowski JQ, Galvin J, et al. Alpha-synuclein cortical Lewy bodies correlate with dementia in Parkinson's disease. Neurology 2000; 54:1916-1921.

Huse DM, Schulman K, Orsini L, Castelli-Haley J, Kennedy S, Lenhart G. Burden of illness in Parkinson's disease. Mov Disord. 2005; 20:1449-1454.

Hyman BT, Phelps CH, Beach TG, et al. National Institute on Aging-Alzheimer's Association guidelines for the neuropathologic assessment of Alzheimer's disease. Alzheimers Dement. 2012; 8:1-13.

Iannaccone S, Cerami C, Alessio M, et al. In vivo microglia activation in very early dementia with Lewy bodies, comparison with Parkinson's disease. Parkinsonism Relat Disord. 2013; 19:47-52.

Ikoma Y, Yasuno F, Ito H, et al. Quantitative analysis for estimating binding potential of the peripheral benzodiazepine receptor with [(11)C]DAA1106. J Cereb Blood Flow Metab. 2007; 27:173-184.

Ikonomovic, MD ,Klunk, WE, Abrahamson EE, et al. Precuneus amyloid burden is associated with reduced cholinergic activity in Alzheimer's disease. Neurology 2011; 77:39-47.

Imamura K, Hishikawa N, Sawada M, et al. Distribution of major histocompatibility complex class II-positive microglia and cytokine profile of Parkinson's disease brains. Acta Neuropathol 2003; 106:518–526.

Inestrosa NC, Marzolo MP, Bonnefont AB. Cellular and molecular basis for estrogen's neuroprotection. Potential relevance for Alzheimer's disease. Mol Neurobiol 1998; 17:73-86.

Innis RB, Cunningham VJ, Delforge J et al. Consensus nomenclature for in vivo imaging of reversibly binding radioligands. J Cereb Blood Flow Metab. 2007; 27:1533-9.

Iqbal K, Alonso Adel C, et al. Tau pathology in Alzheimer disease and other tauopathies. Biochim Biophys Acta. 2005; 1739:198-210.

Iranzo A, Molinuevo JL, Santamaría J, et al. Rapid-eye-movement sleep behaviour disorder as an early marker for a neurodegenerative disorder: a descriptive study. Lancet Neurol. 2006; 5:572-577.

Irwin DJ, White MT, Toledo JB, et al. Neuropathologic substrates of Parkinson disease dementia. Ann Neurol. 2012; 72:587-598.

Ito K, Nagano-Saito A, Kato T, et al. Striatal and extrastriatal dysfunction in Parkinson's disease with dementia: a 6-[18F]fluoro-L-dopa PET study. Brain. 2002; 125:1358–1365.

Jacobs JV, Lou JS, Kraakevik JA, Horak FB. The supplementary motor area contributes to the timing of the anticipatory postural adjustment during step initiation in participants with and without Parkinson's disease. Neuroscience. 2009; 164:877-885.

Jankovic J, McDermott M, Carter J, et al. Variable expression of Parkinson's disease: a base-line analysis of the DATATOP cohort. The Parkinson Study Group. Neurology 1990; 40:1529-1534.

Jaussent I, Bouyer J, Ancelin ML, et al. Excessive sleepiness is predictive of cognitive decline in the elderly. Sleep. 2012; 35:1201-1207.

Jellinger KA. Alpha-synuclein pathology in Parkinson's and Alzheimer's disease brain: incidence and topographic distribution--a pilot study. Acta Neuropathol. 2003; 106:191-201.

Jellinger KA. Lewy body-related alpha-synucleinopathy in the aged human brain. J Neural Transm. 2004; 111:1219-1235.

Jellinger KA. Neuropathology of sporadic Parkinson's disease: evaluation and changes of concepts. Mov Disord. 2012; 27:8-30.

Jellinger KA, Attems J. Does striatal pathology distinguish Parkinson disease with dementia and dementia with Lewy bodies? Acta Neuropathol. 2006; 112:253-260.

Jellinger KA, Attems J Prevalence and impact of vascular and Alzheimer pathologies in Lewy body disease. Acta Neuropathol 2008; 115:427-436.

Jellinger KA. A critical evaluation of current staging of alpha-synuclein pathology in Lewy body disorders. Biochim Biophys Acta.2009; 1792:730-740.

Jenner P, Langston JW. Explaining ADAGIO: a critical review of the biological basis for the clinical effects of rasagiline. Mov Disord. 2011; 26:2316-23.

Jokinen P, Scheinin N, Aalto S, Någren K, Savisto N, Parkkola R, Rokka J, Haaparanta M, Röyttä M, Rinne JO. [(11)C]PIB-, [(18)F]FDG-PET and MRI imaging in patients with Parkinson's disease with and without dementia. Parkinsonism Relat Disord. 2010; 16:666-670.

Kang JH, Irwin DJ, Chen-Plotkin AS, et al. Parkinson's Progression Markers Initiative. Association of cerebrospinal fluid β-amyloid 1-42, T-tau, P-tau181, and α-synuclein levels with clinical features of drug-naive patients with early Parkinson disease. JAMA Neurol. 2013; 70:1277-1287.

Kantarci K, Lowe V, Przybelski SA, et al. APOE modifies the association between Aβ load and cognition in cognitively normal older adults. Neurology 2012; 78:232-240.

Kalaitzakis ME, Walls AJ, Pearce RK, Gentleman SM. Striatal Aβ peptide deposition mirrors dementia and differentiates DLB and PDD from other parkinsonian syndromes. Neurobiol Dis. 2011; 41:377-384.

Kas A, de Souza LC, Samri D, et al. Neural correlates of cognitive impairment in posterior cortical atrophy. Brain 2011; 134:1464-1478.

Kato S, Watanabe H, Senda J, et al. Widespread cortical and subcortical brain atrophy in Parkinson's disease with excessive daytime sleepiness. J Neurol. 2012; 259:318-326.

Katzenschlager R, Lees AJ. Olfaction and Parkinson's syndromes: its role in differential diagnosis. Curr Opin Neurol. 2004; 17:417-423.

Katsuse O, Iseki E, Marui W, Kosaka K. Developmental stages of cortical Lewy bodies and their relation to axonal transport blockage in brains of patients with dementia with Lewy bodies. J Neurol Sci. 2003; 211:29-35.

Kehagia AA, Barker RA, Robbins TW. Neuropsychological and clinical heterogeneity of cognitive impairment and dementia in patients with Parkinson's disease. Lancet Neurol. 2010; 9:1200-1213.

Kerr GK, Worringham CJ, Cole MH, Lacherez PF, Wood JM, Silburn PA. Predictors of future falls in Parkinson disease. Neurology 2010; 75:116-24.

Kilarski LL, Pearson JP, Newsway V, et al. Systematic review and UK-based study of PARK2 (parkin), PINK1, PARK7 (DJ-1) and LRRK2 in early-onset Parkinson's disease. Mov Disord 2012; 27:1522-1529.

Kim SE, Choi JY, Choe YS, Choi Y, Lee WY. Serotonin transporters in the midbrain of Parkinson's disease patients: a study with 123I-beta-CIT SPECT. J Nucl Med. 2003; 44:870-876.

Kish SJ, Shannak K, Hornykiewicz O. Uneven pattern of dopamine loss in the striatum of patients with idiopathic Parkinson's disease. Pathophysiologic and clinical implications. N Engl J Med. 1988; 318:876-880.

Kitada T, Asakawa S, Hattori N, et al. Mutations in the parkin gene cause autosomal recessive juvenile parkinsonism. Nature 1998; 392:605-608.

Klunk WE, Wang Y, Huang GF, Debnath ML, Holt DP, Mathis CA. Uncharged thioflavin-T derivatives bind to amyloid-beta protein with high affinity and readily enter the brain. Life Sci. 2001; 69:1471-1484.

Klunk WE, Wang Y, Huang GF, et al. The binding of 2-(40 methylaminophenyl)benzothiazole to postmortem brain homogenates is dominated by the amyloid component. J Neurosci 2003; 23:2086-2092.

Klunk WE, Engler H, Nordberg A, et al. Imaging brain amyloid in Alzheimer's disease with Pittsburgh Compound-B. Ann Neurol. 2004; 55:306-319.

Knott C, Stern G, Wilkin GP. Inflammatory regulators in Parkinson's disease: iNOS, lipocortin-1, and cyclooxygenases-1 and -2. Mol Cell Neurosci. 2000; 16:724-739.

Koenraadt KL, Roelofsen EG, Duysens J, Keijsers NL. Cortical control of normal gait and precision stepping: an fNIRS study. Neuroimage. 2014; 85:415-422.

Kohutnicka M, Lewandowska E, Kurkowska-Jastrzebska I, Członkowski A, Członkowska A. Microglial and astrocytic involvement in a murine model of

Parkinson's disease induced by 1-methyl-4-phenyl-1,2,3,6-tetrahydropyridine (MPTP). Immunopharmacology. 1998; 39:167-80.

Kok E, Haikonen S, Luoto T, et al. Apolipoprotein E-dependent accumulation of Alzheimer disease-related lesions begins in middle age. Ann Neurol. 2009; 65:650-7.

Kordower JH, Chu Y, Hauser RA, Freeman TB, Olanow CW. Lewy body-like pathology in long-term embryonic nigral transplants in Parkinson's disease. Nature medicine 2008; 14:504-506.

Koshikawa N, Koshikawa F, Tomiyama K, et al. Effects of dopamine D1 and D2 agonists and antagonists injected into the nucleus accumbens and globus pallidus on jaw movements of rats. Eur J Pharmacol 1990; 182:375-380.

Kostić VS, Agosta F, Petrović I, et al. Regional patterns of brain tissue loss associated with depression in Parkinson disease. Neurology 2010; 75:857-863.

Kotagal V, Bohnen NI, Müller ML, Koeppe RA, Frey KA, Albin RL. Cerebral amyloid deposition and serotoninergic innervation in Parkinson disease. Arch Neurol. 2012; 69:1628-1631.

Kotzbauer PT, Cairns NJ, Campbell MC, et al. Pathologic accumulation of α-synuclein and Aβ in Parkinson disease patients with dementia. Arch Neurol. 2012; 69:1326-1331.

Kovacs GG, Milenkovic IJ, Preusser M, Budka H. Nigral burden of alpha-synuclein correlates with striatal dopamine deficit. Mov Disord. 2008; 23:1608-1612.

Kramer ML, Schulz-Schaeffer WJ. Presynaptic alpha-synuclein aggregates, not Lewy bodies,
cause neurodegeneration in dementia with Lewy bodies. J Neurosci. 2007; 27:1405-1410.

Kraybill ML, Larson EB, Tsuang DW, et al. Cognitive differences in dementia patients with autopsy-verified AD, Lewy body pathology, or both. Neurology 2005; 64:2069-2073.

Kreisl WC, Lyoo CH, McGwier M, et al. Biomarkers Consortium PET Radioligand Project Team. In vivo radioligand binding to translocator protein correlates with severity of Alzheimer's disease. Brain 2013; 136:2228-2238.

Kruger R, Kuhn W, Muller T, Woitalla D, Graeber M, Kosel S, et al. Ala30Pro mutation in the gene encoding alpha-synuclein in Parkinson’s disease. Nat Genet 1998; 18:106-108.

Kreutzberg GW. Microglia: a sensor for pathological events in the CNS. Trends Neurosci. 1996; 19:312–318.

Kuhl DE, Minoshima S, Fessler JA, et al. In vivo mapping of cholinergic terminals in normal aging, Alzheimer's disease, and Parkinson's disease. Ann Neurol. 1996; 40:399-410.

Kurz MJ, Wilson TW, Arpin DJ. Stride-time variability and sensorimotor cortical activation during walking. Neuroimage. 2012; 59:1602-1607.

Kuys SS, Brauer SG, Ada L. Test-retest reliability of the GAITRite system in people with stroke undergoing rehabilitation. Disabil Rehabil. 2011; 33:1848-53.

Lammertsma AA, Bench CJ, Hume SP, et al. Comparison of methods for analysis of clinical [11C]raclopride studies. J. Cereb. Blood Flow Metab. 1996; 16:42-52.

Lammertsma AA, Hume SP. Simplified reference tissue model for PET receptor studies.
Neuroimage 1996; 4:153-158.

Landau SM, Mintun MA, Joshi AD, Koeppe RA, Petersen RC, Aisen PS, Weiner MW, Jagust WJ; Alzheimer's Disease Neuroimaging Initiative. Amyloid deposition, hypometabolism, and longitudinal cognitive decline. Ann Neurol. 2012; 72:578-586.

Lang AE, Lozano, AM. Parkinson's Disease. N Engl J Med. 1998; 339:1044-1053.

Lambracht-Washington D, Rosenberg RN. Anti-amyloid beta to tau - based immunization: Developments in immunotherapy for Alzheimer disease. Immunotargets Ther. 2013; 2013:105-114.

Langston JW, Ballard P, Tetrud JW, Irwin I. Chronic Parkinsonism in humans due to a product of meperidine-analog synthesis. Science 1983; 219:979-80.

Langston JW, Forno LS, Tetrud J, Reeves AG, Kaplan JA, Karluk D. Evidence of active nerve cell degeneration in the substantia nigra of humans years after 1-methyl-4-phenyl-1,2,3,6-tetrahydropyridine exposure. Ann Neurol. 1999; 46:598-605.

Lashley T, Holton JL, Gray E, et al. Cortical alpha-synuclein load is associated with amyloid-beta plaque burden in a subset of Parkinson's disease patients. Acta Neuropathol.
2008; 115:417-425.

Lebouvier T, Neunlist M, Bruley des Varannes S, et al. Colonic biopsies to assess the neuropathology of Parkinson's disease and its relationship with symptoms. PLoS One. 2010; 5:e12728.

Lee CS, Schulzer M, de la Fuente-Fernández R, et al. Lack of regional selectivity during the progression of Parkinson disease: implications for pathogenesis. Arch Neurol. 2004; 61:1920-1925.

Lee HJ, Patel S, Lee SJ. Intravesicular localization and exocytosis of alphasynuclein and its aggregates. J Neurosci 2005; 25:6016-6024.

Lee HJ, Suk JE, Patrick C, et al. Direct transfer of alpha-synuclein from neuron to astroglia causes inflammatory responses in synucleinopathies. J Biol Chem 2010; 285:9262-9272.

Leentjens AF, Van den Akker M, Metsemakers JF, Lousberg R, Verhey FR. Higher incidence of depression preceding the onset of Parkinson's disease: a register study. Mov Disord. 2003; 18:414-418.

Lehéricy S, Ducros M, Van de Moortele PF, et al. Diffusion tensor fiber tracking shows distinct corticostriatal circuits in humans. Ann Neurol. 2004; 55:522-529.

Lehnardt S. Innate immunity and neuroinflammation in the CNS: the role of microglia in Toll-like receptor-mediated neuronal injury. Glia 2010; 58:253-263.

Le Ray D, Juvin L, Ryczko D, Dubuc R. Supraspinal control of locomotion: the mesencephalic locomotor region. Prog Brain Res. 2011; 188:51-70.

Lesage S, Durr A, Tazir M, Lohmann E, Leutenegger AL, Janin S, et al. LRRK2 G2019S as a cause of Parkinson’s disease in North African Arabs. N Engl J Med 2006; 354:422-423.

Lesage S, Brice A. Parkinson's disease: from monogenic forms to genetic susceptibility factors. Hum. Mol. Genet. 2009; 18(R1):R48-59.

Lesage S, Condroyer C, Klebe S, et al. Identification of VPS35 mutations replicated in French families with Parkinson disease. Neurology 2012; 78:1449-1450.

Levy G, Tang MX, Cote LJ, et al. Motor impairment in PD: relationship to incident dementia and age. Neurology 2000; 55:539-544.

Levy G, Jacobs DM, Tang MX, et al. Memory and executive function impairment predict dementia in Parkinson’s disease. Mov Disord. 2002; 17:1221-1226.

Levy G, Schupf N, Tang MX, et al. Combined effect of age and severity on the risk of dementia in Parkinson's disease. Ann Neurol. 2002; 51:722-729.

Li JY, Englund E, Holton JL, et al. Lewy bodies in grafted neurons in subjects with Parkinson's disease suggest host-to-graft disease propagation. Nat Med. 2008; 14:501-503.

Li L, Lu J, Tay SS, Moochhala SM, He BP. The function of microglia, either neuroprotection or neurotoxicity, is determined by the equilibrium among factors released from activated microglia in vitro. Brain Res. 2007; 1159:8-17.

Li M, Dai FR, Du XP, Yang QD, Chen Y. Neuroprotection by silencing iNOS expression in a 6-OHDA model of Parkinson's disease. J Mol Neurosci. 2012; 48:225-233.

Liberatore GT, Jackson-Lewis V, Vukosavic S, et al. Inducible nitric oxide synthase stimulates dopaminergic neurodegeneration in the MPTP model of Parkinson disease. Nat Med. 1999; 5:1403-1409.

Libow LS, Frisina PG, Haroutunian V, Perl DP, Purohit DP. Parkinson's disease dementia: a diminished role for the Lewy body. Parkinsonism Relat Disord. 2009; 15:572-575.

Lindvall O. Developing dopaminergic cell therapy for Parkinson's disease--give up or move forward? Mov Disord. 2013; 28:268-273.

Liou HH, Tsai MC, Chen CJ, et al. Environmental risk factors and Parkinson's disease: a case-control study in Taiwan. Neurology 1997; 48:1583-1588.

Litvan I, Aarsland D, Adler CH, et al. MDS task force on mild cognitive impairment in Parkinson's disease: critical review of PD-MCI. Mov Disord. 2011; 26:1814-1824.

Litvan I, Bhatia KP, Burn DJ, et al. Movement Disorders Society Scientific Issues Committee report: SIC Task Force appraisal of clinical diagnostic criteria for Parkinsonian disorders. Mov Disord. 2003; 18:467-486.

Litvan I, Goldman JG, Tröster AI, et al. Diagnostic criteria for mild cognitive impairment in Parkinson's disease: Movement Disorder Society Task Force guidelines. Mov Disord. 2012; 27:349-356.

Liu X, Cheng R, Verbitsky M, et al. Genome-wide association study identifies candidate genes for Parkinson's disease in an Ashkenazi Jewish population. BMC Med Genet. 2011; 12:104.

Lockhart A, Lamb JR, Osredkar T, et al. PIB is a non-specific imaging marker of amyloid-beta (Abeta) peptide-related cerebral amyloidosis. Brain 2007; 130:2607-2615.

Lopresti BJ, Klunk WE, Mathis CA, et al. Simplified Quantification of Pittsburgh Compound B Amyloid Imaging PET Studies: A Comparative Analysis. J Nucl Med. 2005; 46:1959-1972.

Lord S, Galna B, Coleman S, Burn D, Rochester L. Mild depressive symptoms are associated with gait impairment in early Parkinson's disease. Mov Disord. 2013; 28:634-9.

Lord S, Galna B, Verghese J, Coleman S, Burn D, Rochester L. Independent domains of gait in older adults and associated motor and nonmotor attributes: validation of a factor analysis approach. J Gerontol A Biol Sci Med Sci. 2013; 68:820-827.

Lord S, Howe T, Greenland J, Simpson L, Rochester L. Gait variability in older adults: a structured review of testing protocol and clinimetric properties. Gait Posture. 2011; 34:443-450.

Lord S, Rochester L, Hetherington V, Allcock LM, Burn D. Executive dysfunction and attention contribute to gait interference in 'off' state Parkinson's Disease. Gait Posture. 2010; 31:169-174.

Luk KC, Song C, O'Brien P, et al. Exogenous alpha-synuclein fibrils seed the formation of Lewy body-like intracellular inclusions in cultured cells. Proc Natl Acad Sci USA 2009; 106:20051-20056.

Lucking CB, Durr A, Bonifati V, et al. Association between early-onset Parkinson's disease and mutations in the parkin gene. N Engl J Med 2000; 342:1560-1567.

Luk KC, Kehm VM, Zhang B, O'Brien P, Trojanowski JQ, Lee VM: Intracerebral inoculation of pathological alpha-synuclein initiates a rapidly progressive neurodegenerative alpha-synucleinopathy in mice. J Exp Med 2012; 209:975-986.

Luk KC, Kehm V, Carroll J, et al. Pathological a-Synuclein Transmission Initiates Parkinson-like Neurodegeneration in Nontransgenic Mice. Science 2012; 338:949-953.

Lundin-Olsson L, Nyberg L, Gustafson Y. "Stops walking when talking" as a predictor of falls in elderly people. Lancet 1997; 349:617.

Lv Z, Jiang H, Xu H, Song N, Xie J. Increased iron levels correlate with the selective nigral dopaminergic neuron degeneration in Parkinson's disease. J Neural Transm. 2011;118:361-369.

Lyoo CH, Jeong Y, Ryu YH, Rinne JO, Lee MS. Cerebral glucose metabolism of Parkinson's disease patients with mild cognitive impairment. Eur Neurol. 2010; 64:65-73.

Maetzler W, Reimold M, Liepelt I, et al. [(11)C]PIB binding in Parkinson's disease dementia. Neuroimage 2008; 39:1027-1033.

Makizako H, Shimada H, Doi T, et al. Poor balance and lower gray matter volume predict falls in older adults with mild cognitive impairment. BMC Neurol. 2013; 13:102.

Mahieux F, Fenelon G, Flahault A, Manifacier MJ, Michelet D, Boller F. Neuropsychological
prediction of dementia in Parkinson's disease. J Neurol Neurosurg Psychiatry. 1998; 64:178-183.

Malhotra AK, Kestler LJ, Mazzanti C, Bates JA, Goldberg T, Goldman D. A functional polymorphism in the COMT gene and performance on a test of prefrontal cognition. Am J Psychiatry. 2002; 159:652-654.

Mann DM, Yates PO, Hawkes J. The pathology of the human locus ceruleus. Clin Neuropathol. 1983; 2:1-7.

Marder K Cognitive impairment and dementia in Parkinson's disease. Mov Disord. 2010; 25 Suppl 1:S110-6.

Marek K, Innis R, van Dyck C, et al. [123I]beta-CIT SPECT imaging assessment of the rate of Parkinson's disease progression. Neurology. 2001; 57:2089-2094.

Marshall JC, Fink GR. Spatial cognition: where we were and where we are. Neuroimage. 2001; 14:S2-7.

Martinez-Martin P, Rodriguez-Blazquez C, Kurtis MM, Chaudhuri KR; NMSS Validation Group. The impact of non-motor symptoms on health-related quality of life of patients with Parkinson's disease. Mov Disord. 2011; 26:399-406.

Masliah E, Rockenstein E, Mante M, et al. Passive immunization reduces behavioral and neuropathological deficits in an alpha-synuclein transgenic model of Lewy body disease. PLoS One. 2011; 6:e19338.

Masliah E, Rockenstein E, Veinbergs I, et al. Amyloid peptides enhance γ-synuclein accumulation and neuronal deficits in a transgenic mouse model linking Alzheimer's disease and Parkinson's disease. Proc Natl Acad Sci USA 2001; 98:12245-12250.

Masuda-Suzukake M, Nonaka T, Hosokawa M, et al. Prion-like spreading of pathological alpha-synuclein in brain. Brain 2013; 136:1128-1138.

Mathis CA, Bacskai BJ, Kajdasz ST, et al. A lipophilic thioflavin-T derivative for positron emission tomography (PET) imaging of amyloid in brain. Bioorg Med Chem Lett. 2002; 12:295-298.

Mathis CA, Wang Y, Holt DP, Huang GF, Debnath ML, Klunk WE. Synthesis and evaluation of 11C-labeled 6-substituted 2-arylbenzothiazoles as amyloid imaging agents. J Med Chem. 2003; 46:2740-2754.

Martinez-Gonzalez C1, Bolam JP, Mena-Segovia J. Topographical organization of the pedunculopontine nucleus. Front Neuroanat. 2011; 5:22.

Matsui H, Udaka F, Miyoshi T, et al. Three-dimensional stereotactic surface projection study of freezing of gait and brain perfusion image in Parkinson's disease. Mov Disord. 2005 20:1272-7.

McCoy MK, Martinez TN, Ruhn KA, et al. Blocking soluble tumor necrosis factor signaling with dominant-negative tumor necrosis factor inhibitor attenuates loss of dopaminergic neurons in models of Parkinson's disease. J Neurosci. 2006; 26:9365-9375.

McGeer PL, Itagaki S, Boyes BE, et al. Reactive microglia are positive for HLA-DR in the substantia nigra of Parkinson's and Alzheimer's disease brains. Neurology 1988; 38:1285-1291.

McGeer PL, Schwab C, Parent A, et al. Presence of reactive microglia in monkey substantia nigra years after 1-methyl-4-phenyl- 1,2,3,6-tetrahydropyridine administration. Ann Neurol 2003; 54:599-604.

McGeer PL, McGeer EG. Inflammation and the degenerative diseases of aging. Ann. N.Y. Acad. Sci. 2004; 1035:104-116.

McKeith IG, Dickson DW, Lowe J, et al.; Consortium on DLB. Diagnosis and management of dementia with Lewy bodies: third report of the DLB Consortium. Neurology. 2005; 65:1863-1872.

Ménard A, Auclair F, Bourcier-Lucas C, Grillner S, Dubuc R. Descending GABAergic projections to the mesencephalic locomotor region in the lamprey Petromyzon marinus. J Comp Neurol. 2007; 501:260-273.

Menz HB, Latt MD, Tiedemann A, Mun San Kwan M, Lord SR. Reliability of the GAITRite walkway system for the quantification of temporo-spatial parameters of gait in young and older people. Gait Posture. 2004; 20:20-25.

Merlino G, Piani A, Gigli GL, et al. Daytime sleepiness is associated with dementia and cognitive decline in older Italian adults: a population-based study. Sleep Med. 2010; 11:372-377.

Mirelman A, Gurevich T, Giladi N, Bar-Shira A, Orr-Urtreger A, Hausdorff JM. Gait alterations in healthy carriers of the LRRK2 G2019S mutation. Ann Neurol. 2011; 69:193-197.

Mirelman A, Herman T, Brozgol M, et al. Executive function and falls in older adults: new findings from a five-year prospective study link fall risk to cognition. PLoS One. 2012; 7:e40297.

Mito Y, Yoshida K, Yabe I, et al. Brain SPECT analysis by 3D-SSP and phenotype of Parkinson's disease. J Neurol Sci. 2006; 241:67-72.

Miyai I, Tanabe HC, Sase I, et al. Cortical mapping of gait in humans: a near-infrared spectroscopic topography study. Neuroimage. 2001; 14:1186-1192.

Mizoguchi K, Shoji H, Tanaka Y, Maruyama W, Tabira T. Age-related spatial working memory impairment is caused by prefrontal cortical dopaminergic dysfunction in rats. Neuroscience. 2009; 162:1192-1201.

Moehle MS, Webber PJ, Tse T, et al. LRRK2 inhibition attenuates microglial inflammatory responses. J Neurosci. 2012 32:1602-11.

Montero-Odasso M, Verghese J, Beauchet O, Hausdorff JM. Gait and cognition: a complementary approach to understanding brain function and the risk of falling. J Am Geriatr Soc. 2012; 60:2127-2136.

Montine TJ, Shi M, Quinn JF, et al. CSF Aβ(42) and tau in Parkinson's disease with cognitive impairment. Mov Disord. 2010; 25:2682-2685.

Moretto A, Colosio C. Biochemical and toxicological evidence of neurological effects of pesticides: the example of Parkinson's disease. Neurotoxicology. 2011; 32:383-391.

Mori H, Kondo T, Yokochi M, et al. Pathologic and biochemical studies of juvenile parkinsonism linked to chromosome 6q. Neurology 1998; 51: 890-892.

Morris ME, Iansek R, Matyas TA, Summers JJ. Stride length regulation in Parkinson's disease. Normalization strategies and underlying mechanisms. Brain 1996; 119:551-568.

Mortimer JA, Borenstein AR, Nelson LM. Associations of welding and manganese exposure with Parkinson disease: review and meta-analysis. Neurology 2012; 79:1174-1180.

Mrak RE, Griffin WS. Common inflammatory mechanisms in Lewy body disease and Alzheimer disease. J Neuropathol Exp Neurol. 2007; 66:683-686.

Müller ML, Frey KA, Petrou M, et al. β-Amyloid and postural instability and gait difficulty in Parkinson's disease at risk for dementia. Mov Disord. 2013; 28:296-301.

Murphy DD, Rueter SM, Trojanowski JQ, Lee VM. Synucleins are developmentally expressed, and alpha-synuclein regulates the size of the presynaptic vesicular pool in primary hippocampal neurons. J Neurosci. 2000; 20:3214-3220.

Murphy KE, Gysbers AM, Abbott SK, et al. Reduced glucocerebrosidase is associated with increased α-synuclein in sporadic Parkinson's disease. Brain 2014; 137:834-848.

Nakamura K, Nemani VM, Azarbal F, et al. Direct Membrane Association Drives Mitochondrial Fission by the Parkinson Disease-associated Protein **a**-Synuclein. J Biol Chem. 2011; 286:20710-20726.

Nakano I, Hirano A. Parkinson's disease: neuron loss in the nucleus basalis without concomitant Alzheimer's disease. Ann Neurol. 1984; 15:415-418.

Nandhagopal R, Kuramoto L, Schulzer M, et al. Longitudinal progression of sporadic Parkinson's disease: a multi-tracer positron emission tomography study. Brain 2009; 132:2970-2979.

Nelson RL, Guo Z, Halagappa VM, et al. Prophylactic treatment with paroxetine ameliorates behavioral deficits and retards the development of amyloid and tau pathologies in 3xTgAD mice. Exp Neurol. 2007; 205:166-176.

Niethammer M, Tang CC, Ma Y, et al. Parkinson's disease cognitive network correlates with caudate dopamine. Neuroimage. 2013; 78:204-209.

Nitsch RM, Deng M, Tennis M, Schoenfeld D, Growdon JH. The selective muscarinic M1 agonist AF102B decreases levels of total Abeta in cerebrospinal fluid of patients with Alzheimer's disease. Ann Neurol. 2000; 48:913-918.

Oka H, Yoshioka M, Morita M, et al. Reduced cardiac 123I-MIBG uptake reflects cardiac sympathetic dysfunction in Lewy body disease. Neurology 2007; 69:1460-1465.

Olanow CW, Hauser RA, Jankovic J, et al. A randomized, double-blind, placebo-controlled, delayed start study to assess rasagiline as a disease modifying therapy in Parkinson's disease (the ADAGIO study): rationale, design, and baseline characteristics. Mov Disord. 2008; 23:2194-2201.

Olanow CW, Prusiner SB: Is Parkinson's disease a prion disorder? Proc Natl Acad Sci U S A 2009, 106:12571-12572.

Olichney JM, Galasko D, Salmon DP, et al. Cognitive decline is faster in Lewy body variant than in Alzheimer’s disease. Neurology 1998; 51:351-357.

Orimo S, Amino T, Itoh Y, et al. Cardiac sympathetic denervation precedes neuronal loss in the sympathetic ganglia in Lewy body disease. Acta Neuropathol. 2005; 109:583-588.

Orimo S, Uchihara T, Nakamura A, et al. Axonal alpha-synuclein aggregates herald centripetal degeneration of cardiac sympathetic nerve in Parkinson's disease. Brain 2008; 131:642-650.

Ouchi Y, Yoshikawa E, Sekine Y, et al. Microglial activation and dopamine terminal loss in early Parkinson’s disease. Ann Neurol 2005; 57:168-175.

Owen AM, James M, Leigh PN, et al. Fronto-striatal cognitive deficits at different stages of Parkinson's disease. Brain. 1992; 115:1727-1751.

Owen DR, Howell OW, Tang SP, et al. Two binding sites for [3H]PBR28 in human brain: implications for TSPO PET imaging of neuroinflammation. J Cereb Blood Flow Metab. 2010; 30:1608-1618.

Owen DR, Gunn RN, Rabiner EA, et al. Mixed-affinity binding in humans with 18-kDa translocator protein ligands. J Nucl Med. 2011; 52:24-32.

Ozansoy M, Başak AN. The central theme of Parkinson's disease: α-synuclein. Mol Neurobiol. 2013; 47:460-465.

Ozelius LJ, Senthil G, Saunders-Pullman R, et al. LRRK2 G2019S as a cause of Parkinson’s disease in Ashkenazi Jews. N Engl J Med 2006; 354:424-425.

Paisan-Ruiz C, Jain S, Evans EW, et al. Cloning of the gene containing mutations that cause PARK8-linked Parkinson’s disease. Neuron 2004; 44:595-600.

Pakkenberg B, Moller A, Gundersen HJ, et al. The absolute number of nerve cells in substantia nigra in normal subjects and in patients with Parkinson's disease estimated with an unbiased stereological method. J Neurol Neurosurg Psychiatry 1991; 54:30-33.

Palmatier MA, Kang AM, Kidd KK. Global variation in the frequencies of functionally different catechol-O-methyltransferase alleles. Biol Psychiatry. 1999; 46:557-567.

Pankratz N, Wilk JB, Latourelle JC, et al. PSG-PROGENI and GenePD Investigators, Coordinators and Molecular Genetic Laboratories. Genome wide association study for susceptibility genes contributing to familial Parkinson disease. Hum Genet 2009; 124:593-605.

Pappatà S, Santangelo G, Aarsland, et al. Mild cognitive impairment in drug-naive patients with PD is associated with cerebral hypometabolism. Neurology 2011; 77:1357-1362.

Parkinson J. An Essay on the shaking palsy. London: Sherwood, Neely and Jones, 1817

Parkkinen L, Kauppinen T, Pirttila T, et al. Alpha-synuclein pathology does not predict
extrapyramidal symptoms or dementia. Ann Neurol. 2005; 57:82-91.

Parkkinen L, Pirttila T, Alafuzoff I. Applicability of current staging/categorization of alphasynuclein pathology and their clinical relevance. Acta Neuropathol. 2008; 115:399-407.

Paulus W, Jellinger K. The neuropathologic basis of different clinical subgroups of Parkinson's disease. J Neuropathol Exp Neurol. 1991; 50:743-55.

Pavese N, Evans AH, Tai YF, et al. Clinical correlates of levodopa-induced dopamine release in Parkinson disease: a PET study. Neurology 2006; 67:1612-1617.

Pavese N, Gerhard A, Tai YF, et al. Microglial activation correlates with severity in Huntington disease: a clinical and PET study. Neurology 2006; 66:1638-1643.

Pavese N, Metta V, Bose SK, Chaudhuri KR, Brooks DJ. Fatigue in Parkinson's disease is linked to striatal and limbic serotonergic dysfunction. Brain 2010; 33:3434-3443.

Pavese N, Rivero-Bosch M, Lewis SJ, Whone AL, Brooks DJ. Progression of monoaminergic dysfunction in Parkinson’s disease: A longitudinal (18)F-dopa PET study. Neuroimage 2011; 56:1463-1468.

Pearce RK, Hawkes CH, Daniel SE. The anterior olfactory nucleus in Parkinson’s disease. Mov Disord 1995; 10:283-287.

Peppard RF, Martin WRW, Carr GD, et al. Cerebral glucose metabolism in Parkinson’s-disease with and without dementia. Arch Neurol. 1992; 49:1262-1268.

Peterson DS, Pickett KA, Duncan R, Perlmutter J, Earhart GM. Gait-related brain activity in people with Parkinson disease with freezing of gait. PLoS One 2014; 9:e90634.

Petersen RC, Doody R, Kurz A, Mohs RC, Morris JC, Rabins PV, Ritchie K, Rossor M, Thal L, Winblad B. Current concepts in mild cognitive impairment. Arch Neurol. 2001; 58:1985-1992.

Petrou M, Bohnen NI, Müller ML, Koeppe RA, Albin RL, Frey KA. Aβ-amyloid deposition in patients with Parkinson disease at risk for development of dementia. Neurology 2012; 79:1161-1167.

Phani S, Loike JD, Przedborski S. Neurodegeneration and inflammation in Parkinson's disease. Parkinsonism Relat Disord. 2012; 18 Suppl 1:S207-209.

Phillips RJ, Walter GC, Wilder SL, et al. Alpha-synuclein-immunopositive myenteric neurons and vagal preganglionic terminals: autonomic pathway implicated in Parkinson's disease? Neuroscience 2008; 153:733-750.

Piccini P, Morrish PK, Turjanski N, et al. Dopaminergic function in familial Parkinson's disease: a clinical and 18F-dopa PET study. Ann Neurol. 1997; 41:222-229.

Piccini P, Brooks DJ. New developments of brain imaging for Parkinson's disease and related disorders. Mov Disord. 2006; 21:2035-2041.

Picillo M, Barone P, Pellecchia MT, et al. Evolution of mild cognitive impairment in Parkinson disease. Neurology 2014; 82:1384

Pickering RM, Grimbergen YA, Rigney U, et al. A meta-analysis of six prospective studies of falling in Parkinson's disease. Mov Disord. 2007; 22:1892-1900.

Pike VW, Halldin C, Crouzel C, et al. Radioligands for PET studies of central benzodiazepine receptors and PK (peripheral benzodiazepine) binding sites--current status. Nucl Med Biol. 1993; 20:503-525.

Piras F, Caltagirone C, Spalletta G. Working memory performance and thalamus microstructure in healthy subjects. Neuroscience 2010 ;171:496-505.

Pletnikova O, West N, Lee MK, et al. Abeta deposition is associated with enhanced cortical alpha-synuclein lesions in Lewy body diseases. Neurobiol Aging 2005; 26:1183-1192.

Plotnik M, Giladi N, Balash Y, Peretz C, Hausdorff JM. Is freezing of gait in Parkinson's disease related to asymmetric motor function? Ann Neurol. 2005; 57:656-663.

Politis M, Wu K, Loane C, et al. Depressive symptoms in PD correlate with higher 5-HTT binding in raphe and limbic structures. Neurology 2010; 75:1920-1927.

Ponsen MM, Stoffers D, Booij J, van Eck-Smit BL, Wolters ECh, Berendse HW. Idiopathic hyposmia as a preclinical sign of Parkinson's disease. Ann Neurol. 2004; 56:173-181.

Postuma RB, Gagnon JF, Vendette M, Desjardins C, Montplaisir JY. Olfaction and color vision identify impending neurodegeneration in rapid eye movement sleep behavior disorder. Ann Neurol. 2011; 69:811-818.

Price JC, Klunk WE, Lopresti BJ, et al. Kinetic modeling of amyloid binding in humans using PET imaging and Pittsburgh Compound-B. J Cereb Blood Flow Metab. 2005; 25:1528-1547.

Puschmann A. Monogenic Parkinson's disease and parkinsonism: clinical phenotypes and frequencies of known mutations. Parkinsonism Relat Disord. 2013; 19:407-415.

Qian L, Flood PM. Microglial cells and Parkinson's disease. Immunol Res 2008; 41:155-164.

Qian L, Wei SJ, Zhang D, et al. Potent anti-inflammatory and neuroprotective effects of TGF-beta1 are mediated through the inhibition of ERK and p47phox-Ser345 phosphorylation and translocation in microglia. J Immunol. 2008; 181:660-668.

Qian L, Flood PM, Hong JS. Neuroinflammation is a key player in Parkinson's disease and a prime target for therapy. J Neural Transm 2010; 117:971-979.

Qureshi HY, Paudel HK. Parkinsonian neurotoxin 1-methyl-4-phenyl-1,2,3,6 tetrahydropyridine (MPTP) and alpha-synuclein mutations promote tau protein phosphorylation at Ser262 and destabilize microtubule cytoskeleton in vitro. J Biol Chem. 2011; 286:5055-5068.

Raff MC, Whitmore AV, Finn JT. Axonal self-destruction and neurodegeneration. Science 2002; 296:868-871.

Raghavan R, Khin-Nu C, Brown A, et al. Detection of Lewy bodies in trisomy 21 (Down's syndrome). Can J Neurol Sci. 1993; 20:48-51.

Rajput AH. Levodopa prolongs life expectancy and is non-toxic to substantia nigra. Parkinsonism Rel Dis. 2001; 8:95-100.

Racette BA, Criswell SR, Lundin JI, et al. Increased risk of parkinsonism associated with welding exposure. Neurotoxicology 2012; 33:1356-1361

Racette BA. Manganism in the 21st century: The Hanninen lecture. Neurotoxicology. 2013 Oct 19. pii: S0161-813X(13)00157-5.

Ragonese P, Salemi G, Morgante L, et al. A case-control study on cigarette, alcohol, and coffee consumption preceding Parkinson's disease. Neuroepidemiology. 2003; 22:297-304.

Rajput AH, Sitte HH, Rajput A, Fenton ME, Pifl C, Hornykiewicz O. Globus pallidus dopamine and Parkinson motor subtypes: clinical and brain biochemical correlation. Neurology. 2008; 70:1403-1410.

Rao VL, Butterworth RF. Characterization of binding sites for the omega3 receptor ligands [3H]PK11195 and [3H]RO5-4864 in human brain. Eur J Pharmacol. 1997; 340:89-99.

Rees K, Stowe R, Patel S, et al. Non-steroidal anti-inflammatory drugs as disease-modifying agents for Parkinson's disease: evidence from observational studies. Cochrane Database Syst Rev 2011:CD008454.

Reijnders JS, Ehrt U, Weber WE, Aarsland D, Leentjens AF. A systematic review of prevalence studies of depression in Parkinson's disease. Mov Disord. 2008; 23:183-189.

Reiman EM, Chen K, Liu X, et al. Fibrillar amyloid-beta burden in cognitively normal people at 3 levels of genetic risk for Alzheimer's disease. Proc Natl Acad Sci U S A. 2009; 106:6820-6825.

Remy P, Doder M, Lees AJ, Turjanski N, Brooks DJ. Depression in Parkinson's disease: loss of dopamine and noradrenaline innervation in the limbic system. Brain. 2005; 128:1314-1322.

Ries V, Silva RM, Oo TF, et al. JNK2 and JNK3 combined are essential for apoptosis in dopamine neurons of the substantia nigra, but are not required for axon degeneration. J Neurochem. 2008; 107:1578-1588.

Rinne JO, Brooks DJ, Rossor MN, et al. 11C-PiB PET assessment of change in fibrillar amyloid-beta load in patients with Alzheimer's disease treated with bapineuzumab: a phase 2, double-blind, placebo-controlled, ascending-dose study. Lancet Neurol. 2010; 9:363-372.

Rinne JO, Portin R, Ruottinen H, Nurmi E, Bergman J, Haaparanta M, Solin O. Cognitive impairment and the brain dopaminergic system in Parkinson disease: [18F]fluorodopa positron emission tomographic study. Arch Neurol. 2000; 57:470-475.

Rochester L, Hetherington V, Jones D, et al. Attending to the task: interference effects of functional tasks on walking in Parkinson's disease and the roles of cognition, depression, fatigue, and balance. Arch Phys Med Rehabil. 2004; 85:1578-1585.

Rochester L, Yarnall AJ, Baker MR, et al. Cholinergic dysfunction contributes to gait disturbance in early Parkinson's disease. Brain 2012; 135:2779-2888.

Rodier J. Manganese poisoning in Moroccan miners. Br J Industr Med. 1955; 12:21-35.

Rodrigues e Silva AM, Geldsetzer F, Holdorff B, et al. Who was the man who discovered the "Lewy bodies"? Mov Disord. 2010; 25:1765-1773.

Rodriguez-Pallares J, Parga JA, et al. Mechanism of 6-hydroxydopamine neurotoxicity: the role of NADPH oxidase and microglial activation in 6-

hydroxydopamine-induced degeneration of dopaminergic neurons. J Neurochem 2007; 103:145-156.

Rogers JD, Brogan D, Mirra SS. The nucleus basalis of Meynert in neurological disease: a quantitative morphological study. Ann Neurol. 1985; 17:163-170.

Rolinski M, Fox C, Maidment I, McShane R. Cholinesterase inhibitors for dementia with Lewy bodies, Parkinson's disease dementia and cognitive impairment in Parkinson's disease. Cochrane Database Syst Rev. 2012; 3:CD006504.

Rolland AS, Tandé D, Herrero MT, et al. Evidence for a dopaminergic innervation of the pedunculopontine nucleus in monkeys, and its drastic reduction after MPTP intoxication. J Neurochem. 2009; 110:1321-1329.

Roodveldt C, Labrador-Garrido A, Gonzalez-Rey E, et al. Preconditioning of microglia by α-synuclein strongly affects the response induced by toll-like receptor (TLR) stimulation. PLoS One. 2013 8:e79160.

Ros-Bernal F, Hunot S, Herrero MT, et al. Microglial glucocorticoid receptors play a pivotal role in regulating dopaminergic neurodegeneration in parkinsonism. Proc Natl Acad Sci U S A 2011; 108:6632-6637.

Rosano C, Aizenstein H, Brach J, Longenberger A, Studenski S, Newman AB. Special article: gait measures indicate underlying focal gray matter atrophy in the brain of older adults. J Gerontol A Biol Sci Med Sci. 2008; 63:1380-1388.

Rosano C, Brach J, Longstreth Jr WT, Newman AB. Quantitative measures of gait characteristics indicate prevalence of underlying subclinical structural brain abnormalities in high-functioning older adults. Neuroepidemiology 2006; 26:52-60.

Rosenberg RN. Treat Alzheimer disease before it is symptomatic. Arch Neurol. 2011; 68:1237-1238.

Ross CA, Poirier MA. Protein aggregation and neurodegenerative disease. Nat. Med. 2004; 10 (Suppl):S10-7.

Ross GW, Petrovitch H, Abbott RD, et al. Association of olfactory dysfunction with risk for future Parkinson’s disease. Ann Neurol 2008; 63:167-173.

Ryczko D, Grätsch S, Auclair F, et al. Forebrain dopamine neurons project down to a brainstem region controlling locomotion. Proc Natl Acad Sci U S A. 2013; 110:E3235-3242.

Saalmann YB, Pinsk MA, Wang L, Li X, Kastner S. The pulvinar regulates information transmission between cortical areas based on attention demands. Science 2012; 337:753-756.

Sabbagh MN, Adler CH, Lahti TJ, et al. Parkinson disease with dementia: comparing patients with and without Alzheimer pathology. Alzheimer Dis Assoc Disord. 2009; 23:295-297.

Sahyoun C, Floyer-Lea A, Johansen-Berg H, Matthews PM. Towards an understanding of gait control: brain activation during the anticipation, preparation and execution of foot movements. Neuroimage. 2004; 21:568-575.

Salloway S, Sperling R, Fox NC, et al: Bapineuzumab 301 and 302 Clinical Trial Investigators. Two phase 3 trials of bapineuzumab in mild-to-moderate Alzheimer's disease. N Engl J Med. 2014; 370:322-333.

Sapp E, Penney J, Young A, Aronin N, et al. Axonal transport of N-terminal huntingtin suggests early pathology of corticostriatal projections in Huntington disease. J Neuropathol Exp Neurol. 1999; 58:165-1673.

Satake W1, Nakabayashi Y, Mizuta I, et al. Genome-wide association study identifies common variants at four loci as genetic risk factors for Parkinson's disease. Nat Genet. 2009; 41:1303-1307.

Sawada M, Imamura K, Nagatsu T. Role of cytokines in inflammatory process in Parkinson’s disease. J Neural Transm Suppl. 2006:373–381.

Sawaguchi T, Goldman-Rakic PS. D1 dopamine receptors in prefrontal cortex: involvement in working memory. Science 1991; 251:947-950.

Sawle GV, Playford ED, Brooks DJ, Quinn N, Frackowiak RSJ. Asymmetrical presynaptic and postsynaptic changes in the striatal dopamine projection in dopa-naive parkinsonism: diagnostic implications of the D2 receptor status. Brain 1993; 116:853-867.

Scatton B, Javoy-Agid F, Rouquier L, Dubois B, Agid Y. Reduction of cortical dopamine, noradrenaline, serotonin and their metabolites in Parkinson's disease. Brain Res. 1983; 275:321-328.

Schaafsma JD, Giladi N, Balash Y, Bartels AL, Gurevich T, Hausdorff JM. Gait dynamics in Parkinson's disease: relationship to Parkinsonian features, falls and response to levodopa. J Neurol Sci. 2003; 212:47-53.

Scherfler C, Khan NL, Pavese N, et al. Striatal and cortical pre- and postsynaptic dopaminergic dysfunction in sporadic parkin-linked parkinsonism. Brain. 2004; 127:1332-1342.

Schulte EC, Mollenhauer B, Zimprich A, et al. Variants in eukaryotic translation initiation factor 4G1 in sporadic Parkinson’s disease. Neurogenetics 2012; 13:281-285.

Selikhova M, Williams DR, Kempster PA, Holton JL, Revesz T, Lees AJ. A clinico-pathological study of subtypes in Parkinson's disease. Brain 2009; 132:2947-2957.

Sepulcre J, Sabuncu MR, Johnson KA. Network assemblies in the functional brain. Curr Opin Neurol. 2012; 25:384-391.

Shannon KM, Keshavarzian A, Mutlu E, et al. Alpha-synuclein in colonic submucosa in early untreated Parkinson's disease. Mov Disord 2012; 27:709-715.

Sharma M, Ioannidis JP, Aasly JO, et al. GEO-PD Consortium. Large-scale replication and heterogeneity in Parkinson disease genetic loci. Neurology 2012; 79:659-667.

Shechter R, Schwartz M. Harnessing monocyte-derived macrophages to control central nervous system pathologies: no longer 'if' but 'how'. J Pathol. 2013; 229:332-346.

Sherer TB, Betarbet R, Kim JH, et al. Selective microglial activation in the rat rotenone model of Parkinson's disease. Neurosci Lett 2003; 341:87–90

Shen WB, McDowell KA, Siebert AA, et al. Environmental neurotoxin-induced progressive model of parkinsonism in rats. Ann Neurol. 2010; 68:70-80.

Shiba M, Bower JH, Maraganore DM, et al. Anxiety disorders and depressive disorders preceding Parkinson's disease: a case-control study. Mov Disord. 2000; 15:669-677.

Shimada H, Hirano S, Shinotoh H, et al. Mapping of brain acetylcholinesterase alterations in Lewy body disease by PET. Neurology 2009; 73:273-278.

Shulman LM, Taback RL, Bean J, Weiner WJ. Comorbidity of the nonmotor symptoms of Parkinson's disease. Mov Disord. 2001; 16:507-510.

Siderowf A, Xie SX, Hurtig H, et al. CSF amyloid {beta} 1-42 predicts cognitive decline in Parkinson disease. Neurology 2010; 75:1055-1061.

Silveira-Moriyama L, Holton JL, Kingsbury A, et al. Regional differences in the severity of Lewy body pathology across the olfactory cortex. Neurosci Lett. 2009; 453:77-80.

Simon-Sanchez J, Schulte C, Bras JM, et al. Genome-wide association study reveals genetic risk underlying Parkinson's disease. Nat Genet. 2009; 41:1308-1312.

Singleton AB, Farrer M, Johnson J, et al. Alpha-synuclein locus triplication causes Parkinson's disease. Science 2003; 302:841.

Snijders AH, Leunissen I, Bakker M, Overeem S, Helmich RC, Bloem BR, Toni I. Gait-related cerebral alterations in patients with Parkinson's disease with freezing of gait. Brain 2011; 134:59-72

Slifstein M, Laruelle M. Models and methods for derivation of in vivo neuroreceptor parameters with PET and SPECT reversible radiotracers. Nucl Med Biol. 2001; 28:595-608.

Snow BJ, Tooyama I, McGeer EG, et al..Human positron emission tomographic [18F]fluorodopa studies correlate with dopamine cell counts and levels. Ann. Neurol. 1993; 34:324-330.

Sossi V, de la Fuente-Fernandez R, Schulzer M, Troiano AR, Ruth TJ, Stoessl AJ. Dopamine transporter relation to dopamine turnover in Parkinson's disease: a positron emission tomography study. Ann Neurol. 2007; 62:468-474.

Spencer PS, Nunn PB, Hugon J, et al. Guam amyotrophic lateral sclerosis-parkinsonism-dementia linked to a plant excitant neurotoxin. Science 1987; 237:517-522.

Spillantini MG, Schmidt ML, Lee VM, et al. Alpha-synuclein in Lewy bodies. Nature 1997; 388:839-840.

Springer S, Giladi N, Peretz C, Yogev G, Simon ES, Hausdorff JM. Dual-tasking effects on gait variability: the role of aging, falls, and executive function. Mov Disord. 2006; 21:950-957.

Starr JM, Leaper SA, Murray AD, et al. Brain white matter lesions detected by magnetic resonance imaging are associated with balance and gait speed. J Neurol Neurosurg Psychiatry 2003; 74:94-98.

Stepens A, Logina I, Liguts V, et al. A Parkinsonian syndrome in methcathinone users and the role of manganese. N Engl J Med. 2008; 358:1009-1017.

Stern, G. Did Parkinsonism occur before 1817? J Neurol Neurosurg Psychiatry 1989; Special Supplement:11-12

Su X, Federoff HJ, Maguire-Zeiss KA. Mutant alpha-synuclein overexpression mediates early proinflammatory activity. Neurotox Res. 2009; 16:238-254.

Suzuki M, Miyai I, Ono T, et al. Prefrontal and premotor cortices are involved in adapting walking and running speed on the treadmill: an optical imaging study. Neuroimage 2004; 23:1020-1026.

Suzumura A, Sawada M, Marunouchi T. Selective induction of interleukin-6 in mouse microglia by granulocyte-macrophage colony-stimulating factor. Brain Res. 1996; 713:192-198.

Tai YF, Pavese N, Gerhard A, et al. Microglial activation in presymptomatic Huntington's disease gene carriers. Brain. 2007; 130:1759-1766.

Takakusaki K, Habaguchi T, Ohtinata-Sugimoto J, Saitoh K, Sakamoto T. Basal ganglia efferents to the brainstem centers controlling postural muscle tone and locomotion: a new concept for understanding motor disorders in basal ganglia dysfunction. Neuroscience 2003; 119:293-308.

Takakusaki K, Tomita N, Yano M. Substrates for normal gait and pathophysiology of gait disturbances with respect to the basal ganglia dysfunction. J Neurol. 2008; 255

(Suppl 4):19e29.

Takeda A, Hashimoto M, Mallory M, Sundsumo M, Hansen L, Masliah E. C-terminal alpha-synuclein immunoreactivity in structures other than Lewy bodies in neurodegenerative disorders. Acta Neuropathol. 2000; 99:296-304.

Tanaka S, Ishii A, Ohtaki H, Shioda S, Yoshida T, Numazawa S. Activation of microglia induces symptoms of Parkinson's disease in wild-type, but not in IL-1 knockout mice. J Neuroinflammation. 2013; 10:143.

Tansey MG, Goldberg MS. Neuroinflammation in Parkinson's disease: its role in neuronal death and implications for therapeutic intervention. Neurobiol Dis 2010; 37:510-518.

Teismann P, Tieu K, Choi DK, et al. Cyclooxygenase-2 is instrumental in Parkinson's disease neurodegeneration. Proc Natl Acad Sci U S A. 2003; 100:5473-5478.

Tinetti ME, Speechley M, Ginter SF. Risk factors for falls among elderly persons living in the community. N Engl J Med. 1988; 319:1701-1707.

Theodore S, Cao S, McLean PJ, Standaert DG. Targeted overexpression of human alpha-synuclein triggers microglial activation and an adaptive immune response in a mouse model of Parkinson disease. J Neuropathol Exp Neurol. 2008; 67:1149-1158.

Thévenet J, Pescini Gobert R, Hooft van Huijsduijnen R, Wiessner C, Sagot YJ. Regulation of LRRK2 expression points to a functional role in human monocyte maturation. PLoS One. 2011; 6:e21519.

Tolosa E, Wenning G, Poewe W. The diagnosis of Parkinson's disease. Lancet Neurol. 2006; 5:75-86.

Ton TG, Heckbert SR, Longstreth WT Jr, et al. Nonsteroidal anti-inflammatory drugs and risk of Parkinson's disease. Mov Disord 2006; 21:964-969.

Tretiakoff K. Contribution a l'etude de l'anatomie pathologique du locus niger de Soemmering avec quelques deductions relatives a le pathogenie des troubles du tonius musculaire et de la maladie de Parkinson [thesis]. Paris, University of Paris, 1919

Tsigelny IF, Crews L, Desplats P, et al. Mechanisms of hybrid oligomer formation in the pathogenesis of combined Alzheimer's and Parkinson's diseases. PLoS One. 2008; 3:e3135.

Tsuang DW, Wilson RK, Lopez OL, et al. Genetic association between the APOE*4 allele and Lewy bodies in Alzheimer disease. Neurology 2005; 64:509-513.

Tsuang D, Leverenz JB, Lopez OL, et al. APOE ε4 increases risk for dementia in pure synucleinopathies. JAMA Neurol. 2013; 70:223-228.

Turjanski N, Lees AJ, Brooks DJ. In vivo studies on striatal dopamine D1 and D2 site binding in L-dopa-treated Parkinson's disease patients with and without dyskinesias. Neurology 1997; 49:717-723.

Turkheimer FE, Edison P, Pavese N, et al. Reference and target region modeling of [11C]-(R)-PK11195 brain studies. J Nucl Med. 2007; 48:158-167.

Tuschl K, Clayton PT, Gospe SM Jr, et al. Syndrome of hepatic cirrhosis, dystonia, polycythemia, and hypermanganesemia caused by mutations in SLC30A10, a manganese transporter in man. Am J Hum Genet. 2012; 90:457-466.

Uc EY, Rizzo M, Anderson SW, Qian S, Rodnitzky RL, Dawson JD. Visual dysfunction in Parkinson disease without dementia. Neurology 2005; 65:1907-1913.

Uchikado H, Lin WL, DeLucia MW, Dickson DW. Alzheimer disease with amygdala Lewy bodies: a distinct form of alpha-synucleinopathy. J Neuropathol Exp Neurol. 2006; 65:685-697.

Uitti RJ, Baba Y, Whaley NR, Wszolek ZK, Putzke JD. Parkinson disease: handedness predicts asymmetry. Neurology 2005; 64:1925-1930.

Umemura A, Oeda T, Hayashi R, et al. Diagnostic accuracy of apparent diffusion coefficient and 123I-metaiodobenzylguanidine for differentiation of multiple system atrophy and Parkinson's disease. PLoS One 2013; 8:e61066.

Valente EM, Abou-Sleiman PM, Caputo V, et al. Hereditary early-onset Parkinson’s disease caused by mutations in PINK1. Science 2004; 304:1158-1160.

Van de Warrenburg BP, Lammens M, Lucking CB, et al. Clinical and pathologic abnormalities in a family with parkinsonism and parkin gene mutations. Neurology 2001; 56:555-557.

Van Den Eeden SK, Tanner CM, Bernstein AL, et al. Incidence of Parkinson's disease: variation by age, gender, and race/ethnicity. Am J Epidemiol. 2003; 157:1015-1022.

van Hilten JJ, Hoogland G, van der Velde EA, Middelkoop HA, Kerkhof GA, Roos RA. Diurnal effects of motor activity and fatigue in Parkinson's disease. J Neurol Neurosurg Psychiatry 1993; 56:874-877.

Verbaan D, Marinus J, Visser M, van Rooden SM, Stiggelbout AM, van Hilten JJ. Patient-reported autonomic symptoms in Parkinson disease. Neurology 2007 69:333-341.

Verghese J, Robbins M, Holtzer R, et al. Gait dysfunction in mild cognitive impairment syndromes. J Am Geriatr Soc. 2008; 56:1244-1251.

Verghese J, Wang C, Lipton RB, Holtzer R, Xue X. Quantitative gait dysfunction and risk of cognitive decline and dementia. J Neurol Neurosurg Psychiatry 2007; 78:929-935.

Vilarino-Guell C, Wider C, Ross OA, et al. VPS35 mutations in Parkinson disease. Am J Hum Genet. 2011; 89:162-167.

Wakabayashi K, Takahashi H, Takeda S, Ohama E, Ikuta F. Parkinson's disease: the presence of Lewy bodies in Auerbach's and Meissner's plexuses. Acta Neuropathol. 1988; 76:217-221.

Wakabayashi K, Takahashi H, Ohama E, Takeda S, Ikuta F. Lewy bodies in the visceral autonomic nervous system in Parkinson's disease. Adv Neurol 1993; 60:609-612.

Wang C, Wai Y, Kuo B, Yeh YY, Wang J. Cortical control of gait in healthy humans: an fMRI study. J Neural Transm. 2008; 115:1149-1158.

Watts JC, Giles K, Oehler A, et al. Transmission of multiple system atrophy prions to transgenic mice. Proc Natl Acad Sci U S A 2013; 110:19555-19560.

Waxman EA, Giasson BI. Induction of intracellular tau aggregation is promoted by alpha-synuclein seeds and provides novel insights into the hyperphosphorylation of tau. J Neurosci. 2011; 31:7604-7618.

Weingarten MD, Lockwood AH, Hwo SY, Kirschner MW. A protein factor essential for microtubule assembly. Proc Natl Acad Sci U S A 1975; 72:1858-1862.

Wen X, Wu X, Liu J, Li K, Yao L. Abnormal baseline brain activity in non-depressed Parkinson's disease and depressed Parkinson's disease: a resting-state functional magnetic resonance imaging study. PLoS One 2013; 8:e63691.

Whelan PJ. Control of locomotion in the decerebrate cat. Prog Neurobiol. 1996; 49:481-515.

Whone AL, Moore RY, Piccini PP, Brooks DJ. Plasticity of the nigropallidal pathway in Parkinson's disease. Ann Neurol. 2003; 53:206-213.

Williams DR, de Silva R, Paviour DC, et al. Characteristics of two distinct clinical phenotypes in pathologically proven progressive supranuclear palsy: Richardson's syndrome and PSP-parkinsonism. Brain 2005; 128:1247-1258.

Williams-Gray CH, Foltynie T, Brayne CE, et al. Evolution of cognitive dysfunction in an incident Parkinson's disease cohort. Brain 2007; 130:1787-1798.

Williams-Gray CH, Goris A, Saiki M, et al. Apolipoprotein E genotype as a risk factor for susceptibility to and dementia in Parkinson's disease. J Neurol. 2009; 56:493-498.

Williams-Gray CH, Hampshire A, Barker RA, Owen AM. Attentional control in Parkinson's disease is dependent on COMT val 158 met genotype. Brain 2008; 131:397-408.

Williams-Gray CH, Hampshire A, Robbins TW, Owen AM, Barker RA. Catechol O-methyltransferase Val158Met genotype influences frontoparietal activity during planning in patients with Parkinson's disease. J Neurosci. 2007; 27:4832-4838.

Williams-Gray CH, Mason SL, Evans JR, et al. The CamPaIGN study of Parkinson's disease: 10-year outlook in an incident population-based cohort. J Neurol Neurosurg Psychiatry 2013; 84:1258-1264.

Williams GV, Castner SA. Under the curve: critical issues for elucidating D1 receptor function in working memory. Neuroscience 2006; 139:263-276.

Wilson AA, Garcia A, Parkes J, et al. Radiosynthesis and initial evaluation of [18F]-FEPPA for PET imaging of peripheral benzodiazepine receptors. Nucl Med Biol. 2008; 35:305-314.

Winner B, Jappelli R, Maji SK, et al. In vivo demonstration that a-synuclein oligomers are toxic. Proc Natl Acad Sci U S A 2011; 108:4194-4199.

Wooten GF, Currie LJ, Bovbjerg VE, Lee JK, Patrie J. Are men at greater risk for Parkinson's disease than women? J Neurol Neurosurg Psychiatry 2004; 75:637-639.

Wu DC, Jackson-Lewis V, Vila M, et al. Blockade of microglial activation is neuroprotective in the 1-methyl-4-phenyl-1,2,3,6-tetrahydropyridinemouse model of Parkinson disease. J Neurosci 2002; 22:1763-1771.

Wu K, O'Keeffe D, Politis M, et al. The catechol-O-methyltransferase Val(158)Met polymorphism modulates fronto-cortical dopamine turnover in early Parkinson's disease: a PET study. Brain 2012; 135:2449-2457.

Xie W, Wan OW, Chung KK. New insights into the role of mitochondrial dysfunction and protein aggregation in Parkinson’s disease. Biochim Biophys Acta 2010; 1802:935-941.

Yang NY, Lee YN, Lee HJ, Kim YS, Lee SJ. Glucocerebrosidase, a new player changing the old rules in Lewy body diseases. Biol Chem. 2013; 394:807-818.

Yap TL, Gruschus JM, Velayati A, et al. Alpha-synuclein interacts with Glucocerebrosidase providing a molecular link between Parkinson and Gaucher diseases. J Biol Chem. 2011; 286:28080-28088.

Yaqub M, van Berckel BN, Schuitemaker A, Hinz R, Turkheimer FE, Tomasi G, Lammertsma AA, Boellaard R. Optimization of supervised cluster analysis for extracting reference tissue input curves in (R)-[(11)C]PK11195 brain PET studies. J Cereb Blood Flow Metab. 2012; 32:1600-1608.

Yarnall AJ, Breen DP, Duncan GW, et al; ICICLE-PD Study Group. Characterizing mild cognitive impairment in incident Parkinson disease: the ICICLE-PD study. Neurology 2014; 82:308-316.

Yasuno F, Ota M, Kosaka J, et al. Increased binding of peripheral benzodiazepine receptor in Alzheimer's disease measured by positron emission tomography with [11C]DAA1106. Biol Psychiatry 2008; 64:835-841.

Yogev G, Giladi N, Peretz C, Springer S, Simon ES, Hausdorff JM. Dual tasking, gait rhythmicity, and Parkinson's disease: which aspects of gait are attention demanding? Eur J Neurosci. 2005; 22:1248-1256.

Yogev G, Plotnik M, Peretz C, Giladi N, Hausdorff JM. Gait asymmetry in patients with Parkinson's disease and elderly fallers: when does the bilateral coordination of gait require attention? Exp Brain Res. 2007; 177:336-346.

Yogev-Seligmann G, Hausdorff JM, Giladi N. The role of executive function and attention in gait. Mov Disord. 2008; 23:329-342.

Yokokura M, Mori N, Yagi S, et al. In vivo changes in microglial activation and amyloid deposits in brain regions with hypometabolism in Alzheimer's disease. Eur J Nucl Med Mol Imaging 2011; 38:343-351.

Zaccai J, Brayne C, McKeith I, Matthews F, Ince PG. Patterns and stages of alpha-synucleinopathy: Relevance in a population based cohort. Neurology 2008; 70:1042-1048.

Zahrt J, Taylor JR, Mathew RG, Arnsten AF. Supranormal stimulation of D1 dopamine receptors in the rodent prefrontal cortex impairs spatial working memory performance. J Neurosci. 1997; 17:8528-8535.

Zarow C, Lyness SA, Mortimer, JA, Chui, HC. Neuronal loss is greater in the locus coeruleus than nucleus basalis and substantia nigra in Alzheimer and Parkinson diseases. Arch. Neurol. 2003; 60:337-341.

Zarranz JJ, Alegre J, Gomez-Esteban JC, et al. The new mutation, E46K, of alpha-synuclein causes Parkinson and Lewy body dementia. Ann Neurol. 2004; 55:164-173.

Ziegler DA, Wonderlick JS, Ashourian P, et al. Substantia nigra volume loss before basal forebrain degeneration in early Parkinson disease. JAMA Neurol. 2013; 70:241-247.

Zimprich A, Biskup S, Leitner P, et al. Mutations in LRRK2 cause autosomal-dominant parkinsonism with pleomorphic pathology. Neuron 2004; 44:601-607.

Zhang J, Mattison HA, Liu C, et al; Parkinson Study Group DATATOP Investigators. Longitudinal assessment of tau and amyloid beta in cerebrospinal fluid of Parkinson disease. Acta Neuropathol. 2013; 126:671-682.

Zhang W, Wang T, Pei Z, et al. Aggregated alpha-synuclein activates microglia: a process leading to disease progression in Parkinson’s disease. FASEB J. 2005; 19:533-542.